ANKARA YILDIRIM BEYAZIT UNIVERSITY
GRADUATE SCHOOL OF NATURAL AND APPLIED SCIENCES

BEHAVIOR OF SHEAR DEFICIENT REINFORCED CONCRETE COLUMNS JACKETED WITH ENGINEERING CEMENTITIOUS COMPOSITE CONCRETE FOR SEISMIC LOADS

M.Sc. Thesis by

Ali Lilo ALHASAN

Department of Civil Engineering

July, 2024

ANKARA

BEHAVIOR OF SHEAR DEFICIENT REINFORCED CONCRETE COLUMNS JACKETED WITH ENGINEERING CEMENTITIOUS COMPOSITE CONCRETE FOR SEISMIC LOADS

A Thesis Submitted to

the Graduate School of Natural and Applied Sciences of

Ankara Yıldırım Beyazıt University

In Partial Fulfillment of the Requirements for the Degree of Master of Science

in Civil Engineering

by

Ali Lilo ALHASAN

July, 2024

ANKARA

M.Sc. THESIS EXAMINATION RESULT FORM

We have read the thesis entitled "**BEHAVIOR OF SHEAR DEFICIENT REINFORCED CONCRETE COLUMNS JACKETED WITH ENGINEERING CEMENTITIOUS COMPOSITE CONCRETE FOR SEISMIC LOADS**" completed by **ALI LILO ABED ALHASAN** under the supervision of **Prof. Dr. Lutfullah TURANLI** and **Prof. Dr. Afşin SARITAŞ** and we certify that in our opinion it is fully adequate, in scope and in quality, as a thesis for the degree of Master of Science.

Prof. Dr. Lutfullah Turanlı

(Supervisor)

Prof. Dr. Afşin Sarıtaş

(Co-Supervisor)

Assist. Prof. Dr. Mahmut Cem Yılmaz

(Jury Member)

Prof. Dr. Mehmet Baran

(Jury Member)

Assist. Prof. Dr. Ömer Mercimek

(Jury Member)

Prof. Dr. Sadettin Orhan

(Director)

Graduate School of Natural and Applied Sciences

ETHICAL DECLARATION

I hereby declare that, in this thesis which has been prepared in accordance with the Thesis Writing Manual of Graduate School of Natural and Applied Sciences,

- All data, information and documents are obtained in the framework of academic and ethical rules,
- All information, documents and assessments are presented in accordance with scientific ethics and morals,
- All the materials that have been utilized are fully cited and referenced,
- No change has been made on the utilized materials,
- All the works presented are original, and in any contrary case of above statements, I accept to renounce all my legal rights.

Date: 05.07.2024 **Signature**:……………………………..

Name & Surname: Ali Lilo ALHASAN

ACKNOWLEDGEMENTS

First of all, I would like to extend my utmost gratitude to my advisor, **Prof. Dr. Lutfullah Turanlı**, for his unwavering support during my pursuit of master's degree. His benevolence, encouragement and extensive knowledge have been invaluable. Dr. Turanlı office door was consistently accessible whenever I had difficulties or had inquiries regarding my research. He consistently guided me to correct path whenever he deemed it necessary.

My private and sincere gratitude goes out to **Prof.Dr. Afşin Sarıtaş** my co-supervisor for his prompt, helpful responses to my inquiries as well as for his counsel, direction at any stage of my research process. Prof. Dr. Sarıtaş, I am appreciative that I have been educated by someone so amazing, although I didn't say it often. I am lucky to have a wonderful teacher as you. Accept my respect and appreciation.

My father, to your kind soul which never left I dedicate this work. It's given me great pleasure to express my gratitude to my family for their continuous support, tolerance, inspiration, and love during more than two years of my study in Turkey. I must express my gratitude, appreciation, and full thanks to my life partner, my associate in success really, she was a perfect, wonderful wife and carried a lot for me. Also, I would like to say thanks for my great mother and my dear kids, my friends for their unlimited support, without their help, this feat would not have been feasible.

5. July. 2024 **Ali Lilo ALHASAN**

BEHAVIOR OF SHEAR DEFICIENT REINFORCED CONCRETE COLUMNS JACKETED WITH ENGINEERING CEMENTITIOUS COMPOSITE CONCRETE FOR SEISMIC LOADS

ABSTRACT

This study focuses on treating the lack of shear resistance of columns exposed to axial and lateral force, such as earthquake and wind loads. The original columns were strengthened using Engineered cementitious composite ECC jackets, which are characterized by high plastic energy dissipation capability, and a mechanism that allows for the development of multiple tensile microcracks, high tensile resistance, and high hardening strain in tension, using two types of ECC, coated and uncoated fibers. This study bases on simulation and finite element analysis of 40 retrofitted models of experimental columns using the ABAQUS software under conditions similar to those that occurred in the laboratory, by utilizing concrete damage plasticity model to represent concrete behavior under different conditions. The stress-strain relationship and constitutive models in compression and tension have been calibrated. The finite element verification was implemented for all experimental specimens, which exhibit high identical behavior with the tested columns. All models of strengthened specimens with Engineered cementitious composite (ECC) exhibit an increase in lateral load capacity as well as a distinct increasing in ductility that change the sudden shear failure to flexural failure and high enhancement in total and plastic dissipation energy compared with the original experimental columns. The ECC demonstrate excellent compatibility with steel reinforcement and large ability to compensate for the deficiency of shear reinforcement.

Keywords: Concrete damage plasticity (CDP), constitutive model, Abaqus software, material calibration, plastic dissipation energy (PDE), engineering cementitious composites, shear failure, reinforced concrete (RC) column, RC column strengthening

KESMEDE KUSURLU BETONARME KOLONLARIN TASARLANMIŞ ÇİMENTO ESASLI KOMPOZİT BETON İLE DEPREM YÜKLERİNE KARŞI GÜÇLENDİRİLMESİ

ÖZ

Bu çalışma, deprem ve rüzgar yükleri gibi eksenel ve yanal kuvvetlere maruz kalan kolonlarda kesme direnci eksikliğinin giderilmesine odaklanmaktadır. Orijinal kolonlar, yüksek plastik enerji yitim kapasitesi ile karakterize edilen ve iki tip malzeme kullanılarak çoklu çekme mikro çatlaklarının, yüksek çekme direncinin ve çekmede yüksek sertleşme gerinimlerinin oluşmasına izin veren bir mekanizma ile karakterize edilen, tasarlanmış çimento esaslı kompozit ECC hem kaplanmış hem de kaplanmamış liflerle güçlendirildi. Bu çalışma, ABAQUS yazılımını ve farklı koşullar altında beton davranışını temsil etmek için beton hasar plastisite modelini kullanarak, laboratuarda meydana gelenlere benzer koşullar altında 40 adet güçlendirilmiş deneysel kolon modelinin simülasyonuna ve sonlu elemanlar analizine dayanmaktadır. Gerilim-gerinim ilişkisi ve basma ve gerilimdeki malzeme modelleri kalibre edilmiştir. Sonlu eleman doğrulaması tüm deneysel numuneler için uygulanmış olup, test edilen kolonlarla yüksek benzer davranış sergilemiştir. Tasarlanmış çimento esaslı kompozit (ECC) ile güçlendirilmiş tüm kolon modellerinde, orijinal deney numunesiyle karşılaştırıldığında, yanal yük kapasitesinde bir artışın yanı sıra ani kesme kırılmasını eğilme kırılmasına dönüştürmüş ve süneklikte belirgin bir artış ve toplam ve plastik yitim enerjisinde yüksek bir artış sergilemiştir. ECC, çelik takviyeyle mükemmel uyumluluk göstermiş ve kesme takviyesi eksikliğini telafi etme konusunda yüksek seviyede başarı sunmuştur.

Anahtar kelimeler: Beton hasarı plastisitesi (CDP), malzeme modeli, Abaqus yazılımı, malzeme kalibrasyonu, plastik yitim enerjisi (PDE), tasarlanmış çimento esaslı kompozitler, kesme kırılması, betonarme (RC) kolon, betonarme kolon güçlendirmesi

CONTENTS

NOMENCLATURE

ECC	The Engineering cementitious composites
CDP	Concrete Damage Plasticity
DA	Dilation angles
fb/fc	Equiaxial compression yield stress/uniaxial yield stress
V	Rate of applied load in FEA (Viscosity)
e	Eccentricity
M	Mesh size
PD	Plastic dispersion energy
DD	Damage dispersion energy
LL	Light axial load
ML	Moderate axial load
E, E_o	Modulus of elasticity, undamaged modulus of elasticity
dc	Damage parameter in compression
dt	Damage parameter in tension
$\varepsilon_c^{'}$	Compression strain corresponding to ultimate stress
ε_c^{in} , ε_t^{ck}	Inelastic compression strain and crack strain
ε_c^{pl} , ε_t^{pl}	Hardening plastic strain in compression and tension
f_{ck}	Ultimate compression stress
f_{cm}	Average compression stress at 28 days in MPa
f_{1ctm}	Peak tension stress in MPa.
f_{cru}	Ultimate crack stress of ECC corresponding to 3.5% tension strain.
f_{cr1}	First tension stress of ECC corresponding to 1% hardening strain.
ϵ_{cru}	Hardening tension strain of ECC corresponding to peak crack stress.
PDE	Plastic dissipation energy.

LIST OF TABLES

LIST OF FIGURES

CHAPTER 1

INTRODUCTION

1.1 General

Seismic excitations have a significant effect on RC column in multi-story building due to brittleness of normal concrete will cause suddenly failure without any index, as a result of weakness of columns resistance under lateral loads. Excessive axial loads will increase lateral demand and decreasing the ductility [1]. The rehabilitation and strengthen prosses are necessary when few existing facilities meet the life safety requirements of earthquake design codes, a lot of buildings are designed under nonconservative approaches due to economic reasons, or some structures are valuable structures such as cultural and historic buildings to enhance general characteristics to withstand different loading conditions [2]. Strengthening materials contribute to reducing maximum stresses by 30%, decrease story drift, improved shear resistance, in the ground story columns. It can prevent stiffness deterioration, and softening behavior of column during plastic deformations stage [3]. Mostly, concrete jacketing rehabilitation considerably improves peak load capacity by (1.6-3.39), and engineering Cementous composite concrete as a jacket layer of RC column will increase energy dispersion by (4.3-5) times compared with original RC columns [4]. Economic consideration, strengthening techniques depending on the desirable target of these processes, economic consideration, level of expected damage, and the importance of structure. All these factors simultaneously determine the proper approach to achieved rehabilitation [5].

1.2 Purpose and Scope

It is difficult to predict the exact behavior of concrete members due to their brittleness and nonlinearity. This study depends on ABAQUS numerical analysis of fixed RC columns deterioration challenges by using ECC concrete as a retrofitting material. In spite of possessing distinctive characteristics that overcome main limitations of conventional concrete, ECC is not widely used in construction projects due toattributed to high price and unavailability of its components locally. But it has distinct dissipation energy, high ductility, high tension stress, evolution strain-hardening, and high shear resistance, high durability material used to retrofit structures under severe environments such as bridges and offshore piles make it a materials worthy of research[6]. ECC is conducted by using an optimum ratio (1.5%-2%) by volume HPF as PVA polyvinyl alcohol, PE polyethylene, PP polypropylene coupling with fly ash, cement, silica fume, silica sand, and HRWR. These components motivate and improve the mechanical properties of ECC concrete. This study adopt four Christoper Lynn [7] column models with upper and lower pedestals, , exposed to lateral displacement. All specimens suffering from local cracks, low ductility and shear failure except one of them with ductile behavior. ECC jackets used as a strengthening material to beneficial above feedback of ECC to overcome all weakness points of tested samples.

1.3 Thesis Path

This thesis consists of five chapters, summarized as follows:

- Chapter 1: Illustrate general concepts related to strengthening and improving the mechanical properties of structural members by using ECC jacketing and show the target of this study.
- Chapter 2: It explains previous studies regarding with strengthening approach used for existing structural members.
- Chapter 3: This chapter describes concrete damage plasticity theory and FE constitutive models to generate stress-strain relationships in compression and tension and all damage plasticity parameters.
- Chapter 4: It illustrates finite element validation for each specimen and compare it with empirical curves.
- Chapter 5: It presents all simulation results and figures related to it.
- Chapter 6: It involves discussing of the results that were presented from finite element analysis.
- Chapter 7: It summarizes conclusions related with results and recommended future studies.

CHAPTER 2

LITERATURE REVIW

2.1 Overview

The strengthen process of concrete members including enhancement of durability, load capacity, The concept of infrastructure sustainability requirements against any form of decline virtual lifespan. This action is frequently imperative when the initial design specifications are no longer sufficient due to a lot of factors, such as extreme loading scenarios such as earthquakes, hurricanes, or tsunamis, alterations in building codes, the aging of the structure, or the detection of design inadequacies during the operation of buildings. The retrofitting procedure is indispensable to ensure the functionality and safety of the structure and increasing its service life [8][9][10]. Traditional construction materials exhibit weak physical structures and lack the necessary strength to withstand strong seismic forces, resulting in significant damage. Consequently, specialized methods are required to enhance the seismic behavior of these edifices and minimize consequential damage due to large shear stresses and lateral load excitations. privately in heritage and historical structures, including masonry materials such as clay and mud, stone, wood, and brick. It is emphasizing the significance of utilizing specialized methods to promote the seismic behavior of these buildings and minimize destruction. Unfortunately, despite various measures taken, there has not been any notable improvement in the structural performance of these buildings [11]. The proper jacketing methods able to compensate deficiency in shear reinforcement by increasing confinement of columns. This study did not use modern materials for strengthening, as we will discuss in our study, and the presentation of simulations to know the response of the origin gives a visualization of weaknesses and the appropriate way to treat them.

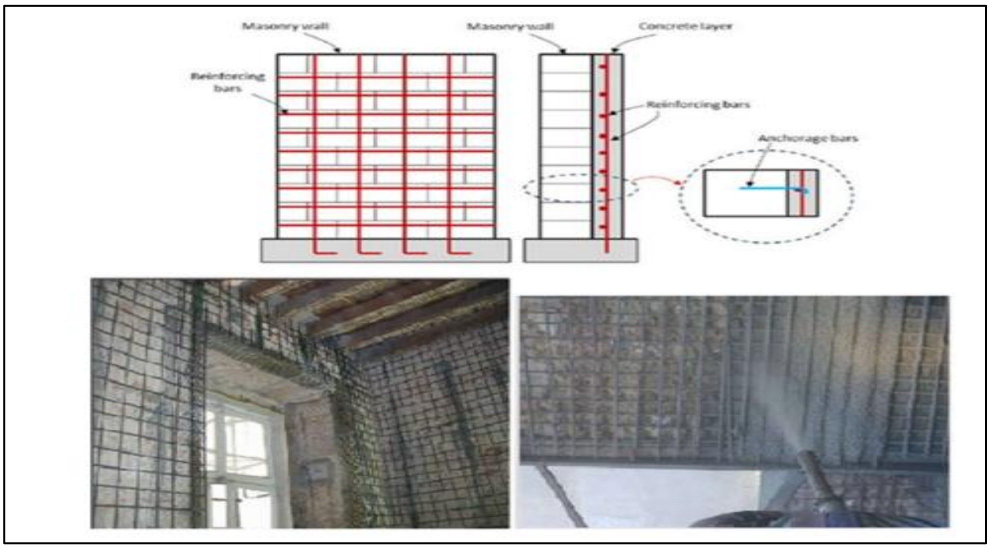

Figure 2.1 Reinforced concrete wall as a strengthening masonry [11]

The serious matter and the challenge are remedying and refurbishing instead of razing them to the ground due to financial considerations. Columns, being essential components of reinforced concrete structures, warrant fortification in old buildings exhibited suboptimal resilience. The manuscript is focused on difference techniques aimed to enhancing the load capacity and ductility of reinforced concrete columns [12].

2.2 Structural Strengthening Types

Mostly, the techniques of strengthen and rehabilitating the structural members have developed significantly with the development of the industry of the materials involved in the strengthening process, as they have differed in the capabilities to dissipate energy and their ability to improve the load capacity and increase the ductility of the concrete members that are characterized by semi-brittle failure. The use of these materials depends on the importance of their origin, the cost of these materials, and their availability. There are multiple strengthening types as the following:

2.2.1 CFRP Jacket Confinement

Carbon fiber reinforced polymer matrix was commonly used due to it exhibits notable efficacy in forecasting the performance of low-strength reinforced concrete columns that have been fortified with CFRP, which increase the ultimate load, CFRP strain, as well as the distribution of concrete strain for instance, (250*250*1680 mm) as a specimen dimension with a very low compression column strength about 7 MPa was adopted. The longitudinal steel was (4ϕ13mm and 8ϕ10 mm). The transverse steel bars (8@50mm) at the plastic hinge with height = 250 mm, while the stirrups in the outside of P. hinge are (8@95mm) a reinforced concrete column retrofitted with 2 plies CFRP, fixed along the height of the column as the figure below:

Figure 2.2 RC column strengthened by two layers of CFRP [10]

This study led to an enhancement the axial load capacity of the jacketing column with CFRP significantly, where the peak axial load increased by 1171 kN, and 1505 kN for the reinforced concrete column and reinforced concrete column strengthened by 2 layers of CFRP, respectively. As a result, the displacement increased, corresponding to the maximum axial force of 4.6 mm, and 15.9mm for the reinforce concreted column and reinforced concrete column retrofitted by 2 layers of CFRP, respectively. At the same time, after reaching to the peak load, both columns decreased in load capacity until failure at 50 mm displacement. The percentage ratio of axial loading capacity of the CFRP-RC column about 28.5% higher than the axial capacity of RC column alone. This research doesn’t catch on effect of CFRP jacket on column ductility, buckling deterioration, and shear force improvement, which are so important items during seismic excitation [5].

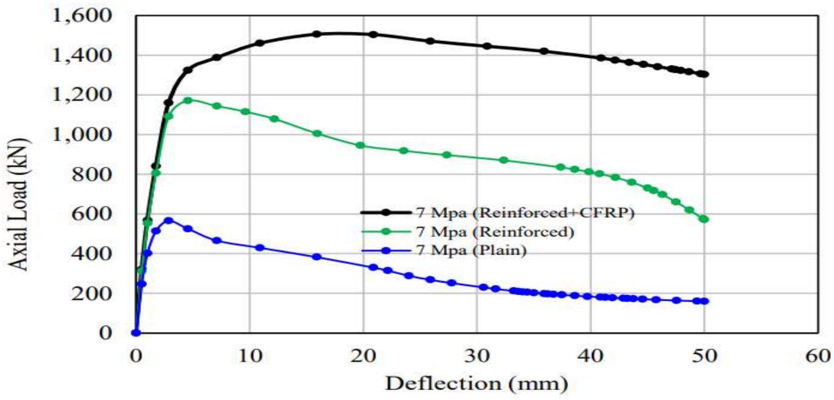

Figure 2.3 Axial load-displacement of RC column strengthened with CFRP [5]

The global study was implemented by A. B. Christianto et al. 2020 which used specimen models achieved by Bisby and Ranger [13] with concrete strengths C30, C40, and eccentricities 30 and 40 mm. The samples have a circular section with 152 mm as a dimeter and 608 mm as a height. It has a 33.2 MPa and 3.557 MPa for compression and tensile strength, respectively.

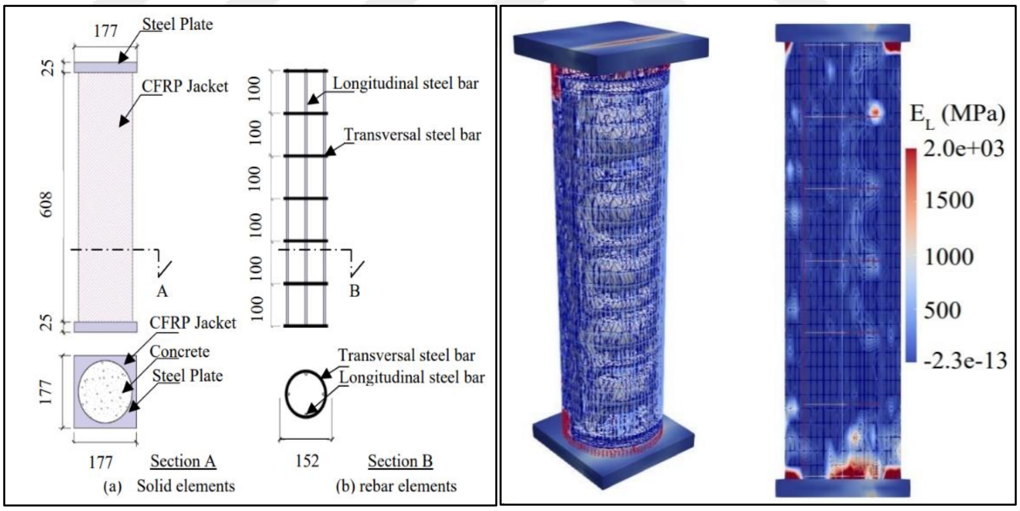

Figure 2.4 Circular column details and retrofitted with CFRP [14]

Substantial disparity in the concrete dilation rate between the core regions of concrete, namely the inner and the outer. This is caused by the adverse effect of confinement experienced by the outer concrete region which is concentrated at stirrups in elastic stage. After that, it disappeared when steel reached to yield stress. The ductility of columns with CFRP jackets was higher for columns with a larger initial load eccentricity [14].

2.2.2 Concrete Jacketing

The application of reinforced concrete jacketing has been extensively employed over the past few decades. There are many studies explained advantages this technique. One of these studies conducted by Dimitra A. which is employed 16 square columns (150*150*500mm) with core compression strength (24,37 MPa) subjected to frequency axial loads. Different pattern of loading and supporting boundary conditions are used for each core and jacket. Generally, the utilization of reinforced concrete jacketing has been experimentally an effective approach to enhance the axial load capacity and corresponding strain at failure. The effectiveness of this technique is reliant upon the behavior of the interface between the pre-existing and concrete jackets [15].

The reinforced concrete jackets were conducted by Vendors and Dristos; they used welding tie tips, to make the columns stronger and more flexible. The lack bonding of the interface caused the jacket has been separated from the original column, because of this, the welding process was insufficient [16]. New study proposed by Liu et.al. demonstrated a methodology to minimize the disturbance of occupancy by utilizing an individual non-symmetric concrete section to strengthen RC columns as shown in the figure (2.5) below, anchor rebars or high-strength bolts were used to fasten the extra piece to the original part. The modified sample has a notable increase in ultimate strength and ductility. Likewise, by using this technique, the stresses between the original and modified sections was reduced. Furthermore, the structure's usability remains unaffected, as the majority of the reinforcement can be performed outdoors. [17].

In recent years, High-performance materials' resilience have make strengthening and maintenance of structural members more efficient, decreasing bent fractures and shear ,improved load-displacement, energy dissipation, and stiffening deterioration of the column, as a results of using HPFR concrete mortar in the plastic hinge of the structural members. According to this, HPFR concrete fix the erosion of damage columns resulted in a reliable increasing in their strength [9][18][19]. Recently, Yao et al. have proposed the employment of textile-reinforced concrete, which is composed of carbon and glass fiber bundles, for the purpose of maintaining corrosion damage of reinforced columns. Seismic performance requirements, including yield force, ductility, peak load capacity, and accumulated energy dissipation, were enhanced as a result of this rehabilitation. However, it was observed that the degree of improvement achieved was determined by the primary corrosion ratio, whereby increasing of initial corrosion ratio correspond to a lower improvement properties[20].

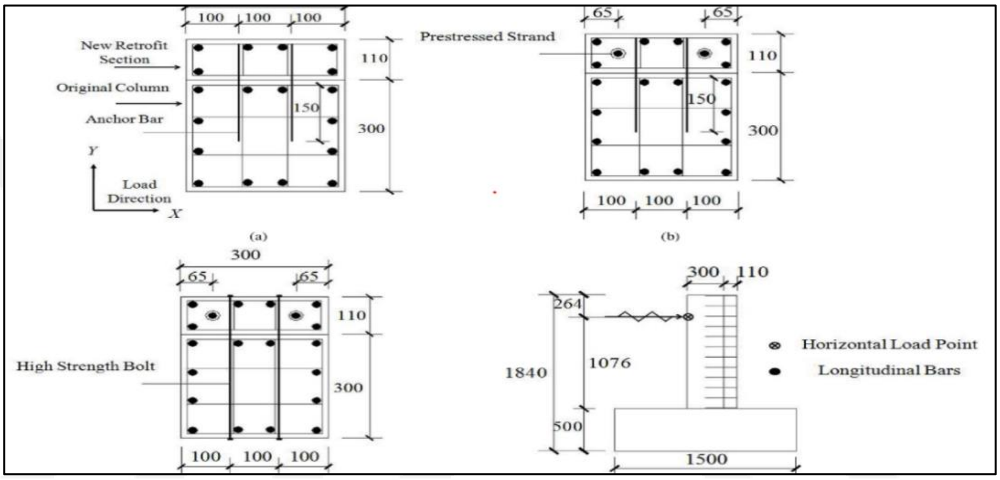

Figure 2.5 Non-symmetric concrete jackets details [20]

2.2.3 Steel Jacketing

In the steel retrofitting process, the structural members should be attached to steel sheets by apply welded or rivets. As a result, a space opens up between them, which was filled by glue materials. Lui. et.al. conducted four simply supported beam retrofits with two steel plates with a thickness 4, 6 mm and different lengths of steel plates,

The connection bolts were placed at various distances.This technique has proven to be effective in enhancement the seismic performance of columns. Also improve shear resistance. However, it is commonly associated with large costs, labor availability, and corrosion issues. In addition, it doesn’t increase section dimensions as concrete jackets so there is no significant change in stiffness of members[21].

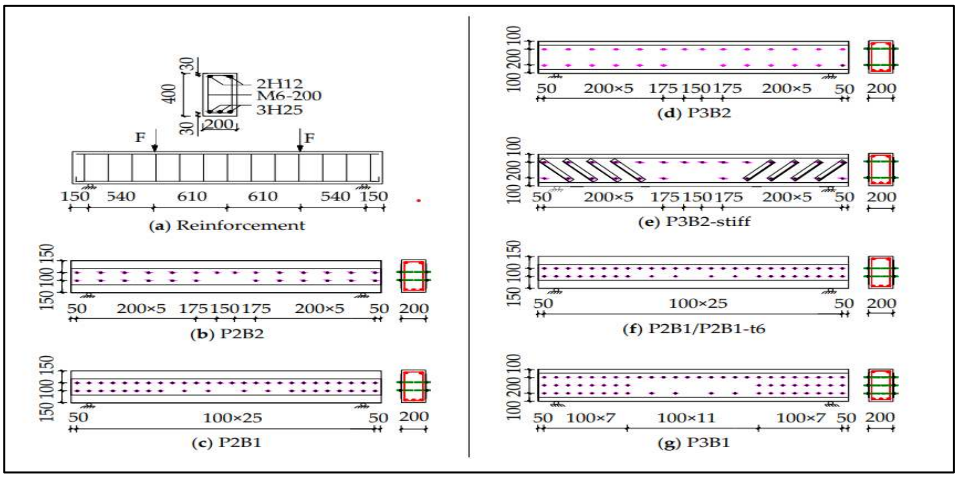

Figure 2.6 Jacketing reinforced beam with steel sheets [21]

The investigation carried out by Daudey and Filiatrault, rectangular reinforced concrete columns were retrofitted with steel jackets. The researchers observed that the original columns collapsed at smaller ductility proportions by (1-2).

Figure 2.7 Steel angles and plates fixed around column [22]

Conversely, each samples appeared a steady cyclic reaction with a ductility proportion of 6 time. The geometric characteristics of the steel jacket, regardless whether it is round or elliptical did not exert any influence on the performance of the reinforced columns. A unique investigation conducted by Wu et al., shown that the attachment of steel sheets to the plastic hinge of the reinforced concrete column successfully prolonged the occurrence of concrete failure. Steel jacketing is a technique that is employed when it is not possible to increase the original dimensions of a given column. Studies have shown that this method is effective method to enhancing the seismic resistance of existing bridge piers. In practice, the steel jacket is fabricated in two shell pieces and is then welded on site around the column. It also uses steel angles and plates fixed to the top of the slab and the bottom of the column which are applied at each of the four coroners then joined together by transverse strips as shown in the figure (2.7) above. However, it should be noted that this approach entails complex welding work. Furthermore, over the long-term corrosion issues are still unresolved [22].

Eight concrete blocks with the same size retrofitted by a steel jacket with a different plate size and exposed to various loading and eccentricity conditions. This study used different distances from anchor bolts and longitudinal and transverse stiffeners and simulate them using ABAQUS software as shown in the figure below:

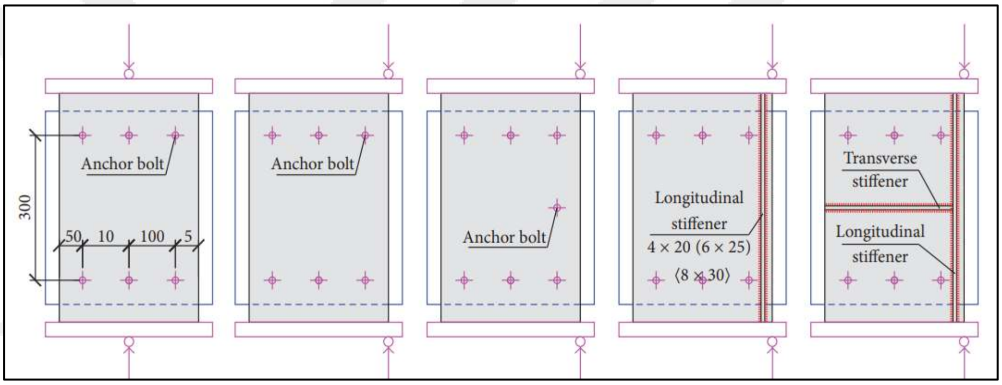

Figure 2.8 Steel jacket fixed by anchor bolts [23]

The structural field capacity of bolted steel plates can be improved through the implementation of a modified arrangement that includes reduced bolt spacing, long side stiffeners, and thicker steel sheet. In addition, the utilization of the first two mentioned restraint measures can produce a significant reduction in lateral buckling deformation [23].

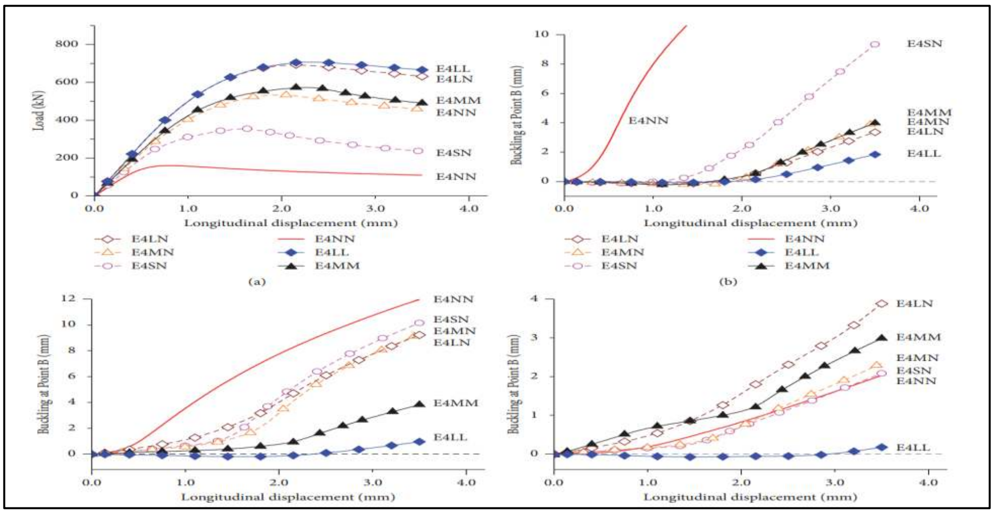

Figure 2.9 Load-displacement and buckling for steel jacket [23]

2.2.4 Hybrid Strengthen Jacketing

2.2.4.1 Concrete Fill Steel Tube and CFRP

P.Kiruthika et.al. utilized a steel pipe with a hollow inner, which agrees with IS 1161-1998 and has a slenderness ratio of (141.5). The tube possesses a circular section with diameter of 42.4mm, 3.2mm as a thickness, and 1500 mm as a height. It has a yield strength of 250 MPa, low-modulus CFRP with 240 kN/mm2 modulus of elasticity and a tensile resistance of 3800 MPa. It has thickness and width are 0.234mm and 600 mm, respectively. The connection type consists of two items, a hardener and a resin, mixed in 100:40 ratio. A mix designed with 27 MPa at 28 days of curing. The behavior of axial compressive for CFST columns reinforced with CFRP was improved with respect to their strength and stiffness. This was achieved by decreasing lateral deformation and load capacity of CFST column increased by 45.12%, 31.71%, and 15.85%, respectively. when use three, two, and one layers of CFRP rather than CS, ultimately resulting in superior performance compare to CFST columns that were not strengthened as shown in the figure below [24].

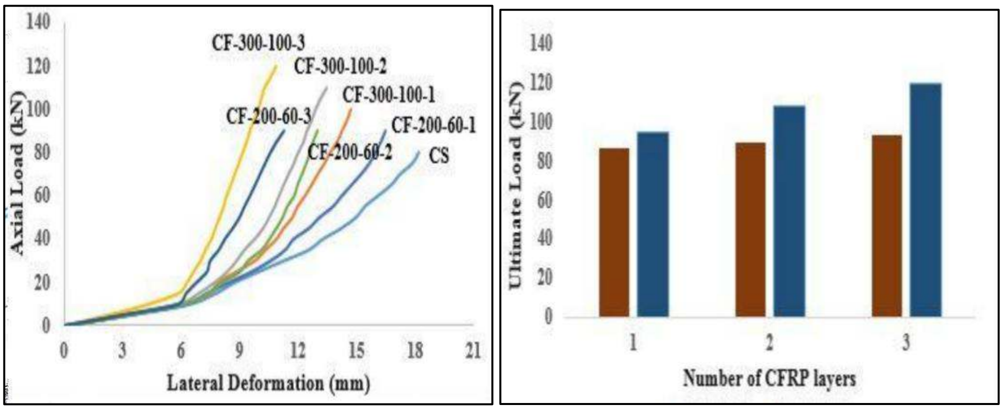

Figure 2.10 Concrete Fill Steel Tube and CFRP load-displacement [24]

2.2.4.2 NSM Bars and FRP Wrapp

The present technique of hybrid jacketing employs the combined use of Fiber-Reinforced Polymer (FRP) sheets and NSM rebars. The FRP sheets are utilized to increase side sway confinement while the NSM bars are used to improve the flexural strength of the column. The outcome of this approach is an improvement in both the internal resistance and ductility of the column. Wu and colleagues employed a methodology that featured the incorporation of glass fiber-reinforced polymer GFRP bars within the plastic hinge region, alongside the implementation of CFRP wraps. According to their findings, this retrofitting approach successfully postponed the deterioration of the concrete and averted the collapse of the longitudinal reinforcement. This led to an improvement in the flexibility and energy dispersion capability of the refurbished columns[25].

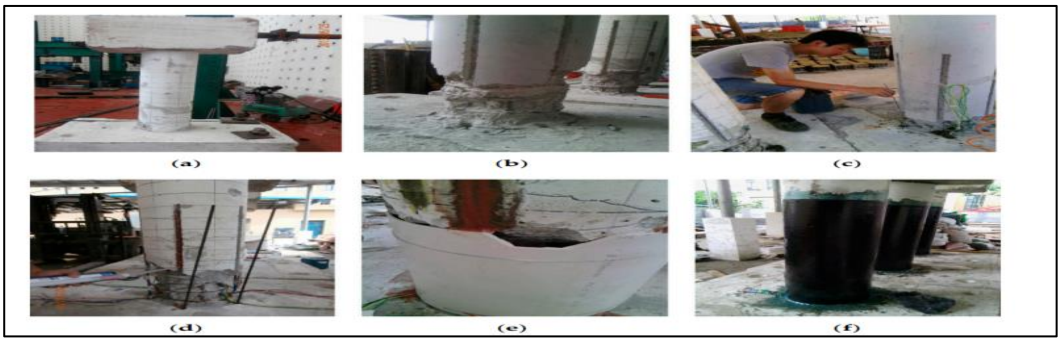

Figure 2.11 Installation stages of NSM bars and CFRP in plastic hinge[25]

2.2.4.3 FRP Sheet and Steel Jacketing

Li et al. conducted an assessment on the efficacy of using combined CFRP and steel jackets for enhancing the seismic response of RC columns suffering from abrasion damage. The results indicated that the application of the combined repairing was more successful in ameliorating the ductility and strength of the damaged columns in comparison to using the materials separately. Additionally, higher levels of reinforcement abrasion in damaged columns resulted in more noticeable improvements in strength augmentation than those with lower corrosion degrees. Notably, an increase in axial force significantly reduced the ductility of the strengthened columns; notwithstanding, the strengthening effect remained superior to that of lower axial load [26][27].

Recently, hybrid jacketing, consists of GFRP-wrapped groove steel pipe, was used to enhance the seismic performance of columns. This kind of groove tube permits to generation a ribbed face between the concrete and FRP. The feedbacks from the practical study appeared a significant growth the drift capacity of the columns with a increasing the number of GFRP layers. Furthermore, the failure changed from shear to flexure with an increase in GFRP layers. Moreover, energy dispersion and shear resistance were increased [26].

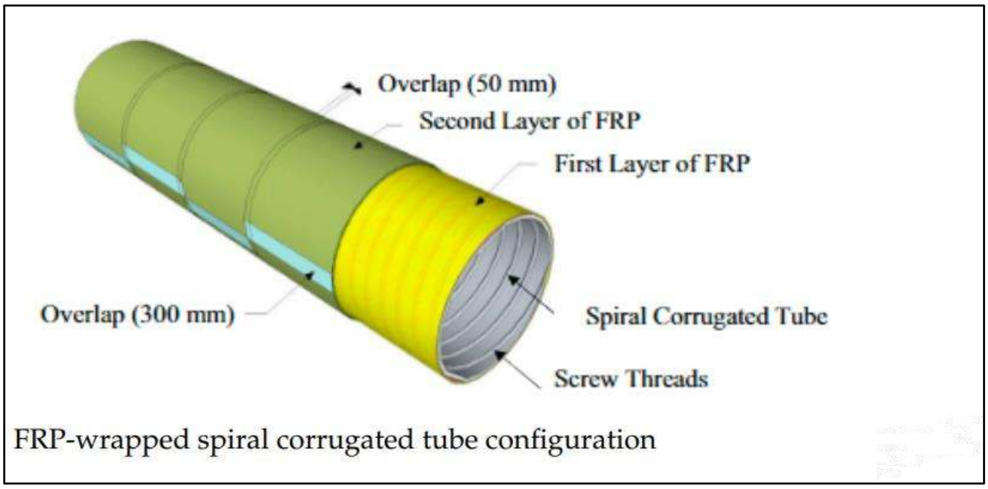

Figure 2.12 Strengthening by using GFRP and steel jacket [26]

2.2.4.4 High-Performance Materials with FRP Wrapping or FRP, Steel Rebars

In the past few years, after a large development in materials manufacturing, high performance materials simultaneously used, FRP and steel rebars, or FRP wrapping is a charming hybrid repair style. Ma and Li achieved study to enhance the seismic performance of reinforced concrete columns that exposed to moderately to severely damaged. The columns were reinforced with basalt fiber-reinforced polymer sheets and fast-treatment, early-strength cement mortar. The results indicated a noteworthy promoting in the energy dispersion and specimens' ductility. The flexural capacity of samples with moderate pre-damage was fully returned, whereas, for samples with severe pre-damage, only a limited return of the flexural capacity was observed. Initial stiffness of the strengthened specimens was not entirely returned[27], as shown in figure below.

Cho et al. referred to ability of (HPFRCC) high-performance fiber-reinforced cementitious composite sprayed mortar with steel rebars to increase the earthquake performance of Columns. In this way, the column cover was splined first, then longitudinal and transverse bars were put in the grooves. Finally, the column was improved by spraying HPFRC mortar. The outcome of the cyclic lateral loading tests carried out on the retrofitted columns was an effective technique to increase both the force and deformation capacities and reduce the bending and diagonal shear cracks [28].

Figure 2.13 Hybrid repair used high performance material and FRP wrapping [28]

2.2.4.5 Thin Cold-Formed Steel Plate and Prestressing Strands

The implementation of prestressing strands coupled with a cold-formed steel plate with small thickness presents a viable, and prompt and easy option to fix the damaged bridge piers. Fakharifar et al. used a hybrid jacket consist of a steel sheet (passive confinement) with fy = 680 MPa, elasticity modulus=207 GPa, and 7ϕ 12mm high-strength strands (active confinement) with maximum tensile strength =1937 MPa, E= 200 GPa. Which applied at 1220 mm.

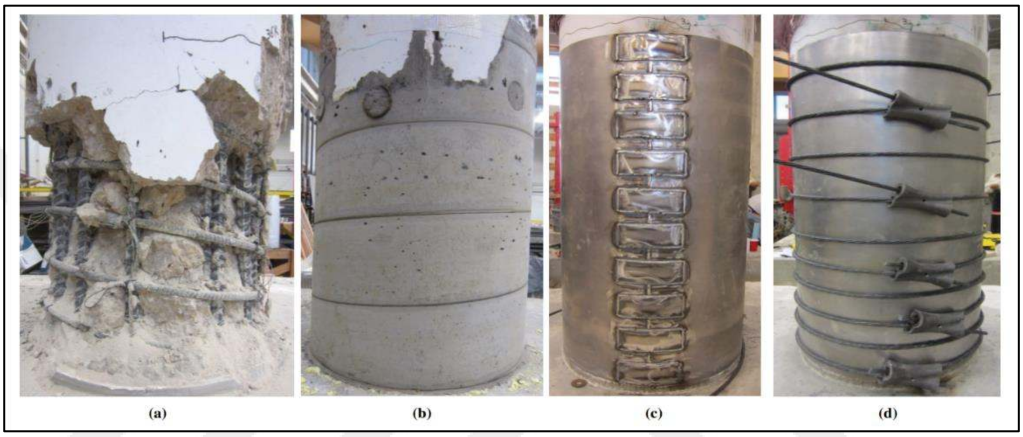

Figure 2.14 Strengthening by use sheet metal wrapping and prestress strands [28]

from the bottom of the damaged column. Its effective way to prevent lap splice defeat and enhance both the flexural behavior and ductility. In addition, it is lightweight and can be considered a viable repair technique for bridge piers in emergency situations. However, the initial stiffness is only partially returned due to spoilage in the concrete and reinforcement. Prestress wire is providing adequate shear transfer between the column and steel sheet, adhesive epoxy is unimportance [28]. The upper method needs heavy equipment to prestressing the wires, accurate work, and skilled workers, in addition to the high cost.

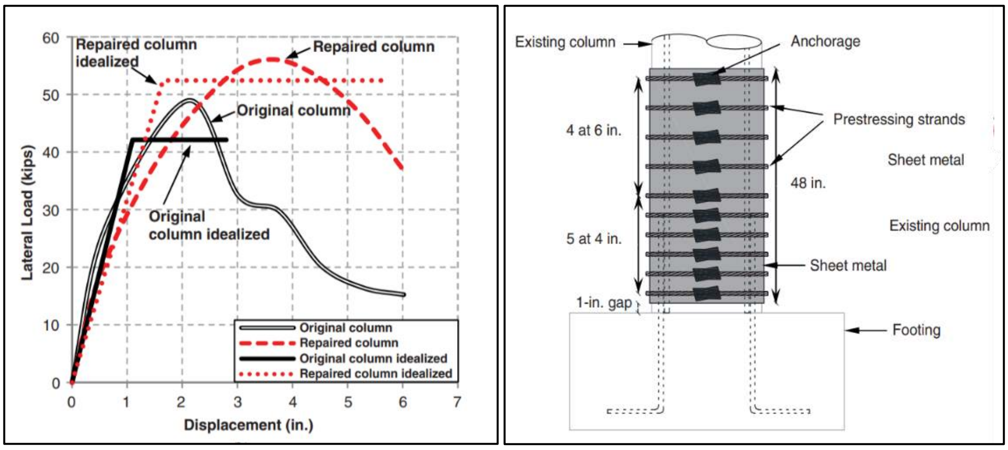

Figure 2.15 Column jacketing with metal and prestress strands details and load-displacement [28]

2.2.5 ECC Concrete Jacketing

As a result of the fact that the failure of the concrete is brittle, it causes a great weakness of the stiffness and shear resistance for concrete members, especially when exposed to seismic excitations, it has become necessary use substantial materials that improve the deficiency of concrete on these sides, such as ductility and energy dispersion, like ECC (Engineered cementitious composites). ECC jackets with (PVA) poly-vinyl-alcohol fiber, 39 µm, 12 mm diameter and length, respectively. It has a tensile strength = 1600 MPa. It used as a jacket to square and circle RC column with dimensions (80*80*400mm), and (90*400mm) for square and circular columns, respectively. The thickness of the ECC material was 20mm, and 22.5 mm for square, and circular column, one by one. ECC jacketing led to increase the strength by about 3.23 times for square columns, and 3.39 times for circular columns. By utilizing ECC as a jacketing, the capacity of columns to absorb energy is notably enhanced, with a significant increasing of around 4.9, and 4.3 for circular and square columns respectively [4]. The best height for ECC layer is determined as 0.8h, which corresponds to the vertical extent of the plastic hinge part of a reinforced concrete column [29].

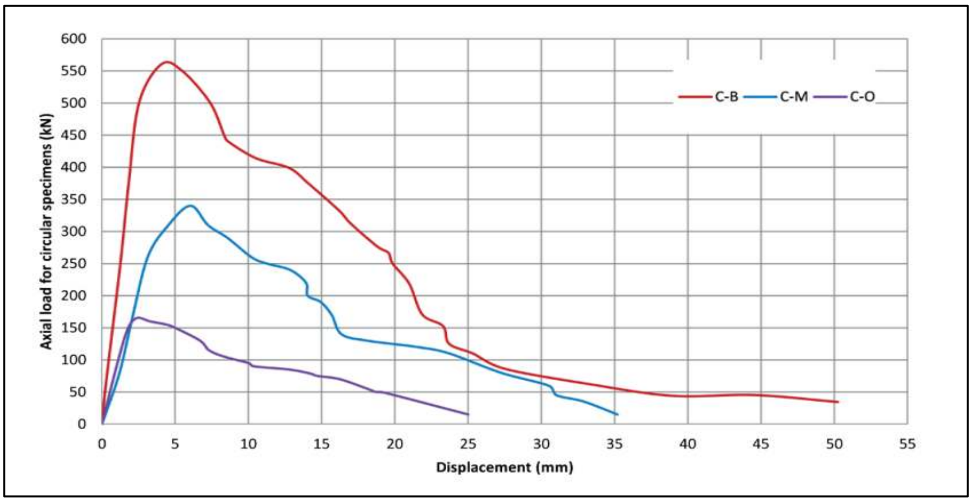

Figure 2.16 Load displacement of column strengthening by ECC layers [29]

2.3 Factors Influence on Strengthening Approach

There are a lot of factors that effect on choosing the proper methods of retrofitting, which is summarized as follows:

1- Cost and financial constraints.

2- Time schedule limitations (work owners' requirements).

3- restricted access to site and availability of primary materials and skilled labor.

4- importance of the project and Architectural limitations.

5- Virtual operation life of the structure (the lower strengthening must be done if the structure will be destroyed in a few years).

6- Original structural members characteristics.

7- Environmental factors and effects of climate [30].

2.4 Comparison between Various Strengthen Considerations

2.4.1 Comparison with Respect to Research

There are many characteristics related to different kinds of repair work and strengthening techniques. It's essentially dependent on what's the target of retrofit and the amount of structural member damages. Several authors focus on types of strengthening and another type needs deeper research, as figure up illustrate research quantity on the last two centuries [10].

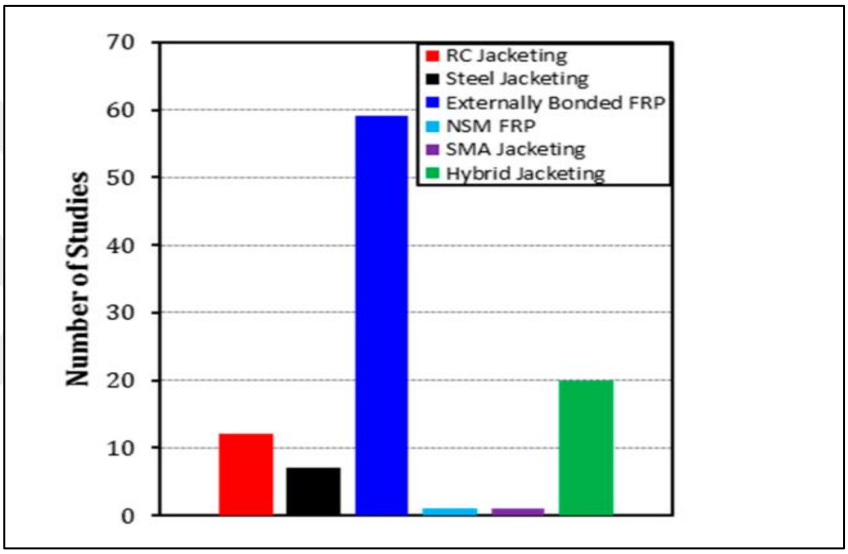

Figure 2.17 Strengthening studies during last two centuries [10]

2.4.2 Comparison with Respect to Performance

On the other hand, some practical studies deal with improving one characteristic or more of structural members, such as strength, ductility, and stiffness [10][12].

Table 2.1 Strength, ductility, and stiffness for different type of jacketing methods [10]

Strengthening Method	Strength and Ductility	Initial Stiffness
RC/Mortar Jacketing		
Concrete jacketing with end-welded stirrups and dowel placement. Shotcrete jacket with bent-down bars	Enhanced	Enhanced
RC jacketing and wing wall installation.	Enhanced	Enhanced
Addition of a single asymmetric concrete section using anchor rebars or high-strength bolts	Enhanced	Enhanced
Addition of a RC flange in the weak axis of the column	Enhanced	Enhanced
High-performance fiber-reinforced cementitious composite (HPFRCC) mortar	Enhanced	Not reported
Self-compacting ultra-high performance fiber-reinforced concrete	Enhanced	Same
Comparison of engineered cementitious composites (ECCs) and ferro-cement jacket	Same strength for both but more ductility with ECCs	Enhanced
Circular or square ferro-cement jackets with steel wire mesh	Improved ductility but no flexural strength improvement	Similar
Steel Jacketing		
Steel tube jacketing with concrete or grout fill	Enhanced	Not reported
Steel plate to flexural faces	Enhanced	Enhanced
Jacketing with steel tube	Enhanced	Not reported
Wrapping with steel jacket	Strength the same, ductility enhanced	Lower
Jacketing with steel angle collars	Enhanced	Not reported
Jacketing with post-compressed steel plates	Enhanced	Enhanced
Externally-bonded Fiber-reinforced polymer (FRP) Jacketing		
Carbon fiber-reinforced polymer (CFRP) wrapping in plastic hinge region	Enhanced	Not reported
Discontinuous CFRP wrapping in strips	Enhanced	Not reported
CFRP jacket confinement in inelastic hinge region	Insignificant increase in strength and considerable increase in ductility	Insignificant increase

2.4.3 Comparison with Respect to Cost

The financial outlays necessary to enhance the structural integrity of a single column utilizing each distinct technique were evaluated and contrasted in Figure below. It was observed that the utilization of the carbon fiber reinforced polymer (CFRP) wrapping method incurred the greatest expenses in comparison to the other techniques. Conversely, the application of steel fibers in circular columns was determined to be the most economical choice of reinforcing columns [12].

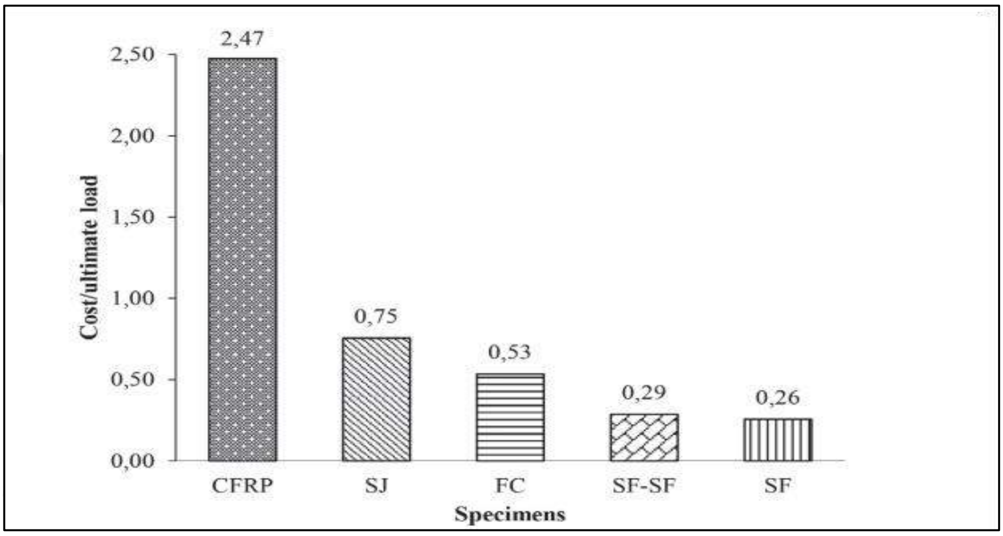

Figure 2.18 Cost to peak load ratio for different kinds of jacketing methods [12]

Where:

CFRP: Carbon fiber reinforced polymer.

SJ: steel jacket.

FC: Ferrocement Confinement.

SF-SF: steel fibers and silica fume.

SF: circular columns having steel fibers.

The difference between a higher and lower one reaches to 89.5% by cost.

CHAPTER 3

THEORETICAL ASPECTS

3.1 Introduction

In order to carefully predict the overall behavior of reinforced concrete elements, the stress-strain relationship of concrete plays a crucial role. Given the wide variety of concrete types used in construction applications, it is essential that the models used to forecast their behavior possess high adaptability. The stress-strain models for unconfined and confined concretes that are now in use have limited application domains, which are defined by the parametric nature of the experimental data taken into account in their creation, according to a thorough review of the existing literature. Additionally, it is noted in earlier evaluations that a comprehensive model that is relevant to all varieties of concrete has not yet been developed[31]. Michal and W. Andrzej[32],The implementation of ABAQUS software provides a valuable path for the simulation and analysis of reinforced concrete structures. This study utilizes the election concrete damaged plasticity model (CDP) that is accessible within the software. Accurate and reliable results within the CDP model are depending on determination of crucial parameters, including the dilation angle, viscosity parameter, Poisson's ratio, and modulus of elasticity. However, the most important matters are stress strain behavior in compression and tension from test results to satisfy accurate results. Unfortunately, A. Christopher. Lynn [7] models adopt in this study didn’t present actual stress-strain relationship, so it was became necessary to generate a relevant constitutive models corresponding to materials properties for CDP ABAQUS requirements.

3.2 Concrete Damage Plasticity Theory Concepts

The nonlinearity behavior of concrete structures can be express by damage, plasticity, fracture energy, and so on, but they aren’t able to represent a carful manner of concrete alone. The pare damage and plasticity theories give an accurate results of nonlinear behavior[33].

The origins of concrete damage plasticity (CDP) can be traced back to the early 1970s, when Lubliner et al.[34] initially introduced it as a fundamental model for concrete. The CDP model is founded upon the integration of two theoretical frameworks, namely plasticity theory and damage mechanics. Damage mechanics deals with the degradation of a material's stiffness and strength as a result of damage, whereas plasticity theory refers to the phenomenon of permanent deformation that a material exhibits when subjected to external forces. Lee and Fenves[34] have evolved and constructed the constitutive relationships for a novel plastic-damage model that incorporates principles from plasticity and continuous damage dynamics.

The utilization of the fracture-energy-based several-hardening parameters is employed for occurrences of tensile and compressive damage. The proper simulation of stiffness loss and recovery resulting from the opening and closing of cracks is achieved separately. Also, it demonstrates proficient management of dilatancy, crucial aspect in the simulation of concrete buildings subjected to multiaxial loading, cyclic loading, and monotonic loading. Li Qingfu et al.[34] showed that the concrete damage plasticity model (CDP model) posits that the concrete material exhibits continuity, isotropy, and uniformity. It also claims that the elastic modulus of concrete diminishes with inelastic strain. under cyclic loading and reduce stuffiness, and it can be partially recalled. To regulate this, a stiffness recovery coefficient, denoted as w, is defined for this purpose. The behavior of concrete under uniaxial cyclic loading exhibits distinct differences in terms of stiffness decrease and restoration between tensile and compressive loading conditions.

$E = (1\text{-}d)\ E_O$

$(1\text{-}d) = (1\text{-}s_t\ d_c)\ (1\text{-}\ s_c\ d_t)$

Where dc, dt: damage parameter in compression and tension and sc, st: stiffness recovery factors in compression and tension, E_O = initial modules of elasticity.

3.3 Finite Element Constitutive Models

The concrete damage plasticity used in the ABAQUS software is applicable for brittle materials such as rocks and concrete[34][35]. This model is capable of simulating the occurrence of tension fracturing and compression crush in concrete. It takes into account the isotropic elastic damage and plastic behavior shown by these materials. Generally, the total strain consists of elastic and plastic part respectively:

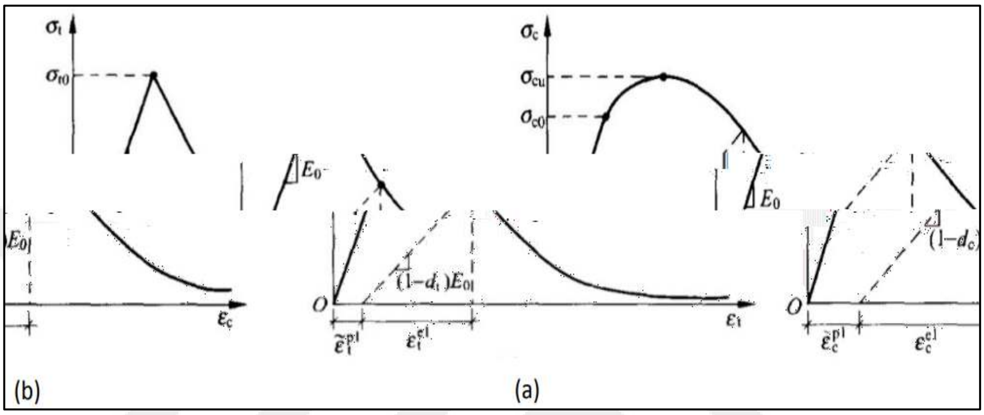

Figure 3.1 Plastic-damage behavior of compression and tension [4][5]

$$\varepsilon_t = \varepsilon^{el} + \varepsilon^{pl}$$

To implement FEM nonlinear analysis in ABAQUS, the stress-strain behavior of concrete in compression and tension must be available from laboratory tests, but this often does not exist. Many fundamental models depend on the internal principle, fracture concept, damage mechanism, viscous-plastic principle, linear elastic approach, nonlinear elastic method, Nevertheless, owing to the complicated characteristics of concrete materials, a universally accepted fundamental model for concrete remains hard to get. In the plastic damage approach, it is suggested that the primary mechanism responsible for the deterioration of concrete material is predominantly attributed to the occurrence of tension cracking and compressive crushing[36]. This study, which adopt on four experimental specimens achieved by Lynn[7], who didn't list actual stress-strain behavior, had to complete the constitutive model in compression and tension. For accurate results, it is crucial to utilize proper constitutive models that can simulate the behavior of materials in practice[37].

3.3.1 CDP for Concrete Compression Behavior

The existing stress-strain models commonly utilize the foundational equations initially proposed by Popovics[38] or Sargin et al.[39], the latter find coefficients in the essential equation by empirical methods. Several models consist of independent nonlinear equations that define the ascending and descending branches. However, these models reveal slightly varying properties, especially for the lower portion of the curve. This study was base on Keun, Yang, et al.[40] to generate a stress-strain curve in compressive, where stipulates on a straightforward and logical stress-strain model for unconfined concretes under compression is developed. This model will cover an extensive range of compressive values between 10 and 180 MPa. Using a regression approach, the modulus of elasticity, the strain at maximum stress, and the strain at 50% of the maximum stress on the branch downward were calculated. Then, create nonlinear formulas, mathematical and statistical studies were carried out. Comparisons with actual stress-strain curves taken from 100 specimens with various compressive strengths and densities helped to demonstrate the validity of the created model as follows, where the data was obtained from the real experimental tests by Lynn's models

Table 3.1 Properties of experimental specimens [7]

Specimen	fc` (MPa)	Young's modulus (MPa)
2CLH18	33	25650
3CLH18	26.89	23718
2CMH18	27.65	23994
3CMH18	25.74	23580

$E_C=A(fc`)^a(w_c/w_o)^b$ MPa.

where, w_o=2300kg/m^3 (A, a and b) are constant equal to (8470,1/3,1.17) respectively, from concrete test results of regression analysis exact values of compression strength ranges of (8.4 to 170) MPa and concrete unit weight ranges of 1200 to 4500 kg/m^3.

$\varepsilon`_C = 0.0016 \exp[240(f_c'/E_C)]$

$\varepsilon`_{C0.5} = 0.0035 \exp [1.2\{(f_0/fc') (w_C/w_0)\}1.75]$

Subsequently, utilizing the analytically derived outcomes, a statistical evaluation was conducted to ascertain the descending and ascending branches shown in the figure below

$\beta_1 = 0.2*\exp (0.73\xi)$ for $\varepsilon_c \leq \varepsilon`_c$

$\beta_1 = 0.41*\exp (0.77\xi)$ for $\varepsilon_c > \varepsilon`_c$

$\xi = (fc'/f_0)0.67\ (w_0/w_c)1.17$ where the standard value for f_0 and w_0 are 10 MPa and 2300 kg/m3, accordingly. Finally, the stress-strain behavior at any compression strain εc calculated based on[40]:

$$fc = fc` \left[\frac{(\beta_1 + 1)\left[\frac{\varepsilon_c}{\varepsilon_0}\right]}{\beta_1 + \left[\frac{\varepsilon_c}{\varepsilon_0}\right]^{(\beta 1+1)}} \right]$$

Table 3.2 Stress-strain constitutive model of 2CLH18

fc (MPa)	**ε**	**fc (MPa)**	**ε**	**fc (MPa)**	**ε**
0	0	32.21232217	0.00175	21.25218193	0.00392880
1.502515409	0.00005	32.39884215	0.0018	20.85943524	0.003978803
3.000561617	0.0001	32.55710047	0.00185	20.47242165	0.004028803
4.489629148	0.00015	32.68864763	0.0019	20.09133286	0.004078803
5.965260179	0.0002	32.79499528	0.00195	19.7163279	0.004128803
7.423107405	0.00025	32.87761163	0.002	19.34753588	0.004178803
8.858982487	0.0003	32.93791788	0.00205	18.98505857	0.004228803
10.26889853	0.00035	32.97728544	0.0021	18.62897282	0.004278803
11.64910721	0.0004	32.99703392	0.00215	18.27933291	0.004328803
12.99613047	0.00045	**33**	**0.00217**	17.93617267	0.004378803
14.30678658	0.0005	31.32281183	0.002678803	17.59950743	0.004428803
15.57820	0.00055	31.00965	0.002728803	17.26933594	0.004478803
16.8078	0.0006	30.67789568	0.002778803	16.94564207	0.004528803

Table 3.2 (continue) Stress-strain constitutive model of 2CLH18

17.99356662	0.00065	30.32941101	0.002828803	16.62839638	0.004578803
19.13345491	0.0007	29.96600237	0.002878803	16.31755762	0.004628803
20.22602496	0.00075	29.58940641	0.002928803	16.01307406	0.004678803
21.27010393	0.0008	29.20128547	0.002978803	15.71488474	0.004728803
22.26484402	0.00085	28.80322304	0.003028803	15.42292064	0.004778803
23.20970838	0.0009	28.39672048	0.003078803	15.13710567	0.004828803
24.10445408	0.00095	27.98319494	0.003128803	14.85735767	0.004878803
24.94911267	0.001	27.56397822	0.003178803	14.58358925	0.004928803
25.74396899	0.00105	27.14031669	0.003228803	14.3157086	0.004978803
26.48953874	0.0011	26.7133719	0.003278803	14.0536202	0.005028803
27.18654529	0.00115	26.28422191	0.003328803	13.79722547	0.005078803
27.8358964	0.0012	25.85386324	0.003378803	13.54642336	0.005128803
28.43866099	0.00125	25.42321328	0.003428803	13.30111089	0.005178803
28.99604652	0.0013	24.99311304	0.003478803	13.06118361	0.005228803
29.50937722	0.00135	24.56433029	0.003528803	12.82653604	0.005278803
29.98007334	0.0014	24.13756283	0.003578803	12.59706208	0.005328803
30.40963175	0.00145	23.71344201	0.003628803	11.728	0.00552
30.79960781	0.0015	23.29253629	0.003678803	10.747	0.00577
31.1515988	0.00155	22.87535484	0.003728803	9.869	0.0061
31.46722883	0.0016	22.46235118	0.003778803	8.655	0.0064
31.74813528	0.00165	22.05392674	0.003828803	7.3942	0.00692
31.99595669	0.0017	21.6504344	0.003878803	6.6583	0.00717

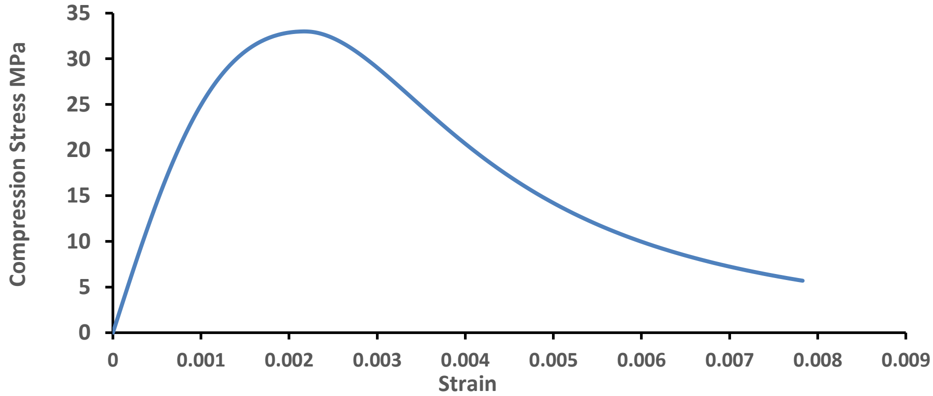

Figure 3.2 Compression stress-strain curve of 2CLH18

Table 3.3 Stress-strain constitutive model of 3CLH18

fc (MPa)	ε	fc (MPa)	ε	fc (MPa)	ε
0	0	26.52121	0.00175	21.18485	0.00345
1.414789	0.00005	26.62586	0.0018	20.89347	0.0035
2.82009	0.0001	26.71114	0.00185	20.60311	0.00355
4.208596	0.00015	26.77835	0.0019	20.31415	0.0036
5.573991	0.0002	26.82871	0.00195	20.0269	0.00365
6.910708	0.00025	26.86338	0.002	19.74165	0.0037
8.213863	0.0003	26.88347	0.00205	19.45866	0.00375
9.479217	0.00035	**26.89**	**0.0021**	19.17817	0.0038
10.70316	0.0004	26.89	0.002100343	18.90038	0.00385
11.88268	0.00045	26.87633	0.00215	18.62548	0.0039
13.01534	0.0005	26.83628	0.0022	18.35361	0.00395
14.09927	0.00055	26.77134	0.00225	18.08493	0.004
15.13309	0.0006	26.68301	0.0023	17.81956	0.00405
16.11593	0.00065	26.57277	0.00235	17.5576	0.0041
17.04732	0.0007	26.44211	0.0024	17.29913	0.00415
17.92721	0.00075	26.29249	0.00245	17.04423	0.0042
18.7559	0.0008	26.12535	0.0025	16.79295	0.00425
19.53399	0.00085	25.94209	0.00255	16.54536	0.0043
20.26238	0.0009	25.74408	0.0026	16.30147	0.00435
20.94215	0.00095	25.53263	0.00265	16.06132	0.0044
21.57462	0.001	25.309	0.0027	15.82492	0.00445
22.16123	0.00105	25.07442	0.00275	15.59229	0.0045
22.70357	0.0011	24.83003	0.0028	15.36341	0.00455
23.2033	0.00115	24.57695	0.00285	15.13828	0.0046
23.66217	0.0012	24.31621	0.0029	14.9169	0.00465
24.08197	0.00125	24.04881	0.00295	14.69923	0.0047
24.4645	0.0013	23.77566	0.003	14.48527	0.00475
24.81157	0.00135	23.49764	0.00305	14.27497	0.0048
25.12499	0.0014	23.21557	0.0031	14.06831	0.00485
25.40654	0.00145	22.9302	0.00315	13.86526	0.0049
25.65798	0.0015	22.64224	0.0032	12.3654	0.0053
25.881	0.00155	22.35235	0.00325	11.2209	0.00565

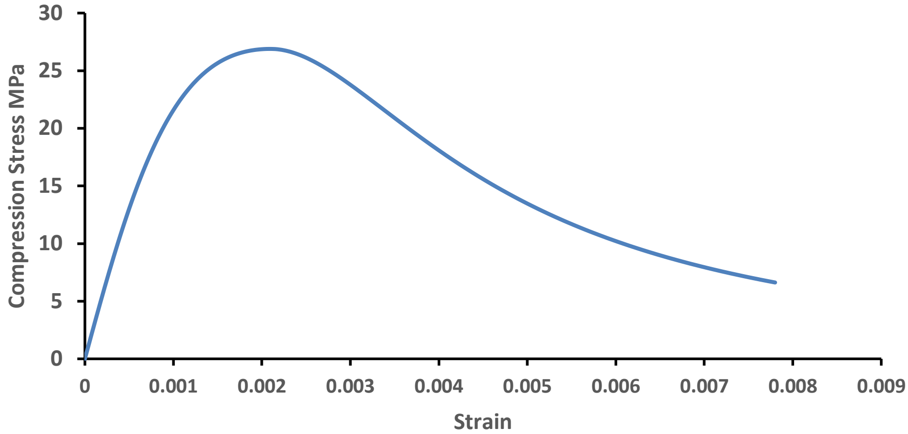

Figure 3.3 Compression stress-strain curve of 3CLH18

Table 3.4 Stress-strain constitutive model of 2CMH18

fc (MPa)	ε	fc (MPa)	ε	fc (MPa)	ε
0	0	27.24203	0.00175	21.64056	0.00346
1.427583	0.00005	27.35512	0.0018	21.33392	0.00351
2.846471	0.0001	27.44782	0.00185	21.02845	0.00356
4.249734	0.00015	27.52145	0.0019	20.72455	0.00361
5.631272	0.0002	27.57729	0.00195	20.42254	0.00366
6.98564	0.00025	27.61653	0.002	20.12274	0.00371
8.307993	0.0003	27.64033	0.00205	19.82543	0.00376
9.594071	0.00035	27.64975	0.0021	19.53084	0.00381
10.84019	0.0004	**27.65**	**0.00211**	19.23919	0.00386
12.04322	0.00045	27.63566	0.00216	18.95069	0.00391
13.20058	0.0005	27.59364	0.00221	18.66549	0.00396
14.31022	0.00055	27.52546	0.00226	18.38375	0.00401
15.37058	0.0006	27.43265	0.00231	18.10559	0.00406
16.38057	0.00065	27.31677	0.00236	17.83112	0.00411
17.33954	0.0007	27.17936	0.00241	17.56042	0.00416
18.24722	0.00075	27.02194	0.00246	17.29358	0.00421
19.10372	0.0008	26.84603	0.00251	17.03066	0.00426
19.90945	0.00085	26.65308	0.00256	16.77169	0.00431
20.66513	0.0009	26.44453	0.00261	16.51672	0.00436
21.3717	0.00095	26.22177	0.00266	16.26577	0.00441
22.03032	0.001	25.98614	0.00271	16.01885	0.00446
22.6423	0.00105	25.73892	0.00276	15.77597	0.00451

Table 3.4 (continue) Stress-strain constitutive model of 2CMH18

23.20913	0.0011	25.48134	0.00281	15.53713	0.00456
23.73239	0.00115	25.21457	0.00286	15.30232	0.00461
24.21372	0.0012	24.93972	0.00291	15.07151	0.00466
24.65487	0.00125	24.65783	0.00296	14.84469	0.00471
25.05759	0.0013	24.36989	0.00301	14.62182	0.00476
25.42367	0.00135	24.07684	0.00306	14.40288	0.00481
25.75488	0.0014	23.77953	0.00311	14.18783	0.00486
26.053	0.00145	23.47879	0.00316	13.97663	0.00491
26.31979	0.0015	23.17536	0.00321	12.419	0.00531
26.55694	0.00155	22.86994	0.00326	11.5585	0.00556
26.76615	0.0016	22.56317	0.00331	10.3383	0.00596
26.94903	0.00165	22.25567	0.00336	9.16676	0.00641
27.10715	0.0017	21.94796	0.00341	8.5948	0.0066

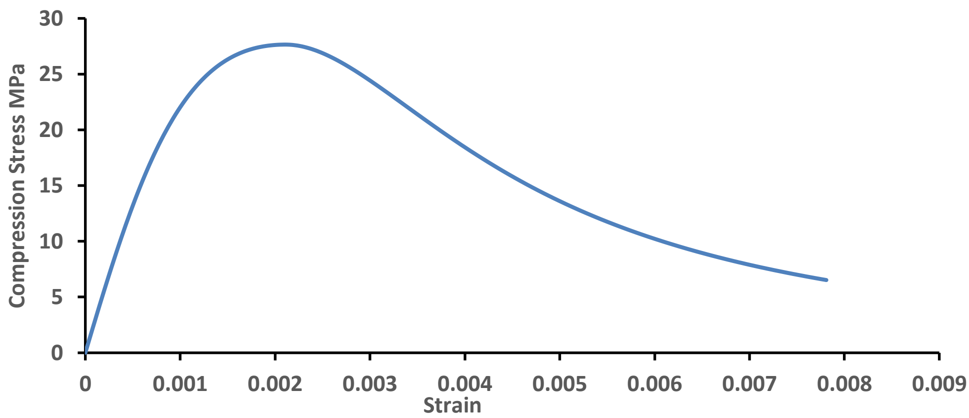

Figure 3.4 Compression stress-strain curve of 2CMH18

Table 3.5 Stress-strain constitutive model of 3CMH18

fc (MPa)	ε	fc (MPa)	ε	fc (MPa)	ε	fc (MPa)	ε
0	0	25.43675	0.00175	20.18248	0.00348	12.38306	0.00523
1.398962	0.00005	25.52756	0.0018	19.91336	0.00353	12.21704	0.00528
2.787029	0.0001	25.60055	0.00185	19.64544	0.00358	12.05392	0.00533
4.156249	0.00015	25.65696	0.0019	19.37902	0.00363	11.89366	0.00538
5.49993	0.0002	25.69795	0.00195	19.11436	0.00368	11.73622	0.00543
6.812305	0.00025	25.7246	0.002	18.8517	0.00373	11.58155	0.00548
8.08842	0.0003	25.73796	0.00205	18.59125	0.00378	11.4296	0.00553

Table 3.5 (continue) Stress-strain constitutive model of 3CMH18

9.324079	0.00035	**25.74**	**0.00208**	18.3332	0.00383	11.28032	0.00558
10.5158	0.0004	25.72722	0.00213	18.07771	0.00388	11.13367	0.00563
11.66076	0.00045	25.68982	0.00218	17.82494	0.00393	10.98961	0.00568
12.75679	0.0005	25.62923	0.00223	17.57501	0.00398	10.84808	0.00573
13.8023	0.00055	25.5469	0.00228	17.32803	0.00403	10.70904	0.00578
14.79625	0.0006	25.44424	0.00233	17.0841	0.00408	10.57245	0.00583
15.73806	0.00065	25.32267	0.00238	16.8433	0.00413	10.43825	0.00588
16.62763	0.0007	25.18357	0.00243	16.6057	0.00418	10.30641	0.00593
17.46524	0.00075	25.02829	0.00248	16.37136	0.00423	10.17687	0.00598
18.25149	0.0008	24.85814	0.00253	16.14032	0.00428	10.0496	0.00603
18.98731	0.00085	24.6744	0.00258	15.91261	0.00433	9.924551	0.00608
19.67386	0.0009	24.47829	0.00263	15.68827	0.00438	9.801678	0.00613
20.31248	0.00095	24.27098	0.00268	15.46731	0.00443	9.680941	0.00618
20.90472	0.001	24.0536	0.00273	15.24974	0.00448	9.562297	0.00623
21.45223	0.00105	23.82721	0.00278	15.03555	0.00453	9.445705	0.00628
21.95676	0.0011	23.59283	0.00283	14.82476	0.00458	9.331125	0.00633
22.42012	0.00115	23.35141	0.00288	14.61735	0.00463	9.218516	0.00638
22.84419	0.0012	23.10386	0.00293	14.4133	0.00468	9.107841	0.00643
23.23084	0.00125	22.85103	0.00298	14.2126	0.00473	8.999059	0.00648
23.58195	0.0013	22.59371	0.00303	14.01522	0.00478	8.892134	0.00653
23.89939	0.00135	22.33265	0.00308	13.82113	0.00483	8.787028	0.00658
24.18498	0.0014	22.06853	0.00313	13.63032	0.00488	8.683704	0.00663
24.44054	0.00145	21.80199	0.00318	13.44273	0.00493	8.582127	0.00668
24.6678	0.0015	21.53365	0.00323	13.25835	0.00498	8.482262	0.00673
24.86847	0.00155	21.26404	0.00328	13.07713	0.00503	8.384075	0.00678
25.04416	0.0016	20.99367	0.00333	12.89903	0.00508	8.287531	0.00683

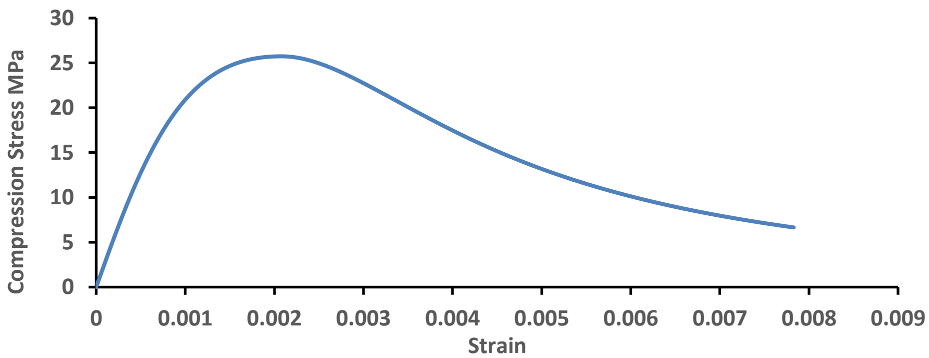

Figure 3.5 Compression stress-strain curve of 3CMH18

3.3.2 Damage Plasticity Requirements of Compression

For employing FEM simulation by ABAQUS needs to present concrete damage plasticity requirements as yield stress, inelastic strain, dc, and damage parameter in compression, which consider a key role in calculate hardening plastic strain $\boldsymbol{\varepsilon}_p$, Lubliner et al.[34] equations based to calculate hardening plastic strain, inelastic strain and corresponding damage parameter in softening behavior as the following:

$$\varepsilon_c^{in} = \varepsilon_c - \frac{\sigma_c}{Eo}$$

$$dc = 1 - \frac{\sigma_c}{\sigma_{cu}}$$

$$\sigma_{c=(1-dc)Eo\left(\varepsilon_c - \varepsilon_c^{pl}\right)}$$

$$\varepsilon_c^{pl} = \varepsilon_c - \frac{\sigma_c}{E_O}\left(\frac{1}{1-dc}\right)$$

$$\varepsilon_c^{pl} = \varepsilon_c^{in} - \frac{dc}{1-dc}\frac{\sigma_c}{E_o}$$

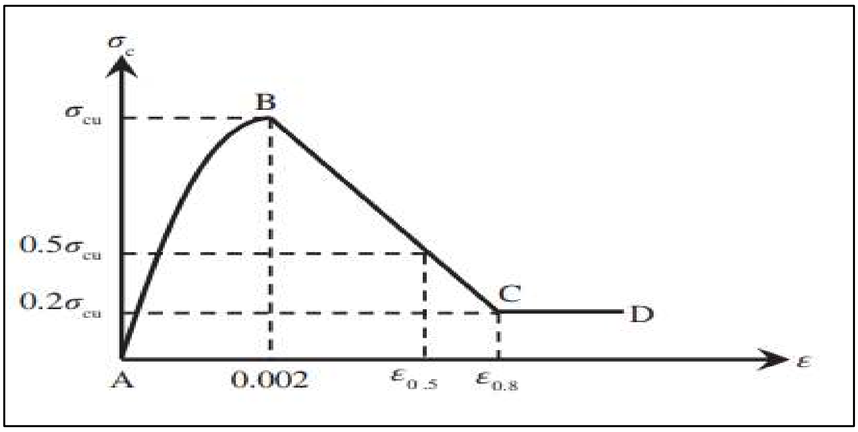

Figure 3.6 Compression damage behavior [11]

Where: σ_c, ε_c, ε_c^{pl}, ε_c^{in}, compression stress corresponding to total concert strain, hardening plastic strain, inelastic strain respectively. σ_{cu}, E_o, d_c, ultimate compression strength, initial modulus of elasticity and compression damage parameter in softening branch sequentially. Kent et.al. and Hognstad [41][42] presented a parabola basic model for unconfined concrete, as illustrated by the subsequent formula. The compression stresses calculated by this equation were so closely related to above Lubliners formula that this study is based on, but the former simplifies softening branch as a straight line

$$\sigma c = \sigma cu \left[2\left(\frac{\varepsilon c}{\varepsilon' c}\right) - \left(\frac{\varepsilon c}{\varepsilon' c}\right)^2 \right]$$

Park[43] presented ε'_C concrete strain corresponding to maximum compression strength =0.002, ε'_c= 2 σ_{CU}/E_O. It is considered so near from ε'_C calculated from equation, which is adopt in this study, which Hognestad strain a little bit more because of the increase in modulus of elasticity.

Table 3.6 FEM damage-plasticity parameters of 2CLH18

Yield stress	**Inelastic strain**	**Damage parameter dc**	**Yield stress**	**Inelastic strain**	**Damage parameter dc**	**Yield stress**	**Inelastic strain**	**Damage parameter dc**
24.94911	2.73E-05	0	29.966	0.001711	0.091939	16.6284	0.003931	0.532639
25.74397	4.63E-05	0	29.58941	0.001775	0.103351	16.31756	0.003993	0.5413
26.48954	6.73E-05	0	29.20129	0.00184	0.115113	16.01307	0.004055	0.549777
27.18655	9.01E-05	0	28.80322	0.001906	0.127175	15.71488	0.004116	0.558073
27.8359	0.000115	0	28.39672	0.001972	0.139493	15.42292	0.004178	0.566191
28.43866	0.000141	0	27.98319	0.002038	0.152024	15.13711	0.004239	0.574133
28.99605	0.00017	0	27.56398	0.002104	0.164728	14.85736	0.0043	0.581902
29.50938	0.0002	0	27.14032	0.002171	0.177566	14.58359	0.00436	0.589502
29.98007	0.000231	0	26.71337	0.002237	0.190504	14.31571	0.004421	0.596936
30.40963	0.000264	0	26.28422	0.002304	0.203508	14.05362	0.004481	0.604207
30.79961	0.000299	0	25.85386	0.002371	0.21655	13.79723	0.004541	0.611317
31.1516	0.000336	0	25.42321	0.002438	0.2296	13.54642	0.004601	0.618271
31.46723	0.000373	0	24.99311	0.002504	0.242633	13.30111	0.00466	0.625071
31.74814	0.000412	0	24.56433	0.002571	0.255626	13.06118	0.00472	0.631721
31.99596	0.000453	0	24.13756	0.002638	0.268559	12.82654	0.004779	0.638224
32.21232	0.000494	0	23.71344	0.002704	0.281411	12.59706	0.004838	0.644583
32.39884	0.000537	0	23.29254	0.002771	0.294166	12.37266	0.004896	0.650801
32.5571	0.000581	0	22.87535	0.002837	0.306807	12.15321	0.004955	0.656881
32.68865	0.000626	0	22.46235	0.002903	0.319323	11.93862	0.005013	0.662827
32.795	0.000671	0	22.05393	0.002969	0.331699	11.72878	0.005072	0.668642
32.87761	0.000718	0	21.65043	0.003035	0.343926	11.52358	0.00513	0.674328
32.93792	0.000766	0	21.25218	0.0031	0.355994	11.32292	0.005187	0.679889

Table 3.6 (continue) FEM damage-plasticity parameters of 2CLH18

32.97729	0.000814	0	20.85944	0.003166	0.367896	11.1267	0.005245	0.685328
32.99703	0.000864	0	20.47242	0.003231	0.379624	10.93481	0.005302	0.690647
33	**0.00089**	**0**	20.09133	0.003296	0.391172	10.74716	0.00536	0.69585
32.9805	0.000943	0.000591	19.71633	0.00336	0.402536	10.56365	0.005417	0.700938
32.9231	0.000995	0.00233	19.34754	0.003425	0.413711	10.38418	0.005474	0.705916
32.82954	0.001049	0.005165	18.98506	0.003489	0.424695	10.20865	0.005531	0.710785
32.70166	0.001104	0.009041	18.62897	0.003553	0.435486	10.03697	0.005587	0.715548
32.54136	0.00116	0.013898	18.27933	0.003616	0.446081	9.869042	0.005644	0.720208
32.35059	0.001218	0.019679	17.93617	0.00368	0.45648	8.5124	0.00614	0.7420
32.13134	0.001276	0.026323	17.59951	0.003743	0.466682	5.463	0.00776	0.8344
31.88563	0.001336	0.033769	17.26934	0.003806	0.476687	5.31716	0.00787	0.8388
31.61546	0.001396	0.041956	16.94564	0.003868	0.486496	3.74249	0.009333	0.886591
30.6779	0.001583	0.070367	16.01307	0.004055	0.115113	3.614455	0.009488	0.890471
30.32941	0.001646	0.080927	15.71488	0.004116	0.127175	3.4243	0.00955	0.9015

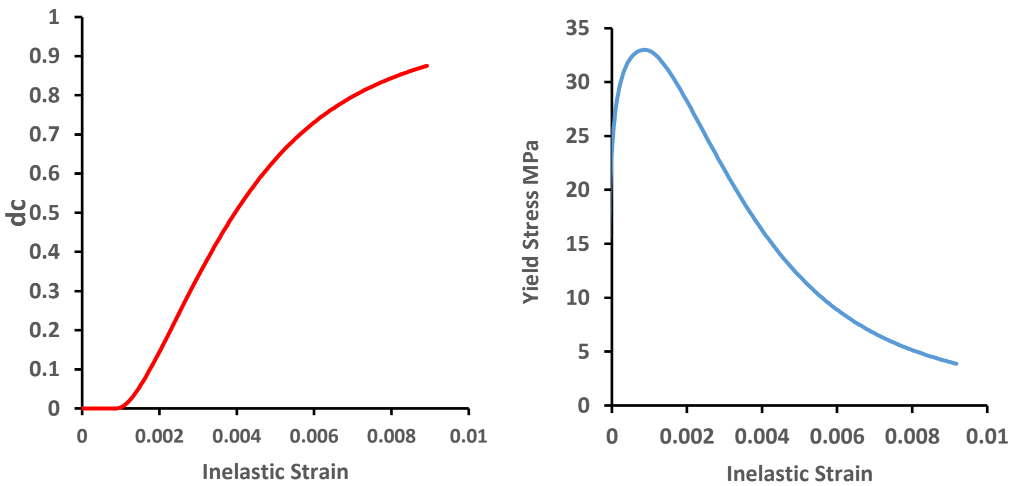

Figure 3.7 Inelastic strain-yield stress and damage in compression of 2CLH18

Table 3.7 FEM damage-plasticity parameters of 3CLH18

Yield stress	Inelastic strain	Damage parameter dc	Yield stress	Inelastic strain	Damage parameter dc	Yield stress	Inelastic strain	Damage parameter dc
19.534	2.6E-05	0	25.309	0.00163	0.058795	15.138	0.00396	0.437029
20.262	4.6E-05	0	25.074	0.00169	0.067519	14.917	0.00402	0.445262
20.942	6.7E-05	0	24.83	0.00175	0.076607	14.699	0.00408	0.453357
21.575	9E-05	0	24.577	0.00181	0.086019	14.485	0.00414	0.461314
22.161	0.00012	0	24.316	0.00188	0.095715	14.275	0.0042	0.469135
22.704	0.00014	0	24.049	0.00194	0.10566	14.068	0.00426	0.47682

Table 3.7 (continue) FEM damage-plasticity parameters of 3CLH18

23.203	0.00017	0	23.776	0.002	0.115818	13.865	0.00432	0.484371
23.662	0.0002	0	23.498	0.00206	0.126157	13.666	0.00437	0.49179
24.082	0.00023	0	23.216	0.00212	0.136647	13.47	0.00443	0.499078
24.464	0.00027	0	22.93	0.00218	0.147259	13.277	0.00449	0.506237
24.812	0.0003	0	22.642	0.00225	0.157968	13.088	0.00455	0.513267
25.125	0.00034	0	22.352	0.00231	0.168749	12.903	0.00461	0.520172
25.407	0.00038	0	22.061	0.00237	0.179579	12.72	0.00466	0.526953
25.658	0.00042	0	21.769	0.00243	0.190438	12.541	0.00472	0.533612
25.881	0.00046	0	21.477	0.00249	0.201306	12.365	0.00478	0.54015
26.077	0.0005	0	21.185	0.00256	0.212166	12.193	0.00484	0.54657
26.248	0.00054	0	20.893	0.00262	0.223002	12.023	0.00489	0.552873
26.396	0.00059	0	20.603	0.00268	0.2338	11.857	0.00495	0.559062
26.521	0.00063	0	20.314	0.00274	0.244546	11.693	0.00501	0.565138
26.626	0.00068	0	20.027	0.00281	0.255229	11.533	0.00506	0.571104
26.711	0.00072	0	19.742	0.00287	0.265837	11.376	0.00512	0.576961
26.778	0.00077	0	19.459	0.00293	0.276361	11.221	0.00518	0.582711
26.829	0.00082	0	19.178	0.00299	0.286792	11.069	0.00523	0.588357
26.863	0.00087	0	18.9	0.00305	0.297122	10.92	0.00529	0.5939
26.883	0.00092	0	18.625	0.00312	0.307346	10.774	0.00535	0.599342
26.89	0.00097	0	18.354	0.00318	0.317456	10.63	0.0054	0.604685
26.89	**0.001**	**0**	18.085	0.00324	0.327448	10.489	0.00546	0.609931
26.876	0.00102	0.000509	17.82	0.0033	0.337316	10.35	0.00551	0.615083
26.836	0.00107	0.001998	17.558	0.00336	0.347059	10.214	0.00557	0.620141
26.771	0.00112	0.004413	17.299	0.00342	0.356671	10.081	0.00563	0.625108
26.683	0.00118	0.007698	17.044	0.00348	0.36615	9.9497	0.00568	0.629985
26.573	0.00123	0.011797	16.793	0.00354	0.375494	9.8209	0.00574	0.634774
26.442	0.00129	0.016656	16.545	0.0036	0.384702	9.6944	0.00579	0.639478
26.292	0.00134	0.022221	16.301	0.00366	0.393772	9.5702	0.00585	0.644097
26.125	0.0014	0.028436	16.061	0.00372	0.402703	9.4482	0.0059	0.648634
25.942	0.00146	0.035251	15.825	0.00378	0.411494	9.3284	0.00596	0.65309

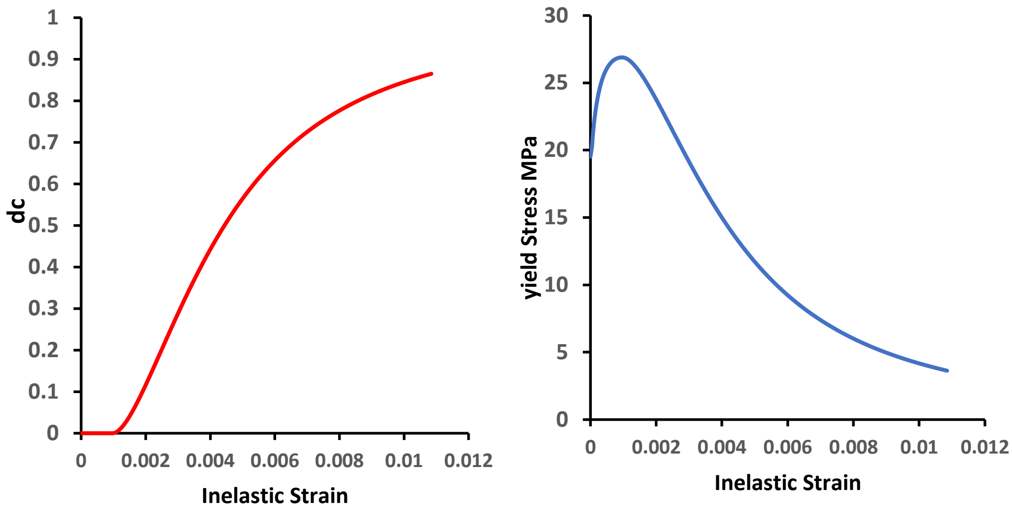

Figure 3.8 Inelastic strain-yield stress and damage in compression of 3CLH18

Table 3.8 FEM damage-plasticity parameters of 2CMH18

Yield stress	Inelastic strain	Damage parameter dc	Yield stress	Inelastic strain	Damage parameter dc	Yield stress	Inelastic strain	Damage parameter dc
19.90945	2.02E-05	0	26.22177	0.001567	0.060176	15.30232	0.003972	0.446571
20.66513	3.87E-05	0	25.98614	0.001627	0.069117	15.07151	0.004032	0.454918
21.3717	5.93E-05	0	25.73892	0.001687	0.078432	14.84469	0.004091	0.463122
22.03032	8.18E-05	0	25.48134	0.001748	0.088081	14.62182	0.00415	0.471182
22.6423	0.000106	0	25.21457	0.001809	0.098021	14.40288	0.004209	0.4791
23.20913	0.000133	0	24.93972	0.00187	0.108216	14.18783	0.004268	0.486878
23.73239	0.000161	0	24.65783	0.001932	0.11863	13.97663	0.004327	0.494516
24.21372	0.000191	0	24.36989	0.001994	0.129228	13.76923	0.004386	0.502017
24.65487	0.000222	0	24.07684	0.002056	0.139981	13.56559	0.004444	0.509382
25.05759	0.000256	0	23.77953	0.002119	0.150858	13.36566	0.004503	0.516613
25.42367	0.00029	0	23.47879	0.002181	0.161832	13.16938	0.004561	0.523711
25.75488	0.000327	0	23.17536	0.002244	0.172878	12.97671	0.004619	0.530679
26.053	0.000364	0	22.86994	0.002307	0.183972	12.7876	0.004677	0.537519
26.31979	0.000403	0	22.56317	0.002369	0.195093	12.60197	0.004735	0.544232
26.55694	0.000443	0	22.25567	0.002432	0.206222	12.41979	0.004792	0.550821
26.76615	0.000484	0	21.94796	0.002495	0.21734	12.241	0.00485	0.557288
26.94903	0.000527	0	21.64056	0.002558	0.22843	12.06552	0.004907	0.563634
27.10715	0.00057	0	21.33392	0.002621	0.239477	11.89332	0.004964	0.569862
27.24203	0.000615	0	21.02845	0.002683	0.250468	11.72432	0.005021	0.575974
27.35512	0.00066	0	20.72455	0.002746	0.261391	11.55848	0.005078	0.581972
27.44782	0.000706	0	20.42254	0.002809	0.272234	11.39573	0.005135	0.587858

Table 3.8 (continue) FEM damage-plasticity parameters of 2CMH18

27.52145	0.000753	0	20.12274	0.002871	0.282986	11.23602	0.005191	0.593634
27.57729	0.000801	0	19.82543	0.002933	0.293641	11.07929	0.005248	0.599302
27.61653	0.000849	0	19.53084	0.002996	0.304188	10.92547	0.005304	0.604865
27.64033	0.000898	0	19.23919	0.003058	0.314622	10.77452	0.005361	0.610325
27.64975	0.000948	0	18.95069	0.00312	0.324937	10.62638	0.005417	0.615682
27.65	**0.000957**	**0**	18.66549	0.003182	0.335127	10.48099	0.005473	0.620941
27.63566	0.001008	0.000519	18.38375	0.003244	0.345187	10.3383	0.005529	0.626101
27.59364	0.00106	0.002038	18.10559	0.003305	0.355113	10.19825	0.005585	0.631166
27.52546	0.001113	0.004504	17.83112	0.003367	0.364903	10.0608	0.00564	0.636138
27.43265	0.001166	0.007861	17.56042	0.003428	0.374554	9.925875	0.005696	0.641017
27.31677	0.001221	0.012052	17.29358	0.003489	0.384063	9.793437	0.005752	0.645807
27.17936	0.001277	0.017021	17.03066	0.00355	0.393429	9.663434	0.005807	0.650509
27.02194	0.001334	0.022715	16.77169	0.003611	0.40265	9.535813	0.005862	0.655124
26.84603	0.001391	0.029077	16.51672	0.003671	0.411726	8.380196	0.00641	0.696919
26.65308	0.001449	0.036055	16.26577	0.003732	0.420656	7.3262	0.007	0.735
26.44453	0.001508	0.043597	16.01885	0.003792	0.42944	6.1736	0.0078	0.7767

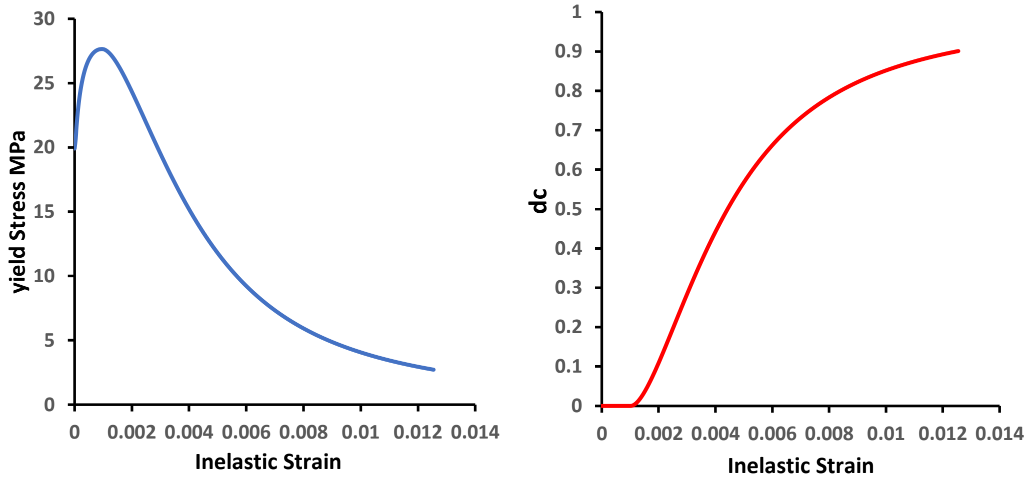

Figure 3.9 Inelastic strain-yield stress and damage in compression of 2CMH18

Table 3.9 FEM damage-plasticity parameters of 3CMH18

Yield stress	**Inelastic strain**	**Damage parameter dc**	**Yield stress**	**Inelastic strain**	**Damage parameter dc**	**Yield stress**	**Inelastic strain**	**Damage parameter dc**
18.25	0.00E+00	0	24.27	0.0017	0.057	14.02	0.0042	0.45
18.99	0.00E+00	0	24.05	0.0017	0.066	13.82	0.0042	0.46
19.67	1.00E-04	0	23.83	0.0018	0.074	13.63	0.0043	0.46
20.31	1.00E-04	0	23.59	0.0018	0.083	13.44	0.0044	0.47
20.9	1.00E-04	0	23.35	0.0019	0.093	13.26	0.0044	0.48
21.45	1.00E-04	0	23.1	0.0019	0.102	13.08	0.0045	0.48
21.96	2.00E-04	0	22.85	0.002	0.112	12.9	0.0045	0.49
22.42	2.00E-04	0	22.59	0.0021	0.122	12.72	0.0046	0.5
22.84	2.00E-04	0	22.33	0.0021	0.132	12.55	0.0046	0.51
23.23	3.00E-04	0	22.07	0.0022	0.143	12.38	0.0047	0.51
23.58	3.00E-04	0	21.8	0.0023	0.153	12.22	0.0048	0.52
23.9	3.00E-04	0	21.53	0.0023	0.163	12.05	0.0048	0.53
24.18	4.00E-04	0	21.26	0.0024	0.174	11.89	0.0049	0.53
24.44	4.00E-04	0	20.99	0.0024	0.184	11.74	0.0049	0.54
24.67	5.00E-04	0	20.72	0.0025	0.195	11.58	0.005	0.54
24.87	5.00E-04	0	20.45	0.0026	0.205	11.43	0.005	0.55
25.04	5.00E-04	0	20.18	0.0026	0.216	11.28	0.0051	0.56
25.2	6.00E-04	0	19.91	0.0027	0.226	11.13	0.0052	0.56
25.33	6.00E-04	0	19.65	0.0027	0.237	10.99	0.0052	0.57
25.44	7.00E-04	0	19.38	0.0028	0.247	10.85	0.0053	0.57
25.53	7.00E-04	0	19.11	0.0029	0.257	10.71	0.0053	0.58
25.6	8.00E-04	0	18.85	0.0029	0.268	10.57	0.0054	0.58
25.66	8.00E-04	0	18.59	0.003	0.278	10.44	0.0054	0.59
25.7	9.00E-04	0	18.33	0.0031	0.288	10.31	0.0055	0.59
25.72	9.00E-04	0	18.08	0.0031	0.298	10.18	0.0055	0.6
25.74	1.00E-03	0	17.82	0.0032	0.308	10.05	0.0056	0.6
25.74	**1.00E-03**	**0**	17.58	0.0032	0.317	9.92	0.0057	0.61
25.73	1.00E-03	0.0005	17.33	0.0033	0.327	9.8	0.0057	0.61
25.69	1.10E-03	0.00195	17.08	0.0034	0.336	9.68	0.0058	0.62

Table 3.9 (continue) FEM damage-plasticity parameters of 3CMH18

25.63	1.10E-03	0.0043	16.84	0.0034	0.346	9.56	0.0058	0.62
25.55	1.20E-03	0.0075	16.61	0.0035	0.355	9.45	0.0059	0.63
25.44	1.30E-03	0.01149	16.37	0.0035	0.364	8.79	0.0062	0.65
25.32	1.30E-03	0.01621	16.14	0.0036	0.373	8.68	0.0063	0.66
25.18	1.40E-03	0.02162	15.91	0.0037	0.382	7.66	0.0069	0.7
25.03	1.40E-03	0.02765	15.69	0.0037	0.391	6.66	0.0075	0.74
24.86	1.50E-03	0.03426	15.47	0.0038	0.399	5.36	0.0087	0.79
24.67	1.50E-03	0.0414	15.25	0.0038	0.408	4.81	0.0093	0.81
24.48	1.60E-03	0.04902	15.04	0.0039	0.416	3.51	0.0113	0.86

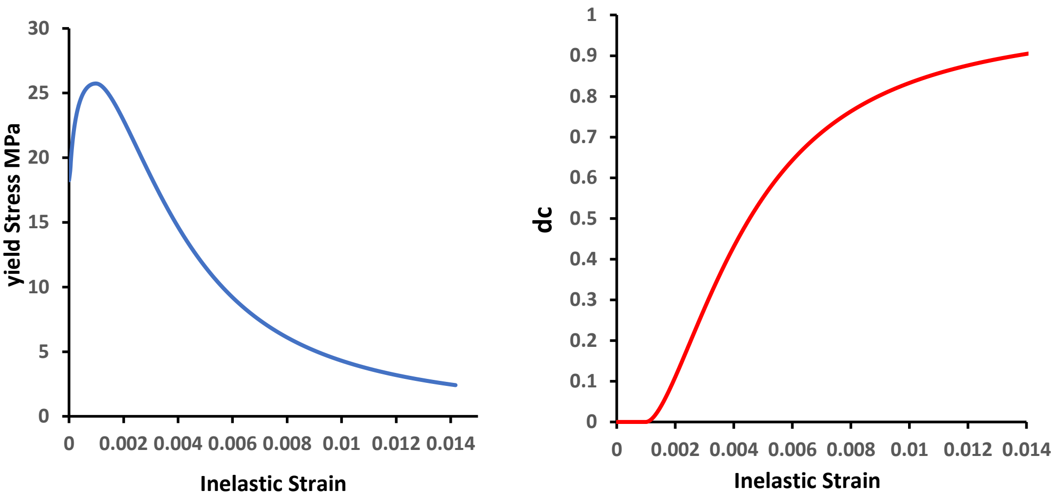

Figure 3.10 Inelastic strain and damage parameter in compression of 3CMH18

3.3.3 CDP for Concrete Tension Behavior

concrete under tension stress, somewhat needs low energy to start and extend cracks within the matrix. The fast growth and interconnectedness of the crack system, which includes existing faults inside the interfacial transition region and newly developed cracks, are one of the biggest drawbacks of concrete in tension, which makes it has brittle failure mode, the tensile behavior of reinforced concrete is influenced by the constraining effect exerted by the reinforcement on crack propagation[44]. Mostly the ratio between tension to compression strength about (7-10%) for low concrete strength, (5-7%) for high concrete strength. The behavior of uniaxial tension is considered more complex than the behavior of compression, that's due to three reasons: the first, the difficulty of matching load axis with the mechanical center during the period of the tests, due to brittle failure under tension, it is difficult to control the load; and finally, the sensitivity to sudden changes in cross-sectional area[45]. Stress-strain curve in tension is necessary in CDP ABAQUS software required to calculate inelastic and plastic strain in hardening and softening branches, Locationally, it can be obtained from BS 1881: Part 117:1983, ASTM C496 splitting tensile strengths, ASTM D-638 for direct tensile testing (dog bone) in order to estimate the tension stress-strain curve in the field. Unfortunately, Lynn[7] didn't list stress-strain in tension except ultimate tensile stress, as follows:

Table 3.10 Tensile stresses of tested specimens

Model	f_{tu} MPa
2CLH18	2.82
3CLH18	2.64
2CMH18	2.75
3CMH18	2.36

so that it has become necessary to generate a relevant constitutive model to plot ascending and descending parts. In this study adoptedEN1992(2004) [46]Eurocode 2: Design of concrete structures to create tension stress-strain curve from following equation for normal concrete:

$f_{cm}=f_{ck}+8$

$f_{ctm}=0.3* f_{ck}^{2/3}$ $\leq$ C50

$f_{ctm}=2.12*\ln\left(1+\frac{fcm}{10}\right)$ > C50

$\eta_l=0.4+0.6*\frac{\varrho}{2200}$

$f_{1ctm}= f_{ctm}* \eta_l$

where: f_{ck}, f_{cm}, f_{1ctm} are ultimate compression strength, average compression strength at 28-day, peak tension stress in MPa respectively. Eurocode also presented empirical equation to calculate modulus of elasticity as:

$E_{cm}=22(f_{cm}/10)^{0.3}$

Mehta (14) exhibit two equations to estimate maximum and minimum tensile stress as:

$f_{ctm,\ min} = 0.95(f_{ck}/10)^{2/3}$

$f_{ctm,\ max}= 1.85(f_{ck}/10)^{2/3}$

$\epsilon_{to}= f_{1ctm} /E_o$

T. Wang, Thomas, et al.[47] presented two equations to estimate tension stress in ascending and descending branches depending on above peak tension stress and corresponding strains following:

$\sigma 1=E_O*\epsilon 1$ for ascending part

$\sigma_1=f_{ck}*(\frac{\epsilon ck}{\epsilon 1})^{0.4}$ for descending part

where: E_o, f_{ck}, ϵ_{ck}, ϵ_1 are undamaged modulus of elasticity, peak tension stress, crack strain, strain corresponding to σ_1. This study takes (0.00005) as strain increment add to previous value: $\epsilon_2=\epsilon_1+0.00005$

Table 3.11 Tension stress-strain constitutive model of 2CLH18

f_t (MPa)	ϵ_t	f_t (MPa)	ϵ_t	f_t (MPa)	ϵ_t	f_t (MPa)	ϵ_t
0	0	0.374468	0.01711	0.28251	0.03461	0.239853	0.05211
2.82	0.00011	0.370178	0.01761	0.280894	0.03511	0.238939	0.05261
1.421015	0.00061	0.366056	0.01811	0.279309	0.03561	0.238036	0.05311
1.118391	0.00111	0.362089	0.01861	0.277756	0.03611	0.237146	0.05361
0.963806	0.00161	0.35827	0.01911	0.276232	0.03661	0.236267	0.05411
0.864979	0.00211	0.354587	0.01961	0.274737	0.03711	0.235399	0.05461

Table 3.11 (continue) Tension stress-strain constitutive model of 2CLH18

0.794441	0.00261	0.351034	0.02011	0.27327	0.03761	0.234543	0.05511
0.74065	0.00311	0.347603	0.02061	0.271831	0.03811	0.233697	0.05561
0.697772	0.00361	0.344286	0.02111	0.270417	0.03861	0.232862	0.05611
0.66249	0.00411	0.341077	0.02161	0.269029	0.03911	0.232037	0.05661
0.632755	0.00461	0.33797	0.02211	0.267665	0.03961	0.231222	0.05711
0.607222	0.00511	0.334961	0.02261	0.266326	0.04011	0.230417	0.05761
0.584966	0.00561	0.332043	0.02311	0.265009	0.04061	0.229622	0.05811
0.565326	0.00611	0.329212	0.02361	0.263715	0.04111	0.228836	0.05861
0.547816	0.00661	0.326464	0.02411	0.262443	0.04161	0.22806	0.05911
0.532068	0.00711	0.323795	0.02461	0.261192	0.04211	0.227293	0.05961
0.517799	0.00761	0.3212	0.02511	0.259962	0.04261	0.226535	0.06011
0.504785	0.00811	0.318677	0.02561	0.258751	0.04311	0.225786	0.06061
0.492849	0.00861	0.316222	0.02611	0.257561	0.04361	0.225045	0.06111
0.481845	0.00911	0.313831	0.02661	0.256389	0.04411	0.224313	0.06161
0.471656	0.00961	0.311503	0.02711	0.255236	0.04461	0.223588	0.06211
0.462183	0.01011	0.309234	0.02761	0.2541	0.04511	0.222872	0.06261
0.453345	0.01061	0.307022	0.02811	0.252982	0.04561	0.222165	0.06311
0.445071	0.01111	0.304865	0.02861	0.251881	0.04611	0.221464	0.06361
0.437302	0.01161	0.302759	0.02911	0.250797	0.04661	0.220772	0.06411
0.429989	0.01211	0.300704	0.02961	0.249729	0.04711	0.220087	0.06461
0.423086	0.01261	0.298696	0.03011	0.248676	0.04761	0.219409	0.06511

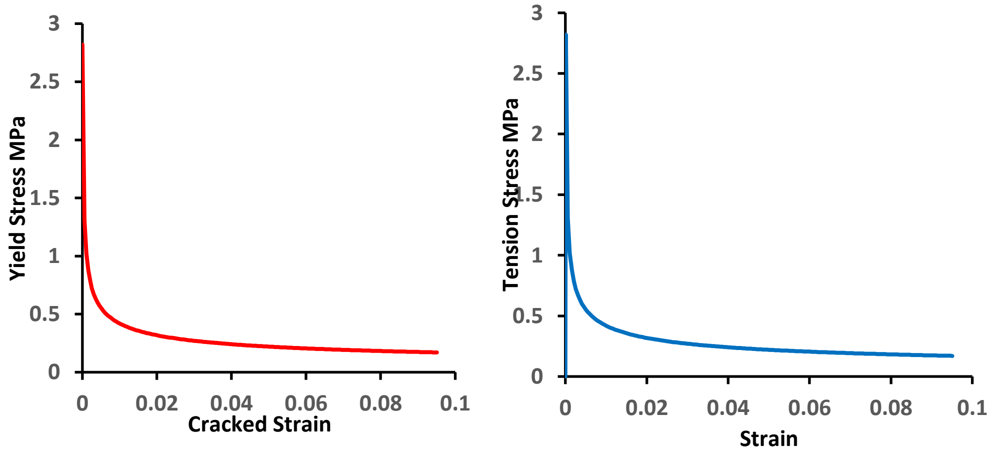

Figure 3.11 Tension stress and cracks strain of 2CLH18

Table 3.12 Tension stress-strain constitutive model of 3CLH18

f_t (MPa)	ϵ_t	f_t (MPa)	ϵ_t	f_t (MPa)	ϵ_t	f_t (MPa)	ϵ_t
0	0	0.352291	0.017111	0.265783	0.034611	0.225653	0.052111
2.64	0.000111	0.348255	0.017611	0.264262	0.035111	0.224793	0.052611
1.335704	0.000611	0.344377	0.018111	0.262772	0.035611	0.223944	0.053111
1.051672	0.001111	0.340646	0.018611	0.261311	0.036111	0.223106	0.053611
0.906448	0.001611	0.337053	0.019111	0.259877	0.036611	0.222279	0.054111
0.813568	0.002111	0.333589	0.019611	0.258471	0.037111	0.221463	0.054611
0.747259	0.002611	0.330246	0.020111	0.257091	0.037611	0.220657	0.055111
0.696686	0.003111	0.327018	0.020611	0.255737	0.038111	0.219861	0.055611
0.65637	0.003611	0.323898	0.021111	0.254407	0.038611	0.219076	0.056111
0.623193	0.004111	0.320879	0.021611	0.253101	0.039111	0.2183	0.056611
0.59523	0.004611	0.317957	0.022111	0.251818	0.039611	0.217533	0.057111
0.571217	0.005111	0.315126	0.022611	0.250558	0.040111	0.216776	0.057611
0.550286	0.005611	0.312381	0.023111	0.249319	0.040611	0.216028	0.058111
0.531815	0.006111	0.309718	0.023611	0.248102	0.041111	0.215289	0.058611
0.515346	0.006611	0.307133	0.024111	0.246905	0.041611	0.214559	0.059111
0.500535	0.007111	0.304621	0.024611	0.245728	0.042111	0.213837	0.059611
0.487114	0.007611	0.302181	0.025111	0.244571	0.042611	0.213124	0.060111
0.474873	0.008111	0.299807	0.025611	0.243432	0.043111	0.212419	0.060611
0.463646	0.008611	0.297497	0.026111	0.242312	0.043611	0.211722	0.061111
0.453296	0.009111	0.295249	0.026611	0.241209	0.044111	0.211033	0.061611
0.443712	0.009611	0.293058	0.027111	0.240124	0.044611	0.210352	0.062111
0.434802	0.010111	0.290924	0.027611	0.239056	0.045111	0.209678	0.062611
0.426488	0.010611	0.288843	0.028111	0.238005	0.045611	0.209012	0.063111
0.418705	0.011111	0.286813	0.028611	0.236969	0.046111	0.208353	0.063611
0.411398	0.011611	0.284833	0.029111	0.235949	0.046611	0.207702	0.064111
0.404518	0.012111	0.282899	0.029611	0.234944	0.047111	0.207057	0.064611
0.398025	0.012611	0.28101	0.030111	0.233954	0.047611	0.20642	0.065111
0.391882	0.013111	0.279165	0.030611	0.232978	0.048111	0.205789	0.065611
0.38606	0.013611	0.277362	0.031111	0.232017	0.048611	0.205165	0.066111
0.380529	0.014111	0.275599	0.031611	0.231069	0.049111	0.204548	0.066611
0.375265	0.014611	0.273874	0.032111	0.230135	0.049611	0.203937	0.067111
0.370249	0.015111	0.272187	0.032611	0.229213	0.050111	0.203332	0.067611
0.365459	0.015611	0.270535	0.033111	0.228305	0.050611	0.202734	0.068111
0.360879	0.016111	0.268918	0.033611	0.227409	0.051111	0.202142	0.068611

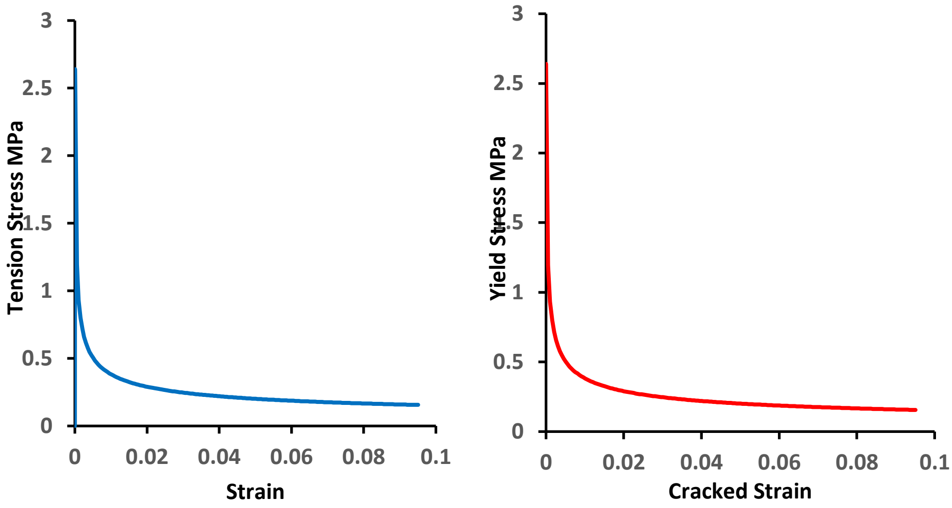

Figure 3.12 Tension stress and cracks strain of 3CLH18

Table 3.13 Tension stress-strain constitutive model of 2CMH18

f_t (MPa)	ϵ_t	f_t (MPa)	ϵ_t	f_t (MPa)	ϵ_t	f_t (MPa)	ϵ_t
0	0	0.367008	0.017615	0.278503	0.035115	0.236909	0.052615
2.75	0.000115	0.362922	0.018115	0.276932	0.035615	0.236015	0.053115
1.404702	0.000615	0.358991	0.018615	0.275392	0.036115	0.235132	0.053615
1.10707	0.001115	0.355205	0.019115	0.273882	0.036615	0.23426	0.054115
0.954547	0.001615	0.351555	0.019615	0.2724	0.037115	0.2334	0.054615
0.856905	0.002115	0.348033	0.020115	0.270946	0.037615	0.232551	0.055115
0.787158	0.002615	0.344631	0.020615	0.269518	0.038115	0.231712	0.055615
0.733944	0.003115	0.341343	0.021115	0.268117	0.038615	0.230884	0.056115
0.691513	0.003615	0.338163	0.021615	0.266741	0.039115	0.230066	0.056615
0.656588	0.004115	0.335083	0.022115	0.265389	0.039615	0.229259	0.057115
0.627149	0.004615	0.3321	0.022615	0.264061	0.040115	0.228461	0.057615
0.601866	0.005115	0.329208	0.023115	0.262755	0.040615	0.227672	0.058115
0.579825	0.005615	0.326402	0.023615	0.261473	0.041115	0.226894	0.058615
0.560373	0.006115	0.323678	0.024115	0.260211	0.041615	0.226124	0.059115
0.543029	0.006615	0.321031	0.024615	0.258971	0.042115	0.225364	0.059615
0.527429	0.007115	0.318459	0.025115	0.257752	0.042615	0.224612	0.060115
0.513293	0.007615	0.315958	0.025615	0.256552	0.043115	0.223869	0.060615
0.5004	0.008115	0.313524	0.026115	0.255371	0.043615	0.223134	0.061115
0.488574	0.008615	0.311155	0.026615	0.254209	0.044115	0.222408	0.061615
0.477672	0.009115	0.308847	0.027115	0.253066	0.044615	0.221691	0.062115
0.467576	0.009615	0.306598	0.027615	0.25194	0.045115	0.220981	0.062615

Table 3.13 (continue) Tension stress-strain constitutive model of 2CMH18

0.458189	0.010115	0.304405	0.028115	0.250832	0.045615	0.220279	0.063115
0.449431	0.010615	0.302266	0.028615	0.249741	0.046115	0.219585	0.063615
0.441232	0.011115	0.300179	0.029115	0.248666	0.046615	0.218898	0.064115
0.433534	0.011615	0.298141	0.029615	0.247607	0.047115	0.218219	0.064615
0.426286	0.012115	0.296151	0.030115	0.246563	0.047615	0.217547	0.065115
0.419445	0.012615	0.294207	0.030615	0.245535	0.048115	0.216882	0.065615
0.412974	0.013115	0.292307	0.031115	0.244522	0.048615	0.216225	0.066115
0.406839	0.013615	0.290449	0.031615	0.243523	0.049115	0.215574	0.066615

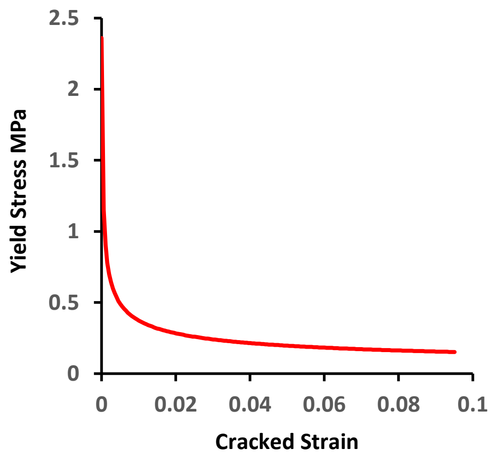

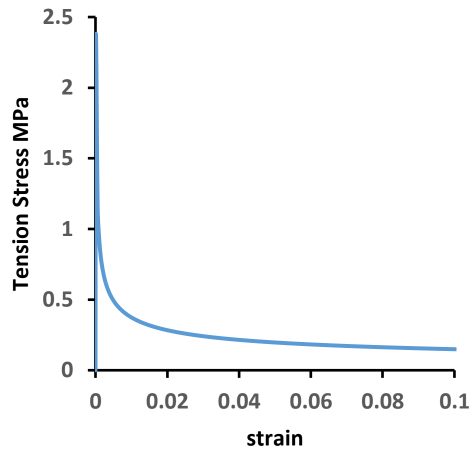

Figure 3.13 Tension stress and cracks strain of 2CMH18

Table 3.14 Tension stress-strain constitutive model of 3CMH18

f_t (MPa)	ϵ_t	f_t (MPa)	ϵ_t	f_t (MPa)	ϵ_t	f_t (MPa)	ϵ_t
0	0	0.301898	0.0171	0.227734	0.0346	0.193341	0.0521
2.36	0.0001	0.298437	0.0176	0.226431	0.0351	0.192604	0.0526
1.152854	0.0006	0.295112	0.0181	0.225154	0.0356	0.191876	0.0531
0.904667	0.0011	0.291913	0.0186	0.223901	0.0361	0.191158	0.0536
0.778757	0.0016	0.288832	0.0191	0.222672	0.0366	0.19045	0.0541
0.698497	0.0021	0.285862	0.0196	0.221467	0.0371	0.18975	0.0546
0.641304	0.0026	0.282996	0.0201	0.220284	0.0376	0.189059	0.0551
0.597737	0.0031	0.280228	0.0206	0.219123	0.0381	0.188378	0.0556
0.563033	0.0036	0.277553	0.0211	0.217984	0.0386	0.187704	0.0561
0.534493	0.0041	0.274965	0.0216	0.216864	0.0391	0.187039	0.0566

Table 3.14 (continue) Tension stress-strain constitutive model of 3CMH18

0.51045	0.0046	0.272459	0.0221	0.215765	0.0396	0.186382	0.0571
0.489811	0.0051	0.270032	0.0226	0.214685	0.0401	0.185733	0.0576
0.471826	0.0056	0.267679	0.0231	0.213623	0.0406	0.185092	0.0581
0.455958	0.0061	0.265396	0.0236	0.21258	0.0411	0.184459	0.0586
0.441814	0.0066	0.263179	0.0241	0.211554	0.0416	0.183833	0.0591
0.429095	0.0071	0.261027	0.0246	0.210546	0.0421	0.183215	0.0596
0.417573	0.0076	0.258934	0.0251	0.209554	0.0426	0.182604	0.0601
0.407065	0.0081	0.256899	0.0256	0.208578	0.0431	0.181999	0.0606
0.397428	0.0086	0.254919	0.0261	0.207618	0.0436	0.181402	0.0611
0.388545	0.0091	0.252992	0.0266	0.206673	0.0441	0.180812	0.0616
0.38032	0.0096	0.251114	0.0271	0.205743	0.0446	0.180228	0.0621
0.372674	0.0101	0.249284	0.0276	0.204828	0.0451	0.179651	0.0626
0.365541	0.0106	0.247501	0.0281	0.203926	0.0456	0.17908	0.0631
0.358863	0.0111	0.245761	0.0286	0.203039	0.0461	0.178516	0.0636
0.352594	0.0116	0.244063	0.0291	0.202164	0.0466	0.177957	0.0641
0.346692	0.0121	0.242405	0.0296	0.201303	0.0471	0.177405	0.0646
0.341122	0.0126	0.240787	0.0301	0.200455	0.0476	0.176859	0.0651
0.335853	0.0131	0.239205	0.0306	0.199619	0.0481	0.176318	0.0656
0.330859	0.0136	0.237659	0.0311	0.198795	0.0486	0.175784	0.0661
0.326115	0.0141	0.236148	0.0316	0.197982	0.0491	0.175255	0.0666
0.321601	0.0146	0.23467	0.0321	0.197182	0.0496	0.174731	0.0671
0.317298	0.0151	0.233223	0.0326	0.196392	0.0501	0.174213	0.0676

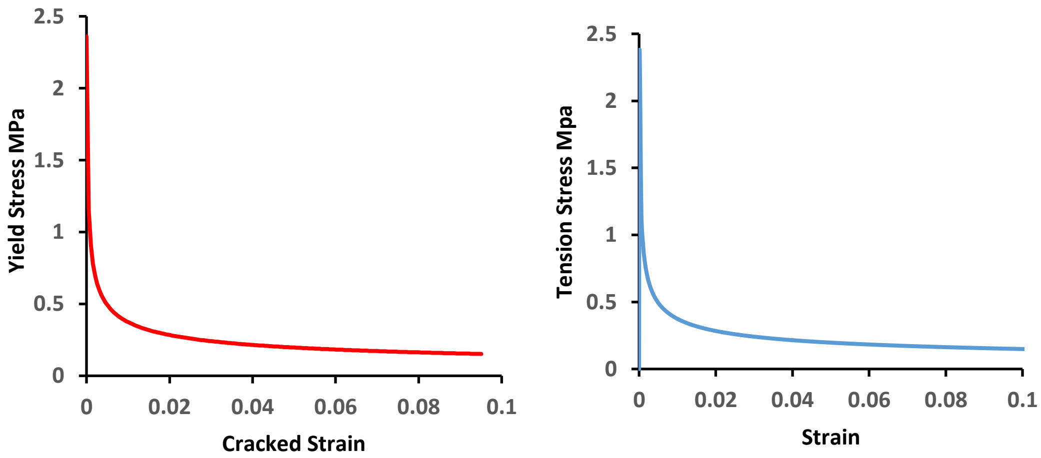

Figure 3.14 Tension stress and cracks strain of 3CMH18

3.3.4 Damage Plasticity Requirements of Tension

Fracture energy theory is widely used as a base to estimate tensile cracking, which is known as energy demanded to consist area of crack. Many fracture mechanisms exist, such as linear elastic fracture mechanism and smeared-crack model. Although, it is use with high efficiency in numerical analysis, there are some disadvantages, such as the lack of balance in the cracks and the difficulty of determining the closing and opening stresses during cyclic loading (4). The damage parameter, denoted as dt, is a measure of a decline in the secant modulus compared to the original elastic modulus after a specific ultimate tensile strength[48][49] as:

$E = (1-d_t)\, E_o$

Nayal & Rasheed, 2006[51] developed two parts of descending tensile stress strain responses defined as the initial cracking zone (0.8 σ_{to}- 0.45 σ_{t0}) and the secondary crack zone (0.45σ_{t0}), This study depends on simplifying the descending branch and using tension hardening and softening values that were generated based on EN1992 (2004) Eurocode 2: Design of concrete structures to calculate crack strain can be considered responsible for the elastic stiffness lost as a result of propagation cracks along tension zone, then use this value to compute plastic strain [51].

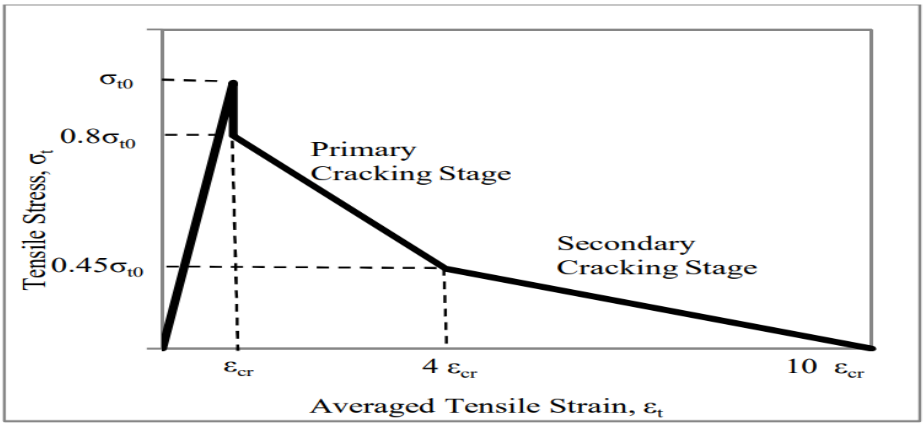

Figure 3.15 Primary and secondary crack staged[50]

$$\varepsilon_t^{ck} = \varepsilon_t - \frac{\sigma_t}{Eo}$$

$$dt = 1 - \frac{\sigma_t}{\sigma_{ck}}$$

$$\sigma_{t = (1-dt)Eo\left(\varepsilon_t - \varepsilon_t^{pl}\right)}$$

$$\varepsilon_t^{pl} = \varepsilon_t^{ck} - \frac{\sigma_t}{E_O}\left(\frac{1}{1-dt}\right)$$

Where: σ_t, ε_t, ε_t^{ck}, ε_t^{pl},tension stress corresponding to total concert strain, crack strain, and hardening plastic strain, respectively. Eo, dc, initial modulus of elasticity and tension damage parameters in softening branches sequentially. Due to the brittle behavior of concrete and ABAQUS software, the relationship between steel bars and concrete was simplified, and the slip of steel bars didn't have a clearness, so the variation of constitutive models was not high effect on numerical analysis[51]. The tables bellow show tension damage factors depend on equations above:

Table 3.15 Tension damage parameters of 2CLH18

Yield stress MPa	**Crack strain**	**Damage parameter dt**	**Yield stress MPa**	**Crack strain**	**Damage parameter dt**
2.82	0	0	0.481845235	0.009091156	0.829132896
1.42101455	0.000554541	0.496094131	0.471656155	0.009591553	0.832746044
1.118391261	0.00106634	0.603407354	0.462183404	0.010091923	0.836105176
0.963806306	0.001572366	0.658224714	0.453344768	0.010592267	0.839239444
0.864979145	0.002076219	0.693269807	0.445070792	0.01109259	0.842173478
0.794440714	0.002578969	0.718283435	0.43730233	0.011592893	0.844928252
0.740649808	0.003081066	0.737358224	0.429988643	0.012093178	0.847521758
0.69777232	0.003582738	0.752563007	0.423085922	0.012593447	0.849969531
0.662490335	0.004084113	0.765074349	0.416556103	0.013093702	0.85228507
0.632755075	0.004585273	0.775618768	0.410365933	0.013593943	0.854480166
0.607221908	0.005086268	0.784673082	0.404486209	0.014094172	0.856565174
0.584965792	0.005587136	0.792565322	0.398891161	0.01459439	0.858549234
0.56532603	0.006087902	0.799529777	0.393557951	0.015094598	0.860440443
0.547816056	0.006588584	0.805738987	0.38846625	0.015594797	0.862246011
0.532068309	0.007089198	0.811323295	0.383597898	0.029598218	0.893367479
0.517799082	0.007589754	0.816383304	0.378936607	0.035098991	0.900392359

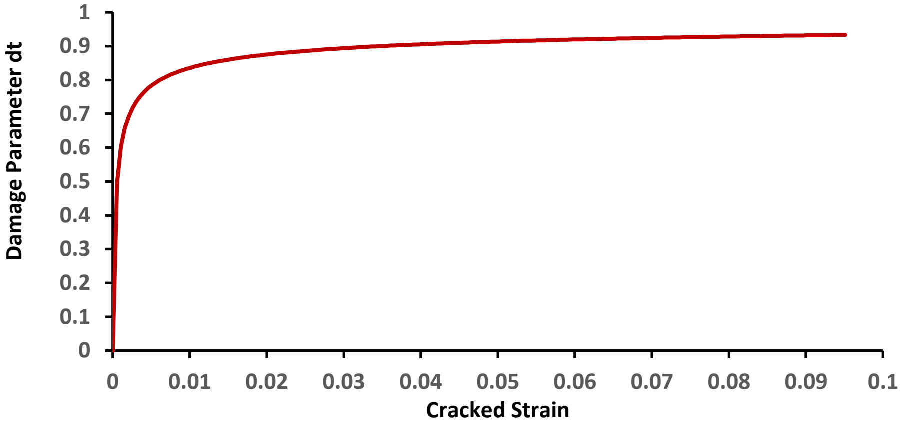

Figure 3.16 Tension damage-cracks strain of 2CLH18

Table 3.16 Tension damage parameters of 3CLH18

Yield stress MPa	Crack strain	Damage parameter dt	Yield stress MPa	Crack strain	Damage parameter dt
2.64	0	0	0.404518003	0.012094253	0.846773484
1.335704157	0.000554992	0.494051456	0.370248622	0.015095697	0.85975431
1.051672496	0.001066967	0.601639206	0.365458911	0.015595899	0.861568594
0.906447928	0.00157309	0.656648512	0.360879285	0.016096092	0.863303301
0.813567601	0.002077006	0.691830454	0.356494424	0.016596277	0.864964234
0.747258805	0.002579802	0.716947422	0.352290547	0.017096455	0.866556611
0.696685989	0.003081934	0.736103792	0.317957079	0.022097902	0.879561712
0.656369612	0.003583634	0.751375147	0.315125827	0.022598022	0.880634156
0.623192577	0.004085033	0.763942206	0.312380893	0.023098137	0.881673904
0.595229743	0.004586212	0.774534188	0.267334447	0.034100036	0.898736952
0.571217436	0.005087224	0.783629759	0.265782919	0.034600102	0.899324652
0.550286214	0.005588107	0.791558252	0.264262457	0.035100166	0.899900584
0.53181503	0.006088885	0.798554913	0.262772009	0.035600229	0.900465148
0.515346486	0.00658958	0.804792998	0.261310574	0.03610029	0.901018722
0.500535033	0.007090204	0.810403397	0.259877197	0.036600351	0.901561668
0.487113938	0.00759077	0.815487145	0.258470967	0.03710041	0.902094331
0.474873481	0.008091286	0.820123681	0.236968869	0.046101317	0.910239065
0.463646115	0.00859176	0.824376472	0.235948791	0.04660136	0.910625458
0.453296101	0.009092196	0.828296932	0.209012086	0.063102495	0.920828755
0.443712104	0.0095926	0.831927233	0.208353376	0.063602523	0.921078267

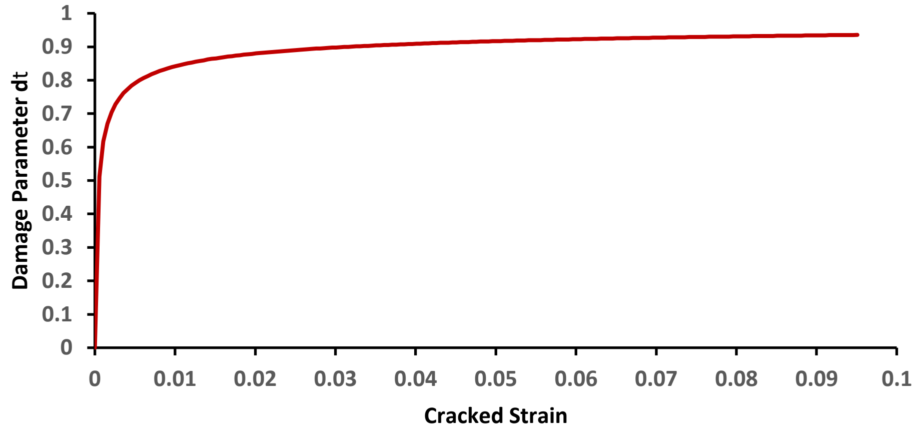

Figure 3.17 Tension damage-cracks strain of 3CLH18

Table 3.17 Tension damage parameters of 2CMH18

Yield stress MPa	Crack strain	Damage parameter dt	Yield stress MPa	Crack strain	Damage parameter dt
2.75	0	0	0.358990631	0.01859965	0.869457952
1.404702319	0.000556068	0.489199157	0.355204546	0.019099808	0.870834711
1.107070366	0.001068473	0.597428958	0.351554629	0.01959996	0.872161953
0.954547272	0.001574829	0.652891901	0.308846975	0.02710174	0.887692009
0.85690452	0.002078899	0.688398356	0.306597869	0.027601834	0.888509866
0.787157813	0.002581806	0.713760795	0.304405063	0.028101925	0.88930725
0.733944346	0.003084023	0.733111147	0.302266185	0.028602014	0.890085024
0.691512501	0.003585792	0.748540909	0.300179	0.029102101	0.890844
0.656588323	0.004087247	0.76124061	0.298141403	0.029602186	0.891584944
0.627148855	0.004588474	0.771945871	0.296151407	0.030102269	0.892308579
0.601865754	0.005089528	0.781139726	0.249740678	0.046104204	0.909185208
0.579824831	0.005590447	0.789154607	0.248665698	0.046604248	0.90957611
0.560372931	0.006091257	0.796228025	0.24760674	0.047104292	0.909961186
0.543028921	0.00659198	0.802534938	0.2465634	0.047604336	0.910340582
0.527429263	0.00709263	0.808207541	0.245535286	0.048104379	0.910714441
0.513293303	0.007593219	0.81334789	0.244522023	0.048604421	0.911082901
0.500400352	0.008093757	0.818036236	0.243523245	0.049104463	0.911446093
0.488574078	0.00859425	0.822336699	0.214930414	0.067105654	0.921843486
0.45818938	0.010095516	0.83338568	0.213038485	0.068605733	0.92253146
0.433533665	0.011596544	0.842351395	0.21120359	0.07010581	0.923198695
0.426285839	0.012096846	0.844986968	0.210604128	0.070605835	0.923416681

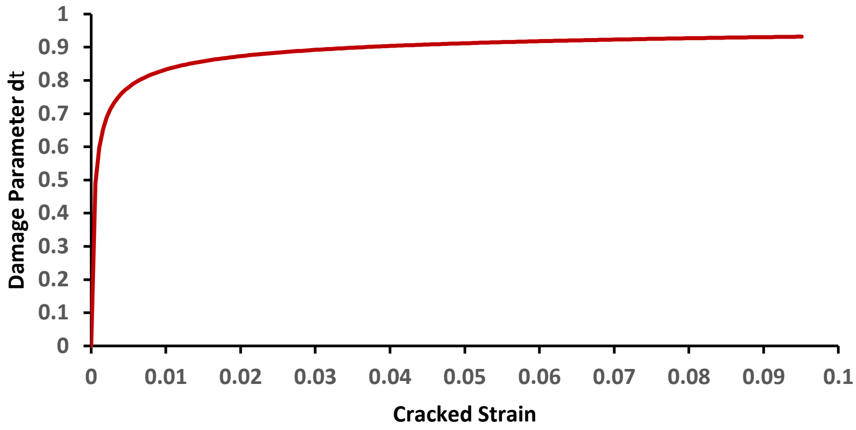

Figure 3.18 Tension damage-cracks strain of 2CMH18

Table 3.18 Tension damage parameters of 3CMH18

Yield stress MPa	Crack strain	Damage parameter dt	Yield stress MPa	Crack strain	Damage parameter dt
2.36	0	0	0.335853316	0.013085842	0.857689273
1.152853781	0.000551194	0.511502635	0.285861787	0.019587962	0.878872124
0.904667139	0.001061719	0.616666466	0.28299589	0.020088083	0.880086487
0.778757213	0.001567059	0.67001813	0.280228099	0.020588201	0.88125928
0.698497007	0.002070462	0.704026692	0.277552794	0.021088314	0.882392884
0.641304486	0.002572888	0.728260811	0.239204988	0.03058994	0.898641954
0.597736606	0.003074736	0.746721777	0.237659213	0.031090006	0.899296944
0.563033442	0.003576207	0.761426508	0.236147844	0.03159007	0.899937354
0.534493155	0.004077418	0.77351985	0.234669589	0.032090133	0.900563734
0.510449694	0.004578437	0.783707757	0.233223223	0.032590194	0.901176601
0.489810763	0.005079313	0.792453066	0.231807584	0.033090254	0.901776447
0.471825536	0.005580075	0.800073925	0.230421572	0.033590313	0.902363741
0.441814004	0.006581348	0.812790676	0.227734285	0.034590427	0.903502421
0.42909541	0.007081887	0.818179911	0.191158271	0.043591978	0.919000733
0.407064714	0.008082822	0.827514952	0.189750075	0.054592038	0.919597426
0.397427752	0.00858323	0.83159841	0.189059444	0.055092067	0.919890066
0.388544806	0.009083607	0.83536237	0.188377532	0.055592096	0.920179012
0.372674155	0.01008428	0.842087222	0.18703912	0.056592153	0.920746135
0.365540539	0.010584583	0.845109941	0.186382264	0.057092181	0.921024464
0.358863067	0.011084866	0.847939378	0.185733411	0.057592208	0.921299402

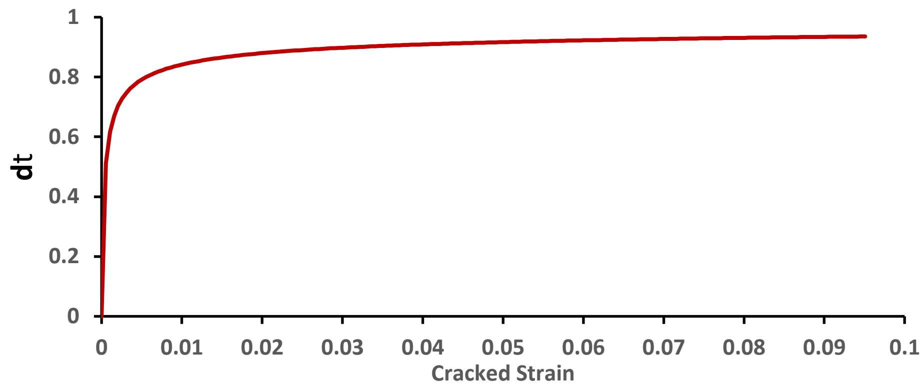

Figure 3.19 Tension damage-cracks strain of 3CMH18

3.3.5 Concrete Damage Plasticity Reequipments for ECC

ECC was called also (HPFRCC) with high ability tension cracking control with micro-cracks distribution by using a coated and uncoated fiber as a polyvinyl alcohol PVA with different sizes. Recently, It has been widely used to increase ductility, durability, large dissipation energy, and increasing of column-beam connection capacity during seismic force. Partially replaced steel-ECC concrete hand over better feedback than entirely used ECC concrete in structural members[52].Tension deformation response of ECC result a two hardening strain parts and multiple micro-cracks with distribution depend on ECC matrix type and propagation in mixture doing together with steel reinforcement to improve ductility response on concrete structural members which lead to decrease early buckling collapse[53]. The shear deformation of HPFRCC concrete assumed same tension response it contribution to reduce transverse reinforcement required to resist shear force[54].

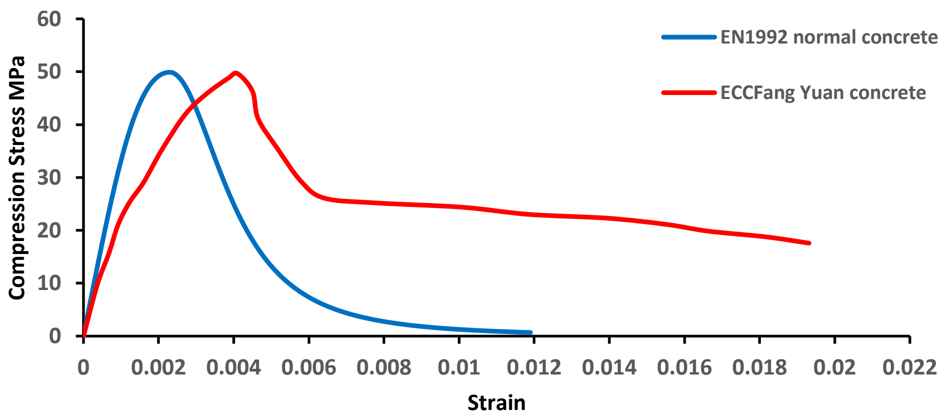

Figure 3.20 Comparison ECC and normal concrete compression strength

The usage ECC significantly decrease shear of stirrups and lower flexural and shear cracks with keeping high load capacity seismic shacking as a result of doubled total strain and strain corresponding to ultimate stress[55]. ECC compression behavior similar normal concrete just the former has approximately twins strain corresponding to ultimate stress so that initial stiffness of ECC and modulus of elasticity less than normal concrete. This study adopt Fang Yuan e. al. ECC real stress strain curve from (100 mm Diameter*200 height mm) cylinder compression field test with 49.6 MPa compression strength and make comparison with normal concrete has same strength 49.6 MPa, and generated stress strain relationship depend on EN 1992(2004)[46] as chart below.

The compression damage of NC at the same strain value reaches more than 90%, in contrast 63% compression deterioration for ECC. The tension behavior of ECC significant effect on finite element analysis and essentially different from NC tensile behavior. Polyvinyl alcohol fibers added to concrete 2% by volume. PVA was split instead of being withdraw out as a result of the high chemical join among skid resistance and cement hydrates. Oil agents (1.2%) are ideally used to improve strain hardening branch by reducing PVA mechanical bond as well as enhancing multiple-tiny cracks instead of single-large cracks[56]. This study suggested two strain-hardening values derivate from the Fang Yuan ECC tensile stress-strain curve (1%,3%) for uncoated and oil-coat PVA, respectively. The strategy followed in this aspect consists of two-part: first, simplify random strain-hardening (ascending) to a straight line by suggest a new constitutive model, and second, modify T.Wang[47] descending (softening branch) for NC to get near to 90% tension damage to prevent stop FEA as follows:

Ascending part: $\varepsilon_n \leq \varepsilon_{cru}$

$$m = (f_{cru}-f_{cri})/(\varepsilon_{cru}-\varepsilon_{cri})$$

$$f_{crn} = f_{cri} + (m*\varepsilon_{crn})$$

Descending part: $ft_n = f_{cru}*(\varepsilon_{cru}/\varepsilon_n)^{2.7}$ $\varepsilon_n > \varepsilon_{cru}$

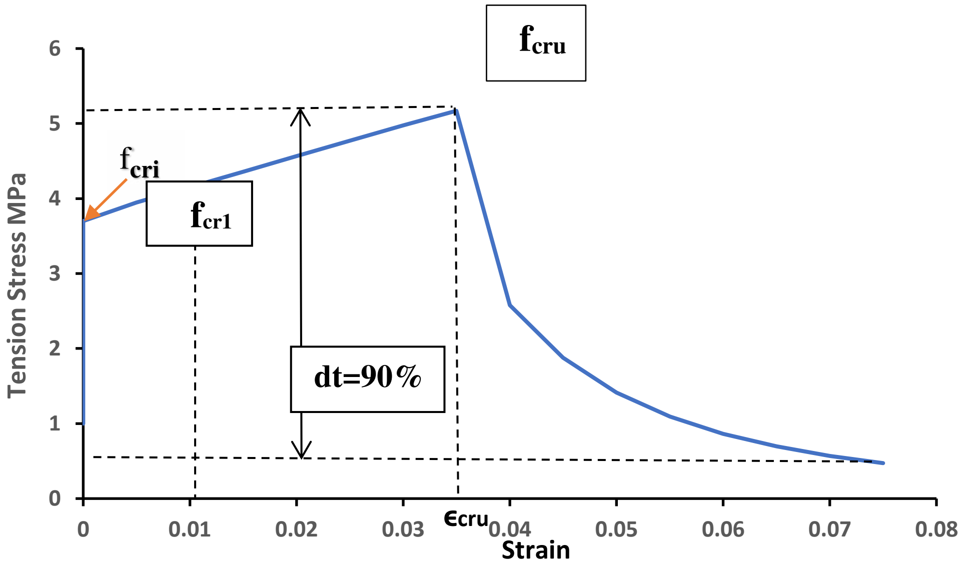

Figure 3.21 New constitutive model for ECC in tension behavior

where: f_{cru}, f_{cri}, ε_{cru}, ε_{cri}, m are ECC ultimate tension stress, initial hardening tension stress ultimate hardening strain corresponding to $\varepsilon = 0.035$, simplified initial strain =0, slope of strain-hardening part respectively**.** FEA achieved by quasi-static analysis to validate above new model and comparison with Fang experimental field tension test as following:

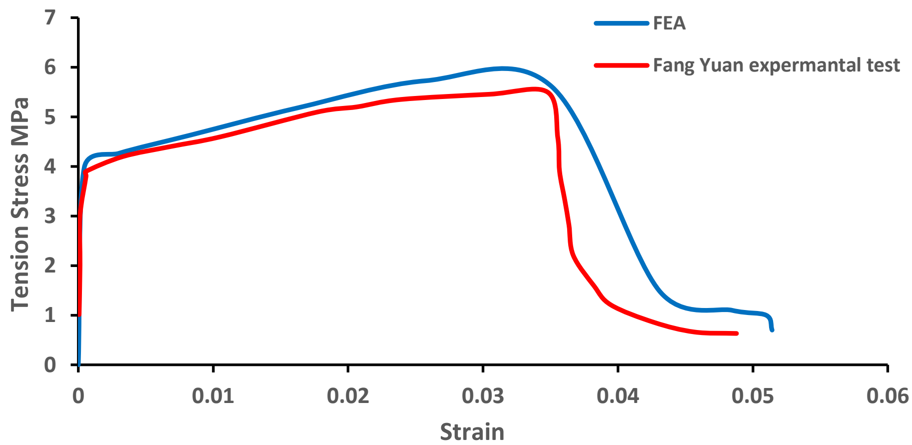

Figure 3.22 FE Verification of new constitutive ECC fang. Model

CHAPTER 4

NUMERICAL VERFICATIONS

4.1 General

In the past few years, numerical analysis programs widely used to simulate reinforced concrete structures. This thesis depends on finite element model analysis by ABAQUS software, which is based on CDP theory to simulate fourth, RC columns. One of the influential factors in numerical analysis is CDP parameter sensitivity, which expresses set of internal and external conditions of reinforced concrete members as well as differences from specimen to another, such as viscosity (rate of applied loads by ABAQUS), dilation angle (internal friction angle of concrete member), fb0/fc0 ratio between biaxial compression stress and uniaxial compression stress in the yield plan, eccentricity of flow potential, and Poisson's ratio. The selection prosses of these parameters must be done with great careful to get the right behavior of specimens, which directly effect on results[32]. For these reasons, validation is necessary to prevent the sensitivity of Concrete damage plasticity parameters. Make sure the proper choice them which is compatible with each specimen to capture the correct plastic and damage behavior of concrete models in tension and compression.

4.2 Numerical Verification of Models

This section expresses FEM analysis for two different experimental members to calibrate stress-strain constitutive models, that have been generated and adopt in this study to satisfy material proprieties and general behavior in each stage of loading, after that, the results were verified and compared with empirical field tests. The first model carried out by (Mark 2004)[57], three points bending beam with (250*500) mm cross section diminutions, effective length = 3000 mm, total length = 3300 mm reinforced by 3ϕ20 mm as a triangle shape in each corner of beam, shear reinforcement ϕ 8mm @150 mm, yield strength of longitudinal and lateral steel bars = 570 MPa, fc '= 35.8 MPa, ft = 3.5MPa. the modulus of elasticity was calculated depend on Eurocode2 E = 32254 MPa as equation below:

Ec= 22(fc ‘/10)$^{\mathbf{0.3}}$ GPa.

Dynamic explicit finite element analysis, C3D8R 8-node linear brick 3D element type and Δt = 116139-time increments had based on implemented this verification and compared the results with experimental load-displacement curve in mid span of beam.

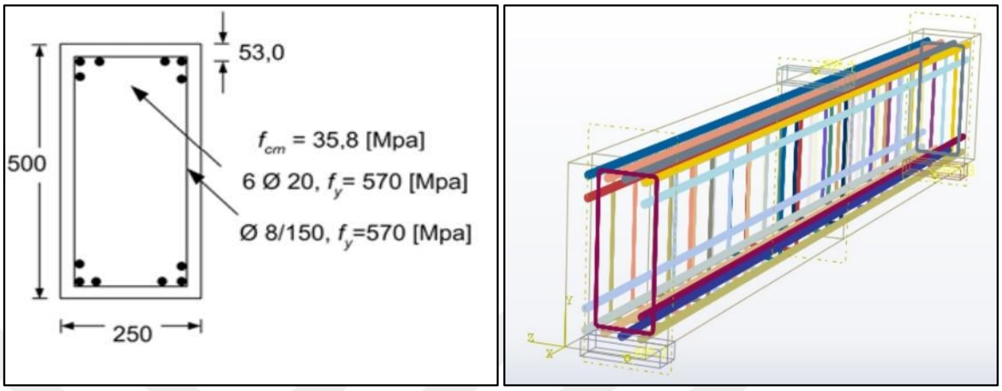

Figure 4.1 Reinforced concrete beam details, Mark 2004[57]

CDP parameters were used in three points bending FE simulation for Marks beam in table below:

Table 4.1 CDP plasticity parameters for Mark sample

Dilation angle	Eccentricity	fb_0/fc_0	k_c	Viscosity
45^O	0.1	1.16	0.67	0.0005

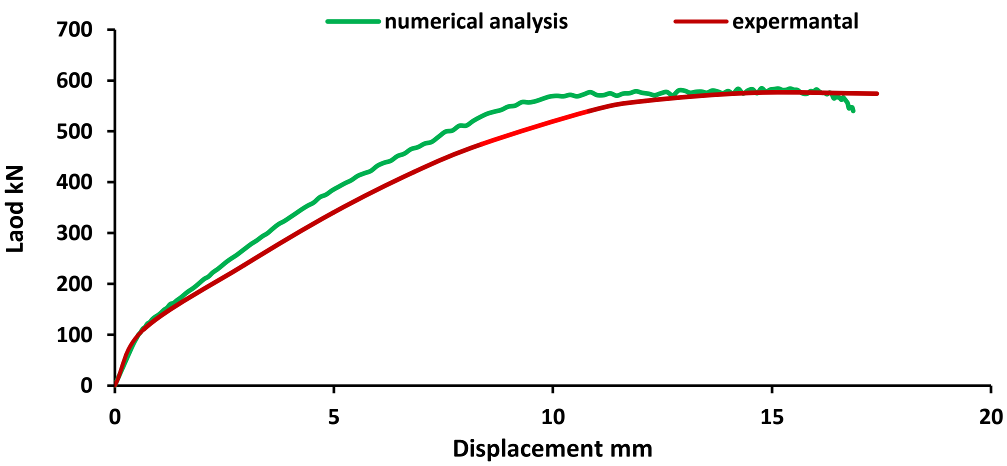

Figure 4.2 FE analysis and experimental load-displacement curve of Mark reinforced concrete beam

It's obviously, the initial stiffness of the numerical analysis increased due to several factors, such as the fracture mechanism, ABAQUS deals with concrete as a homogenous material, it's difficult to know and simulate exact loading, support, internal friction, contact conditions of field test samples, virtual stress-strain relationships, and assumed damage and plasticity behavior. The deviation between FEA and experimental results were about 1.75% of the peak load and 12% of the initial stiffness.

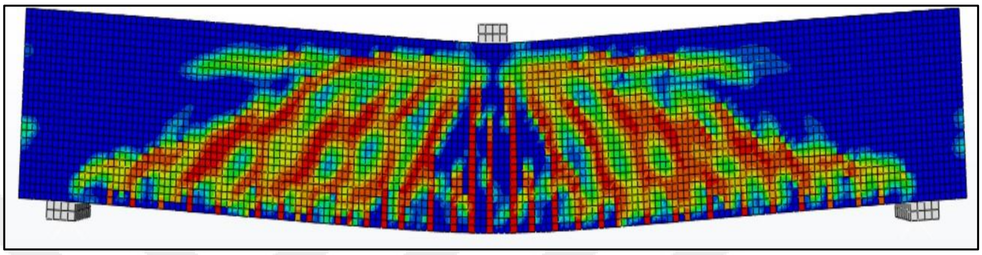

Figure 4.3 Tensile damage distribution of Mark reinforced beam

The second validation was (Toonoenthong, K. Maekawa, 2005)[58]. Three-point bending simply supported reinforced concrete beam with a 250*350 mm cross section and an effective length of 2000 mm, a total length of 2400mm, a compression strength of 35 MPa, the tension strength = 2.8 MPa. boundary conditions, the first support with Uy = 0, and the other Uy = Ux= 0 reinforced longitudinally by 8ϕ19 mm, yield steel stress = 654 MPa, laterally used ϕ6 mm@100 mm with yield stress = 345 MPa. Tensile stress impeded here calculated based on EN1992(2004) Eurocode 2, and Wang (16,17). It was based on the Eurocode2 equation above to estimate the modulus of elasticity for the Maekawa beam, where E=32000MPa, Poisson's ratio is 0.18.

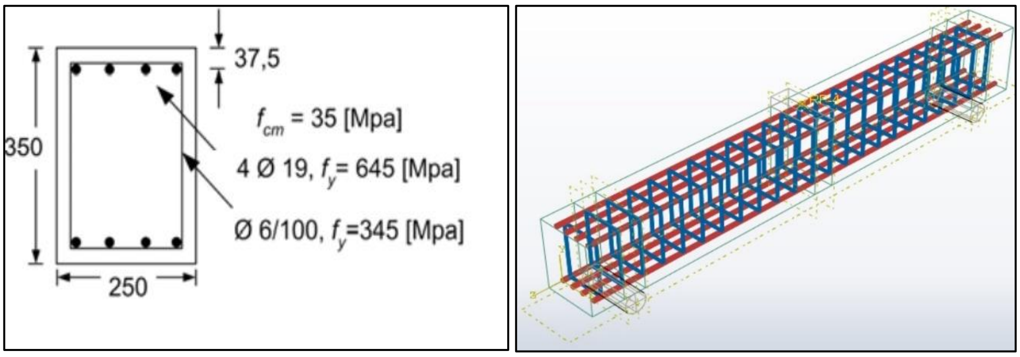

Figure 4.4 Reinforced concrete beam details, Maekawa 2005[58]

Dynamic explicit finite element analysis with C3D8R linear brick 3D element type and mish size 6*8*8 mm with 560522 brick elements were based on carry out this verification and the simulation results were compared with the experimental load-deflection curve in mid-span. The parameters of concrete damage plasticity were used to achievement this validation.

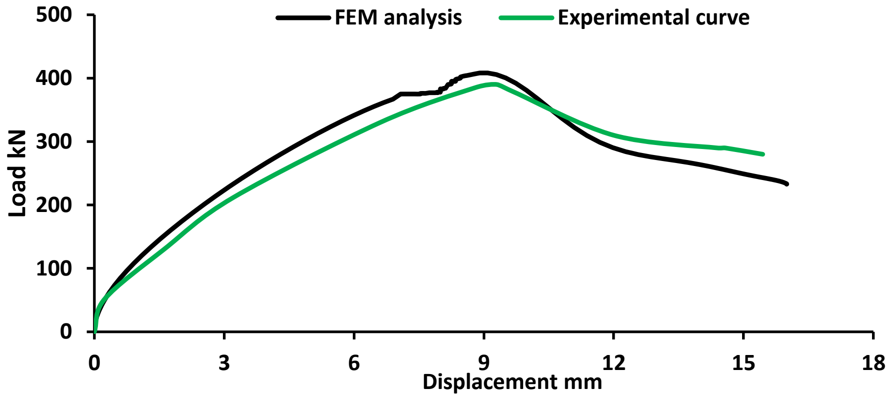

Figure 4.5 FE analysis and experimental load-displacement curve

Table 4.2 CDP plasticity parameters for K. Maekawa, 2005

Dilation angle	Eccentricity	fb_0/fc_0	k_c	Viscosity
45°	0.1	1.16	0.67	0

The figure (4.5) above shows FE simulation and empirical load-deflection curve in mid span, , the former has the same behavior as the Maekawa curve, but it has a higher initial stiffness due to the same reasons illustrated above and a deviation about 2%, 10%, the peak load and initial stiffness, respectively.

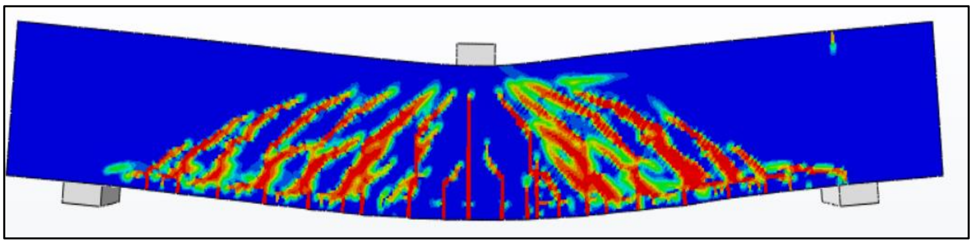

Figure 4.6 Tensile damage distribution of Maekawa reinforced beam

4.3 Finite Element Validation of Empirical Specimens

4.3.1 General Samples Features

Mostly, empirical specimens have been adopted in this thesis a square column (457*457mm), length = 2946 mm, reinforced longitudinally with 8 bars and laterally with ϕ10 mm @ 457 mm, connected to fix-fix two upper and lower pedestals 2460*700*775 mm measured as fit scale from Lynn[7] denoted by many series of symbols, the first style with 3% refer to ϕ32mm, and the another 2% with ϕ25mm, as a diameter of longitudinal rebar respectively, where the longitudinal steel ratio calculated from equation below:

$$\text{Steel ratio}=\frac{\text{No.bar}*\text{area of bar}}{\text{Ag column}}$$

The symbol "C" refers to continuous longitudinal steel bars to upper and lower pedestals, and " L, M" indicate to loading pattern (either light or moderate). It was calculated according to equation below:

LL= 0.12.Ag.fc′

ML=0.35.Ag.fc′

Where: LL: axially applied light load, ML: axially applied moderate load N, Ag: cross sectional area of column =208849 mm^2, fc′: compression resistance 20.68 MPa, was based for each sample to compute axial load," H" hoop stirrups, , and tie spacing 457 mm. All longitudinal bars with grade 40 and ties with grade 60.

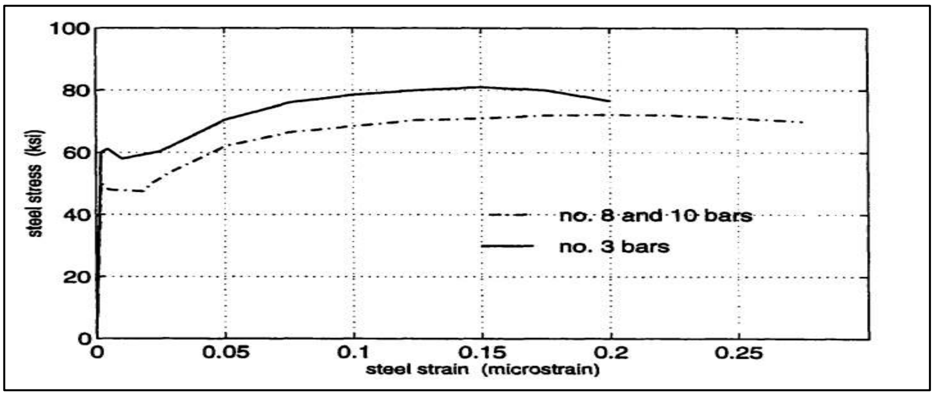

Figure 4.7 Tested longitudinal and ties bars tension stress-strain[7]

The stress-strain curve obtained from the tensile field test as figure (4.7), which shown the stress-strain curve of steel from empirical tests. ABAQUS defines steel bars as an elastic-plastic materials with Young's modulus of 200000 MPa, and Poisson's ratio of 0.3. The yield stress and corresponding plastic strain within the plastic branch are adopt from the figure above as follows:

Table 4.3 FEA yield stresses and plastic strain of reinforcement

Longitudinal bars		**stirrups**	
Yield stress MPa	Plastic strain	Yield stress MPa	Plastic strain
330	0	413	0
420	0.05	482	0.05
462	0.1	537.8	0.1
482	0.15	540	0.12
510	0.2	550	0.15

4.3.2 Validation of 3CLH18 Specimen

ABAQUS software was used to simulate the above model based on concrete damage plasticity theory which indicated in chapter 2, constitutive models in compression, tension, and damage conditions. The experimental results of the field test for specimen 3CLH18, which used to generate the stress-strain relationship illustrated in chapter 3, shown below:

Table 4.4 Proprieties of 3CLH18 experimental specimen

Compression stress MPa	Tensile stress MPa	Modulus of elasticity MPa	Longitudinal bar diameter mm	Tie diameter mm	Cover thickness mm
26.89	2.64	23718	ϕ 32	ϕ 10	37

To satisfy empirical fixed-fixed connection for each specimen, boundary conditions were fully restricted for lower pedestal by (ENCASTRE $Ux = Uy = Uz = URx = URy = URz = 0$), and the upper pedestal was restricted in the X-direction to prevent displacement and rotation in the X-axis ($Ux = URx = 0$), and permit movement in the Z-axis which is direction of applied the lateral load, the figure below show boundary conditions for all samples:

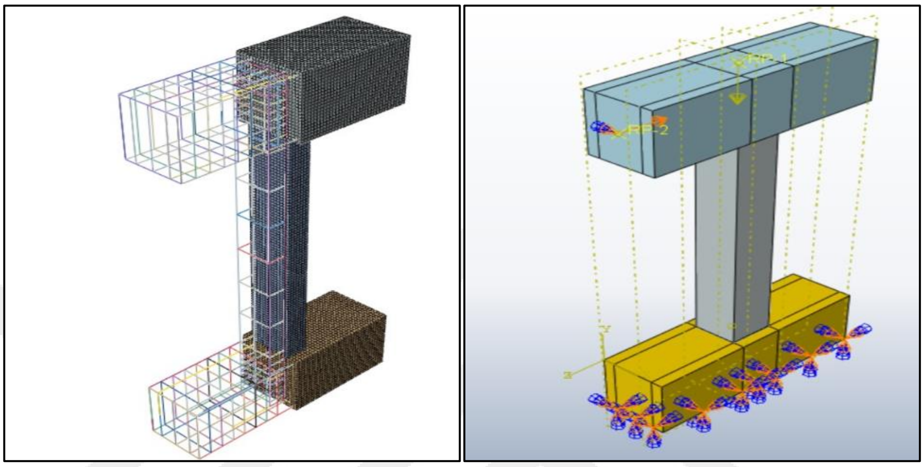

Figure 4.8 Boundary conditions of embedded steel assembly

ABAQUS dynamic explicit FE analysis (central difference analysis) was conducted on 124063 C3D8R 8-node linear brick 3D element divided into 234091-time increments, exposed to a light axial load of 518.28 KN, lateral displacement condition in the Z- axis = 60 mm, and compared results with 3CLH18 back-bone test feedback to reach same behavior of them. The parameters of CDP were embedded in this verification as below:

Table 4.5 CDP plasticity parameters for 3CLH18 specimen

Dilation angle	Eccentricity	fb_0/fc_0	k_c	Viscosity
20^{o}	0.1	1.16	0.67	0

Clearly, from the figure (4.9), FEM captures mostly the proprieties of the tested specimen in a general manner, initial stiffness, peak load capacity, and ductility. When the crack strain reaches value of 0.00055, corresponding to 48% tension damage, column will lose half of its tensile resistance of 1.44 MPa.

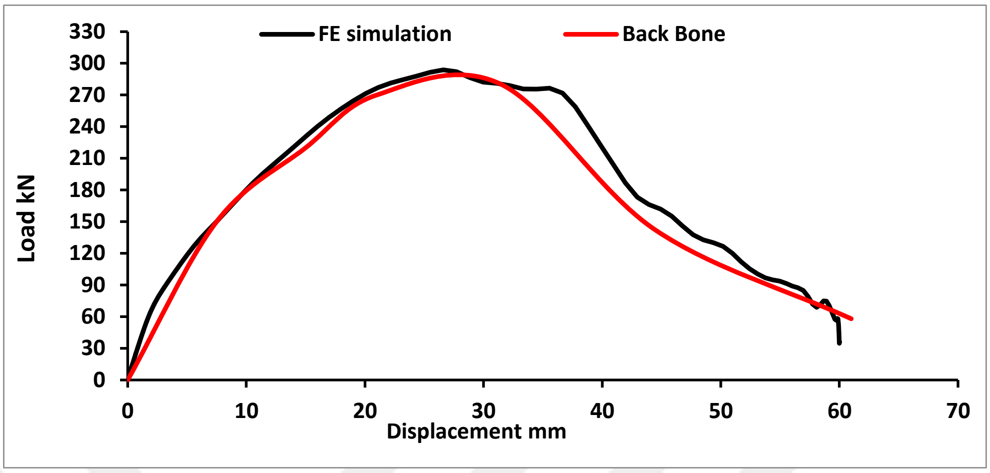

Figure 4.9 FE simulation and tested 3CLH18 load-displacement

After that, both compression and tension damage reached to 90 %, the column will lose its whole capacity, and become cracks deeper and developed in diagonal direction as shear spalling in the Y-Z plan (parallel to lateral applied displacement), It obviously appears cover cracks in the top plastic hinge zone at figure (4.10) which is compatible with field test results as shown below:

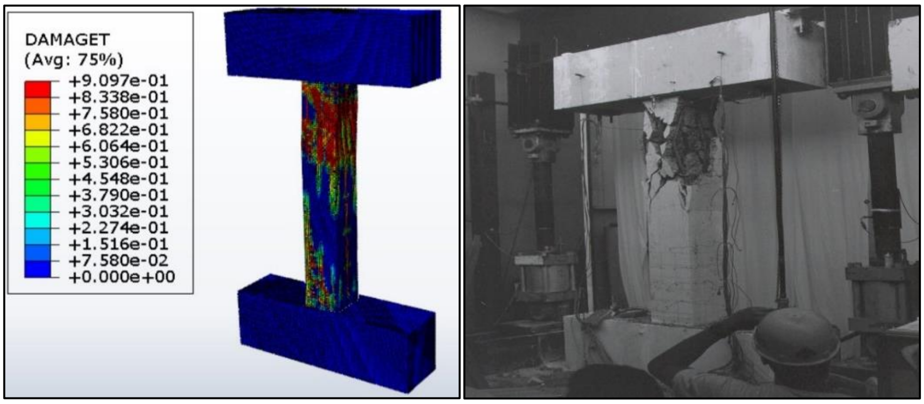

Figure 4.10 FEM cover spalling and loss all axial-load capacity of 3CLH18

Distinctly, both empirical and FEM have the same mechanism of failure start with horizontal cracks, then evaluate to diagonal cover spalling (due to shear force) after reaching stirrup steel to yielding in the top of the column (plastic hinge) and losing most of the load capacity. To ensure that there is no mass excitation, minimum velocity, and moment of inertia inside FEM analysis to garneted stability of dynamic explicit feedbacks, the checking of kinetic energy should be so small as not exceed 5%-10%, of the internal energy (static and plastic energy) according to ABAQUS Manual[59], the kinetic energy was 0.33% of internal energy, which is good evidence of the stability and reasonability of the analysis results.

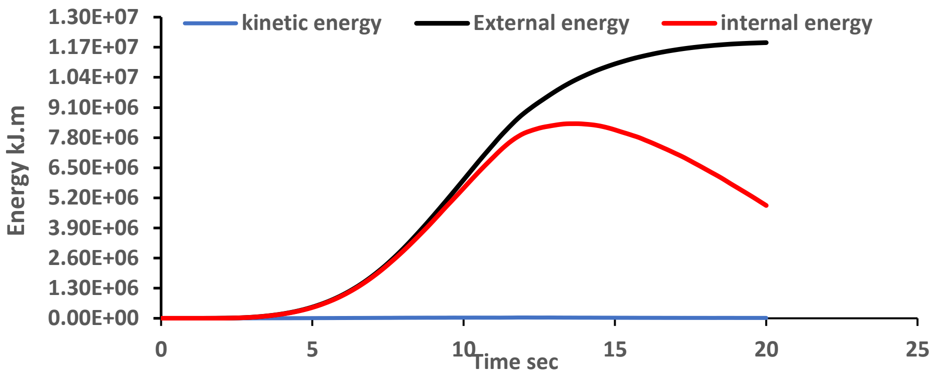

Figure 4.11 Comparison kinetic, internal and external energy of 3CLH18

4.3.3 Validation of 2CLH18 Specimen

Generally, the dimension characteristics and FE boundary conditions of this model similar the former except longitudinal steel with 2% (ϕ25mm), compression and tension test values which are adopt to consist stress-strain curve and based on constitutive models summarize as below:

Table 4.6 Proprieties of 2CLH18 experimental specimen

Compression stress MPa	Tensile stress MPa	Modulus of elasticity MPa	Longitudinal bar diameter (mm)	Tie diameter (mm)	Cover thickness (mm)
33	2.82	25650	ϕ 25	ϕ 10	37

Dynamic explicit FE analysis conduct for 2CLH18 verification with 124063 C3D8R 8-node linear hexahedral (brick) 3D element divided into 233561-time increments, and 2-node truss elements (T3D2) for steel embedded bars, exposed to light axial load=518.28 KN, lateral push over condition in the Z- axis = 90 mm, and the results compared with 2CLH18 back-bone test feedbacks reach to the same behavior. Concrete damage plasticity parameters are adopt in the ABAQUS simulation as follows:

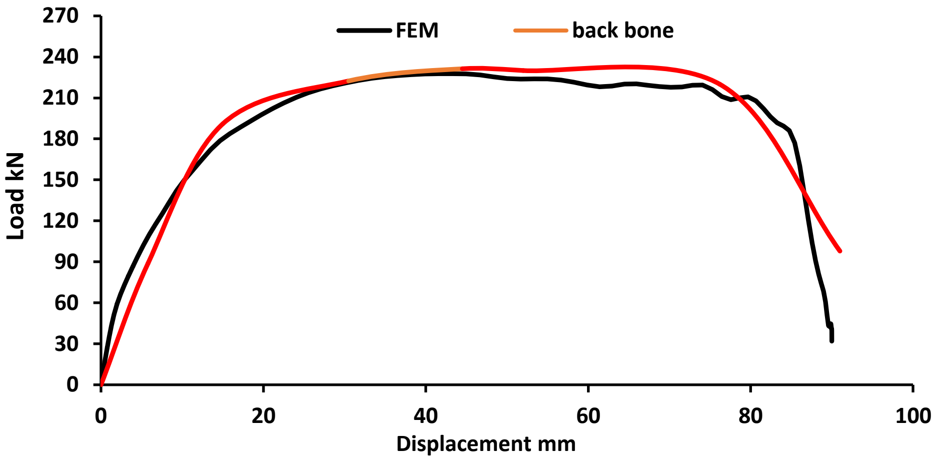

Figure 4.12 FE simulation and experimental 2-CLH18 back bone curve

Table 4.7 CDP plasticity parameters for 2CLH18 specimen

Dilation angle	Eccentricity	fb_0/fc_0	k_c	Viscosity
30°	0.1	1.16	0.67	0.0005

Two curves ensures they have same behavior, ductility, and little bit increased initial stiffness of FEM due the same causes illustrated in Article 4.2. The deviation about 4.1%,12%, the peak load capacity, and the initial stiffness, respectively. When the crack strain reaches value of 0.00055 corresponding to 50% tension damage, column will lose half its tensile resistance, which is of 1.3 MPa. After that, the concrete compression strength reached, the plastic stage and compression damage at inelastic strain of 0. 00093.

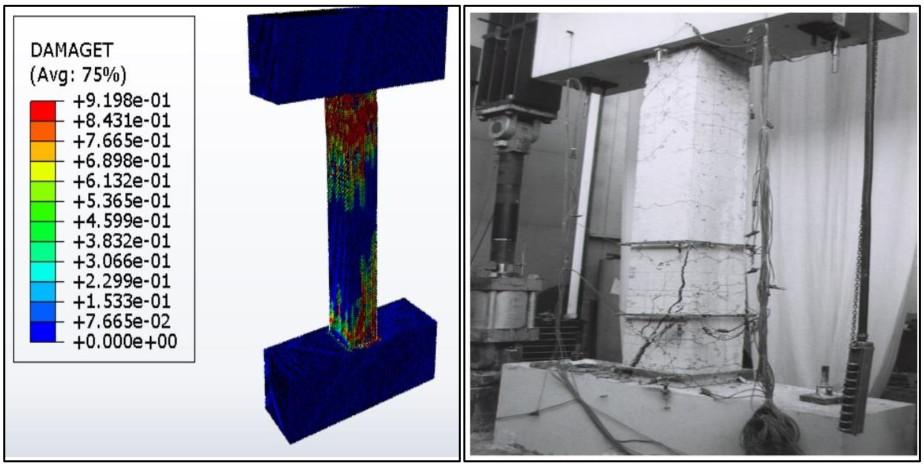

Figure 4.13 FEM verification of 2CLH18 experimental specimen

Clearly, after applied axial and lateral displacement start cover cracking pattern (X-Y plan) perpendicular to the +Z axis; these cracks began horizontally at the top and bottom of the column (plastic hinge zone), then, as a result of rising external applied load, led to propagated diagonal cracks. After reaching 90% damage in tension and compression and yielding tie steel bars, these cracks simultaneously led to spalling cover on the same side of applied lateral displacement because increasing this value to 90 mm caused crushing failure, while opposite side under diagonal shear cracks due to increasing compressive strength. It's obviously showing diagonal local crack at the bottom of plastic hinge due to inadequate transverse steel. The stability of the analysis feedbacks checked by ensuring that the kinetic and internal energy are as shown below. The kinetic energy was 0.15 % of internal energy, which confirms there is no mass excitation and little inertia force in FEM.

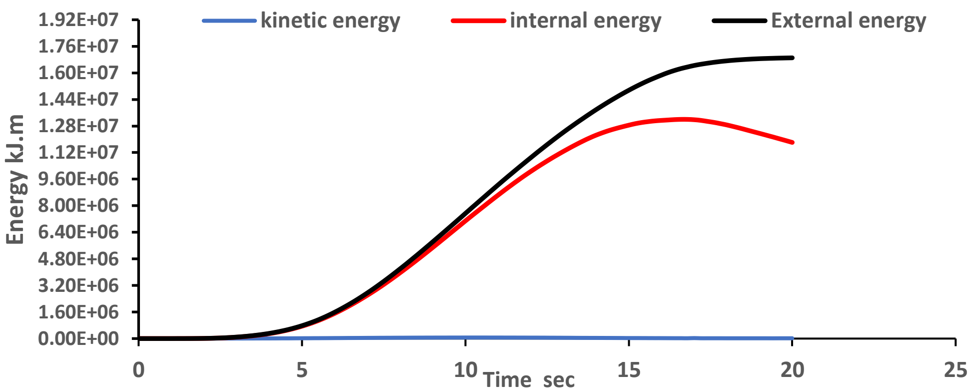

Figure 4.14 Comparison kinetic, internal and external energy of 2CLH18

4.3.4 Validation of 3CMH18 Specimen

The mechanical properties of the model obtained from field tests, which are adopt to consist of a stress-strain curve and based on constitutive models as illustrated in chapter 3, that's summarized as below:

Table 4.8 Proprieties of 3CMH18 experimental specimen

Compression stress MPa	Tensile stress MPa	Modulus of elasticity MPa	Longitudinal bar diameter mm	Tie diameter mm	Cover thickness mm
25.74	2.36	23580	ϕ32	ϕ10	37

It's subjected to a moderate axial load of 1512 KN, maximum lateral displacement of 60 mm in the Z-direction. Dynamic explicit FE analysis conducted 3CMH18 verification with 15361 C3D8R 8-node linear (brick) 3D element divided into 111136-time increments, and 2-node truss elements (T3D2) for steel embedded bars;

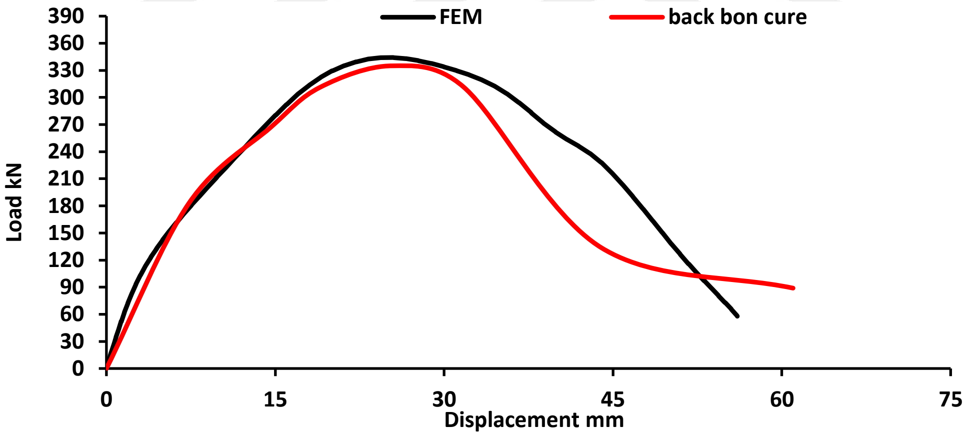

Figure 4.15 FE simulation and experimental 3CMH1

Concrete damage plasticity parameters are adopt in the ABAQUS as follows:

Table 4.9 CDP plasticity parameters for 3CMH specimen

Dilation angle	eccentricity	fb_0/fc_0	k_c	Viscosity
30	0.1	1.16	0.67	0.0005

At all events, the above two curves have a very close demeanor, approximately typical initial stiffness, peak load capacity, and displacement corresponding to them, but FEM has a slopping less than the empirical curve in the softening stage, which gives more ductility in these branches. The deviation 2.9%,6%, the peak load capacity, and the initial stiffness, respectively. When the cracking strain reaches a value of 0.00055, corresponding to 51% tension damage, column will lose half its tensile resistance of 1.15 MPa. After the concrete reached to compression strength, the plastic stage and compression damage were started at inelastic strain = 0.001.

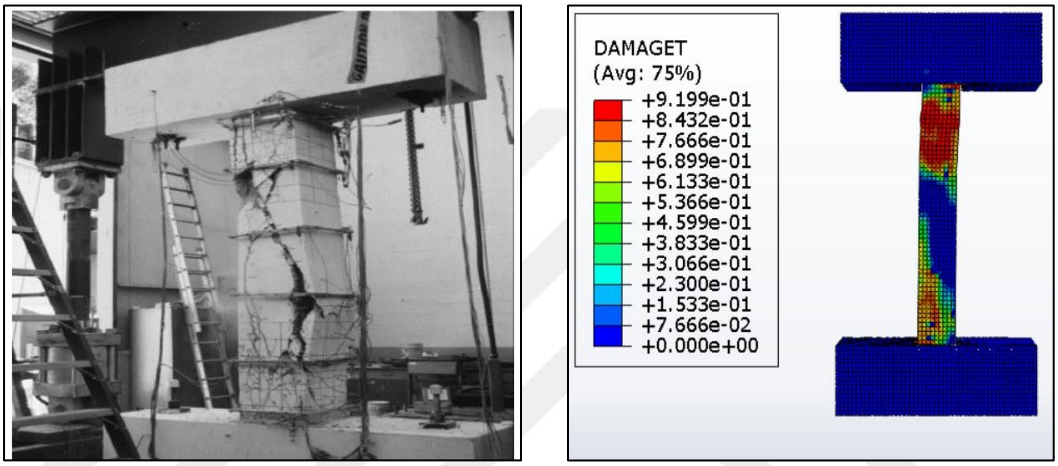

Figure 4.16 FEM ,3CMH18 experimental specimen

After applying external loading horizontal cracks appeared at the top and bottom connecting region between the column and pedestal when lateral displacement was 15.5 mm, then transformed to inclined cracks at the displacement of 31mm due to shear force combination to tension force in the plastic hinge zone, cover spalling, local cracks, steel buckling it will be happening then column loss capacity load at the displacement of 60 mm. It wasn’t clear because FEM has more ductility than empirical specimen in the softening branch. The Stability of analysis results is checked by ensuring that the kinetic and internal energy as shown below. The kinetic energy was 0.06 % of internal energy less than 5%-10%, that’s deduced there is no mass excitation and little inertia force inside FEM.

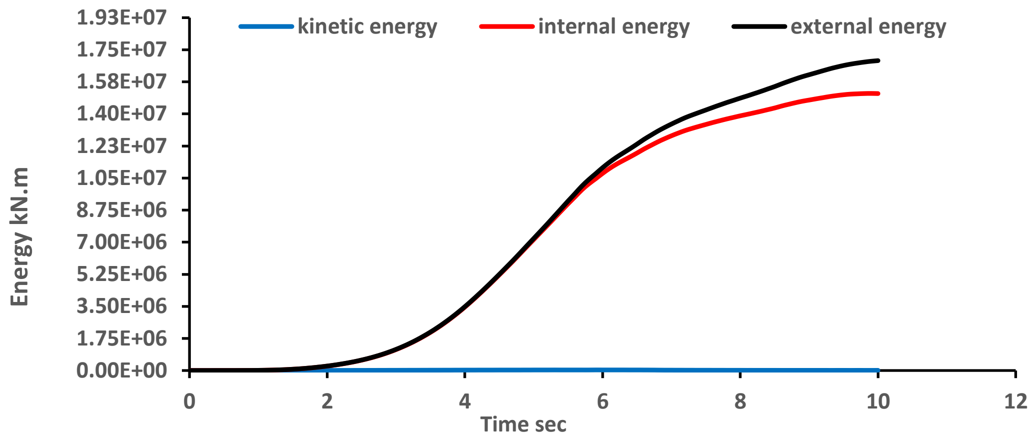

Figure 4.17 Comparison kinetic and internal and external energy of 3CMH18

4.3.5 Validation of 2CMH18 Specimen

This model has the same dimensions and boundary conditions as the other above models. It has the following mechanical properties, which were obtained from laboratory tests in tension and compression with respect to Lynn[7], this information used to construct a stress-strain curve to define yield stress, inelastic strain, tension, and compression damage in various loading stages:

Table 4.10 Proprieties of 2CMH18 experimental specimen

Compression stress MPa	Tensile stress MPa	Modulus of elasticity MPa	Longitudinal bar diameter mm	Tie diameter mm	Cover thickness mm
27.65	2.75	23994	ϕ25	ϕ10	37

It's exposed to a moderate axial load in the y-direction of 1512 KN, lateral displacement of 31 mm in the Z-direction. Dynamic explicit FE analysis was employed for 2CMH18 verification with 124063 C3D8R 8-node linear brick 3D element divided into 207915-time increments, 2-node truss elements (T3D2) for steel embedded bars, compare the results with 2-CMH18 tested back-bone feedbacks reach to the same behavior.

Table 4.11 CDP plasticity parameters for 2CMH18 specimen

Dilation angle	Eccentricity	fb_0/fc_0	k_c	Viscosity
30°	0.1	1.16	0.67	0.0005

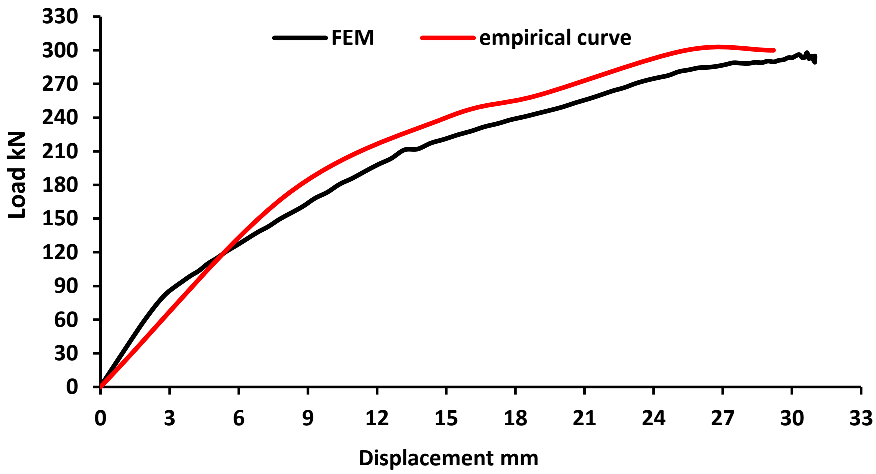

Figure 4.18 FE simulation and experimental 2CMH18

The comparison between the above two curves confirmed they have the same behavior, ductility. A little bit an increase in the initial stiffness of FEM reached to displacement 5mm, and after that, FEM stiffness started to decrease related to chosen 3D mesh size 25 mm, but when taken at 50 mm, mesh size led to an increase FEM stiffness and ductility as well. Because the tested curve has high ductility. So this study based on FEM gives reasonable of simulation results. The deviation 3.4%,16%, the peak load capacity, and the initial stiffness respectively. When the crack strain reaches a value of 0.00055, corresponding to 49% tension damage, column will lose more than half of tensile resistance, which is = 1.41 MPa. After reaching the concrete compression strength, the plastic stage and compression damage at inelastic strain reaches 0.0011. Obviously, horizontal cracks speared at top and bottom (plastic hinge zone) after applied external loads.

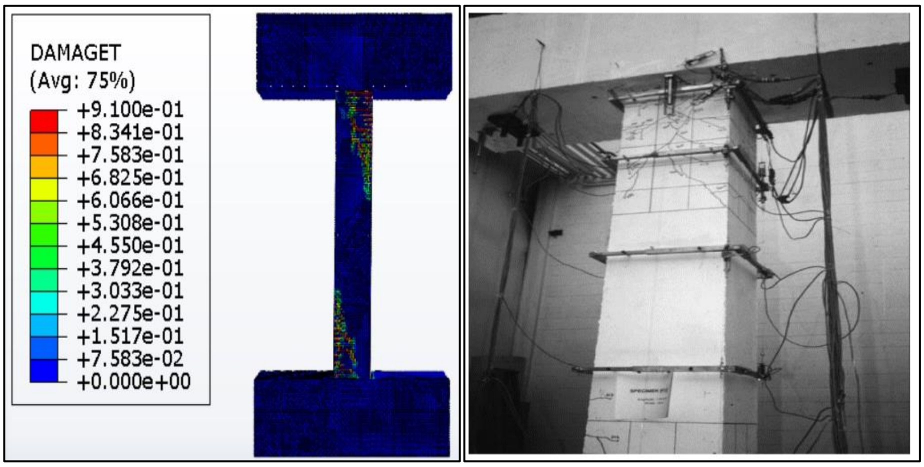

Figure 4.19 FEM ,2CMH18 experimental specimen

The stability of the analysis results checked by ensuring that the kinetic and internal energy as shown below. The kinetic energy was 0.05 % of the internal energy less than 5%-10%,[59], that's why it's deduced there is no mass excitation and little inertia force inside FEM.

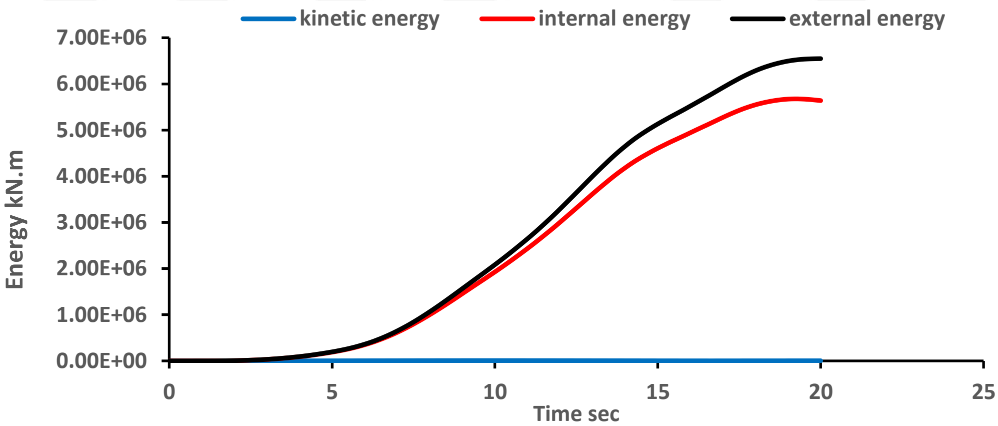

Figure 4.20 Comparison kinetic and internal and external energy of 2CMH18

4.3.6 ECC Model Validation

This study based on Fang Yuan e.al. ECC stress strain curve of 100-mm diameter, and 200-mm height, cylinder compression strength of 49.6 MPa, peak tension stress = 5.17 MPa, modulus of elasticity = 18500 MPa, Poisson's ratio = 0.2. The general behavior of ECC concrete in compression is similar to that of normal concrete, except the former has doubled strain corresponding to peak compression strength. It has a significant tension-hardening branch with high tension strain, which leads to increased ECC deformation ability with multiple distributed cracks. The article discussed a new simplified constitutive model with suggested equation to represent ECC in tension and compression, then use CDP theory and the plasticity parameters of ECC finite element model which will use to conduct ECC retrofitting a above RC columns as table below:

Table 4.12 CDP plasticity parameters of ECC

Dilation angle	Eccentricity	fb_0/fc_0	k_c	Viscosity
45^O	0.1	1.16	0.67	0.00045

Dynamic explicit FEA employed to verify ECC sheet behavior with dimension (350*50*15) mm subjected to 18 mm uniaxial tension displacement in the y- direction and lock all motion and rotation in each other sides, 2100 C3D8R 8-node linear (brick) 3D element, with (5*5*5 mm) mesh size compare results with empirical yang's test feedbacks, due to high resistance of ECC against deformation that's led to increase interior friction angle (45°).

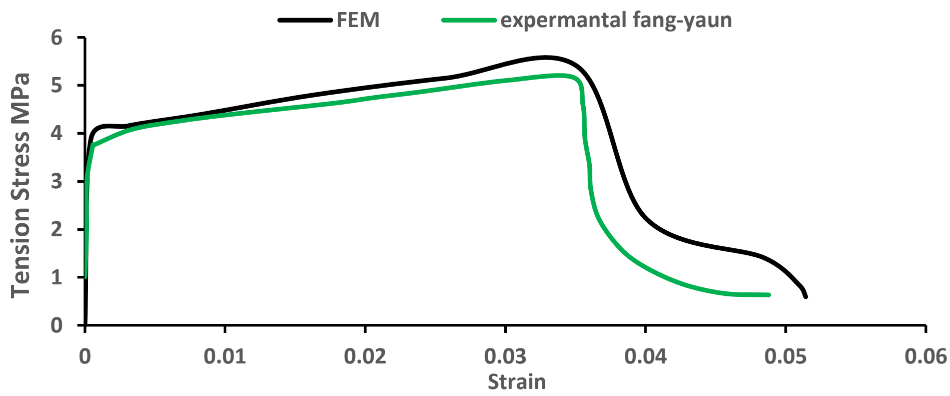

Figure 4.21 FEA of yang's specimen in tension

been hardening stiffness more than Yang's curve; peak tension stress at strain 0.033,0.035 for FEM, Yang's curve, respectively, with a deviation of 6.2%. Maximum tensile load 5.4, 5.17 MPa for FEM, empirical curve, respectively, with a deviation of 4.4%. FEM has softening branch with more ductile failure than Yang's curve. Each curve lost about 90% of tension resistance. It can be a good agreement with general behavior of empirical test result.

4.4 Investigation of CDP Parameters

At the outset, it is a significant matter to calibrate the CDP parameters of all models to reach the right behavior of them. The essential issue is that about most empirical studies didn't show any calculations related with interior friction angle, and eccentricity of applied load, maybe there is no compatibility between the rate of applied loads for field test and FE analysis (viscosity), so it will be important to investigate rational values to capture the correct behavior of RC column. The strategy follows two sides, the first was to change dilation angle, and constant other parameters, the second was to change viscosity values and study the effect of these factors on specimens. Consequently, it was choosing logical parameters for each sample and then conducting mesh size sensitivity to find out the effect of mesh size on load-deflection response as shown below. It is lucid effect of dilation angle on general manner of FEM privately softening part, it was observed when increase DI increase peak load-displacement response, ductility due to rise internal friction resistance of members except 2CMH18 due to exposed to small applied displacement, where all DI value get approximately same response of elastic branch only as figures below:

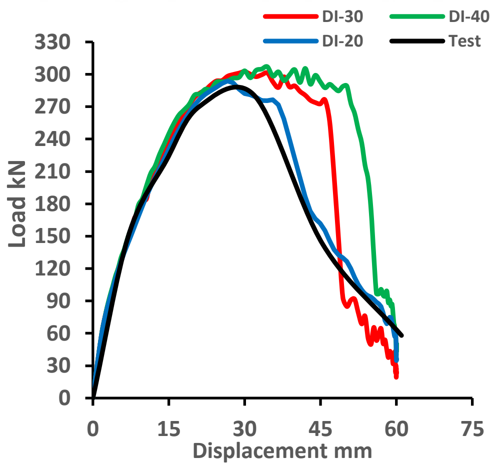

A

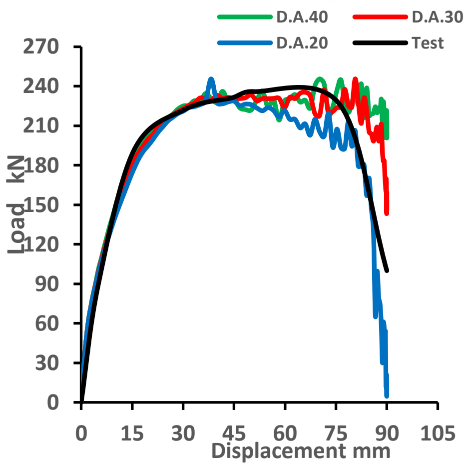

B

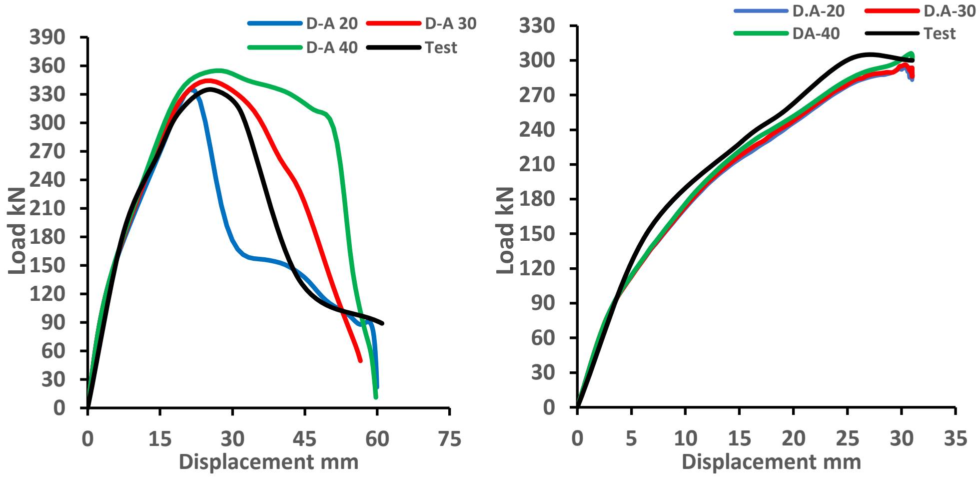

C D

Figure 4.22 Investigation dilation angle of FEM(A) 3CLH18 (B) 2CLH18 (C) 3CMH18 (D) 2CMH18

The second factor that should be calibrated carefully is the rate of applied external loads and their various effects with actual tests, degree of support restrained, perfect ABAQUS reinforced bond effect directly on failure mode of models. Figures below shown all elastic parts of load response weren't affected by change in viscosity.

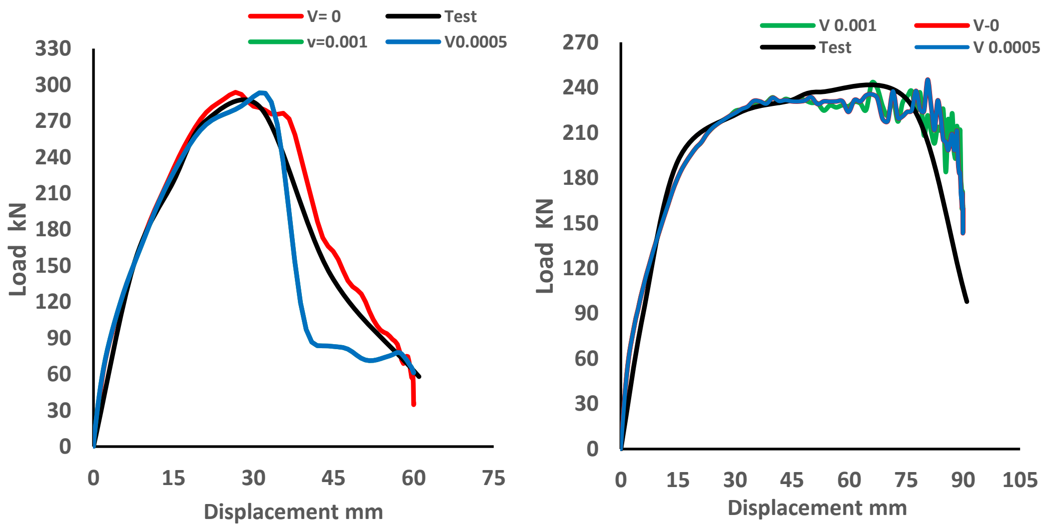

A **B**

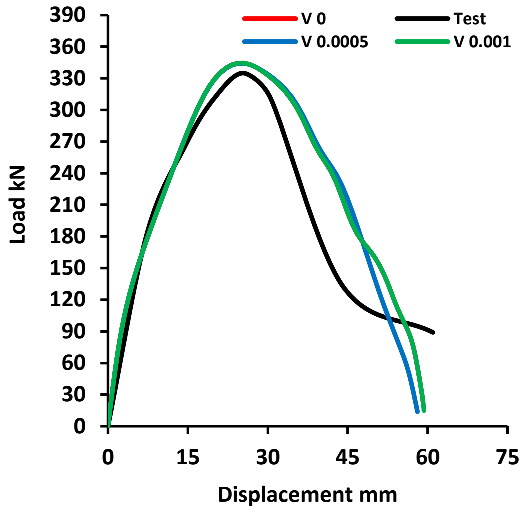

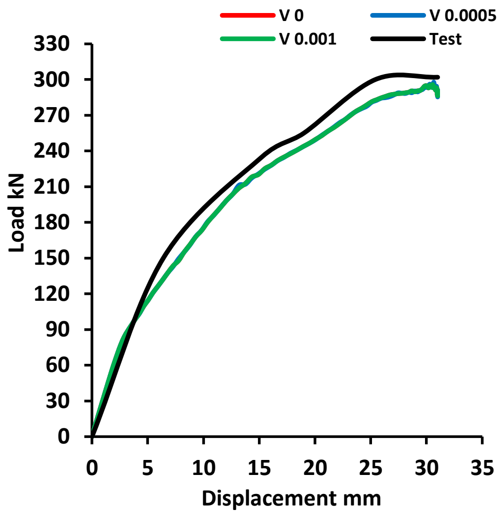

C D

Figure 4.23 Investigation viscosity of FEM (A) 3CLH18 (B) 2CLH18 (C) 3CMH18 (D) 2CMH18

Plastic branch behavior acted by change rate of loading because high nonlinearity of concrete models a, b, and c under biaxial loading, where increase viscosity value led to get a pseudo and steep softening failure, so it should be chosen it carefully, this thesis based on multi-try analysis by constant all parameters, material properties, boundary conditions except viscosity to calibrate a right empirical manner curves

4.5 Mesh Sensitivity

It considers a crucial rule for getting adequate FE analysis in ABAQUS, where it depends on appropriate mesh size and shape of the 3D brick element. This section exhibits three mesh sizes, fine, medium, and coarse 25, 50, 75 mm, respectively, with uniformity hex. Element shape. The result of finite element simulation refers to that good convergence Lynn's models (3CLH18, 3CMH18) in elastic part, but mesh size highly effect on softening branch due to large nonlinearity, not always fine mesh size gives an accurate result because it didn't agree with other computational aspects as 3CMH18 model.

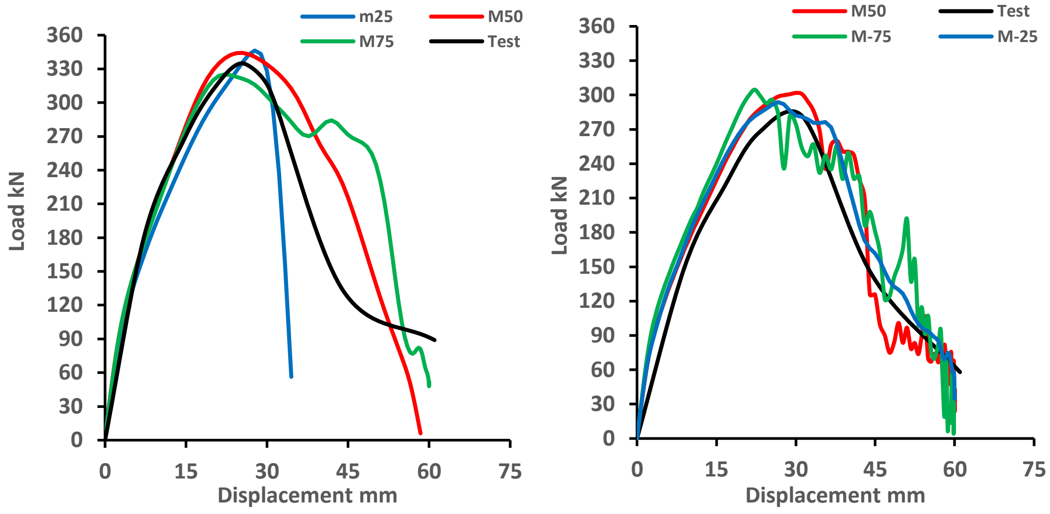

A B

Figure 4.24 Mesh sensitivity of (A) 3CLH18 specimen, (B) 3CMH18 specimen

CHAPTER 5

FINITE ELEMENT SIMULATION OF JACKETED RC COLUMNS

5.1 Overview and Research Significance

Foremost, many studies focused on strengthening and retrofitting structural members because it has a unique approach to improve general structural performance, ductility, general failure style, load and deformation capacities to resist seismic risks, inadequate design capacity, ageing, deterioration of offshore structures by weathering and erosion, saving cost and construction time. Columns were the most important parts of construction benefited from strengthening due to their highest effect by the above deterioration reasons and attributed it most structural stability [60]. The last two centuries have included a lot of research about many strengthening ways with different proportions such as (57% external bond FRP), (19% hybrid jacketing), (12% concrete jacket with various configurations), and (7.8% steel jacket)[10]. Zhang et al.[61] expressed the ECC-polypropylene matrix will be rise shear capacity of beams (20.6%, 107%) for beams without ties and with lateral steel bars, respectively. Few studies have investigated this topic, so this thesis focused on conducting a numerical analysis of RC column jacket with engineering Cementous composite concrete to overcome concrete weakness points such as ductility and seismic resistance [63].

5.2 Methodology

This study adopts FE analysis for two different strategies to simulate ECC concrete jackets and compared with empirical results. The first strategy included 50 mm thickness of ECC jacketing directly connected with, columns cover to simulate strengthening the column capacity in situations of old buildings, and the other strategy includes replacing the damage cover of RC columns with the same thickness of ECC cover to remedy the high damage region in tested models, which concentrated in plastic hinge region at the top and bottom of columns, which is compatible with the theoretical plastic hinge length measured from the upper and lower pedestals. The FEM of jacketed specimens is denoted and displayed as shown in the table below:

Table 5.1 Description of suggested jacketed strategies

Jacket state	ECC jacketing technique	symbol	Inner size (mm)	Outer size (mm)	Thickness (mm)
jacketed layer joined with column	Whole specimen jacketed with ECC and Reinforcement	WR	457*457*2946	557*557*2946	50
	Whole specimen jacketed with ECC	W	457*457*2946	557*557*2946	50
	Top-Bottom Jacketed	TB	457*457*550	557*557*550	50
ECC jacket with replace core cover	Replace Whole column's cover	WC	383*383*2946	457*457*2946	37
	Replace Top-Bottom cover with ECC	TB-C	383*383*550	457*457*550	37

After jacketing, a cross section of column dimension is (557*557) mm, and (457*457) mm, for whole ECC jacketed, and top-bottom jacketed types, respectively. Whole ECC with steel jacketing style reinforced with 4ϕ10 mm as an additional steel bar in long direction installed in middle of the ECC layer and ϕ10 @457 mm as a stirrup as shown in the figure (5.1). All ECC jackets-original columns with (fully tie interactions). The identification of the plastic hinged region by investigators is crucial, particularly in relation to seismic modelling for RC columns. The determination of the plastic range is crucial not only for designing new members but also for fixing and improving the current members[62][63]. The length of op-bottom jacketing adopt in this study with respect to Japan standard[64]. Because it represents the safest option among all other global codes for calculate plastic hinge length, which is a provide adequate jacketed length to shear resistance as following:

L_p= 0.2H-0.1L

Where: H: Net height of column in mm, L: column base length in mm.

Lp =543 mm; for the simplicity; this study adopt (550 mm).

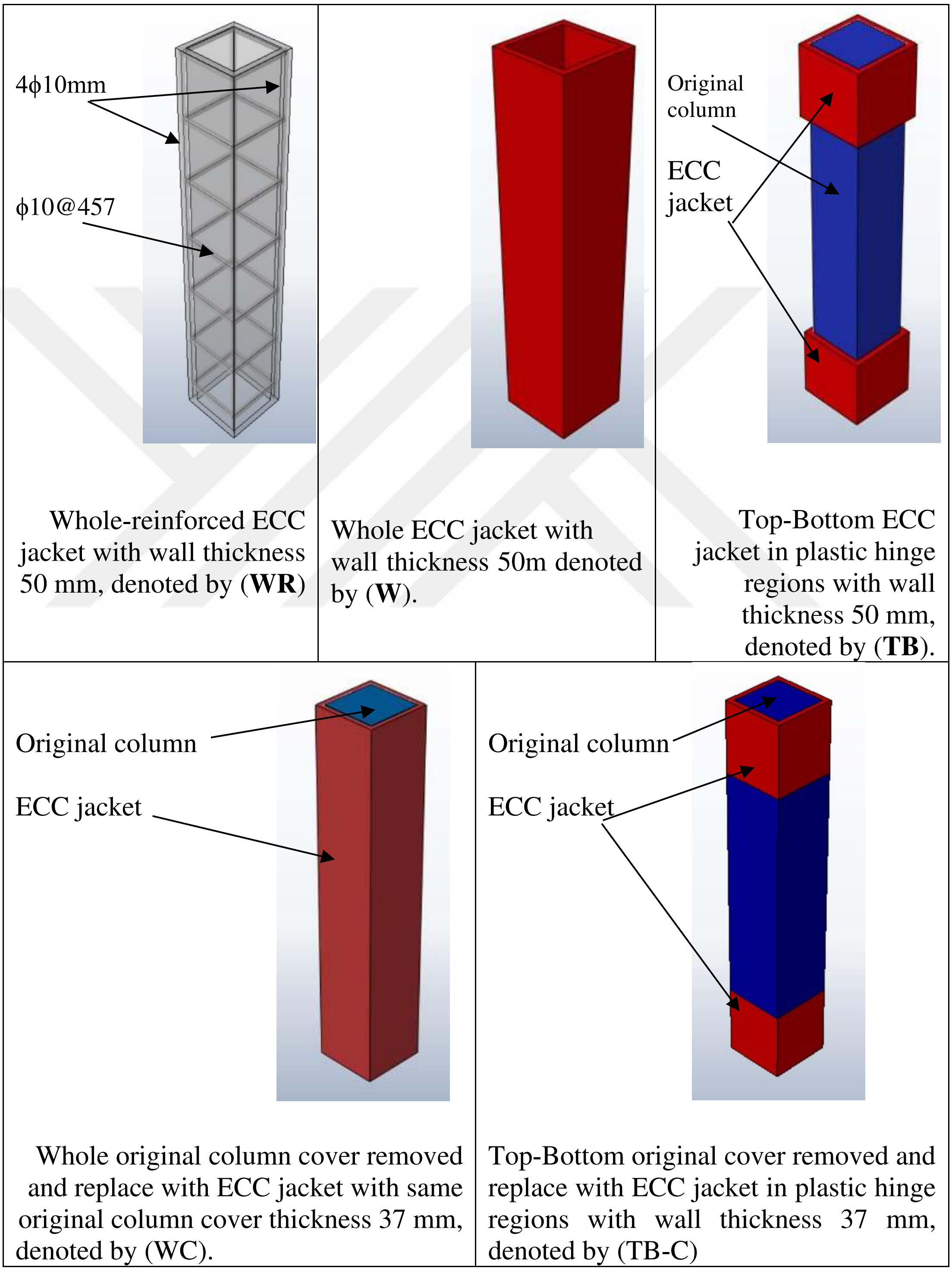

Whole-reinforced ECC jacket with wall thickness 50 mm, denoted by (**WR**)

Whole ECC jacket with wall thickness 50m denoted by (**W**).

Top-Bottom ECC jacket in plastic hinge regions with wall thickness 50 mm, denoted by (**TB**).

Whole original column cover removed and replace with ECC jacket with same original column cover thickness 37 mm, denoted by (WC).

Top-Bottom original cover removed and replace with ECC jacket in plastic hinge regions with wall thickness 37 mm, denoted by (TB-C)

Figure 5.1 Details of suggest FE jacketed strategies

5.3 Ductility and ECC Hardening Strain Criteria

This section discusses crucial terms that play a key role in the performance level of columns exposed to seismic excitations. After finite element analysis, a comparison of simulation with experimental results was achieved, especially for load-deformation response and displacement ductility (μ_δ) which was defined as the ratio of maximum displacement ($\delta_{ult.}$) to yield displacement (δ_{yield}).

$$\mu_\delta = \frac{\delta ult.}{\delta yield}$$

where, δ_u = maximum displacement corresponding to 20% of max. lateral load capacity had lost. δy = yield displacement. This study adopt failure load at the point that represents 20% loss of peak load capacity[65][66][67]. We applied lateral displacement with increments (1.25δ, 1.5δ, 2δ, 3δ, 4δ……. etc.) to capture 20% of the ultimate load drop, which make sense different from sample to other depending on the real maximum displacement of each specimen, the mechanism of retrofitting, and the hardening strain of the ECC. This work simplified the Fang yang [52]empirical data and proposed two strain-hardening values derived from the tensile stress-strain curve of Fang Yuan ECC, specifically at 1% and 3.5% strain, for both uncoated and oil-coated PVA [6]. To satisfy a reasonable result with respect to the two values of ECC hardening strain adopt here, the compression strength of ECC = 49.6 MPa, corresponding to 5.17 MPa, and 3.5 % of the hardening stress and strain respectively, because of this study, additionally based on the 1% ECC strain, it has become necessary to calculate the equivalent ECC compression strength that corresponding to 1% of the strain by making an interpolation direct relationship, which is hand over 39.6 MPa. The approach employed in this regard involves two main steps. Firstly, the random strain-hardening (ascending) is simplified into a straight line by proposing a new constitutive model. Secondly, the descending (softening branch) of Wang[47] is changed for NC in order to achieve around 90% tension damage and avoid the cessation of FEA

5.4 Finite Element Simulation

ABAQUS finite element analysis by dynamic explicit analysis (C3D8R -8 node 3D brick element type) for all (concrete core and ECC jacketing parts); all reinforcement modelled with T3D2-2 node 3D Truss element type was conducted to simulate a high nonlinearity of concrete behavior and to satisfy accurate feedback by using (the central difference equation) as shown below:

$$M\ddot{U} + C\dot{U} + KU = p(t)$$

The interactions between all kinds of ECC jacketing parts and columns were (tie bonds); it is difficult to provide these links in practice, but they were considered to have a high importance on the operation mechanism of these covering layers. The boundary conditions of the top and bottom of all jacketed samples were similar to those of unjacketed specimens, give away the simulation more rationality. To ensure the stability of FE analysis conducted with a the right path, we present kinetic energy, internal and external energy. The kinetic energy should be no more than 5%-10% of the internal energy to emphasize that there is no mass excitation inside the models

5.5 The Results of Finite Element Analysis

5.5.1 3CLH18 Specimen

This section shows the results of FE simulation that were applied various lateral displacements in Z-axis with respect to kind of jacketing, nature of materials christianistic, response of non-jacketing columns, as the displacements series illustrate in Section 5.3 a above until capture 20% of peak lateral capacity absence which based on as a failure point, the sample 3CLH18 exposed to several maximum lateral displacements denoted by ($\delta_{\mathbf{uFEA}}$) as (1.25δ,1.5δ,2δ) corresponding to (75, 90, 120)mm, where TB-C (3.5% and 1% strain) δ_{uFEA} = 75 mm, TB (3.5% and 1% strain) δ_{uFEA} = 90 mm, W,WR,WC (3.5% and 1% strain) δ_{uFEA}= 120 mm, which are compatible with type of ECC jacket as shown in the table. The column jacketing types include top-bottom with 550 mm as a plastic hinge length, whole column jacketed with and without steel by 50 mm ECC thickness, replacing whole the column cover, and top-bottom eliminating only and replacing it by 550 mm of ECC with 37 mm thickness as well. All analyzes above conduct with 3.5% and 1% hardening strains for coating and uncoated ECC, respectively. Each model's hand over a various horizontal response and mode failure because it exposed on different lateral states and developed their capacity by using ECC jackets with multi-types. The figures below shown the lateral response-deflection of FE analysis:

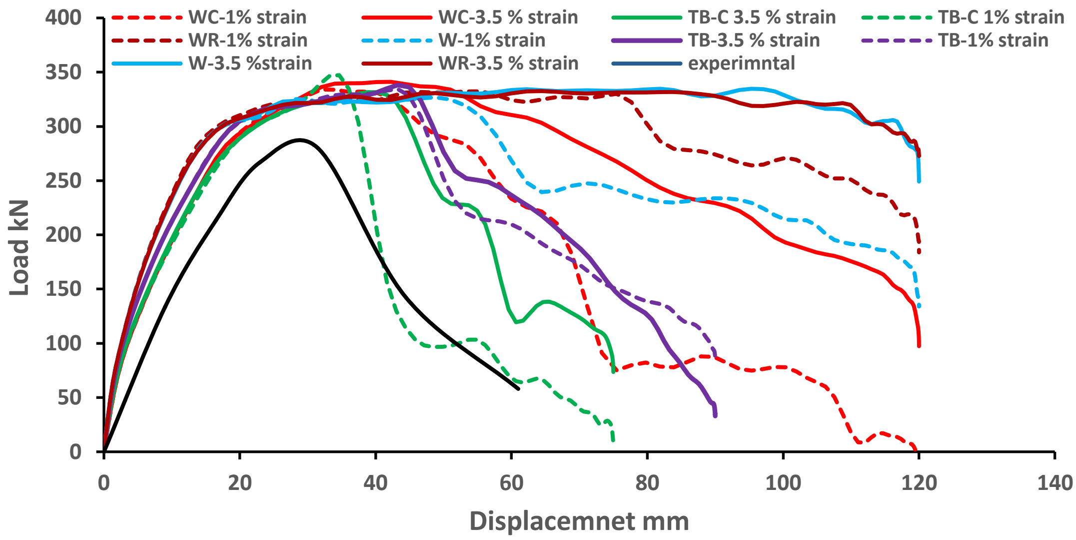

Figure 5.2 Different jacketed techniques of 3CLH18

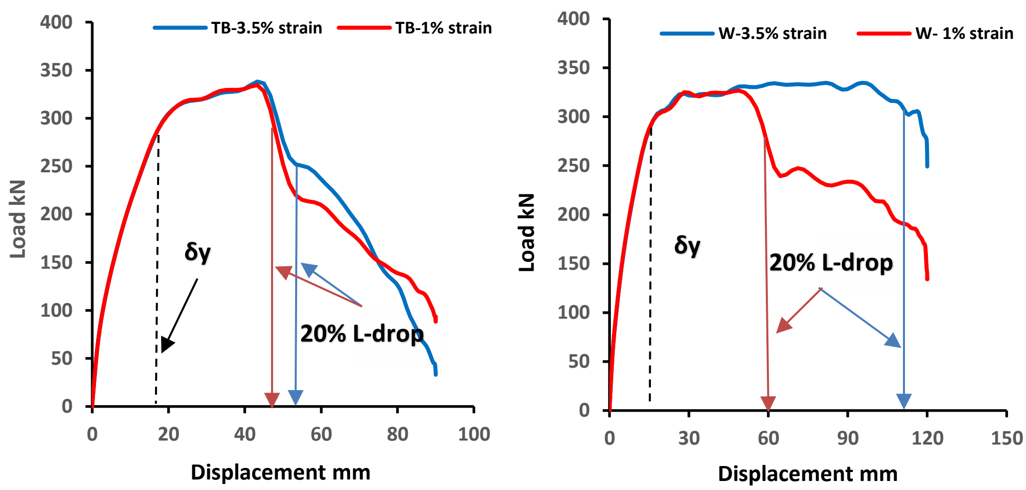

A

B

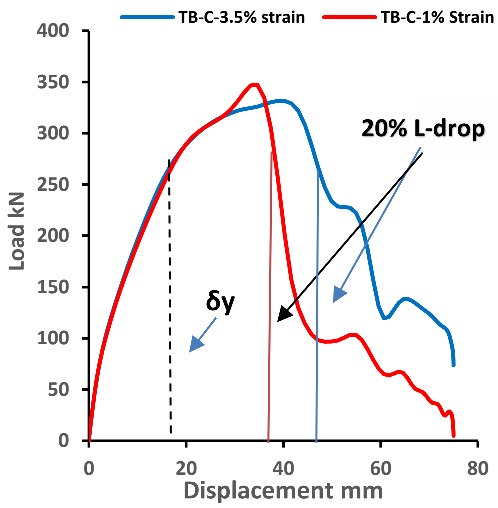

C

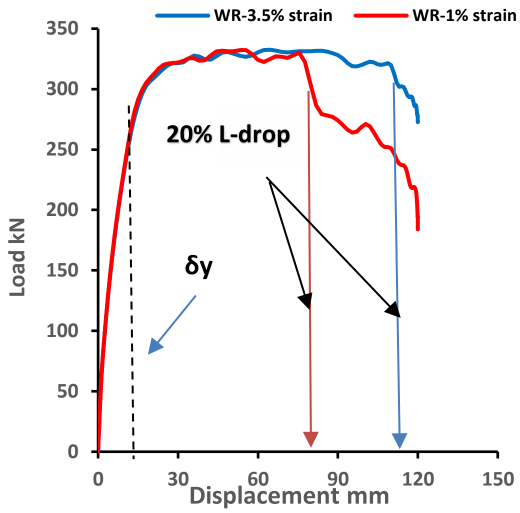

D

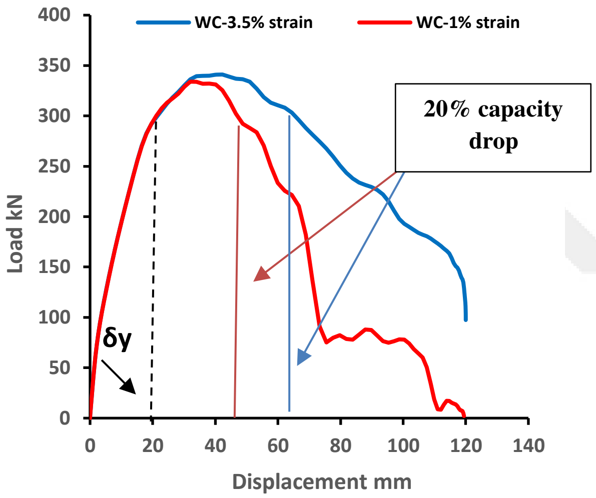

E

Figure 5.3 (A) 3CLH18-top-bottom jacket. (B) 3CLH18-whole ECC jacket (C) 3CLH18-whole ECC jacket with steel bars. (D) 3CLH18-replace top and bottom damage cover of column. (E) 3CLH18-replace whole column cover by ECC cover 37 mm.

Table 5.2 FEA results of 3CLH18 jacketed with 3.5 % ECC tension strain

sample		N_{axial} (kN)	Shear response (KN)	$\frac{V_{FEA}}{V_u}$	$M_{ult.}$ (kN.m)	$\frac{M_{ult.FEA}}{M_{exp}}$	δ_{yield} (mm)	$\delta_{ult.}$ (mm)	μ_Δ	$\frac{\mu_{FEA}}{\mu_{exp}}$
Tested	Jacket technique	518	271.32	-	447.68	-	19	30.5	1.6	-
Finite element analysis 3CLH-model-3.5 % ECC tension strain	TB	518	338	1.24	489	1.09	24	52	2.16	1.35
	W	518	340	1.26	501	1.12	22	110	5	3.12
	WR	518	340	1.26	501	1.12	22	115	5.2	3.26
	TB-C	518	336	1.23	501	1.14	20	50	2.5	1.56
	WC	518	338	1.24	487	1.08	20	70	3.5	2.18

Where:

N_{axial} = applied axial load (kN)

V_U = ultimate shear response of experimental specimen (kN).

V_{FEA} = ultimate shear response of jacketed specimens (KN).

$_{yield}$ = lateral yield displacement (mm). δ

$\delta_{ult.}$ = ultimate lateral displacement corresponding to 20% of load capacity lost (mm).

= displacement ductility. μ Δ

Table 5.3 FEA results of 3CLH18 jacketed with 1 % ECC tension strain

Sample		N_{axial} (KN)	Shear response (KN)	$\frac{V_{FEA}}{V_u}$	$M_{ult.}$ (KN.m)	$\frac{M_{ult.FEA}}{M_{exp}}$	δ_{yield} (mm)	$\delta_{ult.}$ (mm)	μ_{Δ}	$\frac{\mu_{FEA}}{\mu_{exp}}$
Tested	Jacket technique	518	271.32	-	447.68	-	19	30.5	1.6	-
Finite element analysis 3CLH-model- 1 % ECC tension strain	TB	518	338	1.24	487	1.08	24	48	2	1.25
	W	518	332	1.22	498	1.08	22	60	2.7	1.68
	WR	518	340	1.25	501	1.12	22	85	3.86	2.41
	TB-C	518	332	1.22	498	1.11	20	38	1.9	1.18
	WC	518	335	1.23	493.5	1.1	20	55	2.75	1.72

The following charts express the efficiency of jacketing techniques for ECC with 3.5% and 1% hardening strain in tension for the highest and lowest jacketing type, as

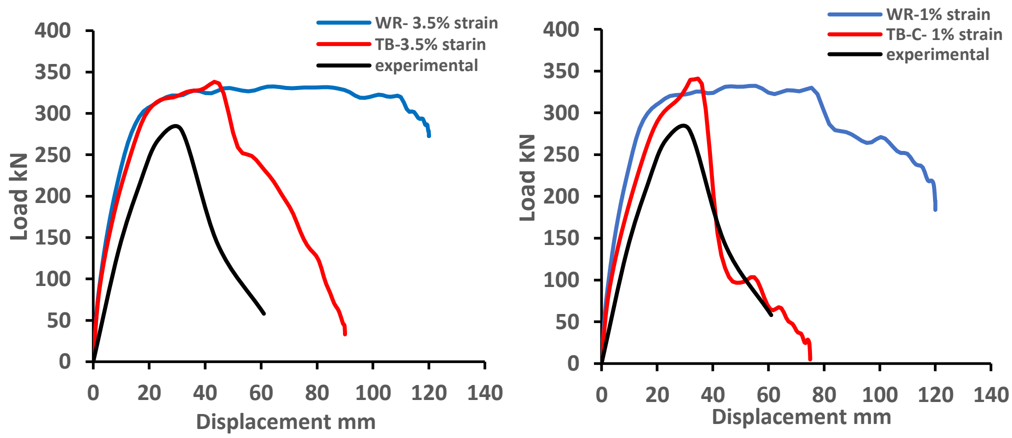

Figure 5.4 Load-displacement the higher and lower jackets specimens of 3CLH18

The following charts are present the Von-Mises stresses and damage tension for the highest and lowest of different jacketing patterns for ECC with 3.5% and 1% hardening strain in tension and compare it with the 3CLH18-tested sample as below:

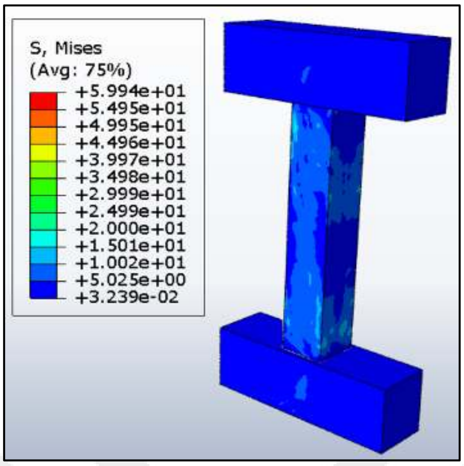

3CLH-WR-3.5% Von-Mises's stress

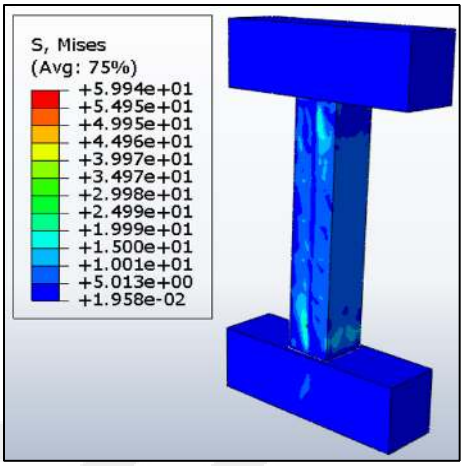

3CLH-WR-1% Von-Mises's stress

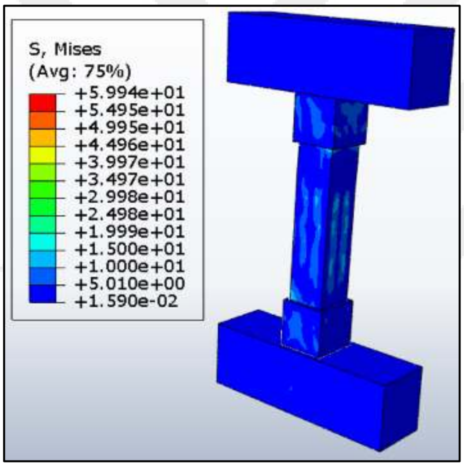

3CLH18-TB-3.5% Von-Mises's stress

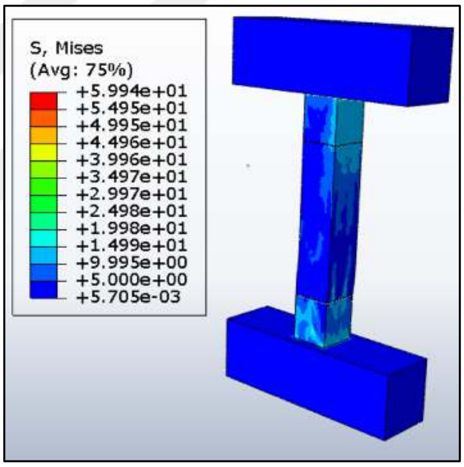

3CLH18-TB-C-1% Von Mises's stress

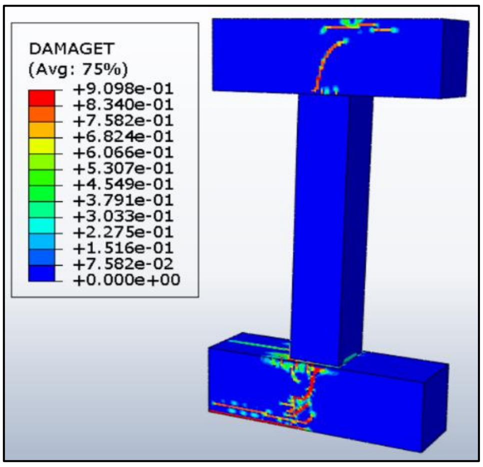

3CLH18-WR-3.5% damage in tension

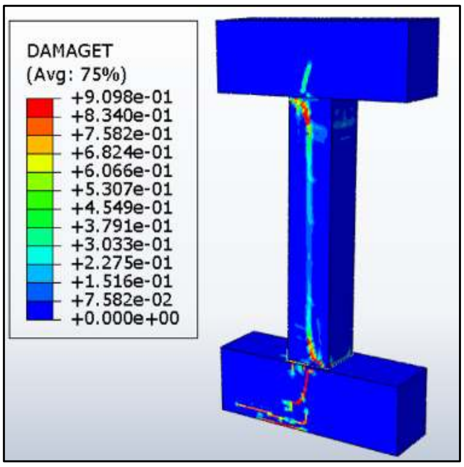

3CLH18-WR-1% damage in tension

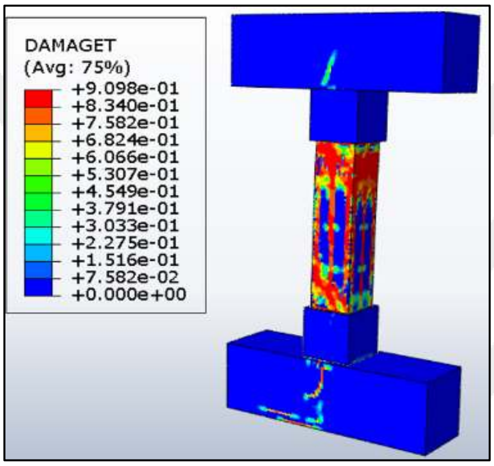

3CLH18-TB-3.5% damage in tension

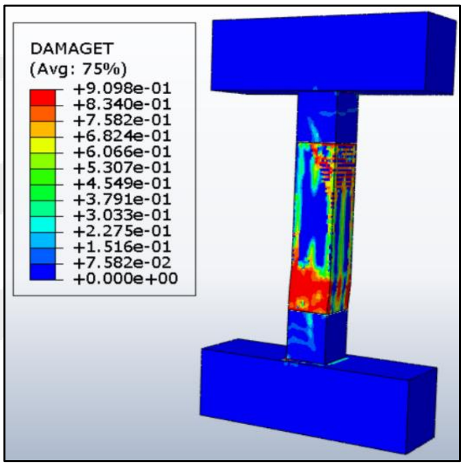

3CLH18-TB-C-1% tension damage

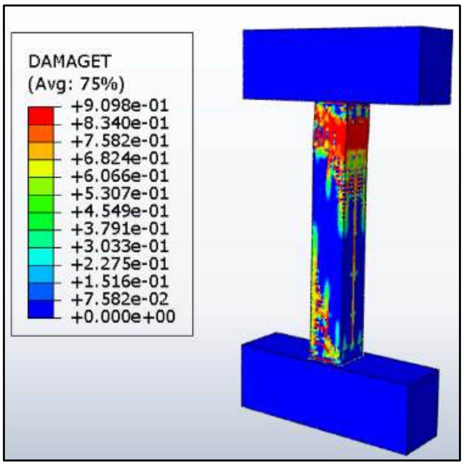

FEA tension damage of tested specimen

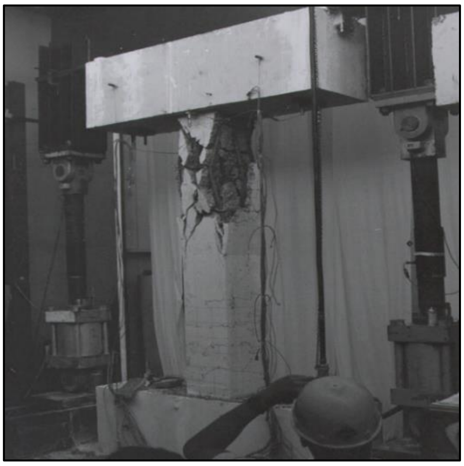

3CLH18-tested cracks propagation

Figure 5.5 FEA stresses and damage in tension of 3CLH18 jacketed specimens

The following schemes show plastic and damage dispersion energy, which can be defined as the ability of structural members to absorb and confuse the dynamic energy without reaching collapse, which is closely related to material ductility and plastic deformation approach as well.

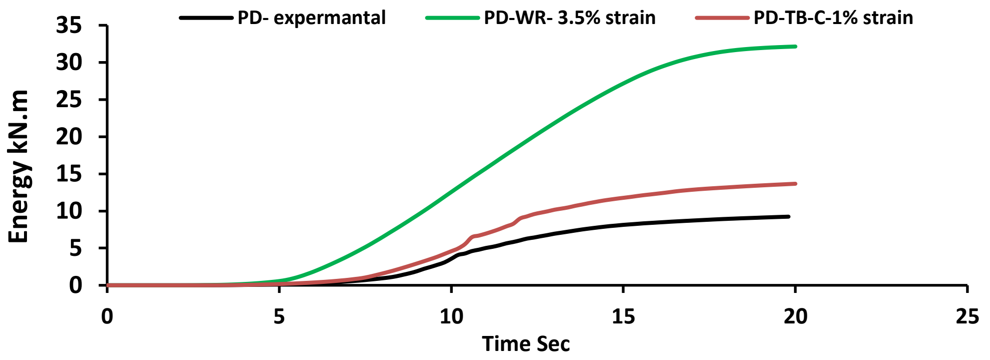

A

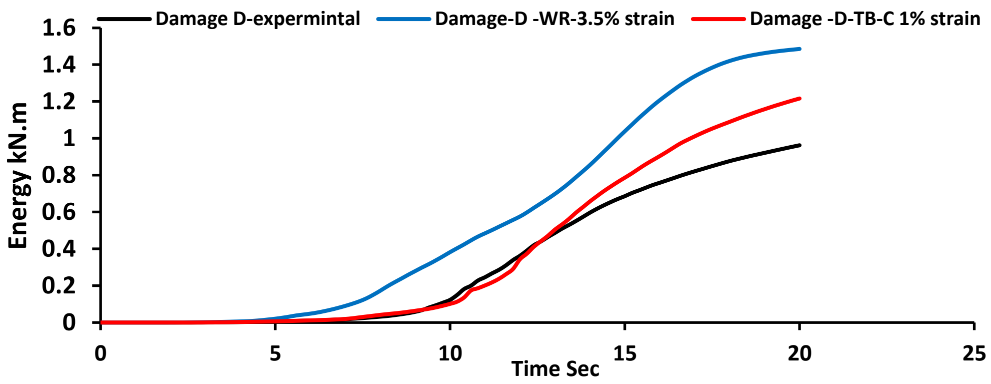

B

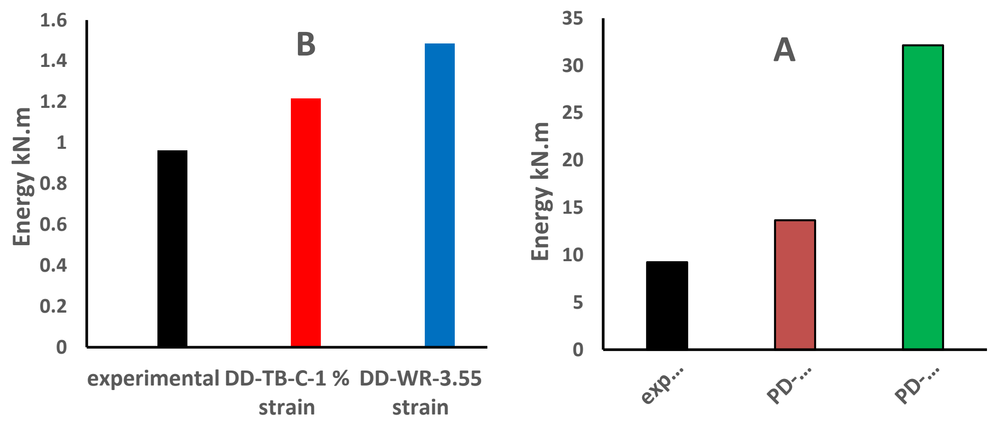

Figure 5.6 A, B plastic, damage dissipation energy for higher and lower FEM 3CLH18 and experimental specimens

5.5.2 2CLH18 Specimen

The 2CLH18 sample was jacketed by all five types in table (5.1) above, the jacketing specimens were exposed to different levels of lateral pushing with multiple values of δ_u= 90 mm, on the middle-top pedestal of the specimen in Z direction. The maximum lateral displacement was applied to each jacketing type of the first strategy (1% ECC tension strain),TB,W,TB-C, and WC, jacketing types were δ_{uFEA} = 180 mm, as a double value of δ_u , and WR-1% (δ_{uFEA})=270 mm, while the ECC jacketing with 3.5% tension strain TB,TB-C, δ_{uFEA} = 180 mm, as a double value of test lateral pushing, W, WC, δ_{uFEA} = 270 mm as a three-times of original test displacement, WR-3.5%, δ_{uFEA} = 360 mm as a four-times of unjacketed column displacement for reaching the point 20% of the maximum force capacity of columns which is considers as a failure point as well. The time step in finite element analysis increases directly with increasing the applied displacement to get a reasonable result and to overcome the results divergence problem. All jacketing type had a mesh size similar to the empirical specimen to avoid the mesh sensitivity issue. The following figures show the FEA load-deflection response for all type of retrofitting and comparison with the experimental results for two tension strain series of 1%, and 3.5%, respectively.

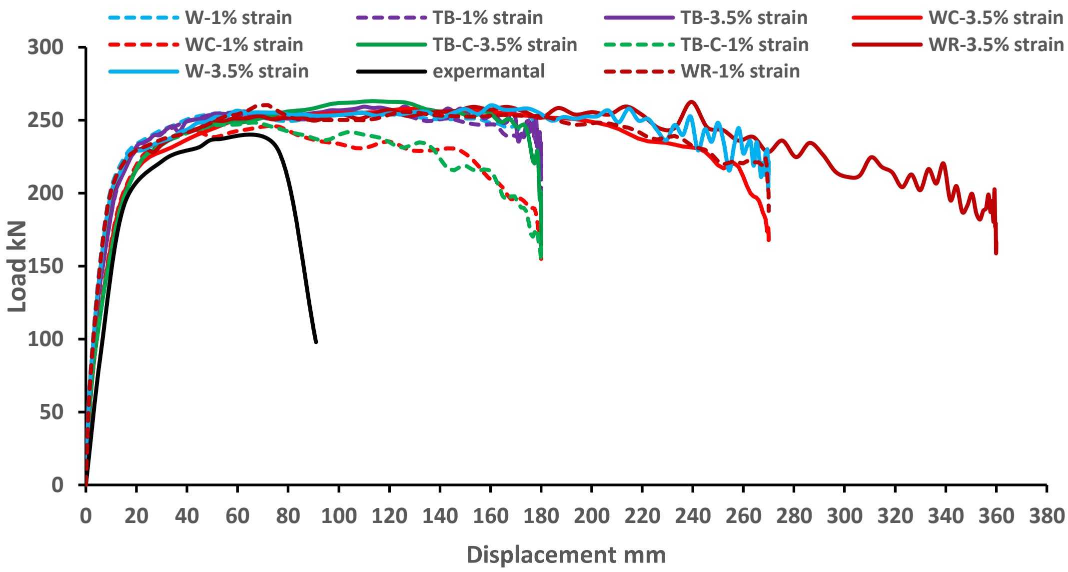

Figure 5.7 Different jacketed techniques of 2CLH18

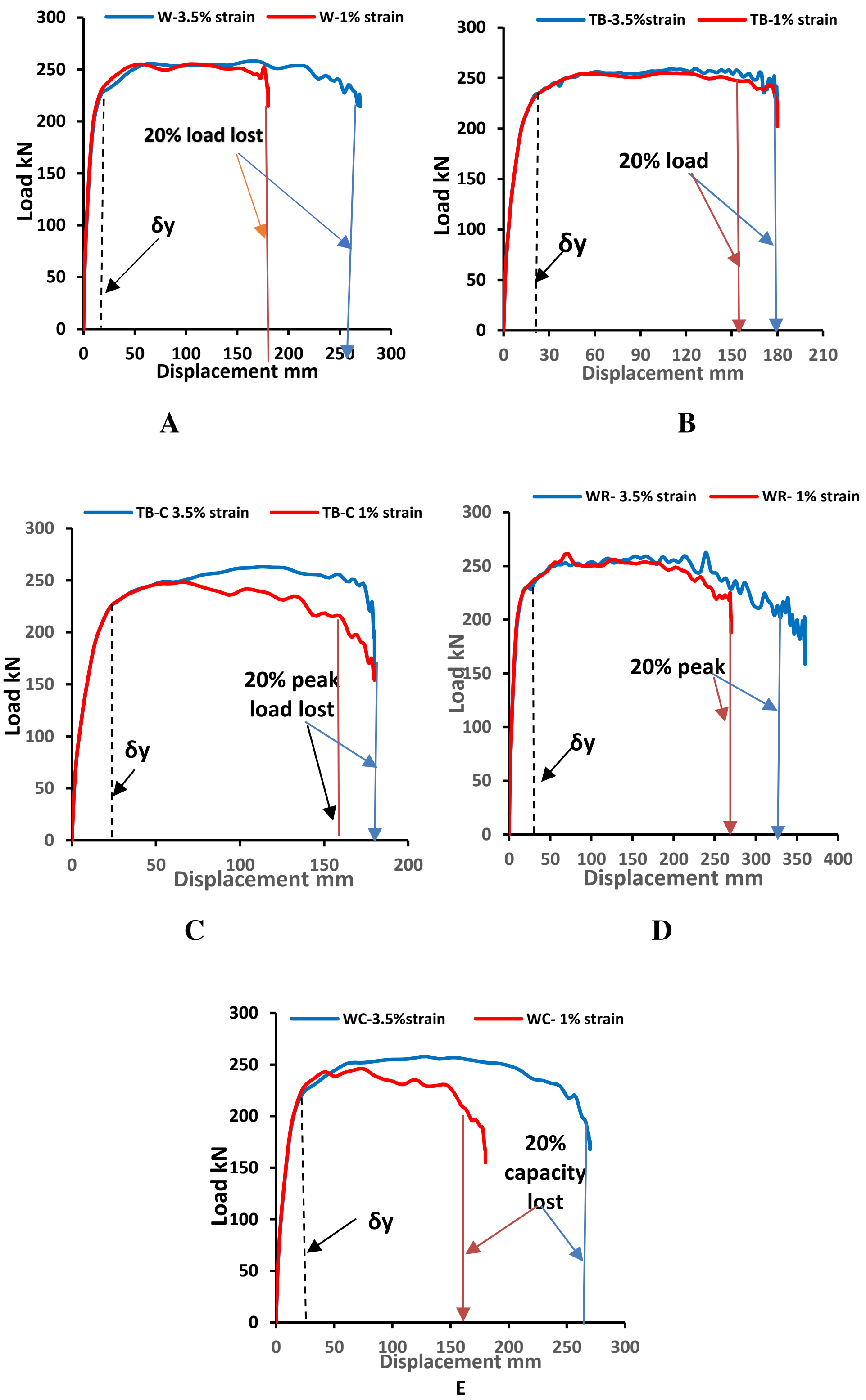

Figure 5.8 (A) 2CLH18-top-bottom jacket. (B) 2CLH18-whole ECC jacket. (C) 2CLH18-whole-steel ECC jacket. (D) 2CLH18-replaceT-B covers of column. (E) 2CLH18-replace whole column cover by ECC cover 37 mm.

Table 5.4 FEA results of 2CLH18 jacketed specimens with 3.5% ECC tension strain

sample		N_{axial} (KN)	Shear response (KN)	$\frac{V_{FEA}}{V_u}$	$M_{ult.}$ (KN.m)	$\frac{M_{ult.FEA}}{M_{exp}}$	δ_{yield} (mm)	$\delta_{ult.}$ (mm)	μ_Δ	$\frac{\mu_{FEA}}{\mu_{exp}}$
Tested	Jacket technique	518	240	-	369.6	-	15	76.2	5.1	-
Finite element analysis 2CLH18-model-3.5 %	TB	518	260	1.08	383	1.03	24	180	7.5	1.47
	W	518	270	1.125	397.7	1.07	20	260	13	2.55
	WR	518	270	1.125	397.7	1.07	22	320	14.5	2.85
	TB-C	518	270	1.125	397.7	1.07	24	178	7.41	1.45
	W	518	255	1.06	375.6	1.01	24	260	10.8	2.1

Table 5.5 FEA results of 2CLH18 jacketed specimens with 1% ECC tension strain

sample		N_{axial} (KN)	Shear response (KN)	$\frac{V_{FEA}}{V_u}$	$M_{ult.}$ (KN.m)	$\frac{M_{ult.FEA}}{M_{exp}}$	δ_{yield} (mm)	$\delta_{ult.}$ (mm)	μ_Δ	$\frac{\mu_{FEA}}{\mu_{exp}}$
Tested	Jacket technique	518	240	-	368	-	15	76.2	5.1	-
Finite element analysis 2CLH18-model- 1%	TB	518	250	1.04	368	1	24	160	6.6	1.3
	W	518	245	1.03	360	0.99	20	180	9	1.76
	WR	518	250	1.04	368	1	22	260	11.8	2.3
	TB-C	518	245	1.03	360	0.99	24	160	6.6	1.3
	WC	518	248	1.033	368	1	24	165	6.87	1.34

The schemes below present various jacketing techniques, which include higher and lower lateral load responses with 3.5% and 1%, hardening strain in tension, and Von-Mises's stress

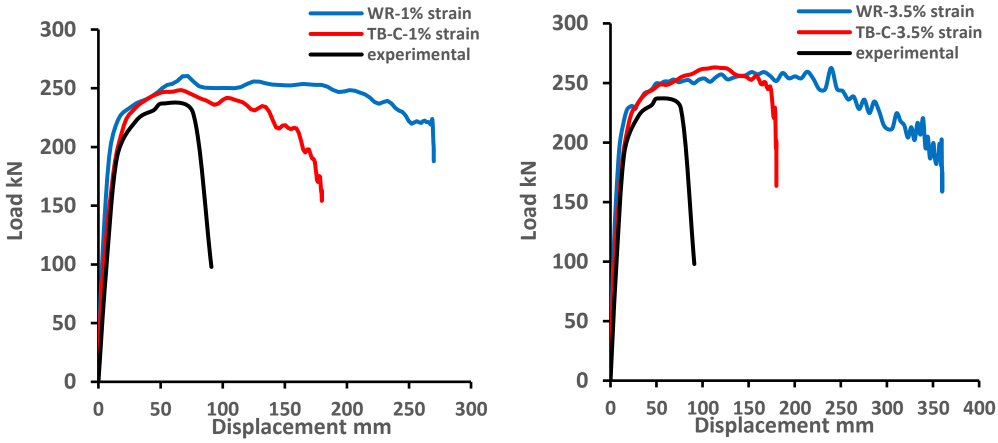

Figure 5.9 Load-displacement of higher and lower of 2CLH18 jacketing specimens

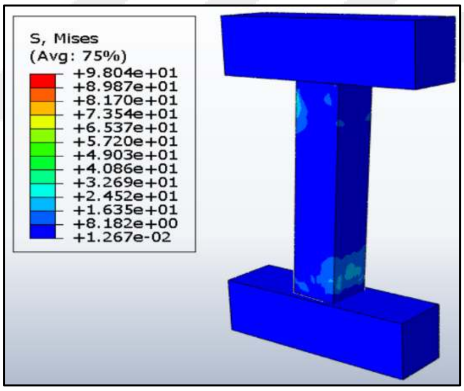

2CLH18-WR-3.5% Von-Mises's stress

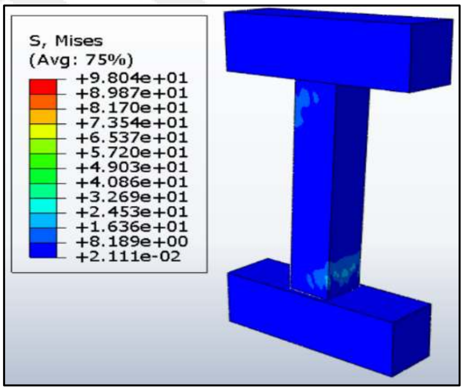

2CLH18-WR-1% Von-Mises's stress

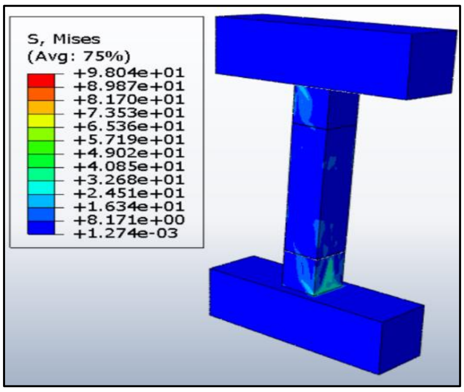

2CLH18-TB-C-3.5% Von-Mises's stress

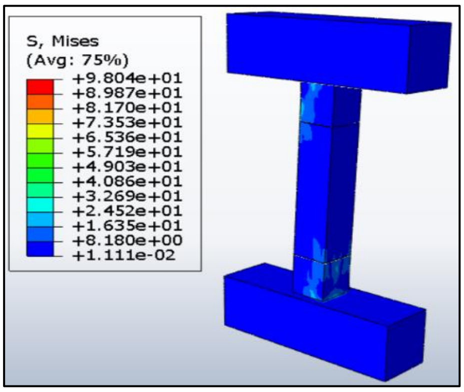

2CLH18-TB-C-1% Von-Mises's stress

The following charts present the damage tension for higher and lower of different jacketing patterns for ECC with 3.5% and 1% hardening strain in tension:

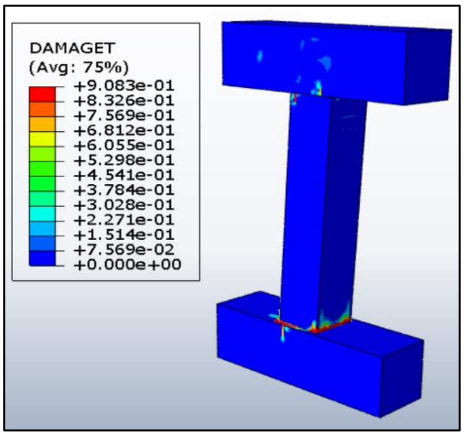

2CLH18-WR-3.5% damage tension

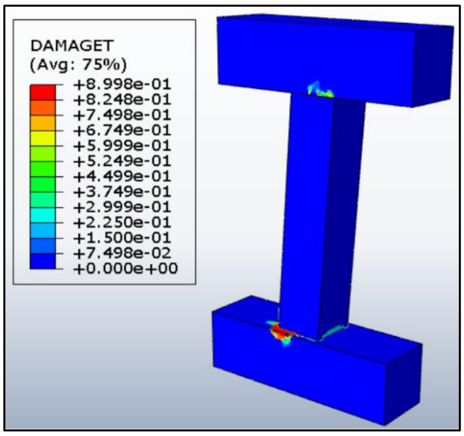

2CLH18-WR-1% damage tension

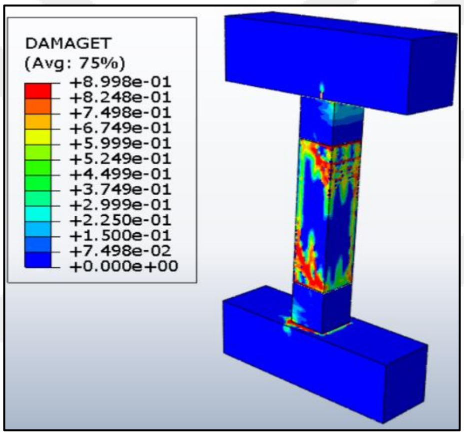

2CLH18-TB-C-3.5% damage tension

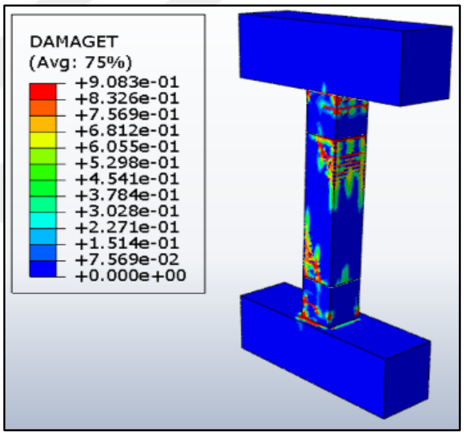

2CLH18-TB-C-1% damage tension

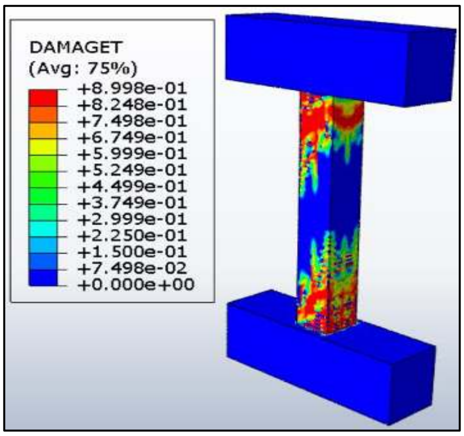

FEM 2CLH18- damage tension

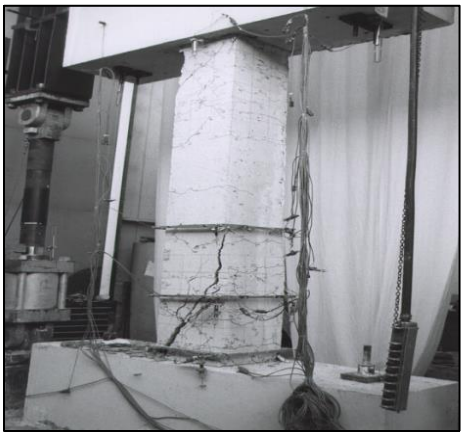

2CLH18-tested cracks propagation

Figure 5.10 FEA stresses and damage in tension of 2CLH18 jacketed specimens

The following schemes show plastic and damage dispersion energy for higher and lower jacketing types which that express the ability of structural members to absorb and confuse the dynamic energy of jacketed specimens:

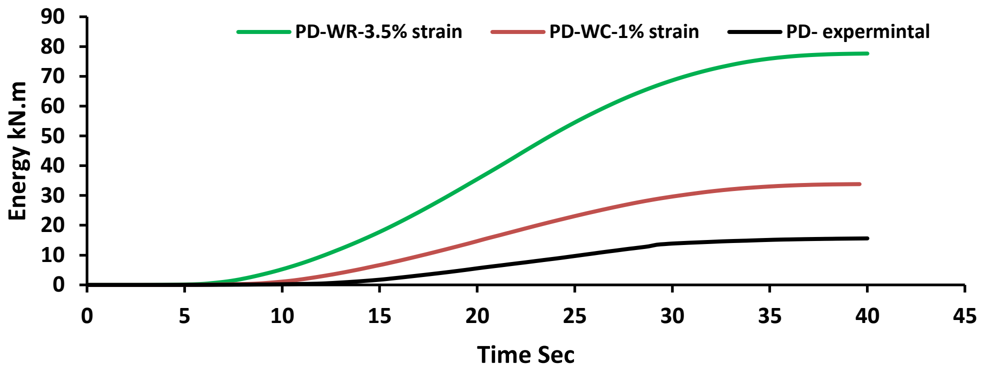

A

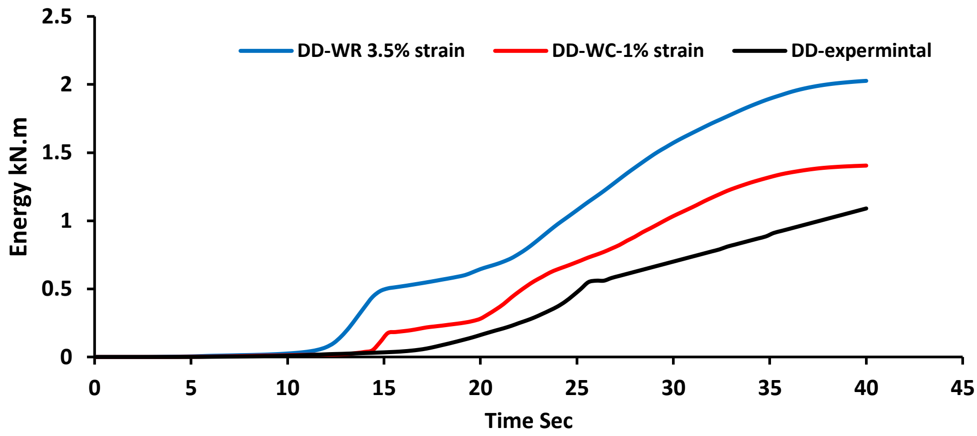

B

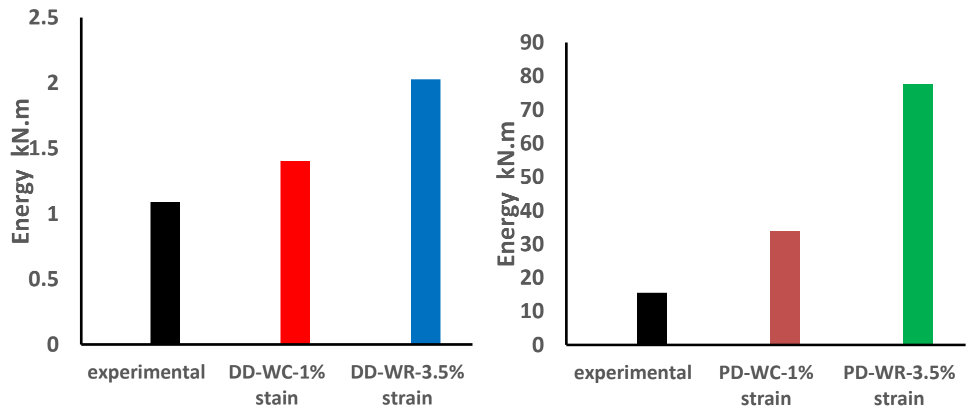

Figure 5.11 A, B, plastic, damage dissipation energy for higher and lower FEM 2CLH18 and experimental specimen.

5.5.3 3CMH18 Specimen

The material features and damage mechanism of the un-jacketed column, the type of strengthening technique, and the applied shearing force play an essential role in the failure approach of retrofitted models as well. The tested specimen suffers from shear failure when displacement reaches 30.5 mm. The jacketing specimens were exposed to different levels of lateral pushing with multiple values of δ_u= 60 mm (applied Z-axis displacement) on the middle-top pedestal of the specimen. The lateral deflection that applied to each jacketing type strategy (3.5%, and 1% ECC tension strain), TB-C and WC jacketing types were δ_{uFEA} = 75 mm, as 1.25 δ_u, but the ECC jacketing TB, with δ_{uFEA} = 90 mm, as a 1.5 time value of test lateral pushing, W, and WR, δ_{uFEA} = 120 mm as a doble times of original tested displacement, for reaching the drop point 20% of the maximum capacity of columns, which is considered as a failure point as well. The time step in finite element analysis increases directly with increasing the applied displacement to get a reasonable result and to overcome the result divergence problems where for displacement increasing (1.25δ,1.5δ,2δ) corresponding to (12.5,15,20) sec. where 10 sec as an un-jacketed 3CMH time of FE analysis. All jacketing types had a mesh size similar to the empirical specimen to avoid the mesh sensitivity issue. The following figures show the FEA load-deflection response for all types of retrofitting and comparison with the experimental results for two tension strain series of 1% and 3.5%, respectively.

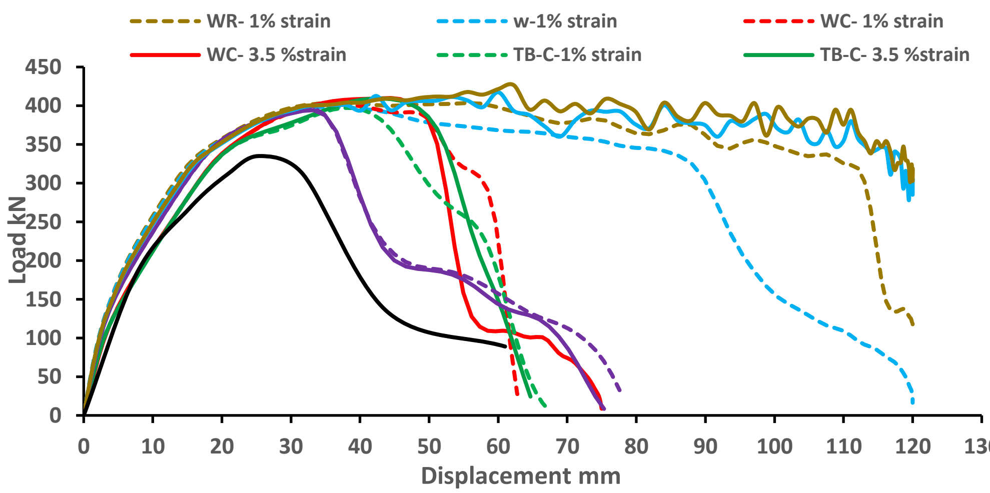

Figure 5.12 Different jacketed techniques of 3CMH18

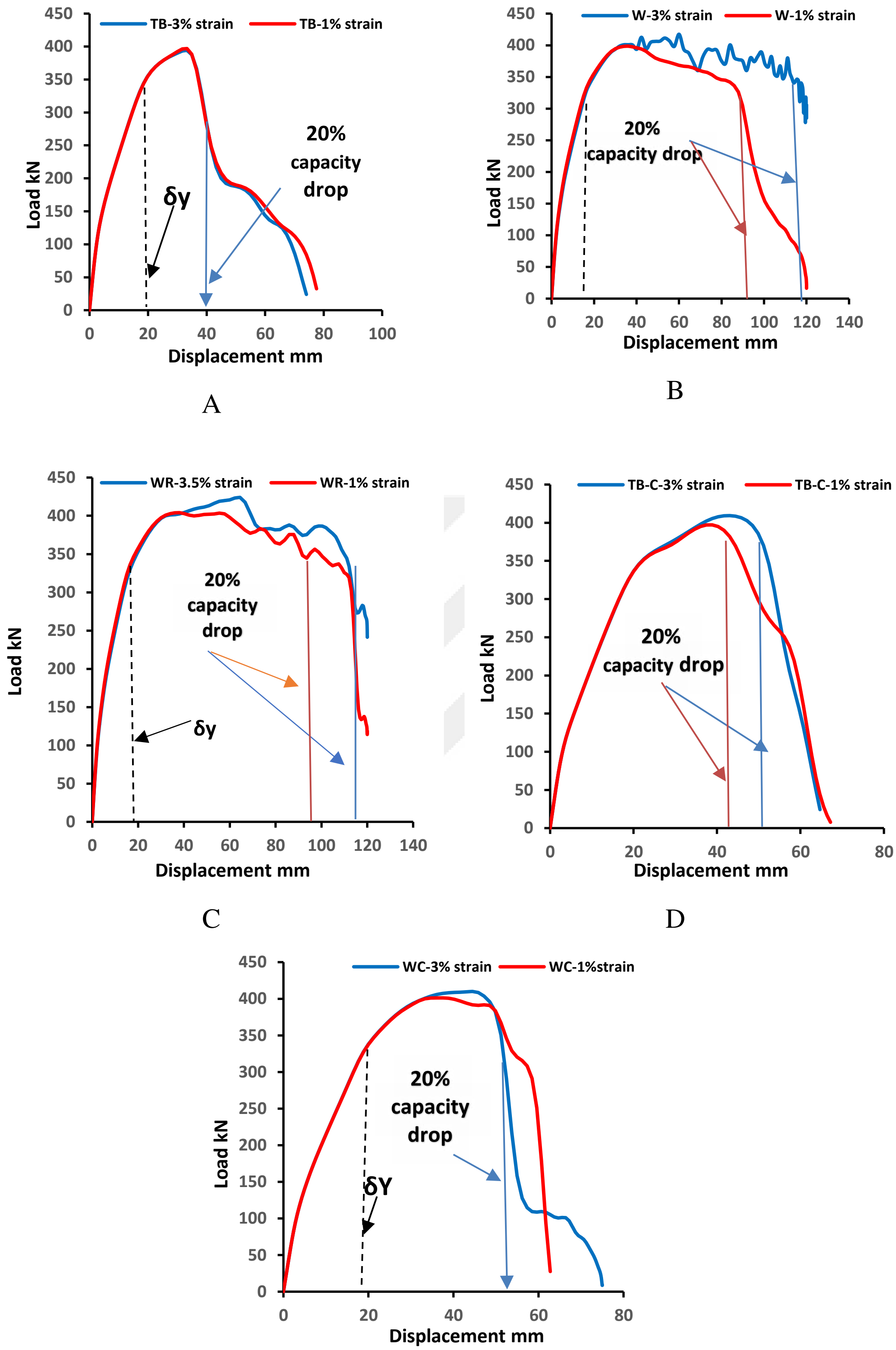

Figure 5.13 **(A)** 3CMH18 top-bottom jacket. (B) whole ECC jacket. (C) whole steel ECC jacket. (D) Replace top-bottom with ECC cover (E) Replace whole cover.

Table 5.6 FEA results of 3CMH18 jacketed specimens- 3.5% ECC tension strain

sample		N_{axial} (KN)	Shear response (KN)	$\frac{V_{FEA}}{V_u}$	$M_{ult.}$ (KN.m)	$\frac{M_{ult.FEA}}{M_{exp.}}$	δ_{yied} (mm)	$\delta_{ult.}$ (mm)	μ_{Δ}	$\frac{\mu_{FEA}}{\mu_{exp}}$
Tested	Jacket technique	1512	338	-	485	-	22.6	30.5	1.3	-
Finite element analysis 3CMH-model-3.5 % ECC	TB	1512	394	1.16	580.3	1.19	20	38	1.9	1.46
	W	1512	417.4	1.23	614.8	1.26	24	115	4.79	3.68
	WR	1512	426.5	1.26	628.2	1.3	24	117	4.87	3.74
	TB-C	1512	409.3	1.21	603	1.24	23	54	2.34	1.8
	WC	1512	410	1.21	604	1.24	23	53	2.3	1.77

Table 5.7 FEA results of 3CMH18 jacketed specimens with 1% ECC tension strain

sample		N_{axial} (KN)	Shear response (KN)	$\frac{V_{FEA}}{V_u}$	$M_{ult.}$ (KN.m)	$\frac{M_{ult.FEM}}{M_{exp.}}$	δ_{yied} (mm)	$\delta_{ult.}$ (mm)	μ_{Δ}	$\frac{\mu_{FEA}}{\mu_{exp}}$
Tested	Jacket technique	1512	338	-	485	-	22.6	30.5	1.3	-
Finite element analysis 3CMH18-model- 1 % ECC	TB	1512	394	1.16	581	1.19	20	38	1.9	1.46
	W	1512	398	1.18	586	1.21	24	90	3.75	2.88
	WR	1512	404	1.2	595	1.22	24	94	3.91	3
	TB-C	1512	397	1.17	585	1.2	23	48	2.1	1.6
	WC	1512	401	1.19	591	1.21	23	56	2.43	1.8

The schemes below present various jacketing techniques, which include higher and lower lateral load responses with 3.5% and 1% hardening strain in tension and Von-Mises’s stress:

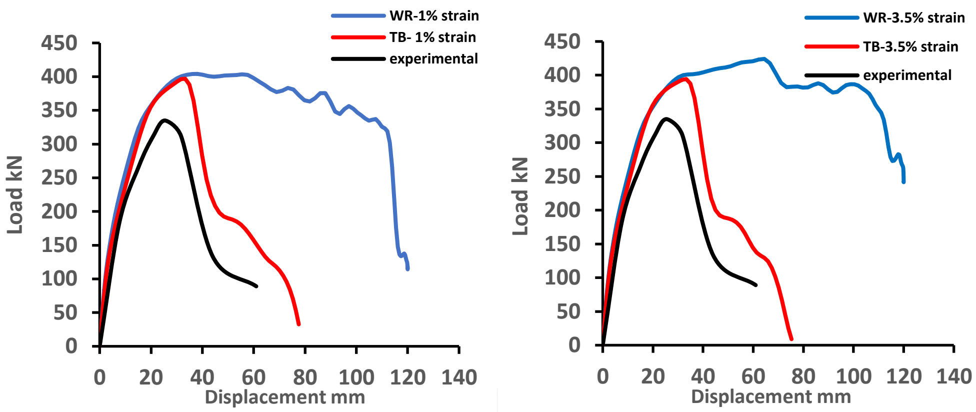

Figure 5.14 Load-displacement of higher and lower of 3CMH18 jacketed specimens

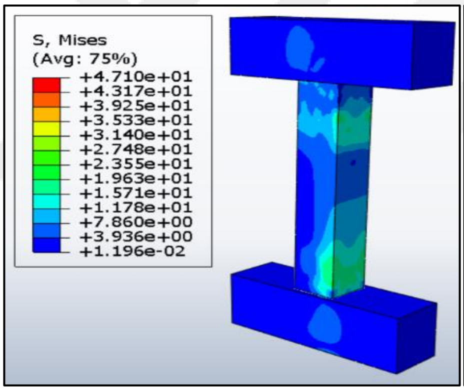

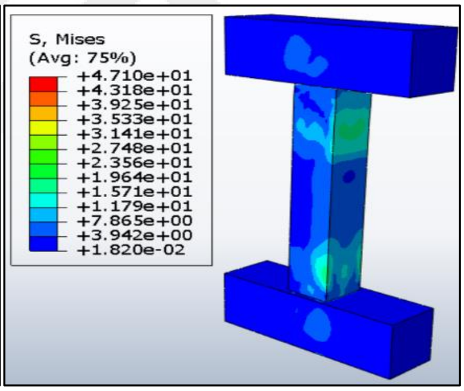

3CMH18-WR-3.5%,Von Mises's stress 3CMH18-WR-1%,Von Mises's stress

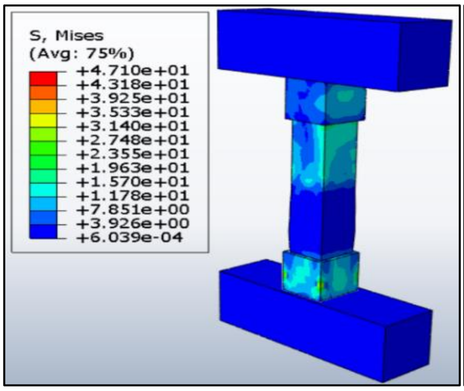

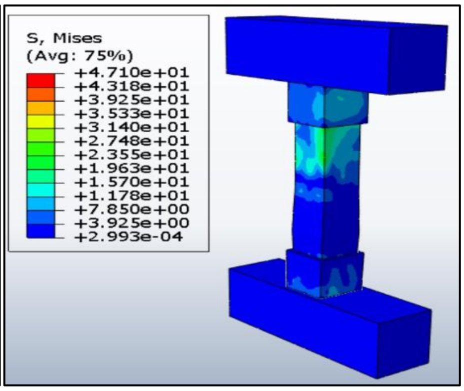

3CMH18-TB-3.5%,Von Mises's stress 3CMH18-TB-1%,Von Mises's stress

The following charts present the damage tension for different jacketing types of ECC

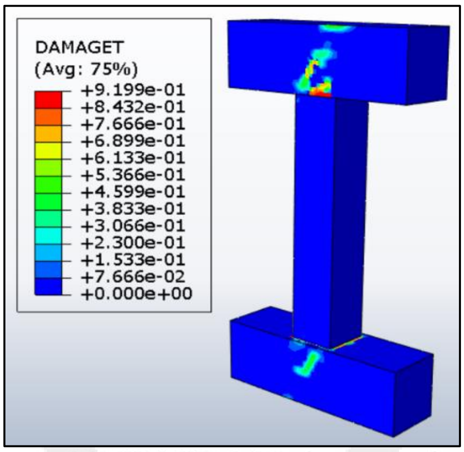

3CMH18-WR-3.5%, damage tension

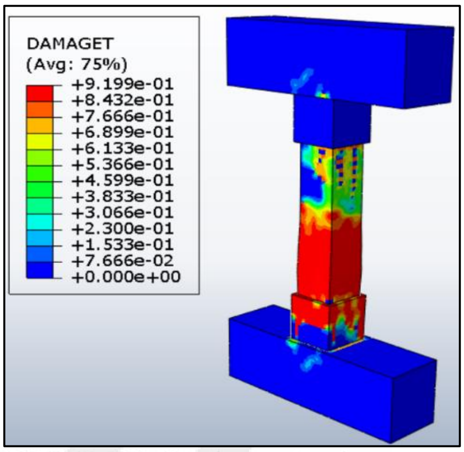

3CMH18-WR-1%, damage tension

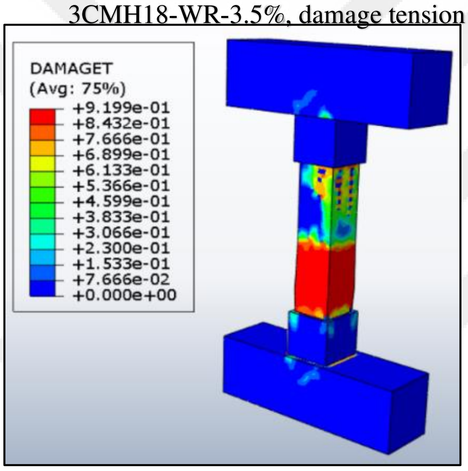

3CMH18-TB-3.5% damage tension

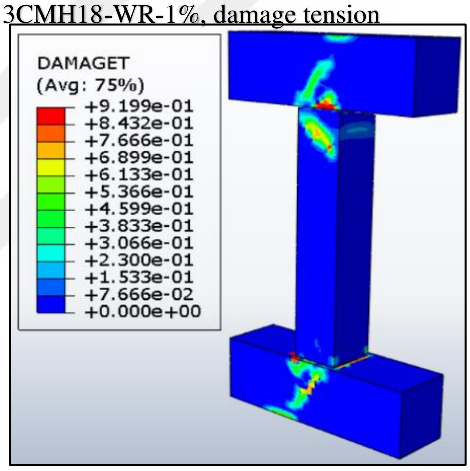

3CMH18-TB-1% damage tension

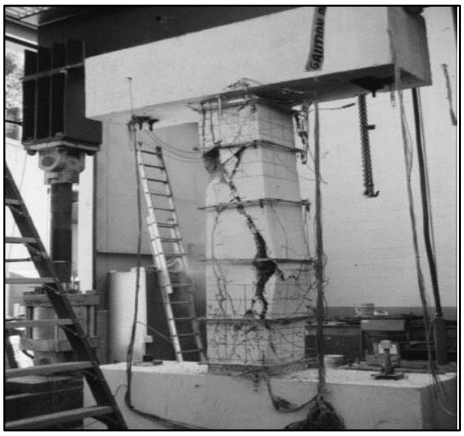

3CMH18-Tested cracks propegation

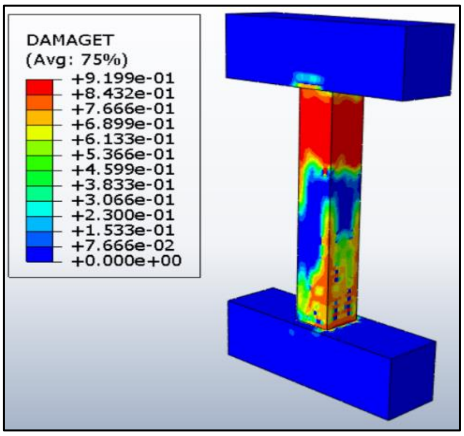

3CMH18 FE cracks

Figure 5.15 FEA stresses and damage in tension of 3CMH18 jacketed specimens

The following schemes show plastic and damage dispersion energy for higher and lower jacketing ways which is express the ability of structural members to absorb and confuse the dynamic energy of jacketed specimen, and compare it with the experimental curve as shown in the figures below:

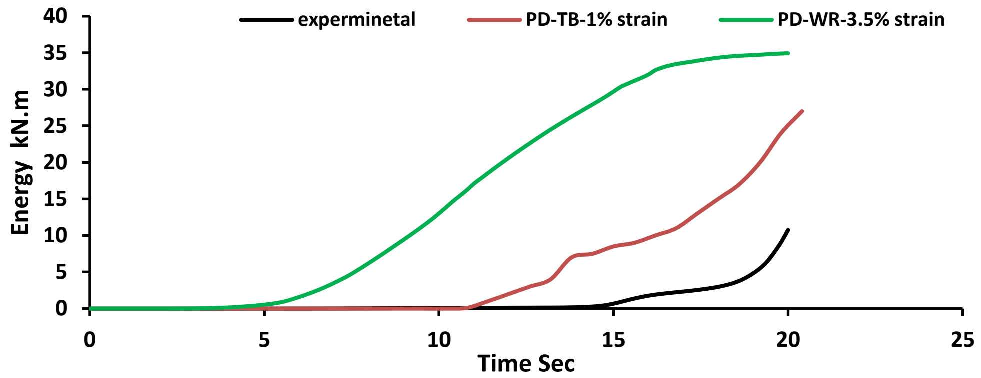

A

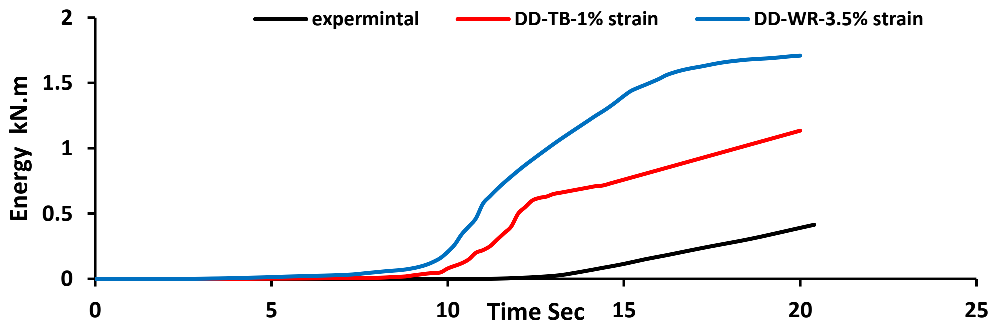

B

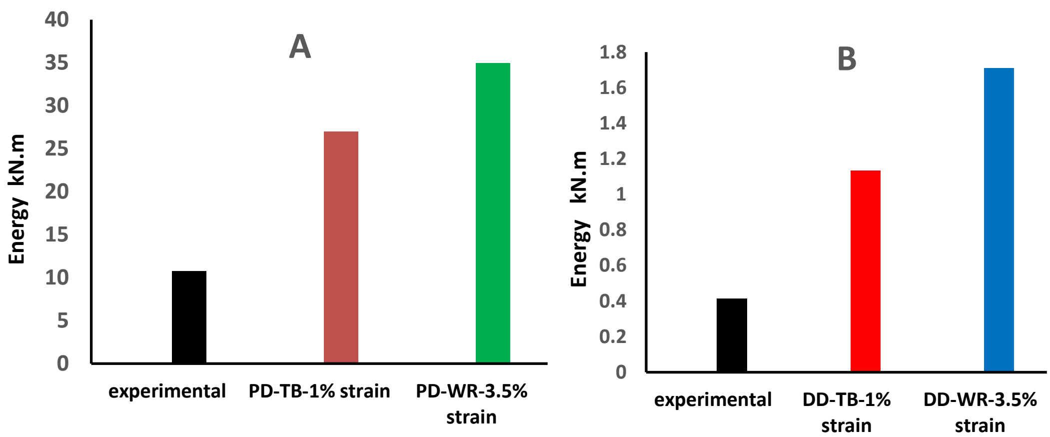

Figure 5.16 A, B, plastic, damage dissipation energy for higher and lower FEM 3CMH18 and experimental specimens.

5.5.4 2CMH18 Specimen

The material features and damage mechanism of the un-jacketed column, type of strengthening technique, and the applied shearing force play an essential role in the failure approach of retrofitted models as well. The tested specimen suffers from shear failure when displacement reaches 30.5 mm. The jacketing specimens were exposed to different patterns of lateral pushing with multiple values of δ_u= 30.5 mm (applied Z-axis displacement) on the middle-top pedestal of the specimen. The lateral deflection that applied on each jacketing types strategy (3.5% and 1% ECC tension strain), TB, and TB-C, jacketing types were δ_{uFEA} = 90 mm, as $3\delta_u$, but the ECC jacketing WC, with δ_{uFEA} = 120 mm, as a four-time value of test lateral pushing , (W and WR, for 1% tension strain), δ_{uFEA} = 150 mm as a five-times of original tested displacement, (W, WR for 3.5% tension strain) were 180 mm (six-times of tested displacement) until capture the drop point 20% of the maximum capacity of columns, which is considered as a failure point as well. The time step in finite element analysis increases directly with increasing the applied displacement to get a reasonable result and to overcome the result divergence problems where for displacement increasing (3δ,4δ,5δ,6δ,) corresponding to (30,40,50,60) sec. where 10 sec is an un-jacketed 2CMH time of FE analysis. All jacketing types had a mesh size similar to the empirical specimen to avoid the mesh sensitivity issue. The following figures show the FEA load-deflection response for all types of retrofitting and comparison with the experimental results for two tension strain series of 1% and 3.5%, respectively. All specimens conducted their FEA with above two hardening strains (ε_t^h) in

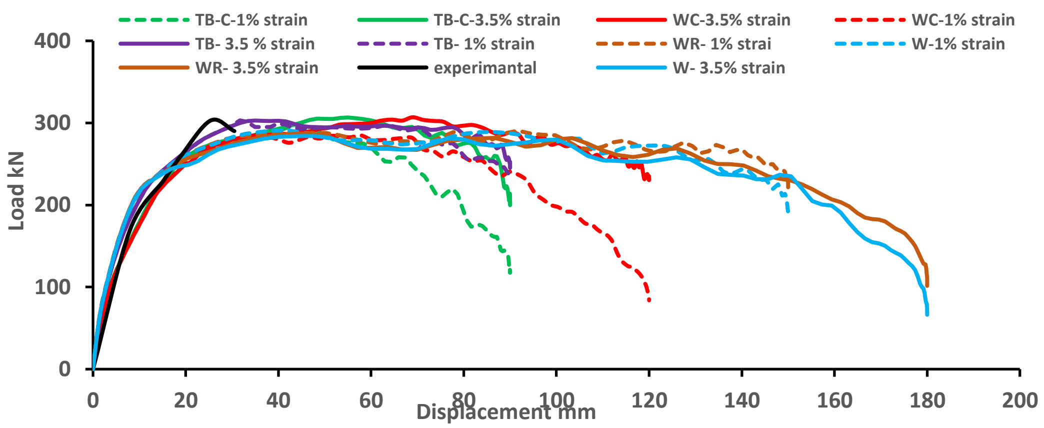

Figure 5.17 Different jacketed techniques of 2CMH18

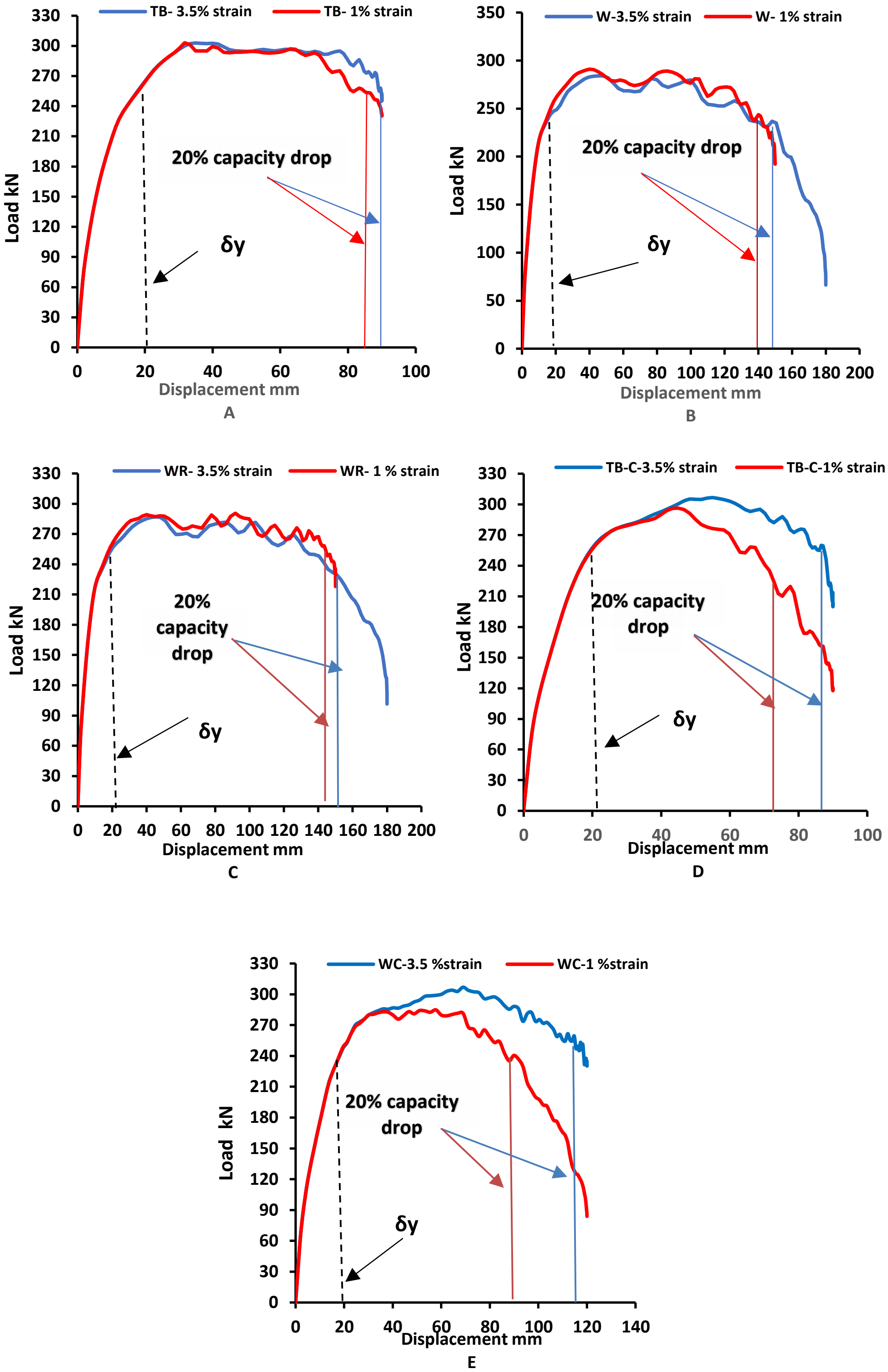

Figure 5.18 (A)2CMH18 top-bottom jacket. (B) whole ECC jacket. (C) whole-steel with ECC jacket. (D) Replace top and bottom damaged cover of column (E) Replace whole-cover with ECC.

Table 5.8 FEA results of 2CMH18 jacketed specimens-3.5 % ECC tension strain

sample		N_{axial} (KN)	Shear response)KN(	$\frac{V_{FEA}}{V_u}$	$M_{ult.}$ (KN.m)	$\frac{M_{ult.FEA}}{M_{exp.}}$	δ_{yield} (mm)	$\delta_{ult.}$ (mm)	μ_Δ	$\frac{\mu_{FEA}}{\mu_{exp}}$
Tested	Jacket technique	1512	290	-	508	-	16.5	30.5	1.8	-
Finite element analysis 2CMH18-model-3.5 %	TB	1512	304	1.04	448	0.88	22	90	4.1	2.27
	W	1512	280	0.96	413.2	0.83	20	145	7.25	4.02
	WR	1512	290	1	423	0.83	20	152	7.6	4.22
	TB-C	1512	306	1.05	451	0.89	20	88	4.4	2.44
	WC	1512	315	1.08	452.2	0.89	22	117	5.3	3.95

Table 5.9 FEA results of 2CMH18 jacketed specimens with 1% ECC tension strain

sample		N_{axial} (KN)	Shear response (KN)	$\frac{V_{FEA}}{V_u}$	$M_{ult.}$ (KN.m)	$\frac{M_{ult.FEA}}{M_{exp.}}$	δ_{yield} (mm)	$\delta_{ult.}$ (mm)	μ_Δ	$\frac{\mu_{FEA}}{\mu_{exp}}$
Tested	Jacket technique	1512	290	-	508	-	16.5	30.5	1.8	-
Finite element analysis 2CMH18-model- 1 % ECC	TB	1512	303	1.04	447	0.9	22	87	3.95	2.2
	W	1512	290	1	423	0.83	20	140	7	3.88
	WR	1512	290	1	423	0.83	20	145	7.25	4
	TB-C	1512	290	1	423	0.83	20	73	3.65	2
	WC	1512	288	1	422	0.82	22	85	3.86	2.14

The schemes below present various jacketing techniques, which include higher and lower lateral load response hardening strain in tension, and Von-Mises's stress:

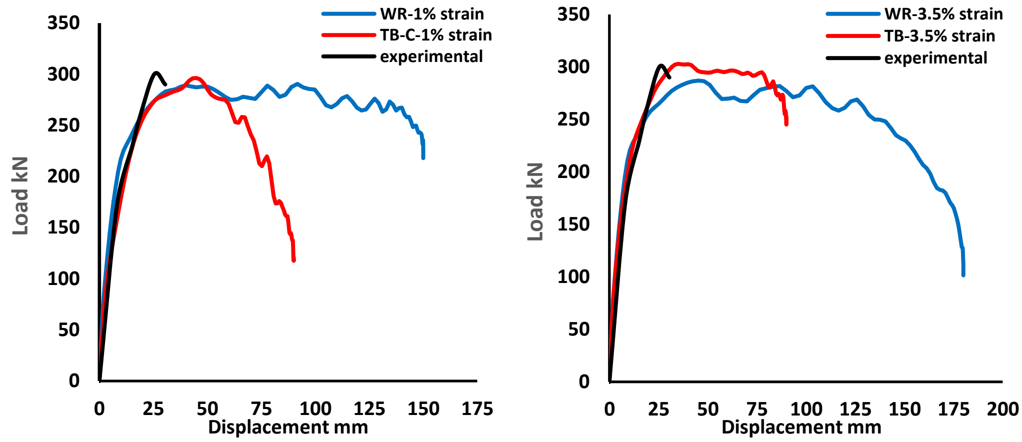

Figure 5.19 Load-displacement of higher and lower of 2CMH18 jacketed specimens

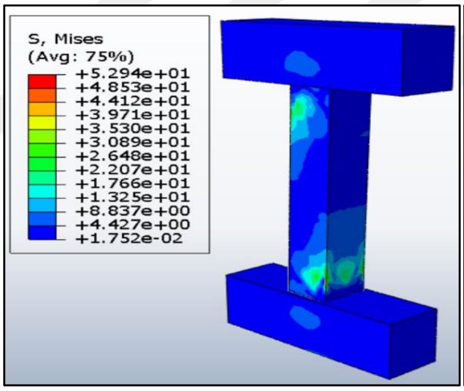

WR-3.5%, Von Mises's stress

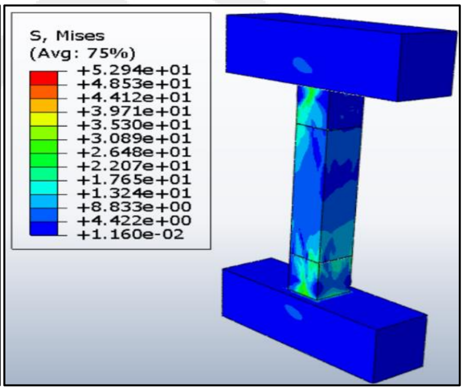

WR-1%, Von Mises's stress

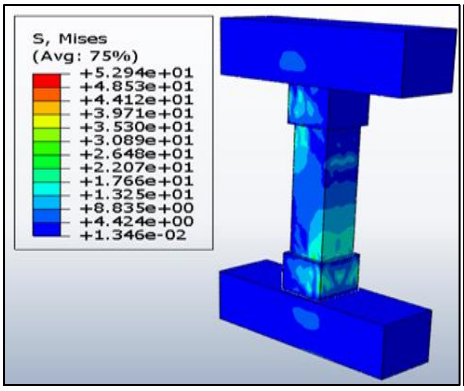

TB-3.5%, Von Mises's stress

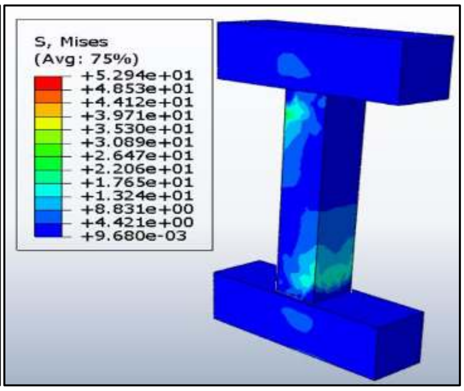

TB-C-1%, Von Mises's stress

The following charts present the damage tension for higher and lower of different jacketing patterns:

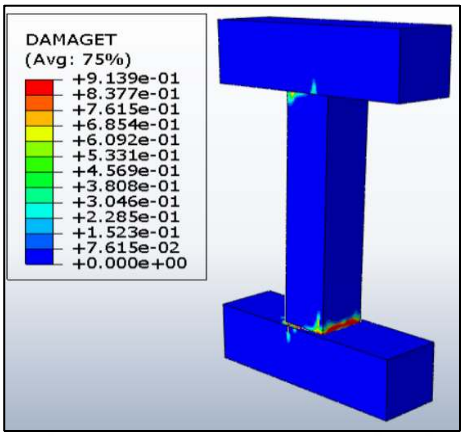

2CMH18-WR-3.5%, damage tension

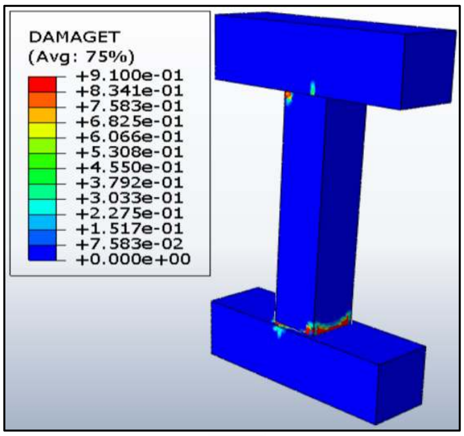

2CMH18-WR-1%, damage tension

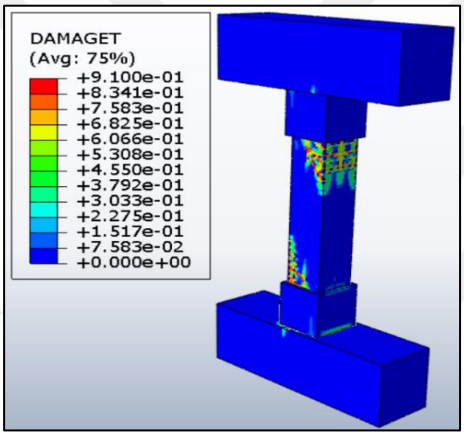

2CMH18-TB-3.5%, damage tension

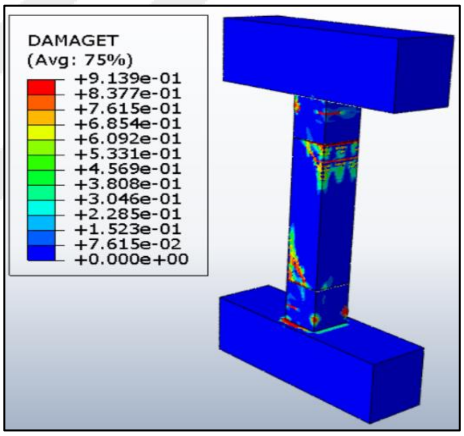

2CMH18-TB-C-1%, damage tension

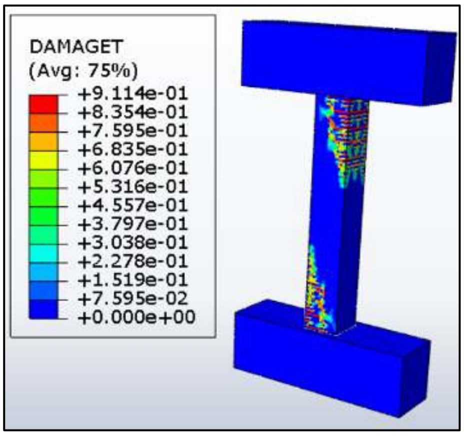

FEA 2CMH18 damage tension

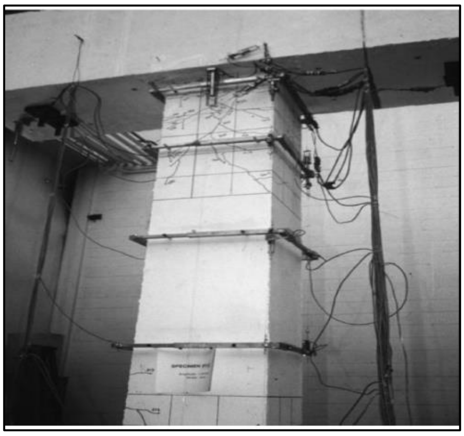

experimental cracks propagation

Figure 5.20 FEA stresses and damage in tension of 2CMH18 jacketed specimens

The following schemes show plastic and damage dispersion energy for higher and lower jacketing approaches and compare it with experimental curve as the figures:

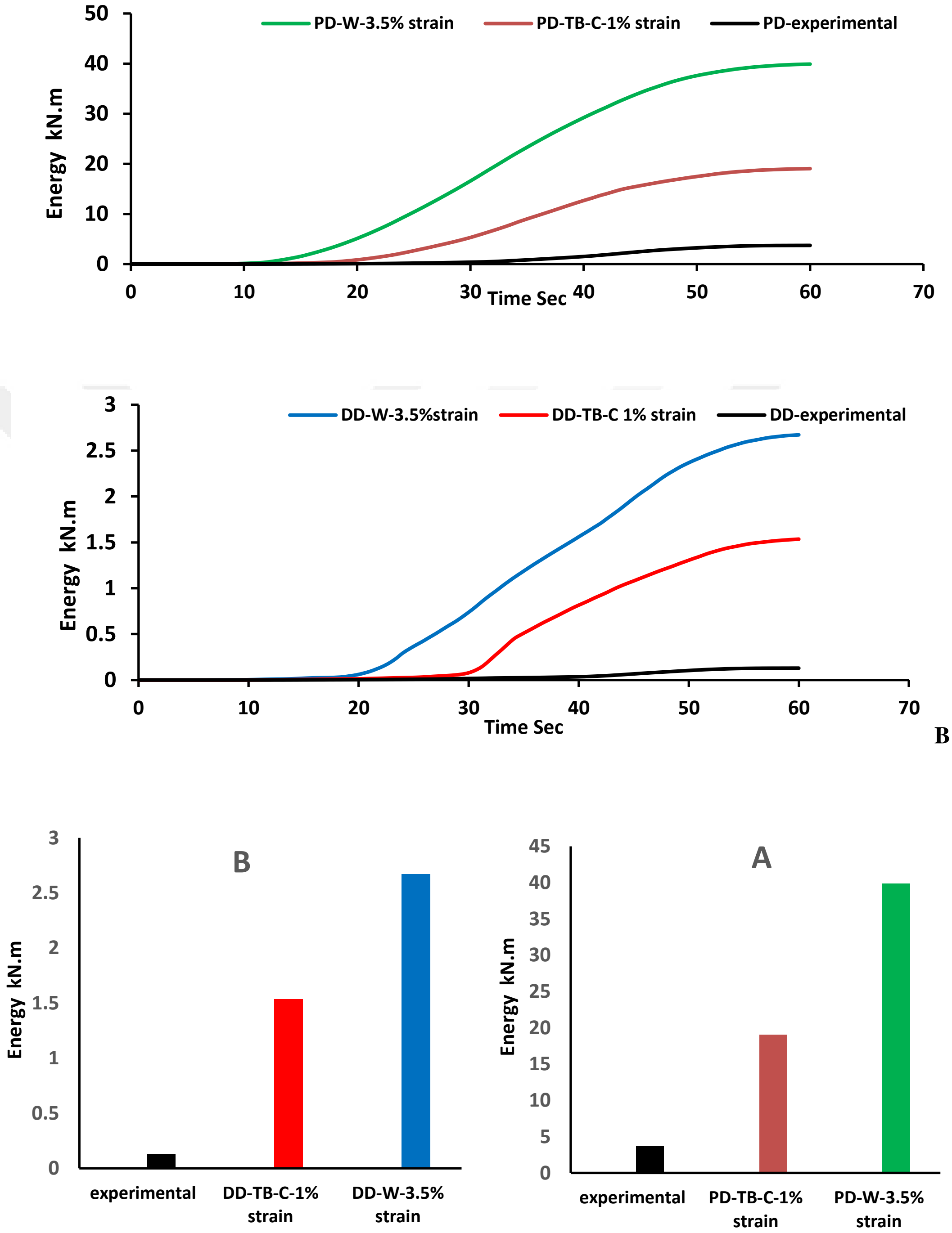

Figure 5.21 A, B, plastic, damage dissipation energy for higher and lower FEM 2CMH18 and experimental respectively.

CHAPTER 6

DISCUSSION OF RESULTS

6.1 Effect of Jacketing Strategies on Lateral Load-Displacement

The figures (5.2, 5.7, 5.12, 5.17) present load-displacement for all jacketed specimens and compare them with experimental samples. I will discuss that in sections below:

6.1.1 3CLH18 Lateral Load-Displacement

This study has base on the average a peak lateral load response to avoid some unreliable results, as shown in figures (5.3, 5.12) due to the rate of applied load, the difference in internal friction angle, and the exaggerated peak load of specimens that led to a maximum load higher than expected before sudden failure.

Obviously, tables (5.2, 5.3) show shear-displacement of FEA 3CLH18 with 3.5% and 1% hardening tension strain of ECC jackets for each five jacketed techniques. The specimen WR-3.5% strain has exhibit highest lateral load response (340 KN), corresponding to a failure displacement =115 mm, which is more than the experimental result, which has the maximum shear force =271.3 kN and the corresponding displacement was 30.5 mm, by 26% and 277%, respectively. The specimen TB-C-1% strain has a lower peak lateral load =332 KN, at failure displacement =38 mm, with 22.5% and 24.6%, increases of lateral load and corresponding deflection, respectively, however, there is a significant difference in the failure pattern following this greatest load.

The peak lateral load values of all jacketed specimens were close to each other's, although the specimens WR, W, and WC (3.5%, 1%) were exposed to lateral displacement =120 mm, which is considered higher than TB, TB-C = 90 mm (3.5% and 1%), and experimental lateral displacement = 60 mm by 33% and 100%, respectively, which are determine the reliability of these methods.

The samples WR-3.5% and W-3.5% have improve lateral displacement ranges that are compatible with peak load staying constant at the curve tip, whereas the former has a (45- 110) mm of constant displacement range without any drop in capacity, and the latter has a (50- 105) mm, displacement range that was increased by 12 and 10 times compared with the tested displacement range (25-30) respectively. The specimens TB-3.5%, TB-1%, TB-C-1% have the same displacement range, corresponding to staying peak load as a constant without enhancing it, and they have a same general behavior, which means these jacketing styles have a lower efficiency between them.

6.1.2 2CLH18 Lateral Load-Displacement

The figure (5.7) and the tables (5.4, 5.5), clarify the lateral load-displacement of FEA 2CLH18 with 3.5% and 1% hardening tension strain of ECC jackets for each of the five retrofitting strategies. The specimen 2CLH18-WR-3.5% strain has exhibit highest peak lateral load response (272 KN), corresponding to a failure displacement =320 mm, at 20% of the peak load have been lost, which is higher than the experimental result, where the shear force of 240 kN and the corresponding displacement=76.2 mm, by 13% and 319% respectively. The specimen TB-C-1% strain has appeared a lower peak lateral load =245 KN, at failure displacement =160 mm, with just 2%, 110%, as an increasing of load and lateral deflection respectively.

The peak load values and mechanism failure of all jacketed specimens were close to each other's, although the specimens WR-3.5% strain was exposed to lateral pushover =360 mm, which is considered higher than W-1%, WC-1%, TB and TB-C (3.5% and 1%), and experimental lateral displacement of 100% and 300%, respectively.

The specimens WR-1%, W-3.5% subjected to maximum lateral displacement = 270 mm, that higher than the other jacketed techniques and tested sample by 50%, 200% respectively, which explains the reliability of these methods.

The specimens WR-3.5%, W3.5%, WR-1%, and WC-3.5% have enhance lateral displacement ranges that are corresponding to peak load staying as constant at the curve tip, where (50-230) mm, (60-180) mm, (55-205) mm, and (60-180) mm, were increased by (6, 5, 4, 4) times compared with the tested displacement range (40-70), respectively. The specimens WC-1%, TB-C-3.5%, and TB-C-1% have the same displacement range corresponding to tested 2CLH18, where the maximum load stays as a constant without enhancing it. All kinds of jacketed specimens have the same general behavior, which means these jacketing styles have a lower effect on maximum shear load because the experimental 2CLH18 has a good ability under applied loads.

6.1.3 3CMH18 Lateral Load-Displacement

The figure (5.12) and the tables (5.6, 5.7) show lateral load-displacement of FEA 3CMH18 with 3.5% and 1% hardening tension strain of ECC jackets for each of five retrofitting strategies. The specimen WR-3.5% strain has given highest lateral load (426.5 KN) at failure displacement of 117 mm, that was higher than the experimental peak lateral load of 338 kN and corresponding displacement of 30.5 mm, with 26% and 283% increases, respectively.

The specimen TB-1% strain present a lower peak lateral load =394 KN, at a failure displacement =38 mm, with 16.5% and 24.6% increasing of peak load and lateral deformation, one by one.

The peak load values and mechanism failure of all jacketed specimens were close to each other's, but there is a significant difference in the failure pattern after peak load.

The specimens WR, W (3.5%, 1%) strain were exposed to maximum lateral displacement =120 mm, which is considered higher than TB, and TB-C (3.5% and 1%) with 90 mm, WC (3.5%, and 1%) with 75 mm, and tested maximum lateral displacement was 60 mm, by 33%, 60% and 100% respectively.

The samples WR-3.5%, and W-3.5%, have improve lateral displacement range that corresponding to the peak load staying constant at the curve tip, where they have (30- 65) mm, which increase by 7 times compared with the tested displacement range (23-28). The spacemen WR-1%, and WC-3.5% have (30- 55) mm and (30- 50) that represent 5 and 4times increase respectively.

The rest of the specimens TB, TB-C (3.5%, 1%), WC-1%, and W-1% have the same displacement range as the 3CMH18 tested sample, which corresponding to staying peak load as a constant without enhancing it, and they have the same general behavior, which means these jacketing styles have a lower efficiency between them.

6.1.4 2CMH18 Lateral Load-Displacement

The figure (5.17) and the tables (5.8, 5.9) show load-displacement of FEA for 2CMH18 with 3.5% and 1% hardening cracks strain of ECC jackets for each the five jacketing strategies. The specimen WC-3.5% strain appeared the highest load response (315 KN) at failure displacement of 117 mm, that was higher than experimental result, where peak lateral load = 290 kN and corresponding displacement=30.5 mm, with 8.6% and 283% increased, respectively.

The specimens TB and TB-C-3.5% strain present an approximately same increasing peak load =304 kN, 306 kN, at the failure displacements =90, 88 mm, respectively, with about 5% and 195% increasing of load and lateral deformation, respectively, while the specimens WR, W capture the same peak load of tested sample because it exposed to lateral displacement bigger than WC-3.5% by 50%, that is confirm whenever increase pushover displacement that led to decrease the peak load.

The specimens WR and W (3.5%, 1%) strain were subjected to a maximum lateral displacement was180 mm, which is considered higher than WR-1% and W-1% strain, with 150 mm, WC (3.5% and 1%) with 120 mm, TB and TB-C (3.5% and 1%) with 90 mm, and tested 2CMH18 with 30.5 mm, by 20%, 50% and 100%, 500%, respectively.

This study proposes equation to predict the shear capacity of ECC jackets for column with shear deficiency depending on Building Code Requirements for Structural Concrete (ACI318-19) [68] by using the net area of ECC jacket and convert it to equivalent Square and postulate the affect of axial load on ECC jackets = 0 as below:

$\mathbf{A_{ECC} = A_T - A_{column}}$

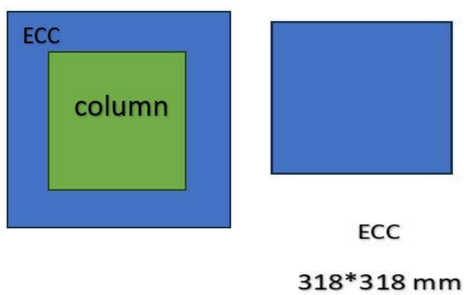

$\mathbf{A_{ECC}} = (557*557) – (457*457)$

$\mathbf{A_{ECC}} = 101400\ mm^2$

dimension of equivalent square ECC = 318*318 mm

1- d $_{ECC}$ =318-102 =216 mm when ECC thickness = 50 mm (All jackets types except no.2).

2- d $_{ECC}$ =250-50 = 200 mm when ECC thickness = 37 mm (Jacket type with replace cover with ECC.

The size effect modification factor λ_s shall be determined by ACI 318-19 (22.5.5.1.3)

$$\lambda_s = \sqrt{\frac{2}{1+0.004\,d}} \leq 1$$

$$\mathbf{V_{ECC} = 0.17\, \lambda s * (\sqrt{fc'_{ECC}}) * bw * d_{ECC}}$$

Where: V_{ECC}, fc'_{ECC}, bw, d_{ECC} are Shear response of ECC jacket, compression strength of ECC, ECC equivalent square dimension, distance from out face of column to center of longitudinal bar.

6.2 Ductility of Jacketed Specimens

This study focuses on one of the most significant properties of structural members, "Ductility" which can be defined as the ability of member to exhibit a high deformation response undergo external excitations prior to failure. It was directly correlated with plastic stage deformation, which is consider a crucial factor under an earthquake and another sever dynamic loading. Thesis has depend on displacement ductility, which represented the ratio of ultimate displacement at 20% of load capacity drop to yield displacement where jacketed techniques present a high area under load-displacement curve as well as ductility.

6.2.1 3CLH18-Specimens Ductility

The development of local inclined cracks, the yielding of reinforcement, early stirrup yielding, which are related to shear strength loss due to brittle behavior, low tensile stress, and the corresponding crack strain of normal concrete, it's required a high ductility, that will lead to a high shear response particularly in columns to avoid the sudden collapse under dynamic load. It is clearly realized by above jacketed strategies.

The tables (5.2, 5.3) present all finite element calculations associated with the ductility of 3CLH18 of different strengthening patterns with 3.5% and 1% of ECC hardening tension strain and compared them with experimental specimen ductility. They are exhibit approximately same yield displacement, but each specimen had a various ultimate displacement (δ_u) corresponding to 20% of peak load response was lost.

All jacketed specimens have an equalize yield displacement of 22 mm on average, with a slight increase about 15% of the tested yield displacement =19 mm. The ultimate displacement considers a predominant factor directly effecting ductility.

The specimens WR and W (3.5% strain) exhibit δ_u = 115 mm and 110 mm, with 277%, and 260% higher than tested δ_u = 30.5 mm, respectively. The specimens TB, TB-C (3.5% strain) appeared δ_u = 52 mm and 50 mm, with rising by 70% and 64% of empirical ultimate displacement.

Under the same principle, WR and W (1% strain) present δ_u= 85 mm and 60 mm, increasing by 178%, and 96% compared with the experimental sample. The specimens TB and TB-C (1% strain) exhibit δ_u= 48 mm, and 38 mm with 57%, 24.6%, as an increase compared with the tested ultimate displacement.

As a result of increasing the ultimate displacement, ductility will increase, where the specimens WR and W (3.5% strain) have given μ_Δ= 5.2, 5 with 226%, 212% higher than tested displacement ductility =1.6, respectively. While the specimens TB and TB-C (3.5% strain) have exhibited μ_Δ= 2.16, 2.5 mm, which corresponding to 35%, 56% higher than tested displacement ductility as well. The specimens WR, and W (1% strain) have given μ_Δ= 3.86, 2.7 with 141%, 68.7% larger than tested displacement ductility, while the samples TB, and TB-C (1% strain) have given μ_Δ= 2, 1.9 with 25%, and 18% higher than empirical displacement ductility.

There are two important matters to discuss, the first, for each two similar techniques, the ductility of the specimen with a 3.5% hardening strain is higher than the ductility with a 1% strain, where an increase in the ECC hardening tension strain led to a delay formation the cracks under the same tension stress, where coated ECC exhibits multiple micro cracks higher than the uncoated ECC. The second, whole jackets technique have present highest ductility associated with large inelastic deformations prior failure and comparing TB, TB-C, due to the former technique was strengthening whole length of column compensated deficiency in transverse reinforcement by increasing confinement of columns, where that’s prevent an expected shear failure, and flexure failure will be occur which extend to the pedestal where weak concrete still there, and absorb large plastic energy than the TB,TB-C as shown in figure (5.5) by 146%, also whole jacketed was distribute the stress over length of column better than the other techniques, the specimens TB, TB-C strengthening will transform plastic hinge toward column center and concentrated the stress on line between ECC-cover and column cover which led to propagate inclined cracks and shear failure will occur.

6.2.2 2CLH18-Specimens Ductility

The tables (5.4, 5.5) present all finite element ductility of 2CLH18 with different strengthening methods using 3.5% and 1% of ECC hardening tension strain and compared it with the ductility of the experimental specimen. Also, they exhibit approximately same yield displacement, but each specimen has a various failure point, where 20% of peak load response was lost, that related with ultimate displacement (δ_u).

All jacketed specimens have an equalized average yield displacement of 22 mm, with increase of 46.6% of the tested yield displacement =15mm. The ultimate displacement is consider a prevalent factor directly affected on ductility.

The specimens WR and WC, W (3.5% strain) have ultimate displacement δ_u= 320 mm and 260 mm, with 319%, and 241% higher than the tested δ_u=76.2 mm, respectively. The specimens TB and TB-C (3.5% strain) exhibit δ_u=180 mm and 178 mm, with increase by 136% and 133% of empirical ultimate displacement.

Under the same principle, WR, and W (1% strain) have ultimate displacement δ_u = 260 and 180 mm, with increasing by 241%, 136% compared with experimental ultimate displacement δ_u = 76.2 mm. The specimens WC, and TB-C (1%strain) have given δ_u = 165 mm, and 160 mm with 116% and 110% an increase compared with tested ultimate displacement.

As a result of increasing the ultimate displacement, it will increase the ability of plastic deformation for jacketed members prior to collapse, where the specimens WR and W (3.5% strain) present displacement ductility of $\mu\Delta$ = 14.5, 13 with 185%, and 155%

higher than tested displacement ductility = 5.1, respectively. The specimens TB and TB-C (3.5% strain) are exhibit μ_{Δ} = 9, 7.4 mm which corresponds to 80% and 45% higher than tested displacement ductility as well. The specimens WR, and W (1% strain) are get μ_{Δ}=11.8, 9 with 131%, and 76% larger than tested displacement ductility, while the samples WC, TB-C (1% strain) present $\mu\Delta$= 6.87, 6.6 with 35%, 35% higher than empirical displacement ductility, the specimens WC and TB-C (1% strain) have the lowest ductility because decreasing the ultimate displacement response and increase the yield lateral displacement =24 mm which ensures, the limited capacity of uncoated ECC.

The significant matter correlation with ductile behavior of the original column core is that for each of the two similar strategies, the ductility of the specimen with a 3.5% hardening strain higher than the ductility with a 1% strain, where an increase in ECC hardening tension strain led to delay formation the cracks under same tension stress, but unjacketed core has given a valuable ductile behavior because it has a high compression strength =33 MPa, a tension stress = 2.82 MPa, undergo light axial load that's led to a good empirical ductility

The whole jacket techniques have a best ductility compared with TB, TB-C due to the former techniques was strengthening whole length of column where prevent an expected shear failure as discuss above, , and absorb large plastic energy than the TB, TB-C as shown in figure (5.5) by 130%, also whole jacketed was distribute the stress over length of column better than the other techniques, the specimens TB,TB-C strengthening will transform plastic hinge in direction of column center and concentrated the stress in join part between ECC-cover and concrete-cover where excessive shear force led to bond-failure and propagate inclined cracks in the plane parallel to the applied lateral load where shear failure will occur.

6.2.3 3CMH18-Specimens Ductility

The tables (5.6, 5.7) present all finite element results associated with the ductility of 3CMH18 with different strengthening using 3.5%, as well as 1% of the ECC hardening tension strain, and compared them with the ductility of experimental specimen. They exhibit approximately the same yield displacement, but each specimen had a clear difference in failure point, where 20% of the maximum lateral response was lost, which refers to ultimate displacement. All jacketed specimens have an equalized average yield displacement 22.8 mm, which is close to the tested yield displacement= 22.6 mm.

The ultimate displacement δu is considered a prevalent factor directly affecting on ductility.

The specimens WR and W (3.5% strain) achieve δ_u = 117 mm, 115 mm, with 283%, and 277% higher than the tested δ_u = 30.5 mm, respectively. The specimens WC, and TB (3.5% strain) have δ_u = 53 mm, 38 mm, with rising by 73%, and 24.5% of empirical ultimate displacement.

Under the same meaning, WR, and W (1% strain) achieve δ_u = 94 mm and 90 mm, respectively, increase by 208%, and 195% compared with the experimental sample. The specimens TB-C, and TB (1% strain) give δ_u = 48 mm, 38 mm with increase by 57%, and 24.6%, respectively, compared with tested ultimate displacement.

As a result of increasing the ultimate displacement, ductility will increase, where the specimens WR, and W (3.5% strain) have μ_Δ= 4.87, and 4.79 with 274%, and 268%, respectively, higher than the tested displacement ductility =1.3. The specimens WC, and TB (3.5% strain) have exhibited μ_Δ= 2.3, 1.9 mm, which corresponds to 77%, 46% higher than the tested displacement ductility as well.

The specimens WR, and W (1% strain) have given μ_Δ=3.91, 3.75 with 200%, 188% larger than tested displacement ductility, while the samples TB-C, and TB (1% strain) have μ_Δ= 2.1, 1.9 with 60%, 46% higher than empirical displacement ductility.

The ductility of all specimens with a 3.5% hardening strain is higher than the ductility with a 1% strain, where the crack mechanism of the coated ECC has exhibit multiple microcracks higher than that of the uncoated ECC.

The whole jacket techniques have highest ductility associated with large inelastic deformations prior to failure except WC, compared with TB and TB-C, due to the former technique was strengthening the whole length of column compensated deficiency in transverse reinforcement by increasing confinement of columns, where that's prevent an expected shear failure, due to the weak compression strength =25.7

MPa, the single local crack in the mid-pedestal is evident, and this ensures high activity of whole jacketing methods , it's clearly WC-1% strain has ductility =2.43 larger than the ductility of WC-3.5% =2.3, that were occurred due to WC-3.5% exposed to lateral displacement 75mm larger than WC-1% = 65 mm where decrease ductility by 5% when increase lateral displacement 15%, this increment led to increase load-capacity by 2.5% and sudden failure will occur which explain reduce the ultimate displacement of WC-3.5% as well as refers to the ductility not just depend on the ECC-tension strain , but also the maximum lateral load which can be applied prior sudden collapse, as shown in the figure (5.12E), and absorb large plastic energy than the TB,TB-C as shown in figure(5.15) by 54%, also whole jacketed was distribute the tensile stress over length of column better than the other techniques, a plastic-hinge region of the specimens TB,TB-C transformed in direction of column center and concentrated the damage, furthermore, excessive cracks in lower- new plastic hinge which led to propagate inclined cracks and occur shear failure, this ensure the bottom jacketing type effaced more than top-jacket whenever increase shear force.

6.2.4 2CMH18-Specimens Ductility

The tables (5.8, 5.9) present all finite element results associated with the ductility of 2CMH18 with different strengthening types using 3.5%, as well as 1% of the ECC hardening tension strain, and compared them with the ductility of an unjacketed specimen. They have given approximately the same yield displacement, but each specimen had a clear difference in failure point, where 20% of the peak lateral capacity was lost, which refers to ultimate displacement δu. All jacketed specimens have an equalized yield displacement 20.8 mm, as average value, that higher than the tested yield displacement= 16.5 mm, by (26%).

The specimens WR, and W (3.5% strain) exhibit δ_u= 152 mm, and 145 mm, with 398%, 375%, respectively higher than tested δ_u = 30.5 mm. The specimens TB, and TB-C (3.5% strain) have δ_u= 90 mm, 88 mm, with 191% higher than empirical ultimate displacement δu.

Under the same principle, WR, and W (1% strain) achieve δ_u = 145 mm, and 140 mm, respectively, increasing by 375%, and 359% compared with the experimental sample.

The specimens TB, and TB-C (1% strain) have δ_u = 87 mm, 73 mm, with 185%, and 139% an increase compared with tested ultimate displacement.

As a result of increasing the ultimate displacement, ductility will increase, where the specimens WR, and W (3.5% strain) have given μ_Δ= 7.6, 7.25 with 322%, and 300% higher than tested displacement ductility =1.8. The specimens TB, and TB-C (3.5% strain) have given μ_Δ= 4.1, 4.4 mm, which corresponds to 127%, 144% higher than tested displacement ductility as well. The specimens WR, and W (1% strain) have μ_Δ=7.25, 7 with 300%, 288% larger than tested displacement ductility, while the samples TB, TB-C (1% strain) have μ_Δ= 3.95, 3.65with 120%, 100% higher than empirical displacement ductility.

Table 6.1 Ductility equations suggest for ECC jacketed specimens

$\mu j = \mu c + 1.8\mu c *(\beta)^{0.8}$	Compression strength of 26.89 MPa, undergo the light axial load and difference maximum lateral displacement.
$\mu j = \mu c + 1.15\ \mu c*(\beta)^{0.5}$	Compression strength of 33 MPa, undergo to the light axial load and difference maximum lateral displacement.
$\mu j = \mu c + 2.3\mu c *(\beta)^{0.8}$	Compression strength of 25.74 MPa, undergo to the moderate axial load and difference maximum lateral displacement.
$\mu j = \mu c + 3\mu c *(\beta)^{0.5}$	Compression strength of 27.65 MPa, undergo to the moderate axial load and difference maximum lateral displacement.

The ductility of all specimens with a 3.5% hardening strain is higher than the ductility with a 1% strain, where the crack mechanism of the coated ECC has exhibit multiple micro cracks prevent formation early local cracks higher than the uncoated ECC.

The whole jacketed techniques have given the highest ductility related to large inelastic deformations prior failure except WC, and compared with TB, TB-C, due to the first techniques were strengthening whole length of column compensated deficiency in transverse reinforcement by increasing confinement of columns, where that's prevent an expected shear failure, while the top-bottom jacketing will generate a new plastic hinge under top jacket , and upper bottom one, which express appeared horizontal cracks in cover which developed to inclined cracks in plane parallel to applied lateral load where expected shear failure will be occur, which requires increasing transverse steel bars at region between top-bottom jacket to prevent shear collapse, and absorb large plastic energy than the TB,TB-C as shown in figure (5.15) by 90%, also whole

jacketed was distribute the tensile stress over length of column better than the other techniques, a plastic-hinge region of the specimens TB, TB-C transformed in direction of column center and concentrated the damage. Furthermore, the unjacketed core has a compression strength of 27.65 MPa, a tension stress = 2.75 MPa, under moderate axial and decreasing maximum lateral response = 30 mm, which led to a delay in the appearance of the inclined shear cracks, and this jacketing method was succussed with this column type. This study suggests an equation to calculate expected ductility of jacketed specimens as below:

Where: $\beta = \frac{L_j}{L_c}$

L_j, L_C are ECC jacket length mm, and length of original column mm, respectively.

μ_j, μ_c are jacketed specimen ductility and original column ductility respectively.

6.3 Fracture Mechanism

Materials quality, stresses distribution, and environmental effects, loading and boundary conditions all play a role in the concrete fracture mechanism. Due to its fragile nature, concrete often breaks abruptly and with little to no deformation which include initial cracks, propagation of cracks, reinforcement effect on failure.

6.3.1 Initial Cracks, Propagation of Cracks and Failure Mechanism

This section shows the fracture stages and correlation stresses for all specimens, which vary depending on the type of jacketing, core specifications as well as maximum applied lateral displacement.

The methodology adopts in this study to capture the first crack stress of all specimens based on the maximum principal stresses corresponding to average damage in tension dt = 0.6, where, it visual seen from tension damage distribution FE analysis, which generated directly after reaching the physical ultimate tensile stress of the core at position where the first crack would be expected to appear due to the low material properties of the column core compering with ECC in tension and compression.

First of all, 3CLH18-jacketed specimens exhibit a different first crack stress that is generated earlier in the cover of the column core depending on the type of strengthening, which can be summarized in the table below:

Table 6.2 First cracks and failure mechanism of 3CLH18-jacketed specimens

Jacketed sample	Mechanism of cracks
WR-3.5 WR-1	First of all, the cracks start at the top and bottom opposite tension regions of the core perpendicular to applied displacement, where crack stress was 2.64 MPa, which is considered ultimate tension stress of the core, but the cracks of WR-1% propagated larger than WR-3.5% under the same lateral displacement = 120 mm (double original maximum displacement), where that’s refers to the high ability of coated ECC to contribute larger plastic deformation than the uncoated ECC as well then, after increase loading led to formation a single local shear crack in the cover at mid-upper and lower pedestals, then continued to pedestal edge.
W-3.5 W-1	Horizontal cracks start at the top and bottom opposite regions of the core perpendicular to applied displacement, where the crack stress was 2.64 MPa, where the cracks propagation of W-1% higher than W-3.5% due to the limited capacity of the uncoated ECC to absorb plastic deformation then a single local shear crack formed in the cover at mid-lower pedestal, then continued to the edge.
TB-3.5 TB-1	Horizontal cracks of the concrete cover of the core at the border line between the ends of the upper and lower jackets with columns, then developed towards the center of the column at a tension stress of 2.64 MPa, then after increasing the lateral displacement to 90 mm (1.5 original displacement), shear failure will occur toward the core center.

Table 6.2 (continue) First cracks and failure mechanism of 3CLH18-jacketed specimens

WC-3.5 WC-1	Horizontal cracks appear in the upper and lower tension zones of the core at a tension stress of 2.64 MPa, then developed at column-pedestal joints, and then local inclined crack just propagated in the lower pedestal. The permanent stress in WC-1% is larger than that in WC- 3.5% which is considered as index of plastic deformation.
TB-C-3.5 TB-C-1	Horizontal cracks appear in the column-ECC, and column-pedestal region, then after reach the applied lateral displacement to 75 mm (1.25 of original maximum displacement), increasing stress in the ECC bottom layer due to the little thickness of ECC layer = 37 mm and the high confinement of the coated ECC, which is represents by increase resistance strength.
Tested	Horizontal cover cracks start in upper, lower column-pedestal joint and propagated towards center of column in plane x-y perpendicular to applied lateral displacement, then developed to shear cracks when increase lateral load.

The table (6.2) expresses various kinds of crack styles. Whole-jacketing types (3.5%, 1% tension strain) worked to delay the appearance of cracks at early time during loading, where the first-crack stress increased by an average of about 715%, and 380% compared with the experimental first-crack stress = 1.4 MPa, respectively. In contrast, TB-C (3.5%, 1%) captures approximately the same first-crack stress at the same degree of damage in the tension of the experimental sample.

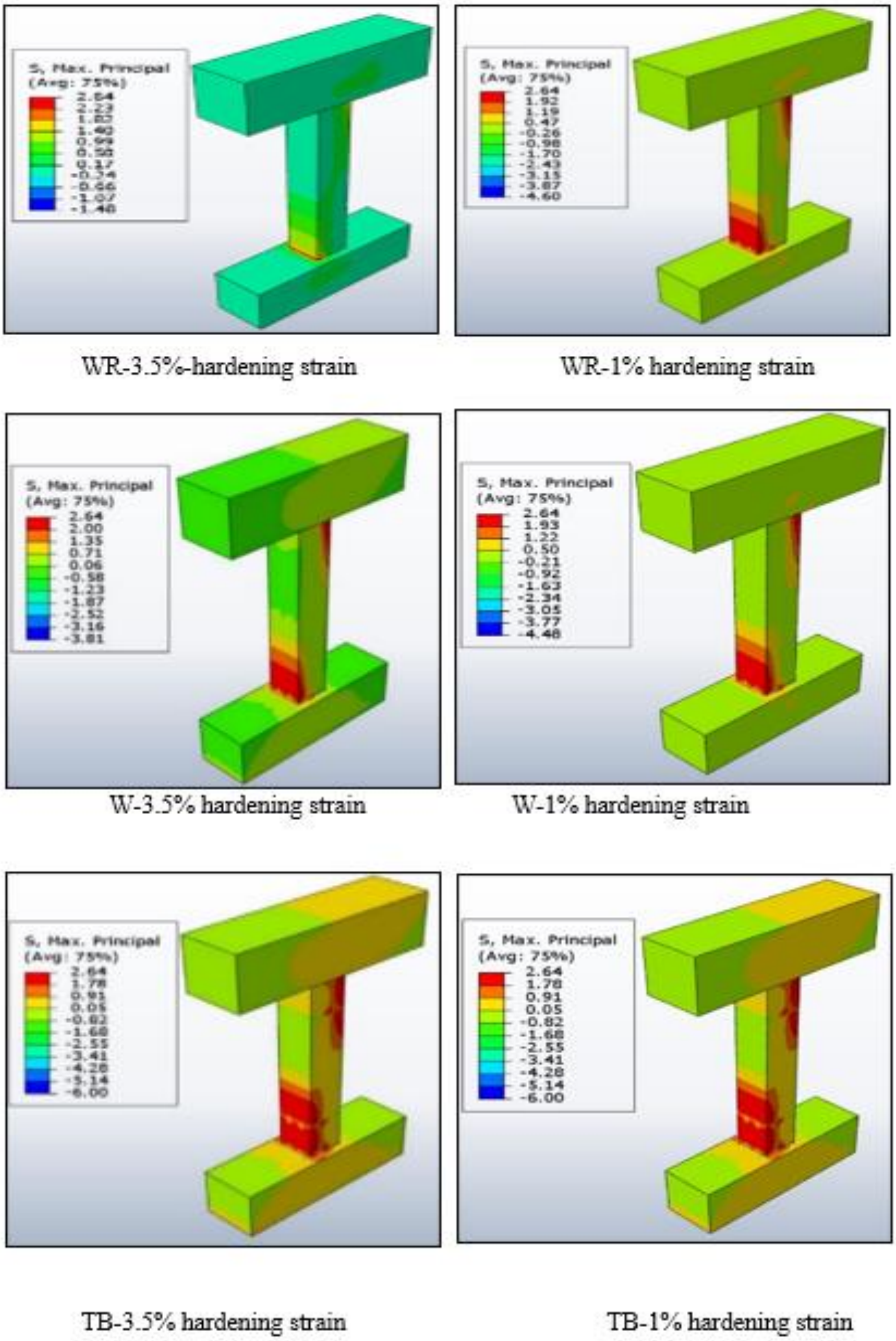

Figure 6.1 Maximum principal stress at first tension cracks for 3CLH18 with difference jacketed techniques

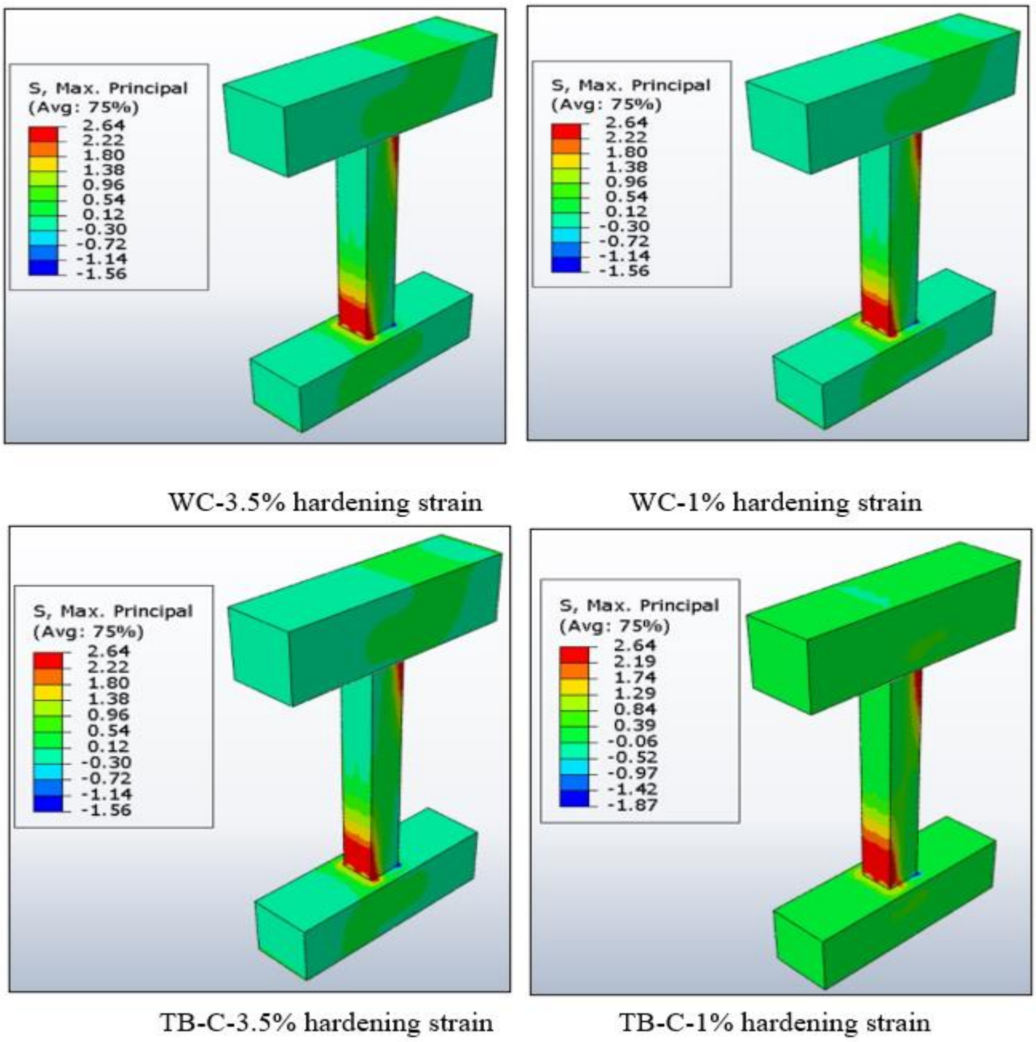

Figure 6.1 (continue) Maximum principal stress at first tension cracks for 3CLH18 with difference jacketed techniques

The table (6.3) below expresses various kinds of crack modes of 2CLH18 column. Whole-jacketing types (3.5%, 1% tension strain) worked to delay the occurrence of cracks at early time of loading where the first-crack stress increased by an average of about 665%, and 360% compared with the experimental first-crack stress = 2 MPa, respectively. In contrast, TB-C (3.5%, 1%) captures approximately the same first-crack stress of experimental sample.

Table 6.3 First cracks and failure mechanism of 2CLH18-jacketed specimens

Jacketed sample	**Mechanism of cracks**
WR-3.5 WR-1	Horizontal cracks start in the X-Y plane at the upper and lower tension side perpendicular to the applied lateral load, as shown in figure (6.2), where the core jacketed with coated-ECC exhibited lower cracks than the core with uncoated-ECC at the same tension stress = 2.85 MPa, due to the high plastic deformation absorption capacity of coated ECC under same lateral displacement =360 mm (4-times of maximum original displacement). For 3.5% strain, a crack formed in upper column-pedestal zone in x-y plane perpendicular to applied-displacement and with same direction of, while in reverse direction of lateral displacement in lower-pedestal. The ECC with 1% strain has the same mechanism but the cracks propagate around all sides of the column bases. The cracks in both cases didn't reach mid-two pedestals due to high compression strength =33 MPa, and good ductility of the core. All damages occur due to concrete crash in compression at upper-column, and crack in tension in lower of column.
W-3.5 W-1	The cracks formed at the upper and lower tension sides perpendicular to the lateral load direction. The core jacketed with coated-ECC exhibited lower cracks than core with uncoated-ECC at the same tension stress = 2.85 MPa, due to the high plastic deformation absorption under the same lateral shear displacement=180 mm Then the cracks propagate at the column-pedestal zone on one side perpendicular to displacement in the +Z and -Z planes, respectively without extending to pedestals because it provided less restriction than WR jacketing methods. All damages occur due to concrete crash in compression at upper-column, and crack in tension in lower of column

Table 6.3 (continue) First cracks and failure mechanism of 2CLH18-jacketed specimens

TB-3.5 TB-1	The horizontal cracks start in the upper and lower tension sides X-Y plane of the core perpendicular to the applied lateral load direction, where they increased in the core jacketed with uncoated ECC due to similar reasons in section above. After that, the cracks extended at ECC-column inside zone of column and propagate toward the column center perpendicular to displacement in +z-direction for top jacket, and -z direction in bottom jacket, after increasing the displacement led to propagation these cracks to both pedestals. In this technique shear failure will be occur due to transport the plastic hinge and concentrated shear stresses in weak region toward center. center and that's mean little available transverse reinforcement in this part.
WC-3.5 WC-1	The cracks start in the upper and lower tension sides X-Y plane of the core. The core jacketed with both coated and uncoated ECC exhibit approximately the same cracks at tension stress = 2.85 MPa, under the same loading conditions due to first cracks directly correlated with core resistance, where the ECC importance stand out in the final stages of failure as well. Then, both column-pedestal regions, after increasing displacement, will extend to both of them due to the decrease jacketed thickness =37 mm, which is available low confinement compared with WR, and W jacketing methods, where that emphasizes high ability of these additional cover to absorb the most energy which caused early damage of the original column-cover.
TB-C-3.5 TB-C-1	The first crack begin tension side X-Y plane of the core then, it appears in both ECC-column and column-pedestals, simultaneously, in this case, due to decrease jacketed thickness=37 mm, and poor control of stresses due to increasing applied lateral displacement =180mm (2-times of maximum applied displacement) that's led to the same effect of both types of ECC. Then, the horizontal cracks perpendicular to displacement will extend to the column center in +Z and -Z planes for the upper and lower jackets respectively. After increase lateral load, led to the shear cracks propagated in parallel to the applied load which that refers to weakness of jackets when

Table 6.3 (continue) First cracks and failure mechanism of 2CLH18-jacketed specimens

Tested	The first crack start in both the top and bottom edges of the column, then horizontal cracks will extend in x-y plane perpendicular to the applied displacement; eventually, they will develop on the other side parallel to lateral load with spalling cover at the corners.

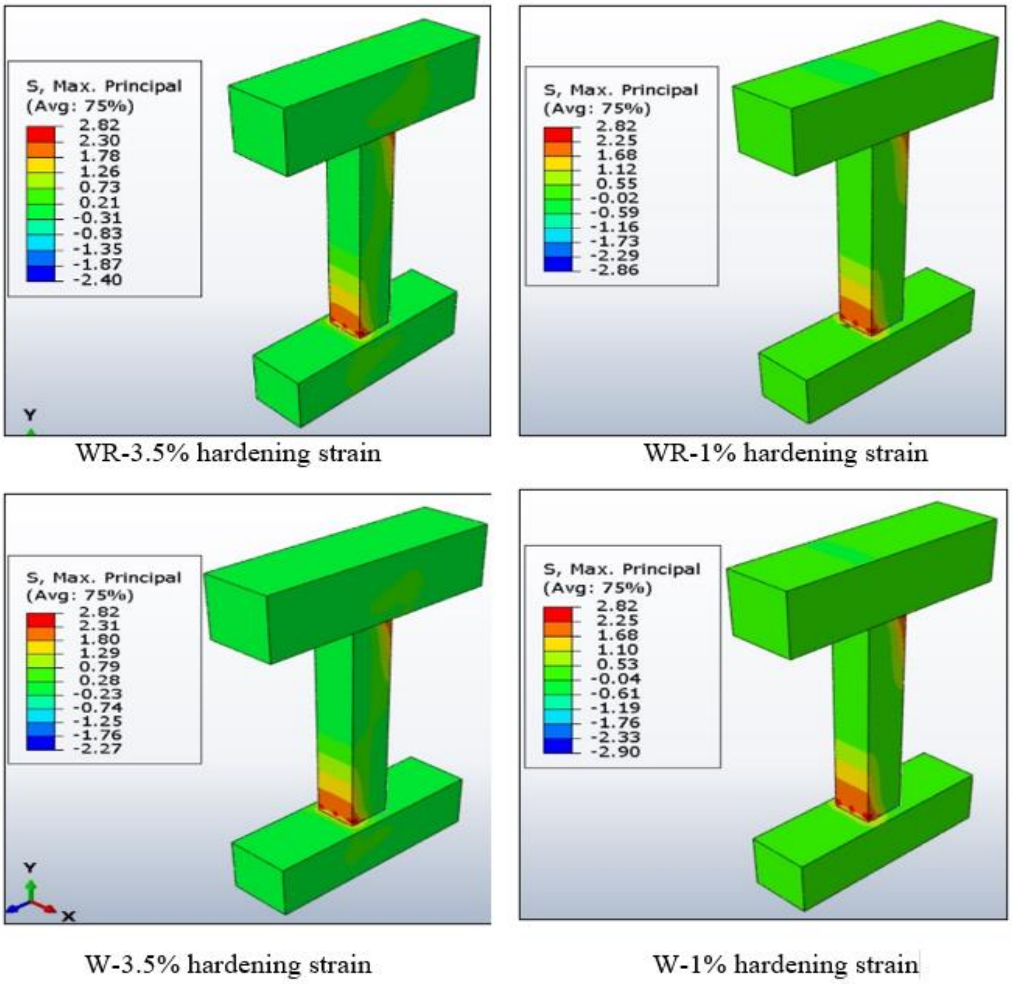

Figure 6.2 Maximum principal stress at first tension cracks for 2CLH18 with difference jacketed techniques

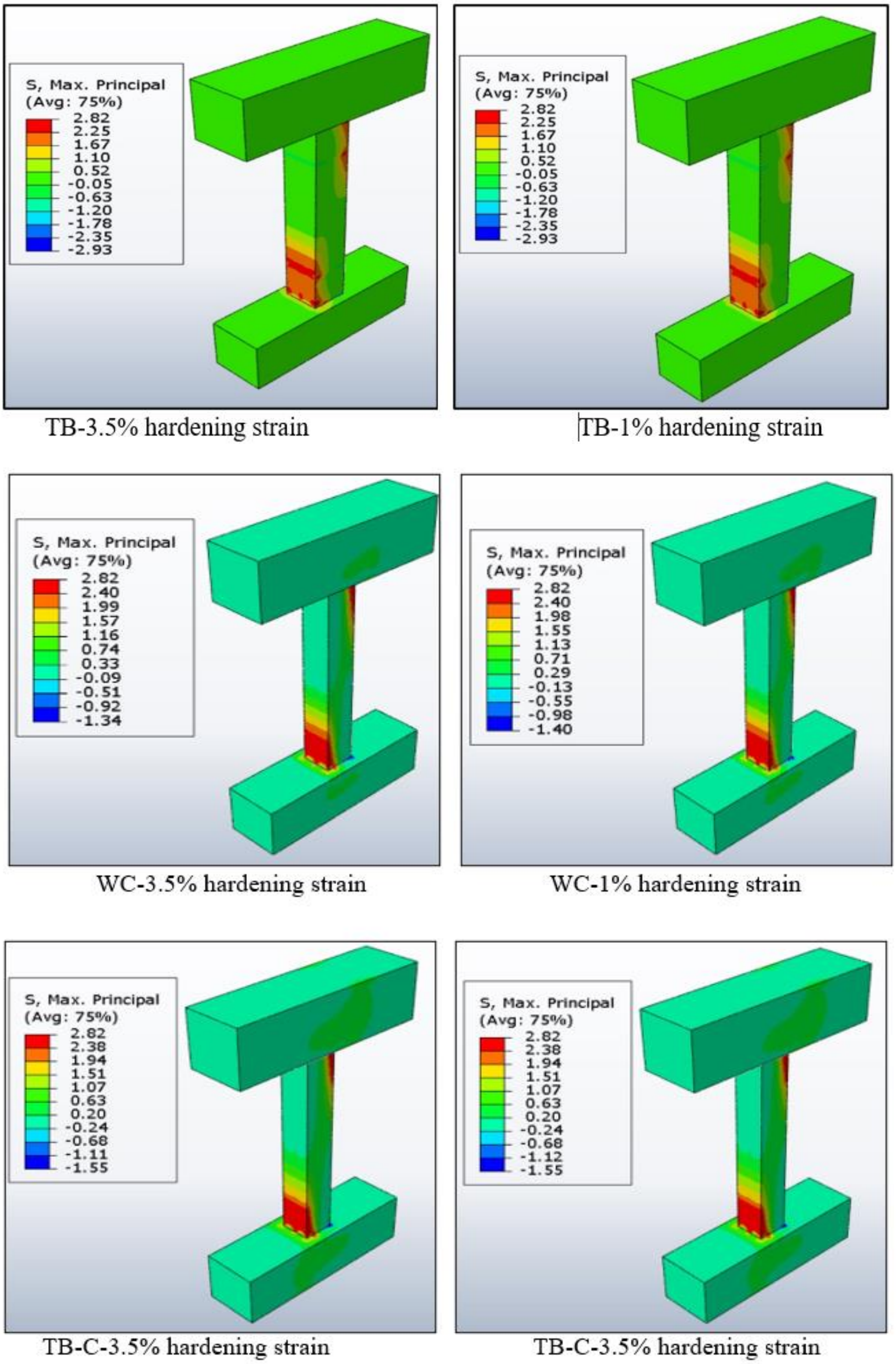

Figure 6.2 (continue) Maximum principal stress at first tension cracks for 2CLH18 with difference jacketed techniques

The table (6.4) below shows the first crack stress and general fracture approach under monotonic loads for 3CMH18-jacketing specimens:

Table 6.4 First cracks and failure mechanism of 3CMH18-jacketed specimens

Jacketed sample	Mechanism of cracks
WR-3.5 WR-1	Horizontal cracks start in the upper and lower tension side X-Y plane of the core as shown in figure (6.3). The core jacketed with coated ECC exhibit cracks less than the uncoated ECC at tension stress=2.36 MPa, under the same loading conditions due to the first cracks directly correlated with the original columns core resistance, where the effect of ECC was little at the first loading stage. The cracks of the WR-3.5 specimen appeared in the upper and lower column-pedestals perpendicular to applied displacement in -Z compression side and +Z tension side direction, respectively, with the local-inclined crack in the mid-both pedestals, due to the high confinement of a 3.5% hardening strain, which led to development this crack in weak section (pedestals), while the WR-1 has same cracks mechanism except the inclined crack appeared in top-plastic hinge due to increasing the lateral load about two times of the tested applied load, which ensures the limited ability of 1% strain.
W-3.5 W-1	The crack begin in both column-pedestals join in two opposite directions -Z (applied lateral displacement direction) and +Z for the upper and lower pedestals, respectively. Then extend cracks around column-pedestal in all sides in addition, the W-1% has exhibit shear cracks in both pedestals then inclined crack directly in upper region of ECC, where that's refers to ability of ECC to developed micro-crack didn't appear until subject excessive lateral load of specimen.

Table 6.4 (continue) First cracks and failure mechanism of 3CMH18-jacketed specimens

TB-3.5 TB-1	The cracks start in the upper and lower tension sides X-Y plane of the core as shown in figure (6.3). There is no big difference in the first crack distribution due to the limited effect of ECC in the first loading stages. After increasing the lateral displacement, horizontal cracks extend from jacket-column region towards center of the column, then it was developed to crush the cover of the half-lower column on all sides because transform plastic hinge close to center and develop the shear-failure in this region.
WC-3.5 WC-1	The cracks start in the upper and lower tension sides of the X-Y plane of the core as shown in figure (6.4). The first cracks distribution for both specimens almost identical due to limited effect of ECC in the first loading stages. Then the horizontal cracks appear in the column-pedestal join in the same direction of applied displacement -Z in upper pedestal (compression side) and opposite side in the lower pedestal (tension side), after increasing inelastic strain by increasing the lateral applied displacement = 90 mm (1.5 time of 3CMH18 lateral displacement), local-inclined cracks in both pedestals will occur parallel to applied load due to the weakness of pedestals then shear failure and cover spalling in all sides of the upper-half of column in the case of W-1% strain.
TB-C3.5 TB-C-1	The cracks start in the upper and lower tension sides of the X-Y plane of the original column core as shown in figure (6.3), due to the same reasons that's described above. Horizontal cracks in both jacket-column and column-pedestals perpendicular to the applied displacement will occur, then it will extend towards column center. After increasing the lateral load, cover crashed on all sides of the mid-half of lower column, while TB-C-1 exhibited little restraint than 3.5% strain which led to lower crack in the same shear failure zone .
Tested	Horizontal cracks in X-Y plane in the upper and lower plastic hinges are perpendicular to the applied load, then extended to the column center, after increasing inelastic strain, inclined cracks in column will occur due to the weakness of column materials which prevent extension the cracks to both pedestals.

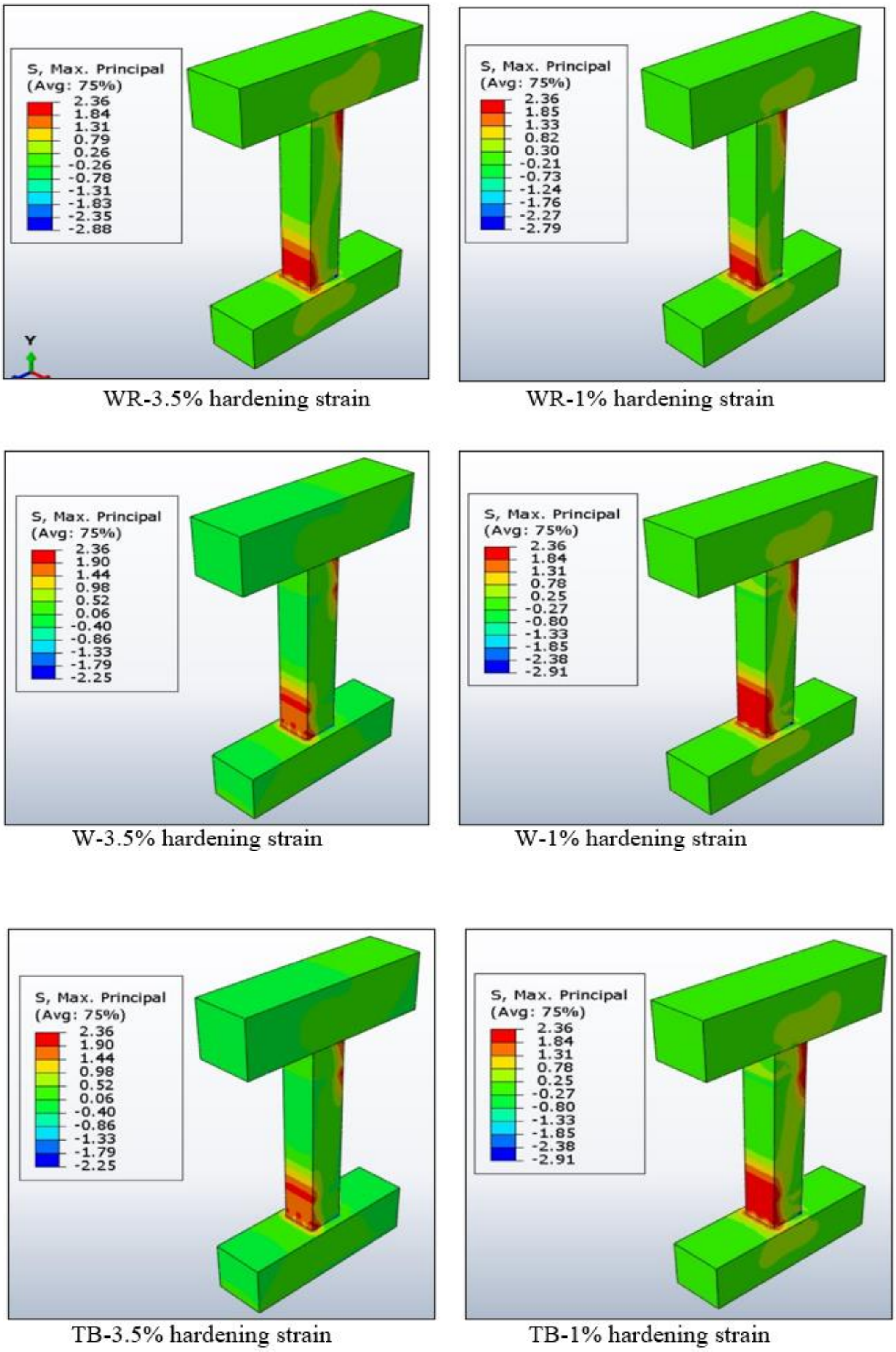

Figure 6.3 Maximum principal stress at first tension cracks for 3CMH18 with difference jacketed techniques

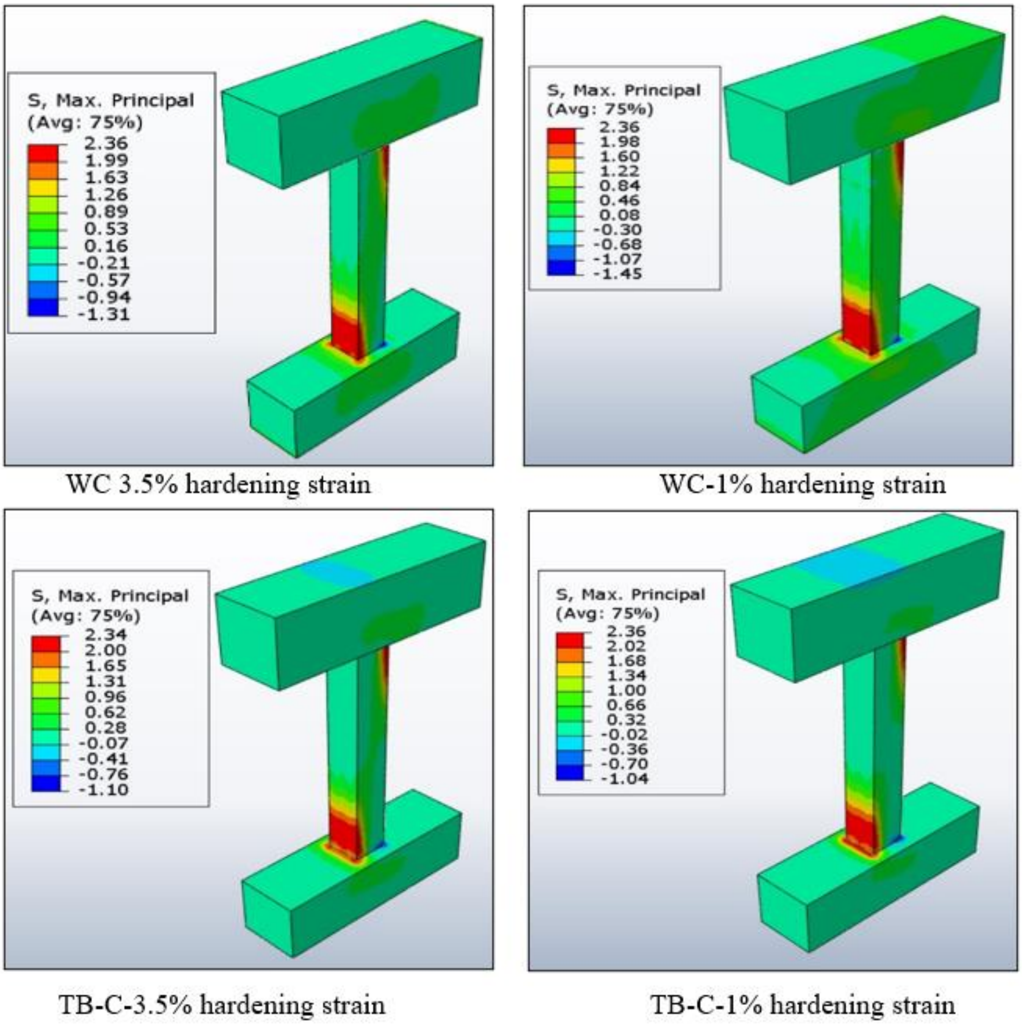

Figure 6.3 (continue) Maximum principal stress at first tension cracks for 3CMH18 with difference jacketed techniques

The table (6.5) below shows the first crack stress and general fracture mechanism under monotonic loads for 2CMH18-jacketing specimens**:**

Table 6.5 First cracks and failure mechanism of 2CMH18-jacketed specimens

Jacketed sample	Mechanism of cracks
WR-3.5 WR-1	The cracks formed in the upper and lower tension sides X-Y plane of the column core as shown in figure (6.4), where the core jacketed with coated ECC exhibit cracks lower than the uncoated ECC at tension stress = 2.75 MPa, under the same loading conditions due to first cracks directly correlated with the core resistance, where the effect of ECC was little at the first loading stage. After that, the cracks appear in both pedestals in the column-pedestal regions. After increasing the lateral displacement to 180 mm (6Δu), this crack will propagate around the column-necks for the WR-3.5 specimen. Both pedestal cracks will increase a little bit because high confinement of the coated ECC and increase lateral load by 20% compared with WR-1, but the Laster has given a perfect behavior compatible with core characteristics.
W-3.5 W-1	The first crack formed in the tension side X-Y plane perpendicular to applied lateral displacement, both types of ECC have almost the same propagation cracks. After that, the cracks formed in the column-pedestal regions, except W-3.5% specimen, exhibit micro-cracks in the compression region due to a 20% increase in displacement compared with W-1%.
TB-3.5 TB-1	The horizontal crack start in the tension side X-Y plane perpendicular to lateral displacement, both types of ECC have almost the same propagation cracks, because the effect of coated and uncoated ECC didn't relate with initial loading stage but it based on the core properties. After that, both jacket-column regions perpendicular to applied displacement 90 mm (3Δu), in compression and tension zones for upper and lower jacket respectively, will propagate towards the column center due to weak material of column and transform plastic-hinge to a new location, whereas TB-1 exhibits some cracks in ECC jacket.

Table 6.5 (continue) First cracks and failure mechanism of 2CMH18-jacketed specimens

WC-3.5 WC-1	The crack appears in the tension side X-Y plane perpendicular to lateral displacement, both types of ECC have nearly identical propagation for the reasons listed above. Then crack pedestal in upper compression and lower tension region in Z direction (applied displacement direction = $4\Delta_u$), then extend in sides Parelle to applied load due to high plastic dissipation of 3.5% strain appear some crack in plastic-hinge in ECC when reach dt to 0.3, corresponding to $\epsilon = 0.013 < 0.035$ while the other tension strain 1% suffering from horizontal crack due to strain reached to 0.026> 0.01 because it is not able to absorb plastic-energy under high displacement($4\Delta_u$).
TB-C-3.5 TB-C-1	The crack start in the tension side X-Y plane perpendicular to lateral displacement, both types of ECC have almost identical propagation for the same reasons listed above. The cracks started in both jacket-column, pedestal-column regions, then extended towards center of column as horizontal cracks, after increasing lateral displacement to 90mm (3Δu). the crack will appear in new plastic-hinge, then due to limited ability of tension strain of ECC with 1%, exhibited cracks in ECC-jacket corner, that's refer to increase inelastic deformation where tension strain > 0.01 corresponding to dt= 0.56 while coated ECC at same displacement appeared 0.042 corresponding dt = 0.56 where the Laster has given a distinct confinement ability but it should be agree with core properties where it didn't prevent shear failure in mid-column due to transform plastic-hinge close to center where origin column hadn't a little transverse reinforcement as well.
Tested	Horizontal cracks began in X-Y plane on the tension side at upper and lower plastic hinges perpendicular to the applied load, then extended to the column center. After increasing inelastic strain, an inclined cracks in the column will occur due to weakness of column materials prevent extension the cracks to both pedestals.

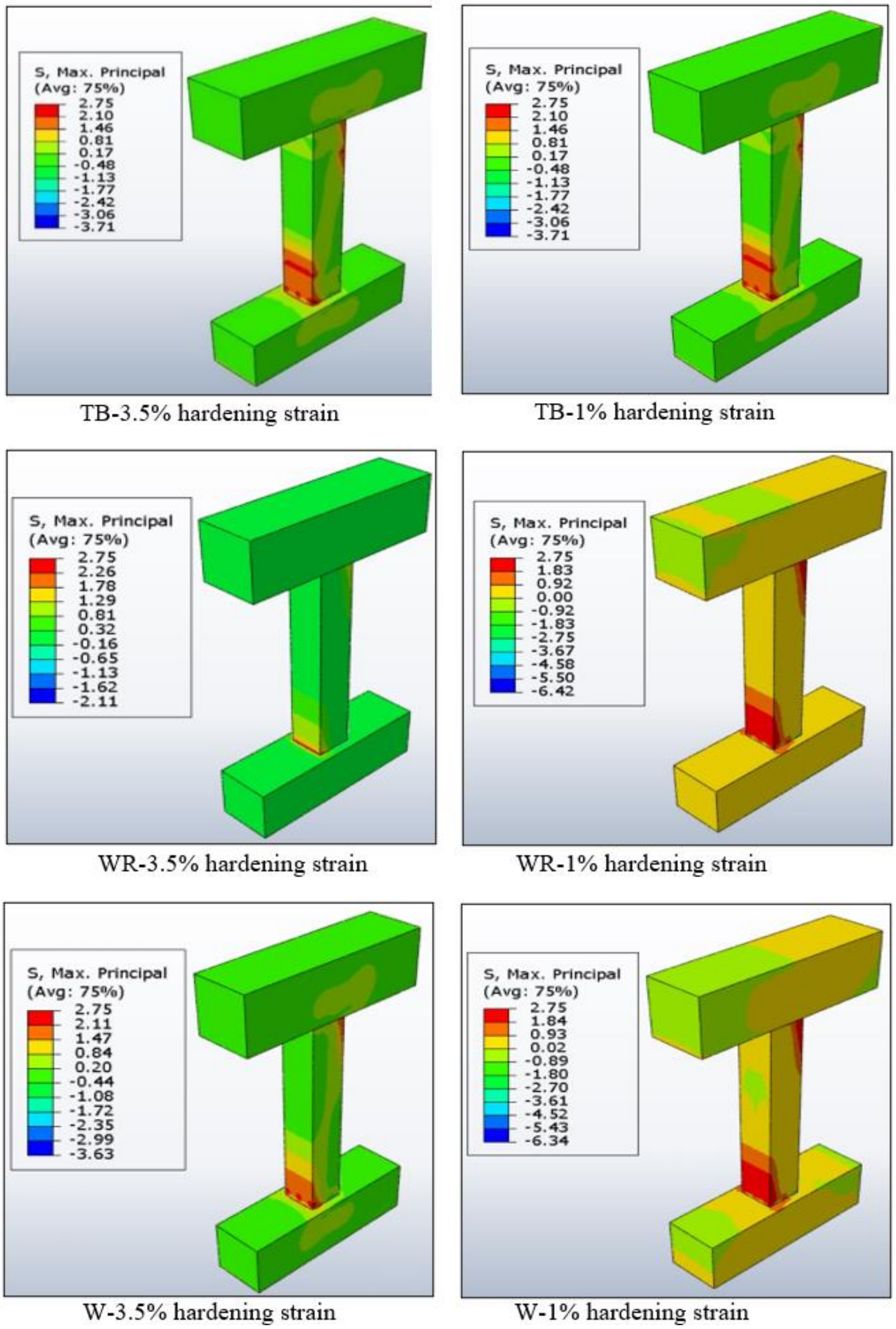

Figure 6.4 Maximum principal stress at first tension cracks for 2CMH18

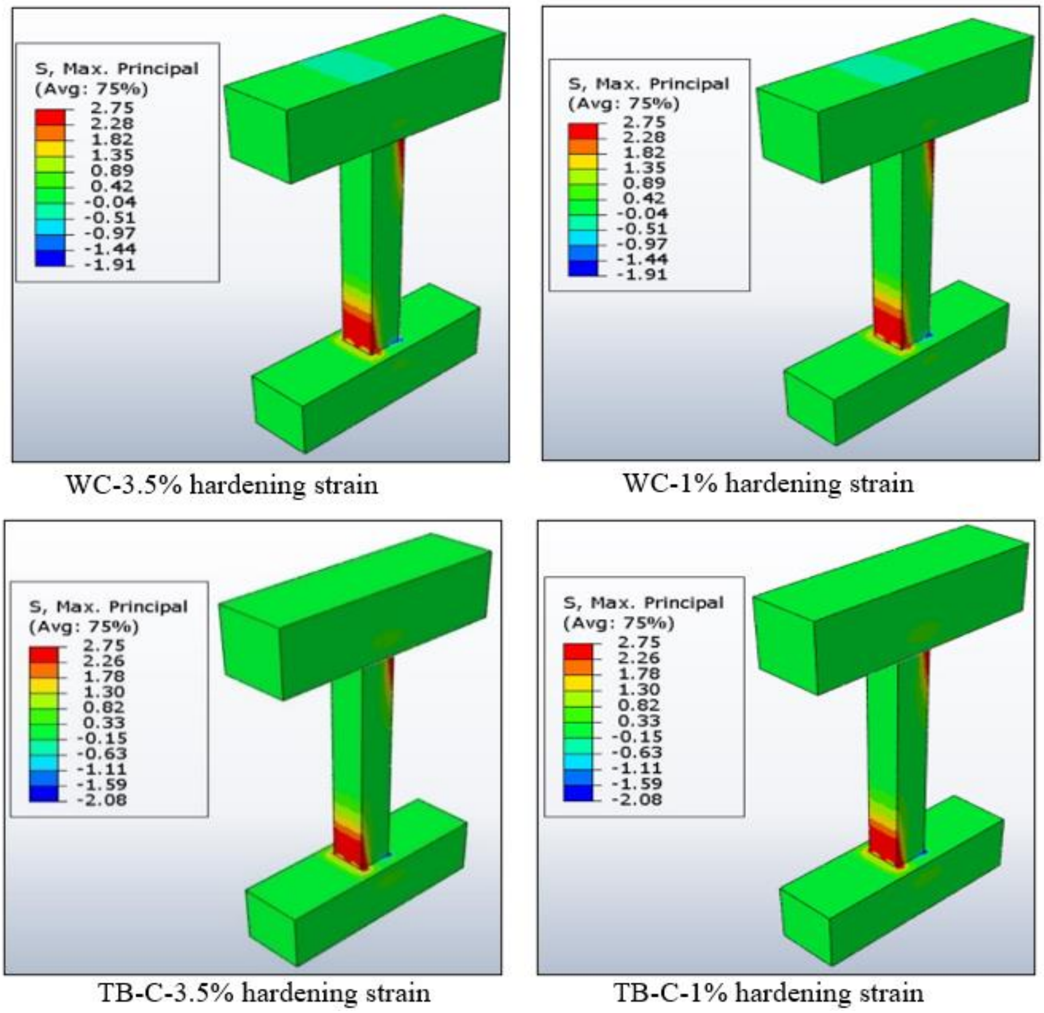

Figure 6.4 (continue) Maximum principal stress at first tension cracks for 2CMH18

6.3.2 Yielding of Shear Reinforcement

This study adopts methodology to capture transverse reinforcement yielding in terms finite element lateral displacement where determine stirrups yield stress = 413 MPa, then capturing the corresponding lateral displacement as below:

Table 6.6 Displacement at shear reinforcement yield of jacketed specimens

Jacket type	**3CLH18**		**2CLH18**		**3CMH18**		**2CMH18**	
	δty*	**δmax****	**tyδ**	**δmax**	**tyδ**	**δmax**	**tyδ**	**δmax**
Experimental	**30.5**	**60**	**76.2**	**90**	**30.5**	**60**	**30.5**	**30.5**
FE simulation	**31**	**60**	**78**	**90**	**34**	**60**	**30**	**30.5**
WR-3.5%	100	120	76.3	360	63.7	120	74	180
WR-1%	60	120	76	270	61	120	75.2	150
W-3.5%	73	120	72	270	35.4	120	74	180
W-1%	55.6	120	77	180	38	120	75	150
WC-3.5%	59	120	76	180	60	120	84	120
WC-1%	49	120	82	180	56.7	120	88	120
TB-3.5%	48.5	90	77	180	38	90	90	90
TB-1%	45	90	78	180	38	90	90	90
TB-C-3.5%	40	90	77	180	35.3	75	54	90
TB-C-1%	35.5	90	55	180	36	75	56	90

***δty** = lateral displacement at the tie reinforcement has been yielded in mm.

****δmax** = maximum applied lateral displacement in mm.

The table (6.6), both specimens 3CLH18 and 3CMH18 (original columns with shear deficiency) combined with same transverse yielding behavior, where the whole steel jackets technique improve displacement value corresponding to tie yielding by (2-3.27) times under double maximum applied lateral displacement compared with tested specimens, in other words, this ECC jackets delayed the transverse steel reach to the yield stress three times higher than original column, that's are overcome the shear deficiency has been predicted in both tested columns above, due to high confinement of ECC jacket along the columns which compensated inadequate of shear reinforcement in tested specimens.

In a related study, the whole ECC jackets with replace cover exhibit increase in displacement corresponding to stirrups yielding by (1.6-2) times, due to removal the old column cover which consider as a weak part between ECC and stirrups, that's give index to increase tie activity when it directly contacts with ECC.

The top-bottom specimens exhibit displacement at shear reinforcement yield close to tested specimens due to high diagonal cracks propagation at middle-column effect on general behavior of ECC which covered a limit area of column.

Most of 2CLH18-jacketed specimens exhibit displacement at transverse yield close to displacement for tested 2CLH18 (original column with flexural behavior), although increasing maximum applied lateral displacement (2-4) times, where ECC jackets increase the general flexural behavior with the same above increasing ratio, except TB-C 1% which appeared displacement lower than experimental with doubled maximum displacement where this technique can be effect on the original flexure and give a reverse effect under external lateral excitation not more than double.

For 2CMH18-jacketed specimens improve shear reinforcement yielding ability by (2.5 time with 6 δmax), (2.5 time with 5 δmax), (2.8 time with 4 δmax), (1.8-3 time with 3 δmax) for WR, W, WC, TB specimens respectively.

WR-jackets improve shear reinforcement yielding higher than other jackets due to high confinement and plastic dissipation energy, while Top-Bottom specimens exhibit lower ability, the low maximum applied lateral displacement of tested specimen =30 mm and moderate elasticity modulus of concrete, permit to the TB specimens improve tie yielding at maximum displacement of 90 mm, On the contrary, the WR improve close value of TB specimens with 180 mm, for same reasons the steel bars of ECC are not contribution of tie yielding.

6.3.3 Yield Stresses and Plastic Dissipation Energy

6.3.3.1 Stresses Distribution of Steel Bars and Components of Plastic Dissipation Energy

The longitudinal reinforcement yield is associated with loading level, design considerations, steel characteristics themselves, and the general behavior of structural members and joints. The figure (6.6) below illustrates rebar stresses distribution that directly depends on the magnitude of the lateral load, characteristic of the concrete and plastic capacity of the structural system.

The methodology adopts in this study base on yielded area of reinforcement which considered as a criterion of the flexural behavior as well as ductility, where it has been shown a lot of bars of WR-3%, WR-1% exceeded yield stress=330 MPa, which consider as index to increasing contribution of longitudinal steel bars simultaneously with ECC- jacket layer to transport the general behavior from shear to flexural, although doubled the lateral displacement to 120 mm as well. The figure shown below the yield stresses of longitudinal reinforced bars:

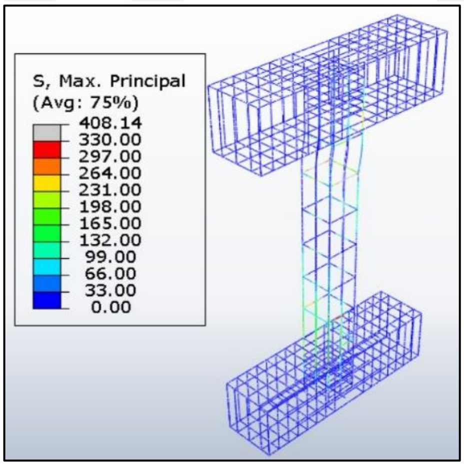

Figure 6.5 Stresses distribution of longitudinal bars of experimental and various 3CLH18- jacketed techniques at maximum displacement

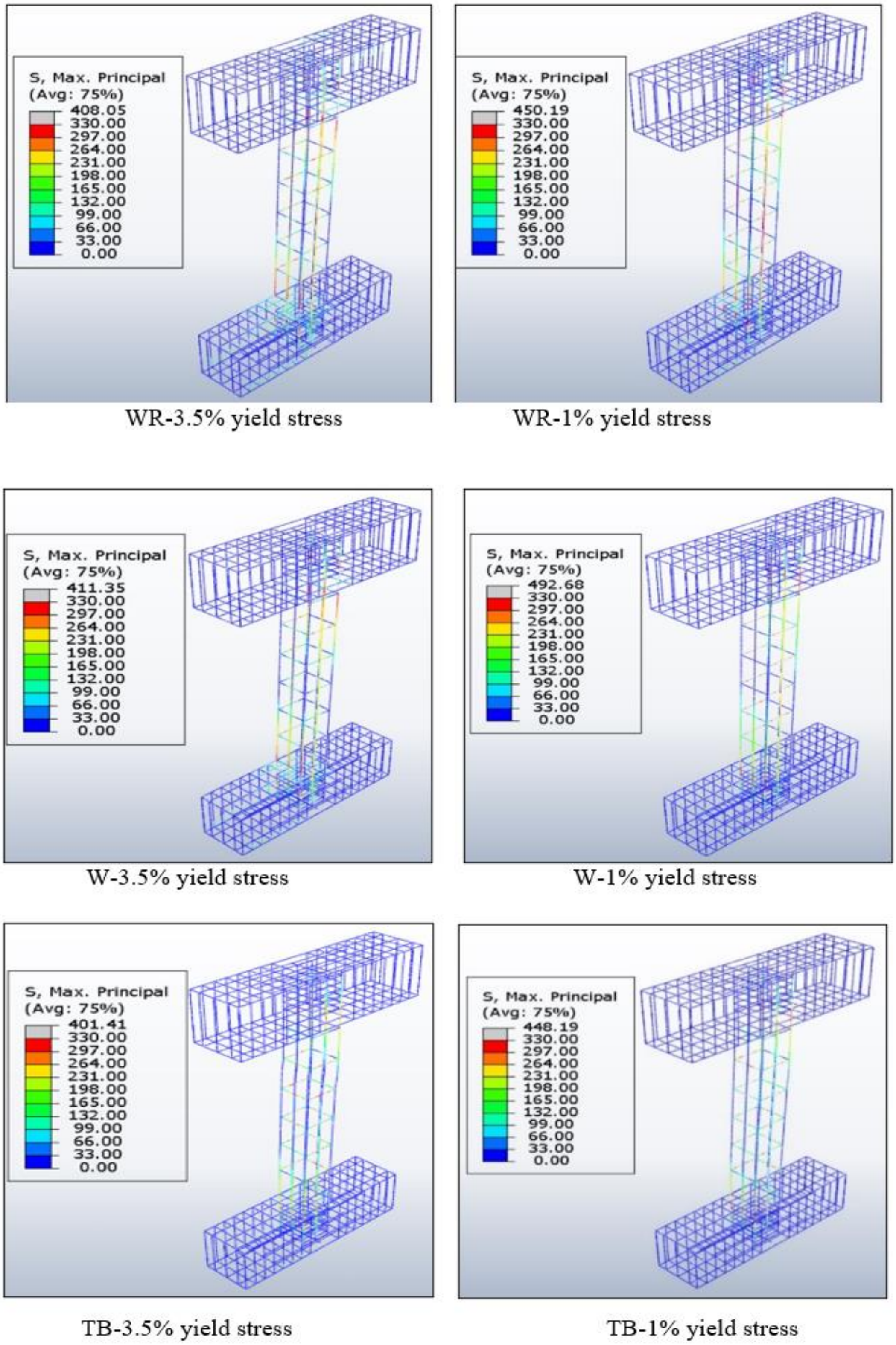

Figure 6.5 (continue) Stresses distribution of longitudinal bars of experimental and various 3CLH18-jacketed techniques at maximum displacement

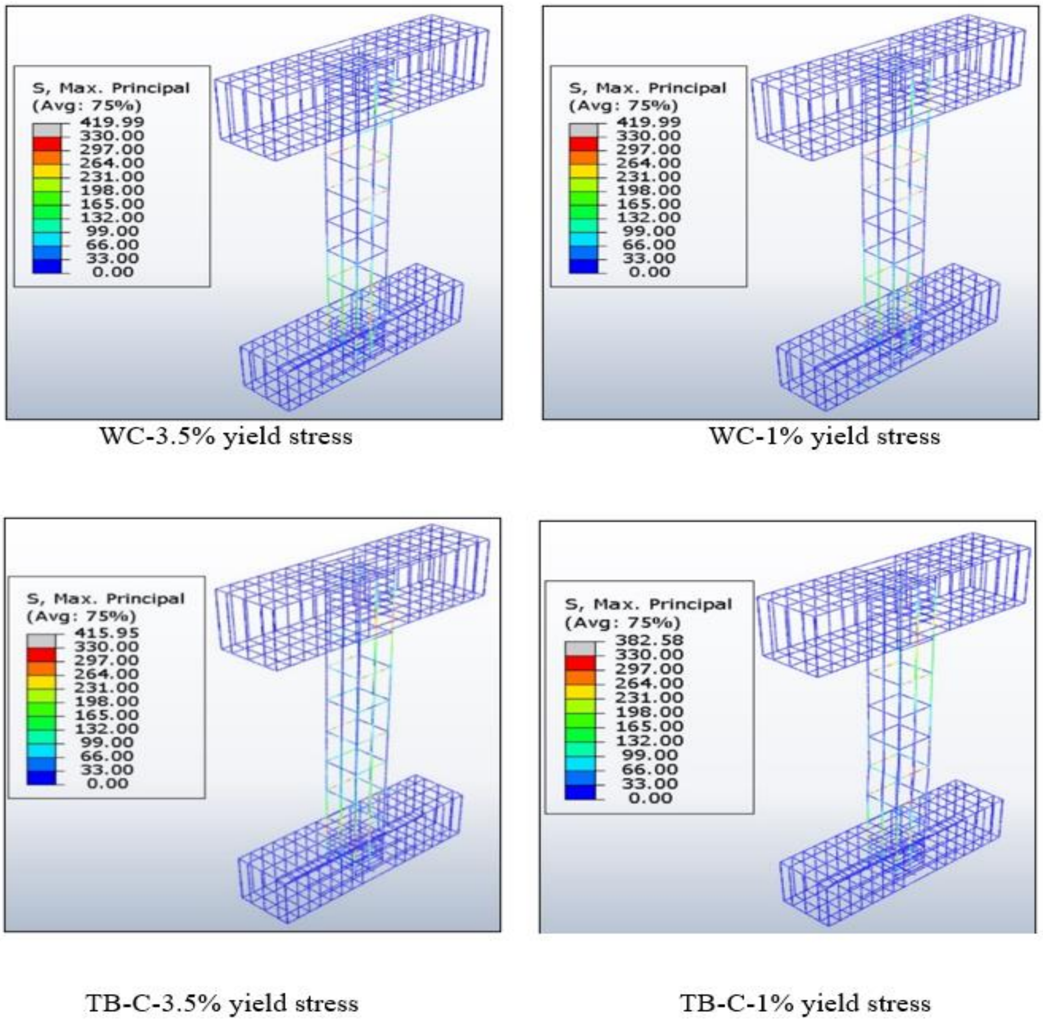

Figure 6.5 (continue) Stresses distribution of longitudinal bars of experimental and various 3CLH18-jacketed techniques at maximum displacement

The figure (6.5) shows the yield stress of longitudinal bares, where it is obviously seen the number and area of longitudinal bares of WR, W (3.5%, 1% hardening strain) have been yielded and contributed in improvement the ductility larger than other specimens, that's suffering from shear failure, where the former with whole ECC jacket techniques increase the core efficiency by provided it with high confinement to resist shear failure and increase the total column capacity to permit high contribution of steel bars in spite of increase lateral displacement to 120mm (doubled tested displacement).

To confirm this hypothesis, this study adopts plastic dissipation energy (PDE components) which are considered a standard for the contribution of steel reinforcement, ECC jackets, and normal concrete of columns by conducting finite element analysis for WR-3.5% and TB-C-1% and compared the results with experimental results, based on the following equation:

$$E_P = E_{core} + E_{ECC} + E_{steel}$$

Where:

E_P: Total plastic dissipation energy of structural system in kJ.

E_{core}: Plastic dissipation energy by normal concrete of column in kJ.

E_{ECC}: Plastic dissipation energy by Engineering cementitious composite in kJ.

E_{steel}: Plastic dissipation energy by reinforced bars and ties in kJ.

The figure shown below plastic energy for **3CLH18** FE models:

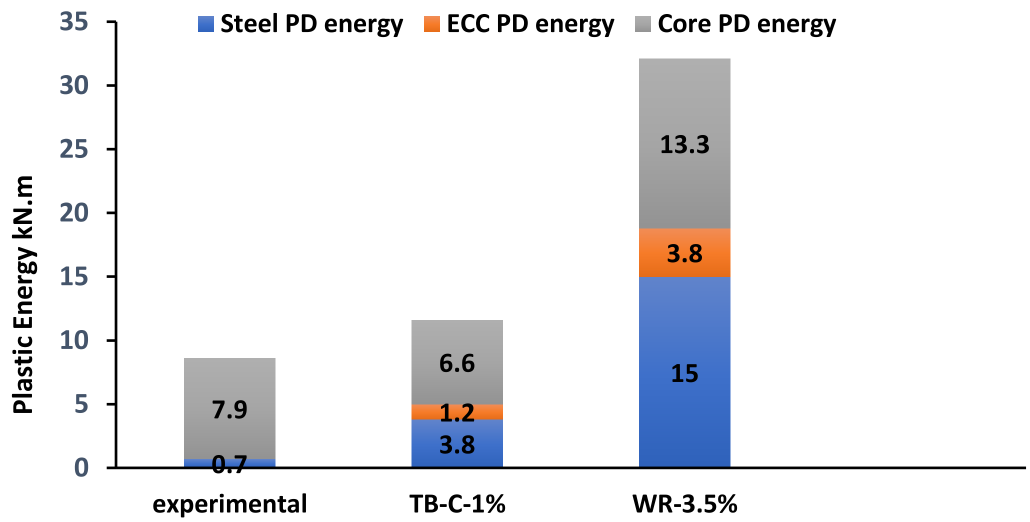

Figure 6.6 Contribution of steel bars, ECC jacket and column core in plastic dissipation energy for 3CLH18 specimens at maximum displacement

The yield stresses of reinforced steel bars shown in the figure below:

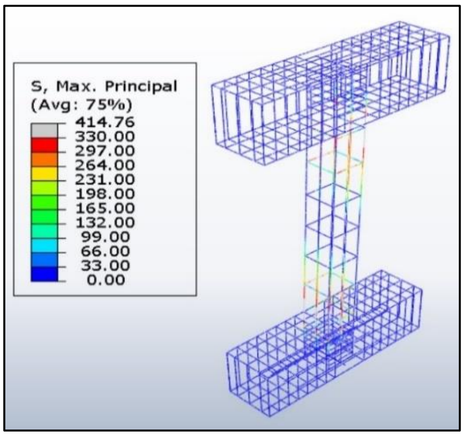

yield stress of longitudinal bars for **2CLH18** experimental specimen

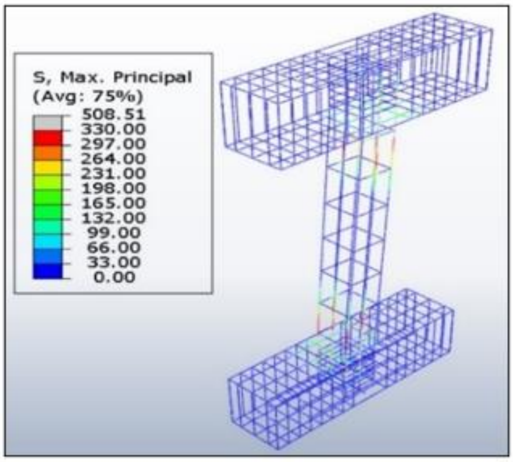

WR-3.5% yield stress

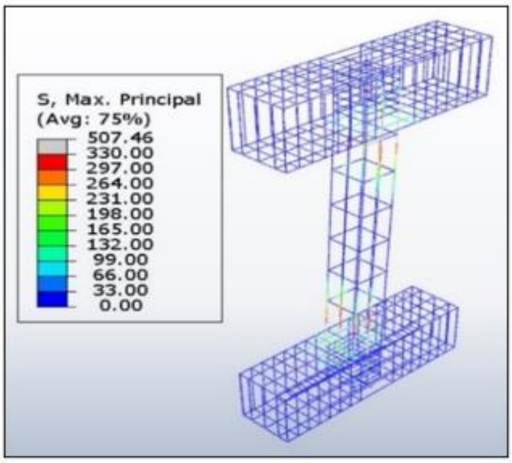

WR-1% yield stress

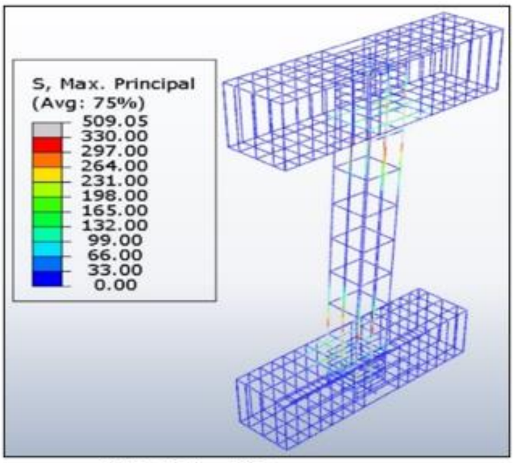

W-3.5% yield stress

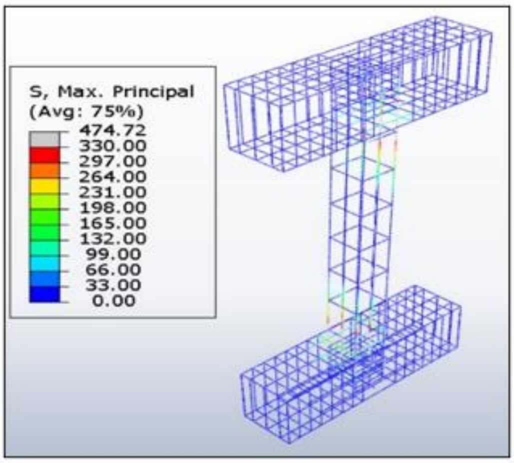

W-1% yield stress

Figure 6.7 Stresses distribution of longitudinal bars for different 2CLH18 jacketed techniques at maximum displacement

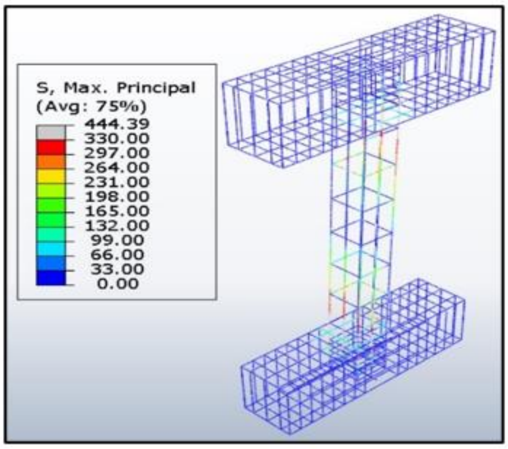

TB-C-3.5% yield stress

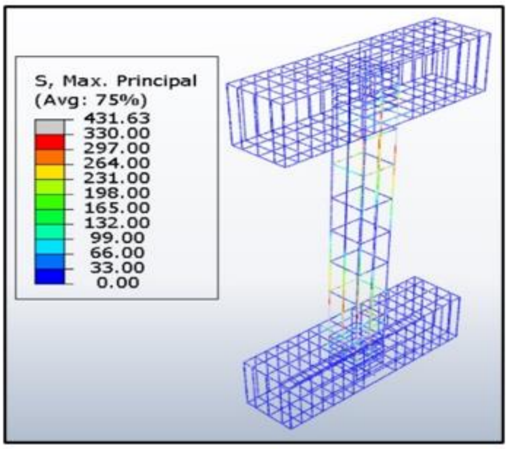

TB-C-1% yield stress

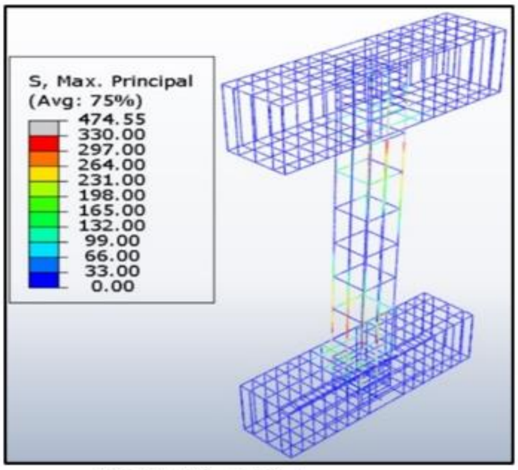

TB-3.5% yield stress

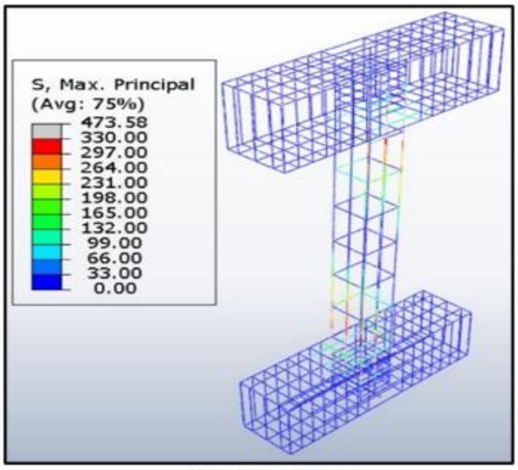

TB-1% yield stress

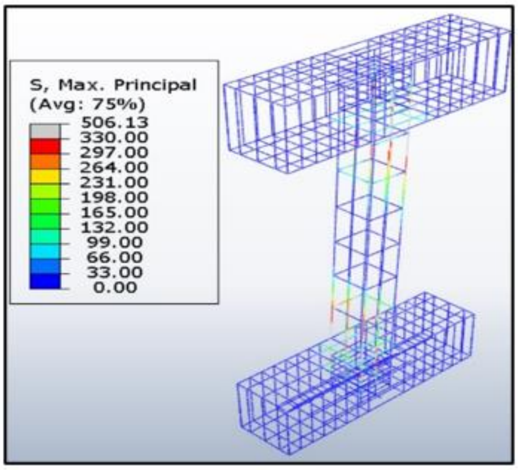

WC-3.5% yield stress

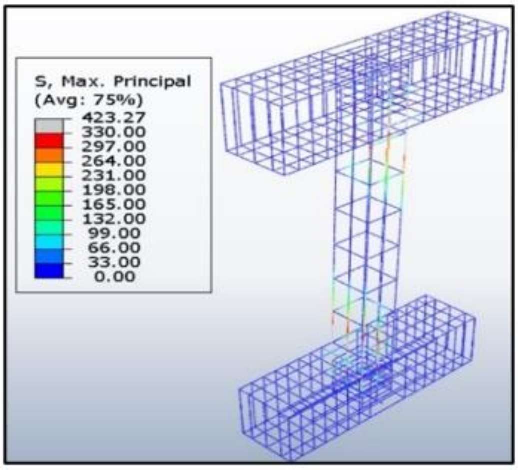

WC-1% yield stress

Figure 6.7 (continue) Stresses distribution of longitudinal bars for different 2CLH18 jacketed techniques at maximum displacement

The figure (6.7) expresses the yield stress of longitudinal bares, where it is clearly show the number and area of longitudinal bares of all specimens have been yielded and contributed to improvement of the ductility due to good 2CLH18 ductility, although the difference in applied displacement between them, where the jacketed specimens kept the flexural behavior.

High original column ductility of 2CLH18 (μ=5.1) led to close ECC contribution of WR3.5% and TB-C1% specimens (4, 3.7) kJ respectively, with (8% PDE difference between them), in plastic dissipation energy, on the contrary, 3CLH18 has a low original column ductility, where the ECC plastic dissipation energy is increase and based on the jacketed technique as well as WR3.5% and TB-C1% (3.8, 1.2) KJ respectively, with (216% PDE difference between them).

It ensures the high activity of ECC jacket for original column with shear deficiency as shown below in the figure (6.8):

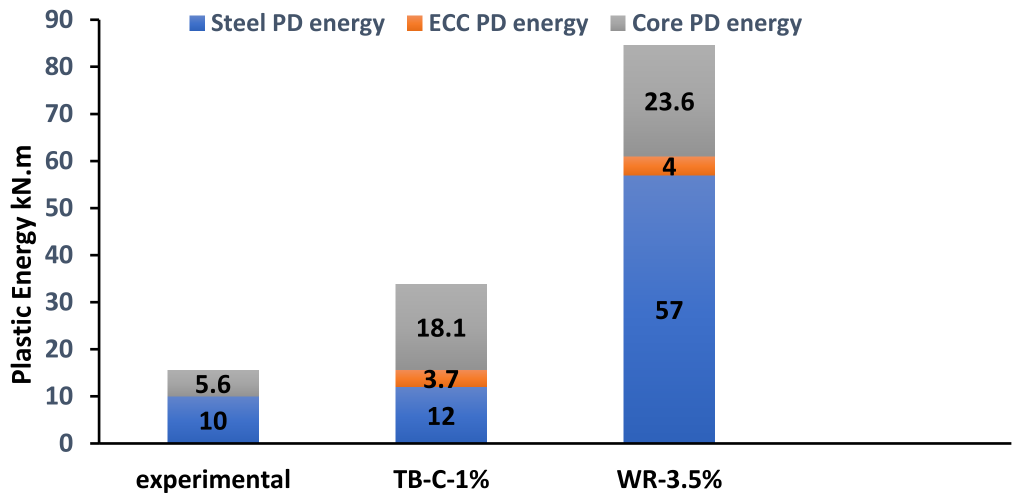

Figure 6.8 Contribution of steel bars, ECC jacket and column core in plastic dissipation energy for 2CLH18 specimens at maximum displacement

The yield stresses of longitudinal reinforced bars shown in the figure below:

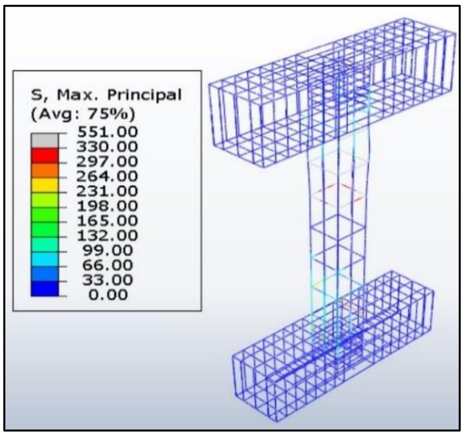

yield stress of longitudinal bars for **3CMH18** experimental specimen

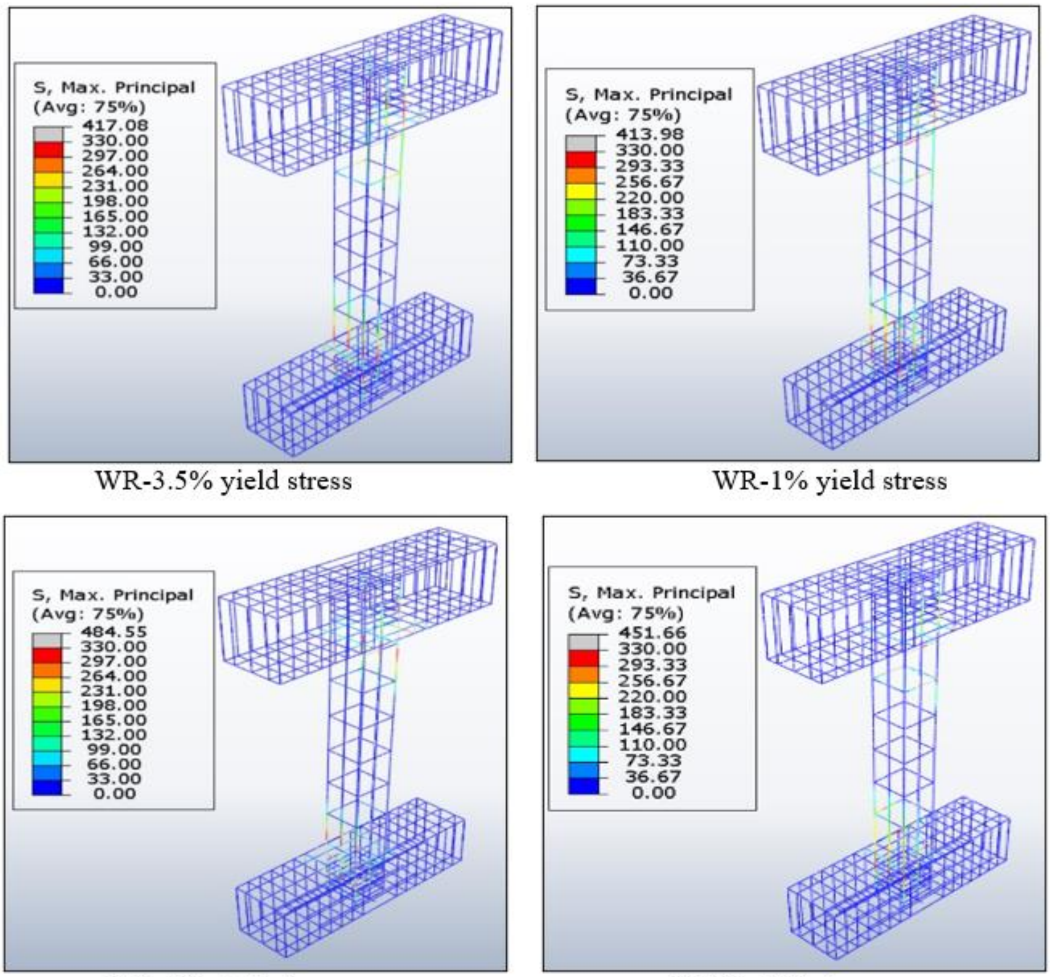

WR-3.5% yield stress — WR-1% yield stress

W-3.5% yield stress — W-1% yield stress

Figure 6.9 Stresses distribution of longitudinal bars of experimental and various 3CMH18 jacketed techniques at maximum displacement

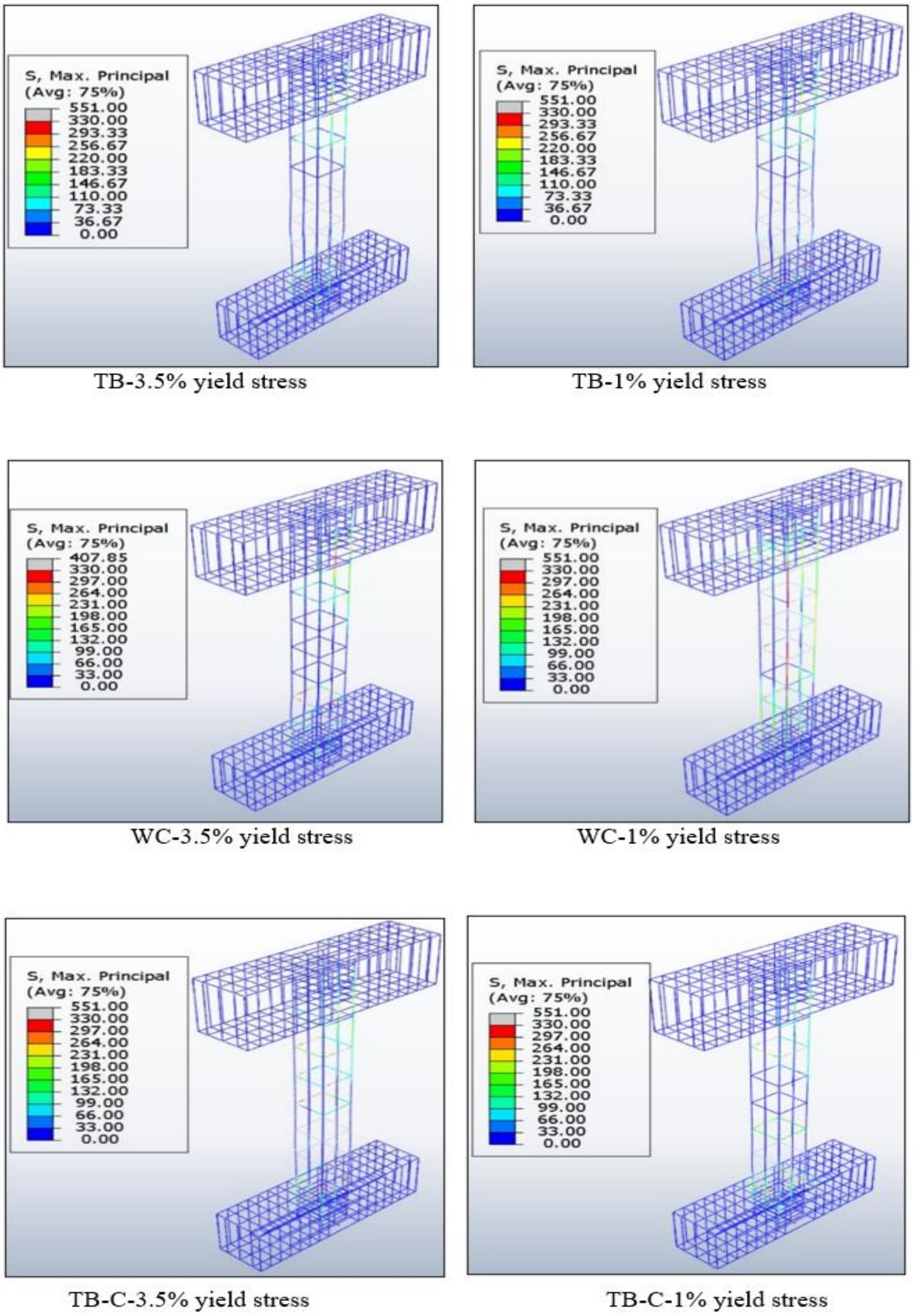

Figure 6.9 (continue) Stresses distribution of longitudinal bars of experimental and various 3CMH18 jacketed techniques at maximum displacement

The figure (6.9) expresses the yield stress of longitudinal bares, where the number and area of longitudinal bares of WR, W (3.5% and 1% hardening strain) have been yielded and contributed to improvement the ductility larger than the other specimens, that's suffering from shear failure, where the former with whole ECC jacket techniques increase the original core efficiency by provide it with high confinement to resist shear failure and increase the total core capacity to permit high contribution of steel bars in spite of increase lateral displacement to 120mm (doubled tested maximum displacement).

Low original column ductility and properties of 3CMH18 (μ=1.3) led to higher ECC contribution of WR3.5% in term plastic dissipation energy than TB-C1% specimen (3.4, 2.1) kJ, respectively, with (62% PDE increasing between them).

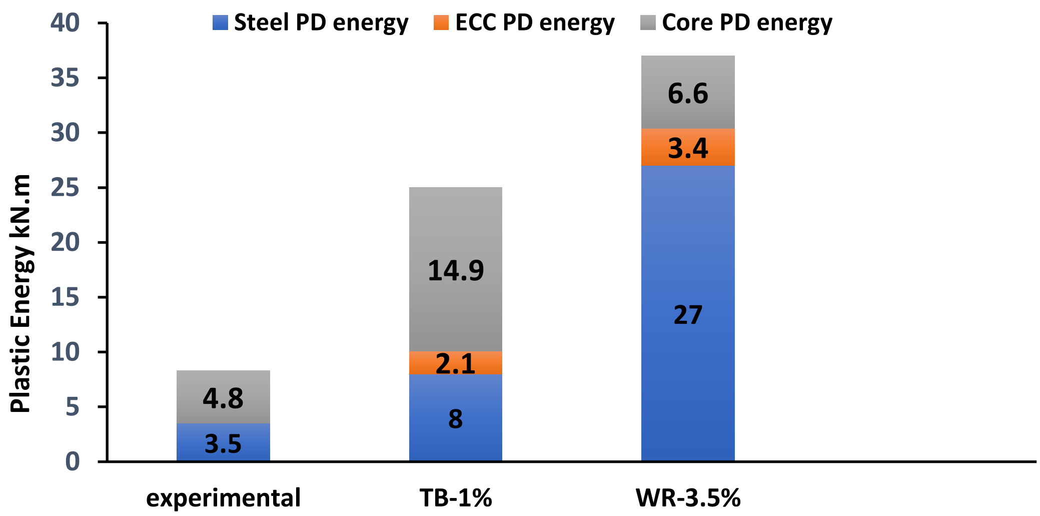

Figure 6.10 Contribution of steel bars, ECC jacket and column core in plastic dissipation energy for 3CMH18 specimens at maximum displacement

The yield stresses of longitudinal reinforced bars shown in the figure below:

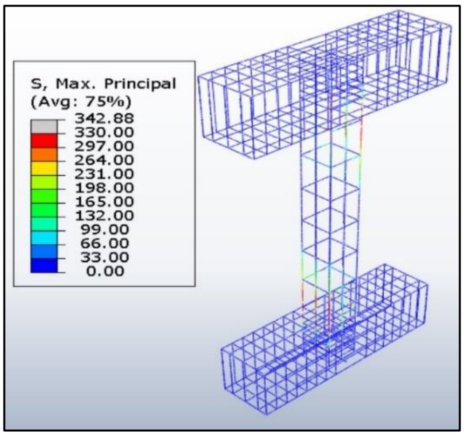

yield stress of longitudinal bars for **2CMH18** experimental specimen

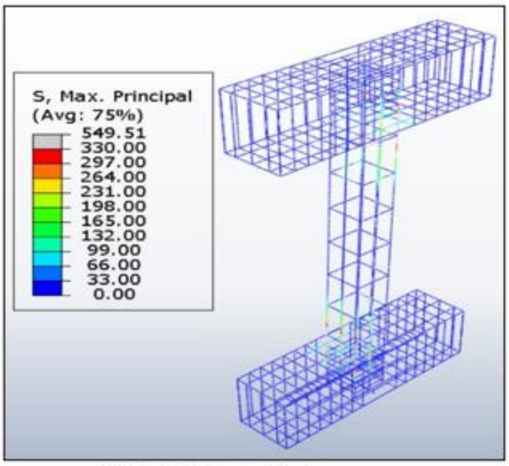

WR-3.5% yield stress

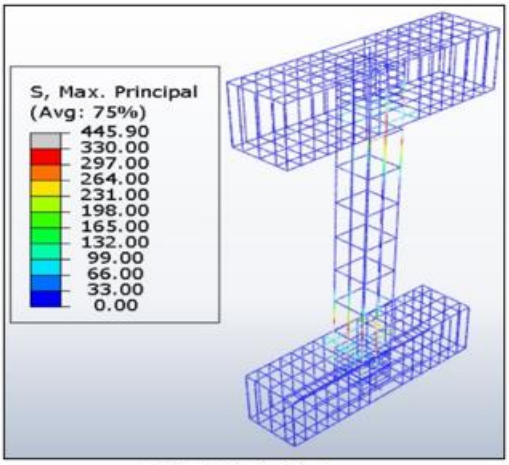

WR-1% yield stress

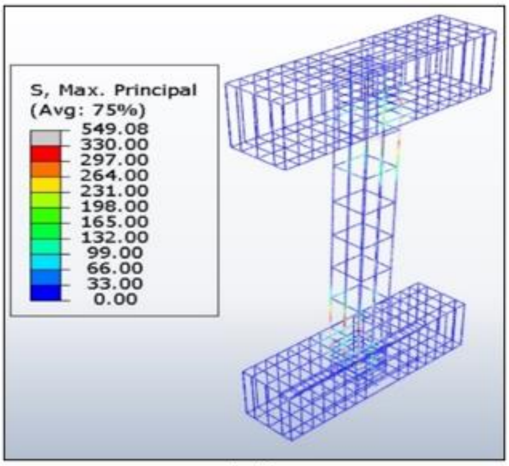

W-3.5% yield stress

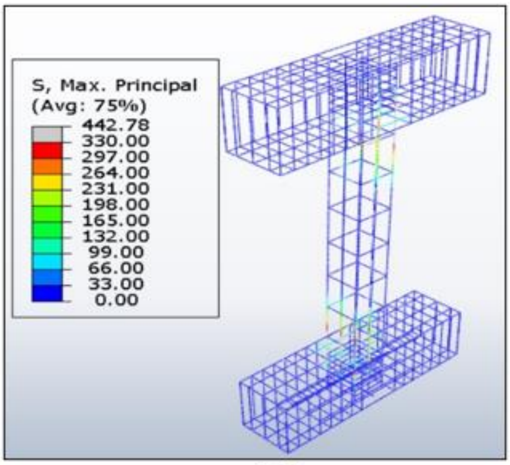

W-1% yield stress

Figure 6.11 Stresses distribution of longitudinal bars of experimental and various 2CMH18 jacketed techniques at maximum displacement

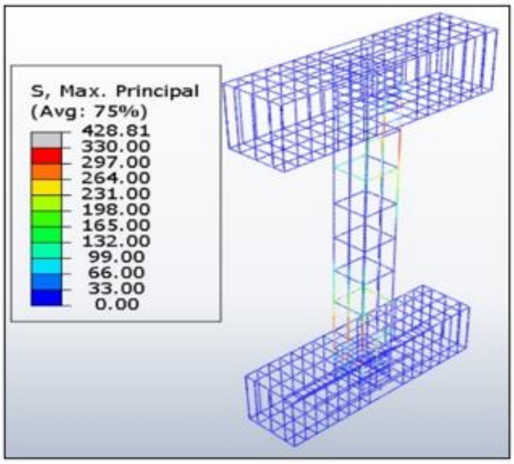

TB-C-3.5% yield stress

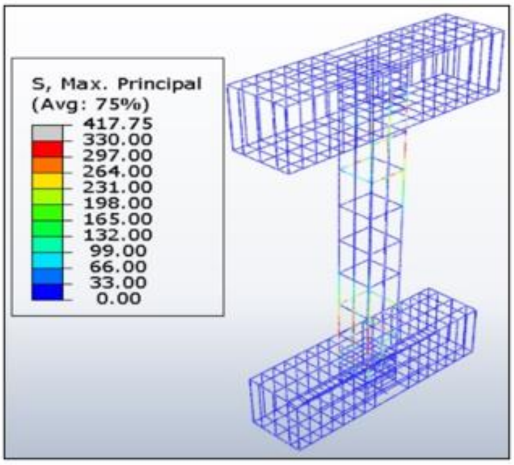

TB-C-1% yield stress

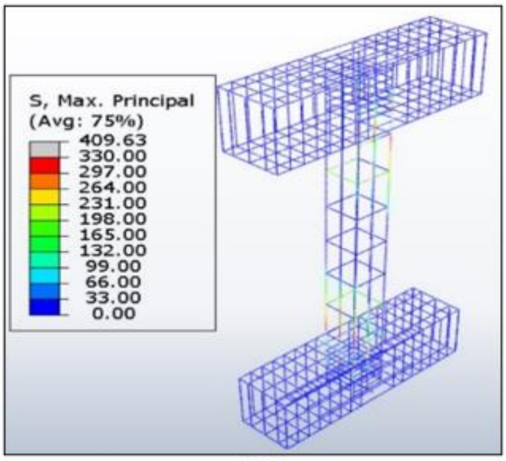

TB-3.5% yield stress

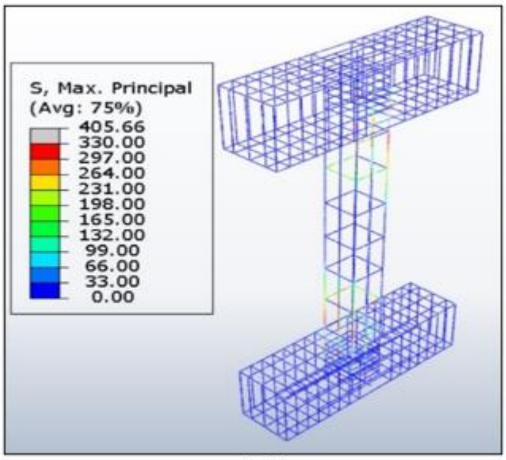

TB-1% yield stress

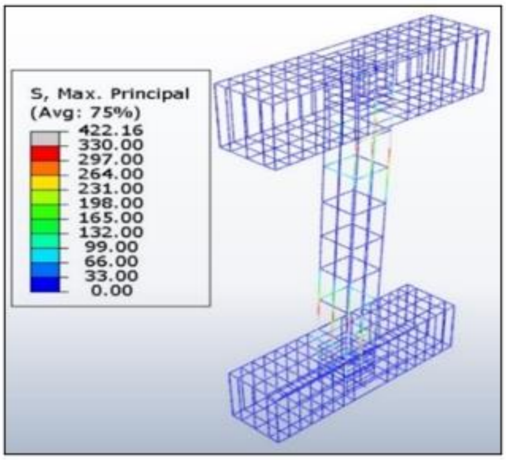

WC-3.5% yield stress

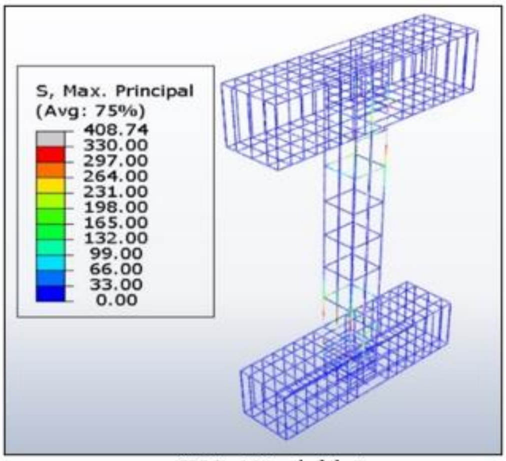

WC-1% yield stress

Figure 6.11 (continue) Stresses distribution of longitudinal bars of experimental and various 2CMH18 jacketed techniques at maximum displacement

The figure (6.11) above shows the yielded stress of steel bares where the flexural behavior of whole-steel jacketed with coated ECC specimens higher than the other samples, although increasing lateral displacement to (6 times of maximum lateral displacement of tested 2CMH18) for WR-3.5% model which confirm the plastic dissipation energy will be increased with the used ECC jacket simultaneously.

Low original column ductility of 2CMH18 led to close ECC contribution of plastic dissipation energy for WR3.5% and TB-C1% specimens (3.68, 3.16) kJ respectively, with (15.8% PDE increasing between them).

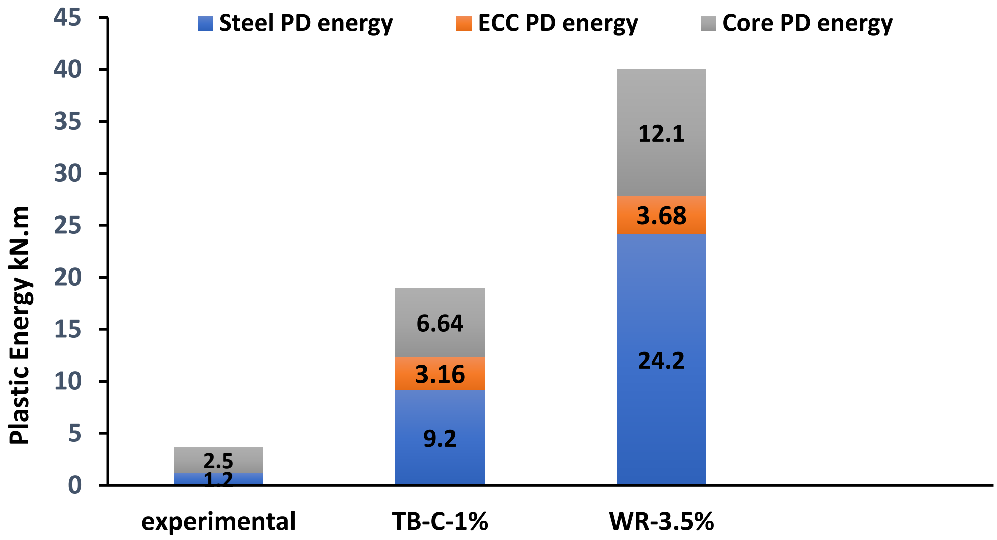

Figure 6.12 Contribution of steel bars, ECC jacket and column core in plastic dissipation energy for 2CMH18 specimens at maximum displacement

Table 6.7 Contribution of various components of plastic dissipation energy

Specimen		plastic dissipation energy kJ				δ_{max} mm	μ	PDE Contribution %		
		Column Core	ECC	Steel	Total			Core	ECC	Steel
3CLH18	WR-3.5%	13.3	3.8	15	**32.1**	120	5.2	41.4	11.8	46.7
	TB-C-1%	6.6	1.2	3.8	**11.6**	75	1.9	56.8	10	32.7
	Tested	7.9	-	0.7	**8.6**	60	1.6	91.8	-	8.4
2CLH18	WR-3.5%	16.6	4	57	**77.6**	360	14	21.3	5	73.4
	TB-C-1%	18.1	3.7	12	**33.8**	180	6.6	53.5	11	35.5
	Tested	5.6	-	10	**15.6**	90	5.1	35.9	-	64
3CMH18	WR-3.5%	6.6	3.4	27	**37**	120	4.8	17.8	9.1	73
	TB-1%	14.9	2.1	8	**25**	90	1.9	59.6	8.4	32
	Tested	4.8	-	3.5	**8.3**	60	1.3	57.8	-	42.1
2CMH18	WR-3.5%	12.1	3.7	24.2	**40**	180	7.6	30	9.2	60.5
	TB-C-1%	6.64	3.1	9.2	**19**	90	3.6	35	16	48.4
	Tested	2.5	-	1.2	**3.7**	30	1.8	67.5	-	32.4

Where:

μ = displacement ductility.

δ = maximum applied lateral displacement mm.

Core contribution = (plastic energy of original core /total plastic energy) *100%.

ECC contribution = (plastic energy of ECC/total plastic energy) *100%.

Steel contribution = (plastic energy of steel bars/total plastic energy) *100%.

The table (6.7) above shows the contribution of various structural components of plastic dissipation energy for highest and lowest jacketed techniques, and compared it with tested specimens.

The first component present plastic dissipation energy and corresponding contribution ratio of normal concrete of columns core under symbol (column core), that are got from finite element analysis, where the original column with shear deficiency of tested specimens exhibit PDE of columns core more than PDE of steel bars which consider one reasons to occur shear failure as a result to low plastic dissipation energy ability of normal concrete. In contrary, all WR-3.5% specimens results refer to the contribution of column core in plastic dissipation energy for less than PDE of reinforcement, which led to decrease sudden failure caused by brittleness of concrete core as well as increase ductility by increase steel contribution in plastic energy compared with tested results.

In contrary, the contribution of the columns core in plastic energy more than reinforcement PDE for Top-Bottom (1% strain) technique except and TB-1% 2CMH18 which appear the contribution ratio of reinforcement PDE more than column core, in contrary, decrease plastic energy of steel bars, due to Significant restriction for top and bottom and concentrated the stresses toward the column center and bad stress distribution which led to consisting the shear cracks close the center, these reasons made the concrete of column carried plastic energy more than tested specimens where increasing the brittleness of the whole structural system which is clearly seen Slight increases ductility of TB jacketed (6.6, 1.9) column no. 8 in table above, for TB-C1% 2CLH18, TB-1%3CMH18 respectively, close to experimental value.

The second component shows in the table (6.7) above which present the plastic energy and corresponding contribution ratio of ECC under symbol (ECC), where it obviously show, in the original column with shear deficiency such as 3CLH18 and 3CMH18, which are suffering from low ductility, whenever increase lateral displacement led to slightly increase in ECC plastic energy contribution and directly increase reinforcement plastic energy contribution so it improved ductility of jacketed samples with large difference between WR3.5% and TB1% techniques μ = (5.2, 1.9), (4.87, 1.9) of WR3.5% , TB-C1% of 3CLH18 and WR3.5%, TB1% of 3CMH18 respectively, which corresponding with slightly difference in ECC contribution between them, that’s mean the ECC jacket increase flexural provided by steel bars and decrease the normal concrete brittleness

On other side, the coated ECC improve total plastic dissipation energy higher than the uncoated ECC, depending on maximum lateral displacement, and strengthen technique, although increase maximum lateral displacement led to decrease PDE of

ECC contribution this didn't forbid improve the steel plastic energy and decrease core brittleness, which provide extra ductility to the jacketed specimens.

The third component is the plastic energy and corresponding contribution of steel reinforcement, where each jacketed specimens improve difference value of the plastic dissipation energy of steel reinforcement compared with tested samples depending on the original column properties, original ductility and maximum lateral applied displacement.

The whole-steel with coated ECC technique (WR-3.5) exhibit highest plastic dissipation energy of steel by (20.4, 4.7, 6.7, 19.2) times corresponding steel PDE for tested 3CLH18, 2CLH18, 3CMH18 and 2CMH18 respectively. The improvement of steel PDE for weak original column ductility as WR-3.5 3CLH18 and WR-3.5 2CMH18 (20.4, 19.2) is greater than that the steel PDE of the high original column ductility as WR-3.5 2CLH18 (4.7).

In other words, that's confirms highest activity of whole-coated ECC jacketed low original column ductility which leads to transformation of their shear failure to flexural failure.

The top-bottom with the uncoated ECC technique (TB-1%) appear the lowest plastic dissipation energy of steel by (4.4, 0.2, 1.3 and 6.6) times the corresponding steel PDE for tested 3CLH18, 2CLH18, 3CMH18 and 2CMH18 respectively. The improvement of steel PDE for weak column ductility as TB-C-1% 3CLH18 and TB-C-1% 2CMH18 (4.4, 6.6) are greater than the steel PDE for high column ductility as TB-C-1% 2CLH18 (0.2), that's ensures the lowest activity of top-bottom-uncoated ECC jacketed although, slightly increasing the steel PDE compared with tested specimens which are led to stay the shear failure except 2CLH18.

6.3.3.2 Plastic Dissipation Energy of Jacketed Specimens

This section demonstrates difference plastic dissipation energy PDE of all jacketed specimens and its relationship with corresponding ductility as well as failure behavior, then compared them with experimental specimens' data.

It is clear from the figure (6.13) below, ductility was directly proportional to plastic energy, where the ductility of jacketed column increase by increase the plastic dissipation energy compared with the tested column due to the ECC jacket's ability to improve the total plastic energy, as well as the PDE components (increase the contribution PDE of steel) as discussed in the previous section.

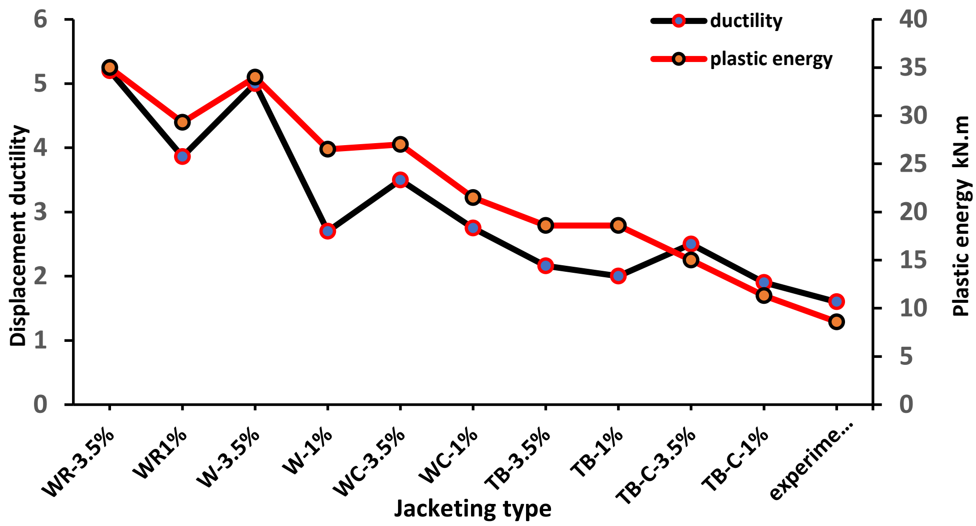

Figure 6.13 PDE and ductility for 3CLH18 jacketed specimens

Also, this improvement capacity depends on the jacketing technique, maximum lateral displacement, and type of ECC jackets. All ECC jacket types exhibit a clear difference of PDE and corresponding ductility due to their weak column core characteristics. The whole jacket techniques have the highest PDE and corresponding ductility, as well as convert the general failure from sudden shear failure to flexural. In the other side, the coated ECC appear PDE, and ductility higher than uncoated ECC for the same technique.

The figure below explains PDE and ductility for 2CLH18 jacketed specimen:

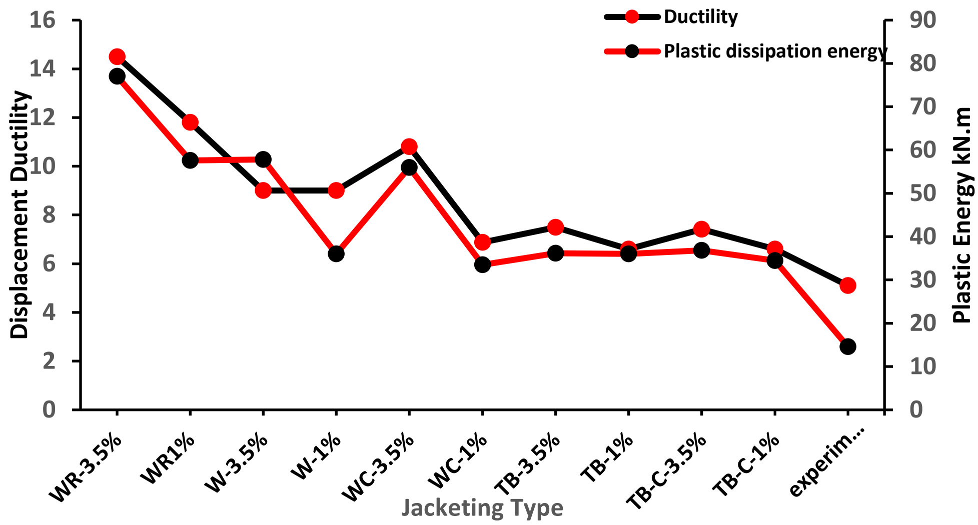

Figure 6.14 PDE and ductility for 2CLH18 jacketed specimens

It is obviously, the figure (6.14) above, the ductility was directly proportional to plastic energy, where the ductility of the jacketed column increase by increase the plastic dissipation energy compared with the tested column due to the ECC jacket's ability to improve the total plastic energy, as well as the PDE components (increase the contribution PDE of steel) as discussed in the previous section.

All whole jacket types (3.5% and 1% hardening strain) exhibit clear difference PDE and corresponding ductility depend on jacket technique and the ECC type, but there is a slight difference in both (top-bottom) techniques due to the high core characteristics, where the former strategies more suitable than the later types in these cases. The whole jackets technique appear highest PDE and corresponding ductility in the other side, the coated ECC appear higher PDE and ductility than uncoated ECC for the same technique except (Top-Bottom) jackets types.

The figure below explains PDE and ductility for 3CMH18 jacketed specimens:

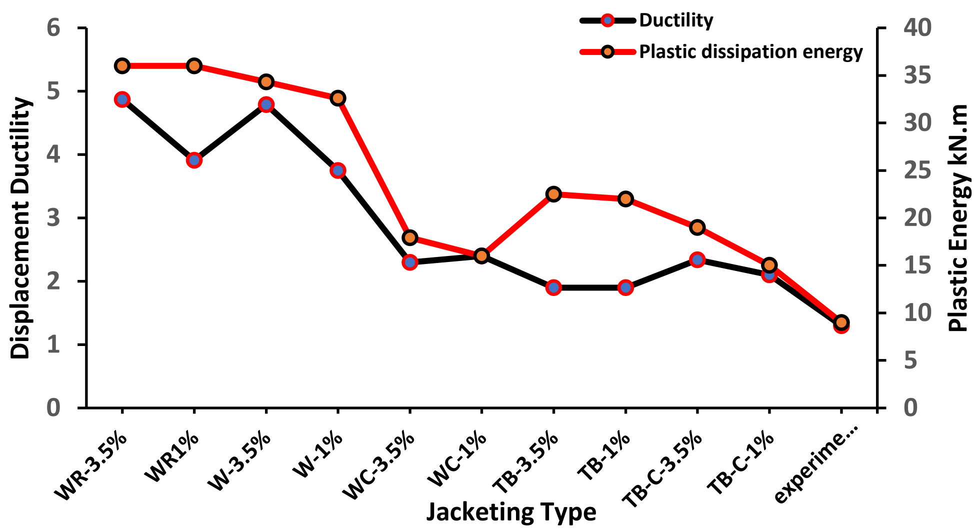

Figure 6.15 PDE and ductility for 3CMH18 jacketed specimens

It is clearly, the figure (6.15) above, the ductility was directly proportional to plastic energy, where the ductility of jacketed column increase by increase the plastic dissipation energy compared with the tested column due to the ECC jacket's ability to improve the total plastic energy, as well as the PDE components (increase the contribution PDE of steel) as discussed in the previous section.

All whole jacket types (3.5%, 1% hardening strain) exhibit a clear difference PDE and corresponding ductility depend on jacket techniques, maximum lateral displacement and ECC type, but, in spite of increasing PDE of both (top-bottom) techniques, the ductility is still decreasing compared with whole jacket types due to the limited ECC ability to enhance the PDE component because it concentrated in top and bottom which led to just a local improvement of PDE without significant increasing of ductility to resist the shear deficiency in mid-column, while this issue does not occur in 2CLH18, where the former strategies are more suitable than the later types in this case. The whole jackets technique appeared highest PDE and corresponding ductility, in the other side, the coated ECC appeared the higher PDE and ductility for same technique except (Top-Bottom) jackets types.

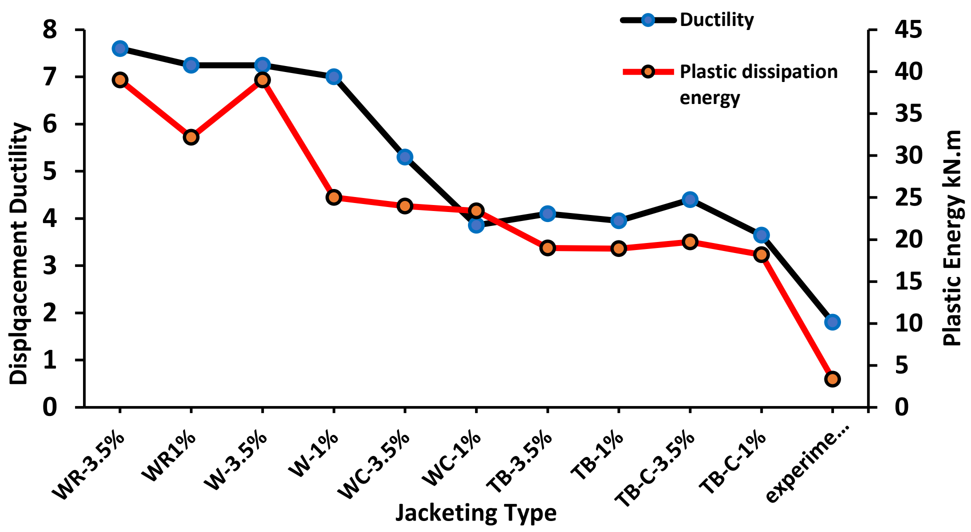

Figure 6.16 PDE and ductility for 2CMH18 jacketed specimens

In the figure (6.16) above, all whole jacket types (3.5%, 1% hardening strain) exhibits a clear difference in PDE and corresponding ductility depending on jacket technique and ECC type, but there is a slight difference in both (top-bottom) techniques due to the same reasons which discussed in section above, where the former strategies are more suitable than the later types in this case. The whole jackets technique appears highest PDE and corresponding ductility in the other side, the coated ECC has PDE and ductility higher than uncoated ECC for same technique except (Top-Bottom) jackets types.

CHAPTER 7

CONCLUSIONS AND FUTURE STUDIES

The essential objectives of this study are provide strengthening of four RC columns which are employed by Lynn, where three of them suffering from shear resistance deficiency and low ductility, while the latter with flexural and ductile behavior. Two gropes of engineering cementitious composite concrete (coated ECC with 3.5% tension hardening strain and uncoated ECC with 1% tension hardening strain) were used as a jacketed material. They have a unique ability to dissipation plastic energy, high tension stress, development multi-micro cracks instead of single local cracks and enhancement seismic performance level of RC columns as well as whole structure performance controlled by flexural behavior which prevent loss of axial load due to excessive shear force. This study adopts difference jackets techniques such as whole ECC with and without reinforcement, ECC jacket in plastic hinge regions, and replace damage cover. The finite element analysis of jacketed specimens is conducts by ABAQUS software depend on concrete damage plasticity theory (CDP).

Based on the results of analysis, the lateral load-displacement, ductility, failure mechanism, yielding of longitudinal bars, plastic dissipation energy summarized as following

7.1 Lateral Load-Displacement Behavior

One of the most important targeted features is load-displacement response of columns to resist lateral force due to earthquakes and wind loads etc. A structure's peak load capacity is the highest load prior significantly deformed. In contrast, story drift occurs when various stories of a building move laterally relative to one another as a result of lateral loads. A structural behavior under sever conditions can be understood by examining the relationship between peak load capacity and story drift. Lateral load-displacement of ECC jacketed specimens can summarized as following:

1. For original columns with shear deficiency, Whole ECC jacketed specimens exhibited increase peak lateral load (18%-26%) higher than top-bottom ECC jacketed specimens (4%-24%), whereas, for original column with flexural failure, whole ECC jacketed specimens increased peak lateral load (3%-12.5%) higher than top-bottom ECC jacketed specimens (3%-8%).
2. All specimens jacketed with coated ECC have increased lateral load capacity higher than uncoated ECC.
3. All jacketed specimens improved the displacement range, corresponding to constant load capacity (plastic deformation prior failure). For original columns with shear deficiency, whole ECC jacketed specimens improve lateral displacement corresponding to constant peak load (45-110) mm higher than experimental displacement range (25-30) mm by (4-12) time, while top-bottom ECC jacketed specimens have displacement range close to experimental so that they have low plastic deformation. For original column with flexural failure, whole ECC jacketed specimens improve lateral displacement corresponding to constant peak load (50-230) mm higher than experimental displacement range (40-70) mm by (4-6) time, while top-bottom ECC jacketed specimens have displacement range close to experimental.
4. The whole jackets with coated ECC exhibited the highest shear response and corresponding lateral displacement due to it provides significant confinement and good stress distribution along the whole cross-sectional area of column, but the specimens jacketed with replace cover top-bottom ECC have shear failure under applied lateral displacement that was lower than displacement which applied on the former model.
5. The ECC jacket techniques increase the maximum applied lateral displacement to (double of maximum applied displacement) in original columns with shear deficiency, while will reaching to (6 times of the maximum applied lateral displacement of experimental specimen) In original column with flexural failure.

7.2 Ductility Improvement

One of the most desirable properties is improve the ductility to resist dynamic loads**,** which was discussed with more details in chapter six of this study, Ductility of ECC jacketed specimen's conclusion summarized as following:

1. All specimens strengthened with ECC-jackets are improve ductility with difference values based on the technique type, original column ductility and the type of ECC-jacket.
2. All specimens strengthened with (the whole jacket-reinforced technique WR) exhibit largest ductility compared with other techniques.
3. All specimens jacketed with coated-ECC are exhibit ductility larger than specimens jacketed with uncoated-ECC.
4. All specimens with (whole jacket-reinforced technique WR) are improve the ductility higher than specimens with (whole jacket unreinforced technique W) by (1.6%-11.5%) and (3.5%-43%) for coated and uncoated ECC respectively. This is confirmed high efficiency of ECC side by side with steel reinforcement simultaneously.
5. For original columns with shear deficiency, the whole jacket-reinforced with coated ECC technique exhibits increase in ductility larger than uncoated ECC jackets by (2.25-2.74), (1.41-2) times of experimental ductility, for coated and uncoated ECC respectively, while for original column with flexural failure, whole jacket-reinforced technique exhibits increase in ductility (1.85-3.22), (1.3-3) times, where the efficiency of ECC jackets with original ductile column more than original columns with shear deficiency.
6. The specimens jacketed by top-bottom with replace cover (TB-C), and top-bottom (TB) techniques exhibit lowest increase in ductility compared with other techniques, where the ductility is increased for original column with shear deficiency and original column with flexural failure are (0.35-1.44), (0.18-1.2) times the original column ductility, for coated and uncoated ECC, respectively.

7. The ductility increased directly with increasing plastic dissipation energy for all jacketed specimens except the top-bottom jacketed techniques for original

column with shear deficiency, which are decreased ductility whenever there was increased plastic dissipation energy due to the effect of early shear failure on ECC activity which are generated near the center of column, this is confirm the importance selection of jacketed types which effect on general failure behavior.

8. On the contrary, for original column with flexural failure, slightly increase in ductility with close values of plastic dissipation energy for top-bottom techniques which is confirmed Inefficiency of this jacket types with ductile columns.

7.3 Failure Mechanism

1. All specimens strengthened with whole coated and uncoated ECC jackets (WR, W) exhibit flexural failure at the final loading stage, where they convert shear failure of original columns with shear deficiency to flexural failure due to the high confinement of the ECC jackets along the columns which compensated the deficiency of shear reinforcement in tested specimens, while all top-bottom jackets techniques (TB and TB-C) maintain shear failure except the original column with flexural failure which exhibit a flexural failure at the final stage of loading.
2. There is no significant effect of ECC-jackets on the elastic behavior of jacketed specimens, where all samples exhibit approximately yield displacement close to tested yield displacement until with increase applied lateral loads, but the effect was worthy increasing in the plastic deformation stage due to the high ability of ECC to develop cracks mechanism related to the hardening strain of ECC in tension, which is confirms the high ECC activity with high lateral excitation.
3. The whole ECC jackets improve the yield stress of transverse reinforcement and compensated the deficiency of shear reinforcement in tested columns, where they have been improved the tie yielding (2 - 3.27) times of tested stirrup yielding of original columns with shear deficiency as 3CLH18 and 3CMH18.
4. Top-bottom jacketed techniques exhibit a lower effect on the yield stress of transverse reinforcement and the shear failure remained as a dominant failure

in the final loading stages due to the high strengthening available in plastic hinge regions, which led to rapid propagation of cracks towards the columns center, which is already suffering from inadequate shear reinforcement.

5. The whole-cover replace (W-C) jacketed techniques exhibit a significant increase in yield stress of transvers reinforcement due to elimination of the concrete cover of columns, which is considered as a weak layer between ECC and stirrups. That's refers to increasing the ECC efficiency whenever directly contact with stirrups, as well as shear resistance by ECC.
6. The cracks propagation of the columns core jacketed with uncoated ECC higher than coated ECC, where the latter developed high-performance multiple cracks mechanism which are prevent early cracks formation of columns core, especially in original columns with shear deficiency. That's means the permanent stress of uncoated ECC jackets larger than that in jacketed specimens with coated ECC, which is considered as index of plastic deformation.
7. The cracks of the top-bottom jacketed techniques started in the jacket-column join, then propagated towards the center of the columns, where in the high ductile original column 2CLH18, where is assisted to formation diagonal cracks close to column center, which explained no significant increase in ductility in this type of jackets.

7.4 Yielding of Longitudinal Reinforcement

1. The whole ECC-jackets improve the area of longitudinal steel bars yielded greater than top-bottom techniques of original columns with shear deficiency as 3CLH18 and 3CMH18, and therefore increased flexural capacity
2. All ECC jacketed types didn't have a valuable increase yielding area of longitudinal steel bars for original column with flexural failure 2CLH18.

7.5 Plastic Dissipation Energy

1. All ECC-jacketed techniques improve the total plastic dissipation energy of the strengthened systems.
2. All ECC-jacketed techniques enhance the contribution of plastic dissipation energy of normal concrete with different values depending on the jacket technique, ECC type, and unjacketed columns properties. The whole-steel with coated ECC improve PDE of columns core (1.37-4.8) of experimental PDE which is increase whenever with original columns with flexural failure. Top- bottom with uncoated ECC (0.83-3.2) of experimental PDE of columns core depend on maximum lateral displacement and original columns properties.
3. The whole-steel with coated ECC jacketed technique exhibits an increase in total plastic dissipation energy PDE by (3.7-10.8) times of PDE for the experimental specimens which are consider higher than other techniques and provide RC columns a significant plastic deformation prior failure.
4. The top-bottom with uncoated ECC jacketed technique exhibits an increase in total plastic dissipation energy by (1.34-5.1) times of total PDE for the experimental specimens which are consider lower than other techniques. In spite of enhance PDE but remained the shear failure in columns center as a dominant failure especially in original column with shear deficiency due to concentrated PDE around plastic hinge regions.
5. For original columns with shear deficiency, whole-steel with coated ECC jacket techniques improve plastic dissipation energy PDE provide by steel rebars by (7.7-21.4) times, compared with experimental specimens, whereas original column with flexural failure exhibits lower improvement of PDE provided by steel rebars by (5.7 or less), where this explains high efficiency of above technique with original columns suffering from shear deficiency.
6. For original columns with shear deficiency, top-bottom (TB-C) with uncoated ECC jacket techniques improve plastic dissipation energy PDE provide by steel rebars by (2.3-7.6) times, compared with experimental specimens, whereas original column with flexural failure exhibits lower improvement of PDE provided by steel rebars by (1.2 or less).

7. The lack of compressive strength of the original column led to little participation of steel reinforcement, which is overcome by ECC jackets. This confirms the uselessness of a large amount of rebar with weak compressive strength, as it gives opposite results, high compatibility and efficiency of the ECC jackets with steel rebars.

7.6 Future Studies and Recommendations

Depending on the results which obtained from finite element analysis of jacketed specimens by using engineering cementitious composite concrete. The following recommendations are suggested further future studies:

1. Conducting empirical tests for RC columns retrofitted by ECC to study the bond properties between core and ECC and effect it on general behavior of member because the prefect bond which used in this study hard to handle practically in the sites, where the bond problems consider a big challenge for all jacket types not only ECC.
2. Studying the effective thickness of ECC on strengthening characteristics of RC columns.
3. Investigating the relationship between increasing axial loads and general behavior of RC columns jacketed with ECC.
4. Conducting comparison among structural members strengthened with ECC and CFRP.
5. Studying effect of cyclic loading on RC columns strengthening with ECC jacket through experimental and numerical tests.
6. ECC jackets can be used to retrofit piers of bridges, offshore piles, and marine structures exposed sever conditions as humidity and corrosion.

REFERENCES

[1] A. Yassin, "Seismic Performance Evaluation of Stiffness Irregular Rc Buildings Due To Story Height Difference Addis Ababa, Ethiopia," 2019.

[2] A. S. Mokha, N. Amin, M. C. Constantinou, and V. Zayas, "Seismic Isolation Retrofit of Large Historic Building," *J. Struct. Eng.*, vol. 122, no. 3, pp. 298–308, 1996, doi: 10.1061/(asce)0733-9445(1996)122:3(298).

[3] R. Vicente, H. Rodrigues, H. Varum, and J. A. R. Mendes da Silva, "Evaluation of Strengthening Techniques of Traditional Masonry Buildings: Case Study of a Four-Building Aggregate," *J. Perform. Constr. Facil.*, vol. 25, no. 3, pp. 202–216, 2011, doi: 10.1061/(asce)cf.1943-5509.0000164.

[4] B. Dadmand, M. Pourbaba, and R. Riahi, "Experimental and Numerical Investigation of Different Types of Jacketing Effect on Retrofitting RC Short Columns Using ECC Concrete," *Period. Polytech. Civ. Eng.*, vol. 66, no. 2, pp. 603–613, 2022, doi: 10.3311/PPci.19114.

[5] P. Kurniawan, H. Kasyanto, and L. M. Mauludin, "Numerical modeling of low strength reinforced concrete column strengthened with CFRP jacketing," *J. Phys. Conf. Ser.*, vol. 1839, no. 1, 2021, doi: 10.1088/1742-6596/1839/1/012007.

[6] M. S. Thesis and A. J. Mahmoodsami, "ANKARA YILDIRIM BEYAZIT UNIVERSITY GRADUATE SCHOOL OF NATURAL AND APPLIED SCIENCES USE OF NATURAL POZZOLANS IN LIGHTWEIGHT ENGINEERED CEMENTITIOUS COMPOSITE."

[7] A. C. Lynn, J. P. Moehle, S. A. Mahin, and W. T. Holmes, "Seismic evaluation of existing reinforced concrete building columns," *Earthq. Spectra*, vol. 12, no. 4, pp. 715–739, 1996, doi: 10.1193/1.1585907.

[8] R. O. and V. M. Ciprian Cozmanciuc, "Strengthening Techniques of RC Columns Using Fibre Reinforced Polymeric Materials," *Univ. Teh. „Gheorghe Asachi" din Iaşi Tomul LV (LIX), Fasc. 3, 2009 Secţia CONSTRUCŢII.*

ĂRHITECTURĂ, vol. 17, no. Lix, 2009, [Online]. Available: http://www.ce.tuiasi.ro/~bipcons/Archive/158.pdf

[9] S. Boukais, A. Nekmouche, N. Khelil, A. Kezmane, and A. Overview, "Numerical Investigation of the Jacketing Method of Reinforced Concrete Column," vol. 14, no. 1, pp. 26–29, 2020.

[10] S. Raza, M. K. I. Khan, S. J. Menegon, H. H. Tsang, and J. L. Wilson, "Strengthening and repair of reinforced concrete columns by jacketing: State-of-the-art review," *Sustain.*, vol. 11, no. 11, 2019, doi: 10.3390/su11113208.

[11] B. Wafaei Baneh and K. W. B. Wafaei Baneh, "Review of the Methods for Strengthening and Retrofitting Cultural Heritage Structures," *UKH J. Sci. Eng.*, vol. 4, no. 6, pp. 45–56, 2020, doi: 10.25079/ukhjse.v4n1y2020.pp45-56.

[12] S. R. Tariq, L. A. Qureshi, B. Ali, and M. U. Rashid, "Structural Behavior of RC Columns Improved by Different Strengthening Techniques," *Slovak J. Civ. Eng.*, vol. 28, no. 3, pp. 20–28, 2020, doi: 10.2478/sjce-2020-0020.

[13] L. Bisby and M. Ranger, "Axial–flexural interaction in circular FRP-confined reinforced concrete columns," *Constr. Build. Mater.*, vol. 24, no. 9, pp. 1672–1681, 2010.

[14] A. B. Christianto, B. Piscesa, M. M. Attard, Faimun, and P. Aji, "3D Finite element modeling of circular reinforced concrete column confined with CFRP under different eccentric loads," *IOP Conf. Ser. Mater. Sci. Eng.*, vol. 930, no. 1, 2020, doi: 10.1088/1757-899X/930/1/012047.

[15] Dimitra Achillopoulou, " Force transfer between existing concrete columns with reinforced concrete jackets subjected to axial loading," *15th World Conf. Earthq. Eng.*, no. January, 2012.

[16] K. G. Vandoros and S. E. Dritsos, "Concrete jacket construction detail effectiveness when strengthening RC columns," *Constr. Build. Mater.*, vol. 22, no. 3, pp. 264–276, 2008.

[17] C. Liu, H. Ma, L. Chen, Z. Li, and D. Yang, "Experimental study on seismic

performance of reinforced concrete column retrofitted by asymmetric increased single lateral section," *Adv. Struct. Eng.*, vol. 20, no. 9, pp. 1325–1339, 2017.

[18] C. G. Cho, Y. Y. Kim, L. Feo, and D. Hui, "Cyclic responses of reinforced concrete composite columns strengthened in the plastic hinge region by HPFRC mortar," *Compos. Struct.*, vol. 94, no. 7, pp. 2246–2253, 2012, doi: 10.1016/j.compstruct.2012.01.025.

[19] A. Meda, S. Mostosi, Z. Rinaldi, and P. Riva, "Corroded RC columns repair and strengthening with high performance fiber reinforced concrete jacket," *Mater. Struct.*, vol. 49, pp. 1967–1978, 2016.

[20] L. Yao, Y. Shi-ping, and C. Wen-jie, "Seismic behavior of corrosion-damaged RC columns strengthened with TRC under a chloride environment," *Constr. Build. Mater.*, vol. 201, pp. 736–745, 2019.

[21] X. Liu, Z. D. Lu, and L. Z. Li, "The use of bolted side plates for shear strengthening of RC beams: A review," *Sustain.*, vol. 10, no. 12, 2018, doi: 10.3390/su10124658.

[22] K. Heiza, A. Nabil, M. Tayel, K. Heiza, and N. Meleka, "State-of-the Art Review: Strengthening of Reinforced Concrete Structures-Different Strengthening Techniques Concrete Structures View project Behavior and Analysis of Reinforced Concrete Voided Slabs View project State-of-the Art Review: Strengthening of Reinforced Concrete Structures-Different Strengthening Techniques," 2014. [Online]. Available: https://www.researchgate.net/publication/260991475

[23] X. L. Xu, Z. D. Lu, L. Z. Li, and C. J. Jiang, "Numerical Study on the Local Buckling Behaviour of Bolted Steel Plates in Steel Jacketing," *Adv. Mater. Sci. Eng.*, vol. 2017, 2017, doi: 10.1155/2017/1352084.

[24] P. Kiruthika, S. Balasubramanian, M. C. Sundarraja, and J. Jegan, "Strengthening of Concrete Filled Steel Tubular Columns using FRP Composites," *Int. J. Innov. Res. Sci. Eng. Technol. (An ISO*, vol. 3297, pp. 2250–2259, 2007, doi: 10.15680/IJIRSET.2015.0404081.

[25] Y.-F. Wu, T. Liu, and L. Wang, “Experimental investigation on seismic retrofitting of square RC columns by carbon FRP sheet confinement combined with transverse short glass FRP bars in bored holes,” *J. Compos. Constr.*, vol. 12, no. 1, pp. 53–60, 2008.

[26] R. Realfonzo and A. Napoli, “Cyclic behavior of RC columns strengthened by FRP and steel devices,” *J. Struct. Eng.*, vol. 135, no. 10, pp. 1164–1176, 2009.

[27] G. Ma and H. Li, “Experimental study of the seismic behavior of predamaged reinforced-concrete columns retrofitted with basalt fiber–reinforced polymer,” *J. Compos. Constr.*, vol. 19, no. 6, p. 4015016, 2015.

[28] C.-G. Cho, B.-C. Han, S.-C. Lim, N. Morii, and J.-W. Kim, “Strengthening of reinforced concrete columns by High-Performance Fiber-Reinforced Cementitious Composite (HPFRC) sprayed mortar with strengthening bars,” *Compos. Struct.*, vol. 202, pp. 1078–1086, 2018.

[29] L. Xu, J. Pan, and J. Cai, “Seismic behavior of steel reinforced ECC or ECC/concrete composite short columns,” 2016, doi: 10.21012/fc9.142.

[30] J. H. Paul, “REPAIR, RENOVATION AND STRENGTHENING OF CONCRETE STRUCTURES ‘Evaluation and Rehabilitation of Concrete Structures’ Mexico City,” pp. 1–11, 2002.

[31] J. C. Lim and T. Ozbakkaloglu, “Stress–demon model for normal-and light-weight concretes under uniaxial and triaxial compression,” *Constr. Build. Mater.*, vol. 71, pp. 492–509, 2014.

[32] M. Szczecina, “Calibration of the CDP model parameters in Abaqus,” *Civ. Eng. J.*, vol. 8, no. 2, pp. 225–237, 2015.

[33] M. Labibzadeh, M. Zakeri, and A. A. Shoaib, “A new method for CDP input parameter identification of the ABAQUS software guaranteeing uniqueness and precision,” *Int. J. Struct. Integr.*, vol. 8, no. 2, pp. 264–284, 2017, doi: 10.1108/IJSI-03-2016-0010.

[34] J. Lubliner, J. Oliver, S. Oller, and Ejij. Onate, “A plastic-damage model for

concrete," *Int. J. Solids Struct.*, vol. 25, no. 3, pp. 299–326, 1989.

[35] J. Lee and G. L. Fenves, "Plastic-damage model for cyclic loading of concrete structures," *J. Eng. Mech.*, vol. 124, no. 8, pp. 892–900, 1998.

[36] V. Birtel and P. Mark, "Parameterised finite element modelling of RC beam shear failure," in *ABAQUS users' conference*, 2006.

[37] E. Noroozieh and A. Mansouri, "Lateral strength and ductility of reinforced concrete columns strengthened with NSM FRP rebars and FRP jacket," *Int. J. Adv. Struct. Eng.*, vol. 11, no. 2, pp. 195–209, 2019, doi: 10.1007/s40091-019-0225-5.

[38] S. Popovics, "A numerical approach to the complete stress-strain curve of concrete," *Cem. Concr. Res.*, vol. 3, no. 5, pp. 583–599, 1973.

[39] M. Sargin, S. K. Ghosh, and V. K. Handa, "Effects of lateral reinforcement upon the strength and deformation properties of concrete," *Mag. Concr. Res.*, vol. 23, no. 75–76, pp. 99–110, 1971.

[40] K.-H. Yang, J.-H. Mun, M.-S. Cho, and T. H. K. Kang, "Stress-strain model for various unconfined concretes in compression," *ACI Struct. J.*, vol. 111, no. 4, p. 819, 2014.

[41] D. C. Kent and R. Park, "Flexural members with confined concrete," *J. Struct. Div.*, vol. 97, no. 7, pp. 1969–1990, 1971.

[42] E. Hognestad, "Study of combined bending and axial load in reinforced concrete members," *Univ. Illinois. Eng. Exp. Station. Bull. no. 399*, 1951.

[43] R. Park and W. L. Gamble, *Reinforced concrete slabs*. John Wiley & Sons, 1999.

[44] D. J. Carreira and K.-H. Chu, "Stress-strain relationship for reinforced concrete in tension," in *Journal Proceedings*, 1986, pp. 21–28.

[45] B. L. Iverson and P. B. Dervan, *No 主観的健康感を中心とした在宅高齢者における 健康関連指標に関する共分散構造分析Title*.

[46] C. Arya, "Eurocode 2: Design of concrete structures," *Des. Struct. Elem.*, vol. 3, pp. 334–394, 2015, doi: 10.1201/b18121-18.

[47] T. Wang and T. T. C. Hsu, "Nonlinear finite element analysis of concrete structures using new constitutive models," *Comput. Struct.*, vol. 79, no. 32, pp. 2781–2791, 2001.

[48] L. Qingfu, G. Wei, and K. Yihang, "Parameter calculation and verification of concrete plastic damage model of ABAQUS," in *IOP conference series: Materials science and engineering*, IOP Publishing, 2020, p. 12036.

[49] A. Belarbi and T. T. C. Hsu, "Constitutive laws of concrete in tension and reinforcing bars stiffened by concrete," *Struct. J.*, vol. 91, no. 4, pp. 465–474, 1994.

[50] B. Wahalathantri, D. Thambiratnam, T. Chan, and S. Fawzia, "A material model for flexural crack simulation in reinforced concrete elements using ABAQUS," in *Proceedings of the first international conference on engineering, designing and developing the built environment for sustainable wellbeing*, Queensland University of Technology, 2011, pp. 260–264.

[51] M. Hafezolghorani, F. Hejazi, R. Vaghei, M. S. Bin Jaafar, and K. Karimzade, "Simplified damage plasticity model for concrete," *Struct. Eng. Int.*, vol. 27, no. 1, pp. 68–78, 2017.

[52] F. Yuan, J. Pan, and C. K. Y. Leung, "Elastoplastic time history analysis of reinforced engineered cementitious composite or engineered cementitious composite-concrete composite frame under earthquake action," *Adv. Struct. Eng.*, vol. 20, no. 4, pp. 491–503, 2017, doi: 10.1177/1369433216655809.

[53] G. Fischer and V. C. Li, "Effect of matrix ductility on deformation behavior of steel-reinforced ECC flexural members under reversed cyclic loading conditions," *Struct. J.*, vol. 99, no. 6, pp. 781–790, 2002.

[54] V. C. Li and D. K. Mishra, "Structural applications of engineered cementitious composites," 1996.

[55] F. Yuan, J. Pan, L. Dong, and C. K. Y. Leung, “Mechanical Behaviors of Steel Reinforced ECC or ECC/Concrete Composite Beams under Reversed Cyclic Loading,” *J. Mater. Civ. Eng.*, vol. 26, no. 8, 2014, doi: 10.1061/(asce)mt.1943-5533.0000935.

[56] B. Alfarah, F. López-Almansa, and S. Oller, “New methodology for calculating damage variables evolution in Plastic Damage Model for RC structures,” *Eng. Struct.*, vol. 132, pp. 70–86, 2017, doi: 10.1016/j.engstruct.2016.11.022.

[57] P. Mark, “Stahlbetonträger mit zweiachsiger Querkraftbeanspruchung,” *Beton- und Stahlbetonbau*, vol. 99, no. 9, pp. 744–753, 2004.

[58] K. Toongoenthong and K. Maekawa, “Computational performance assessment of damaged RC members with fractured stirrups,” *J. Adv. Concr. Technol.*, vol. 3, no. 1, pp. 123–136, 2005.

[59] A. M. Britto, “Running ABAQUS 6.4.” Online, 2005.

[60] C. Rupakumar and T. Swedha, “Experimental Investigation of Column Retrofitted with Steel Mesh and HPFRC under Cyclic Loading”.

[61] R. Zhang, K. Matsumoto, J. Niwa, T. Hirata, and Y. Ishizeki, “Experimental study on shear behavior of PP-ECC beams with different stirrup ratios,” in *Proceedings of the Thirteenth East Asia-Pacific Conference on structural engineering and construction (EASEC-13)*, The Thirteenth East Asia-Pacific Conference on Structural Engineering and …, 2013, p. B-5.

[62] C.-L. Ning and B. Li, “Probabilistic approach for estimating plastic hinge length of reinforced concrete columns,” *J. Struct. Eng.*, vol. 142, no. 3, p. 4015164, 2016.

[63] A. C. Aydin, B. Bayrak, M. Maali, M. Kiliç, and H. G. Alcan, “Shear wall design within the light of prominent standards,” *Civ Eng Beyond Limits*, vol. 4, pp. 13–19, 2020.

[64] Y. M. A. Hashash, J. J. Hook, B. Schmidt, I. John, and C. Yao, “Seismic design and analysis of underground structures,” *Tunn. Undergr. Sp. Technol.*, vol. 16,

no. 4, pp. 247–293, 2001.

[65] W. M. Hassan and M. Farag, “Seismic performance of steel-reinforced concrete composite columns in existing and modern construction,” *Soil Dyn. Earthq. Eng.*, vol. 151, p. 106945, 2021.

[66] M. ElGawady, M. Endeshaw, D. McLean, and R. Sack, “Retrofitting of rectangular columns with deficient lap splices,” *J. Compos. Constr.*, vol. 14, no. 1, pp. 22–35, 2010.

[67] O. Ozcan, B. Binici, and G. Ozcebe, “Improving seismic performance of deficient reinforced concrete columns using carbon fiber-reinforced polymers,” *Eng. Struct.*, vol. 30, no. 6, pp. 1632–1646, 2008.

[68] ACI 318-19, “318M-19: Building Code Requirements for Concrete and Commentary,” *Aci 318-19M*, p. 628, 2019.

CURRICULUM VITAE

PERSONAL INFORMATION

Name Surname : Ali Lilo Al Hasan
Date of Birth :
Phone :
E-mail :

EDUCATION

High School : GRADUATE SCHOOL OF NATURAL AND APPLIED SCIENCES
Bachelor : Basrah university / Civil Engineering
Master Degree : ANKARA YILDIRIM BEYAZIT UNIVERSITY/ Civil Engineering

WORK EXPERIENCE

Research Assist. :

TOPICS OF INTEREST

- Dynamic of structure -
Strengthening RC Column
- Shear Deficint -
Earthquake resistance resistance of Existing Building

PRESENT ORGANIZED SOURCES / PRESENTATION